

THE MOLECULAR BASIS OF ANTAGONISM BY
PPADS AT THE HUMAN P2X1 RECEPTOR

Thesis Submitted for the Degree of
Doctor of Philosophy
at the University of Leicester

By Hong Huo

Department of Molecular and Cell Biology

University of Leicester

June 2018

Abstract

The Molecular Basis of Antagonism by PPADS at the Human P2X1 Receptor

- **Hong Huo**

P2X receptors (P2XRs) activated by ATP are widely expressed throughout the human body and mediate various physiological and pathophysiological roles. Crystal structures have provided a major advance in understanding agonist and subtype selective antagonist actions. However, the molecular basis of antagonism of general antagonists is poorly understood. PPADS is an effective antagonist at most mammalian P2XRs. Previous studies suggested lysine residue 249 (K249) (numbering for P2X1R) was involved in PPADS action. The aim of this study was to determine the PPADS binding site in a molecular model of the human P2X1R based on the zebra fish P2X4R (zfP2X4R) crystal structure. Contributions of individual residues in a ring centred on K249 with a radius of the length of PPADS were investigated by cysteine mutagenesis. The effect of their cysteine substitutions on accessibility following PPADS binding and on PPADS sensitivity were tested.

A cluster of positively charged residues (K70, K190 and K249) at the orthosteric pocket showed decreases in both accessibility and sensitivity to PPADS, suggesting they are directly involved in binding of the antagonist. These data allow validation of molecular docking to provide the first model of PPADS binding. Some residues outside the orthosteric area showed decreased accessibility following PPADS binding but on change in antagonist sensitivity, indicating PPADS binding induced significant conformational changes from the apo state. In addition, the charge and conformational changes at the cysteine rich head (CRH) region also contributed to antagonist action by showing a mutation at a positively charged residue (K138C) increased accessibility following PPADS binding and decreased PPADS sensitivity.

In summary, this thesis has advanced the understanding of antagonist PPADS action and provided a template to develop subtype selectivity based on the differences between subunits around the orthosteric P2XR binding site and the CRH region.

Publications

Papers

Huo, H., Fryatt, A. G., Farmer, L. K., Schmid, R. and Evans, R. J. (2018) Mapping the binding site of the P2X receptor antagonist PPADS reveals the importance of orthosteric site charge and the cysteine rich head region. *J Biol Chem.* 2018 Aug 17, 293(33): 12820-12831

Abstracts

Hong Huo, Richard J. Evans. The molecular basis of PPADS antagonism at P2X1 receptors. *Poster presentation at 1st UK/Italian Purine Club Meeting, Bristol, UK.*

Hong Huo, Richard, J. Evans, The molecular basis of PPADS antagonism at P2X1 receptors. *Poster presentation at the Purines 2017 conference, Rome, Italy.*

Acknowledgements

Firstly, I would like to give a massive thank to my brilliant supervisor Prof. Richard Evans. I started my studies as a master student and Prof. Evans provided me the opportunity to continue to a PhD. Throughout my PhD, he gave me excellent teaching and invaluable support. His vast knowledge and enthusiasm for scientific research inspired me to work hard and obtained good work in the end. I am also grateful for his patience with me during my writing up status. I improved a lot in writing skills with his guidance. Moreover, I would like to thank all the academic staff who gave me expert advice and feedback about my project, especially my committee members Prof. John Challiss and Dr. John Micheson. Many thanks to Dr Ralf Schmidt for teaching me the modelling and docking work and provided me many docking models.

I would also like to thank everyone in the lab for their help and teaching me practical skills. Especially thanks to Alistair who is very patient to teach me new techniques and answer me lots of questions. We have been good friends even now he finished his contract. I am very grateful to Manijeh for her weekly oocytes preparation and general lab assistance. Thank Adam for his support and providing laughs to me. His optimism encouraged me a lot when I felt frustrated and upset.

Also, I would like to give a huge thank to my boyfriend for his support. He is always there when I needed. He shares with me in good days and cheers me up in my bad days. I would also thank all my friends in Leicester, especially Yan, Shou, Xianguo and Tiya for accompanying me and made me not feel lonely here.

Finally, I would like to say thank you to my family who support me for studying and living in UK. I feel so lucky to have been raised in such a loving and supportive family.

Abbreviations

2-meSATP	2-methylthio-adenosine-5'-triphosphate
5-BDBD	5-(3-Bromophenyl)-1,3-dihydro-2 <i>H</i> -benzofuro[3,2- <i>e</i>]-1,4-diazepin-2-one
A-740003	N-(1-[(cyanoimino)(5-quinolinylamino)methyl]amino-2,2-dimethylpropyl)-2-(3,4-dimethoxyphenyl)aceta-mide
A-804598	2-cyano-1-[(1 <i>S</i>)-1-phenylethyl]-3-quinolin-5-ylguanidine
ACh	Acetylcholine
ADP	Adenosine diphosphate
AFM	Atomic force microscopy
Am	<i>Amblyomma maculatum</i>
AMP	Adenosine monophosphate
ATP	Adenosine 5' Triphosphate
ATP₉₀	Concentration of ATP that gives 90% of the maximal response
ATP_γS	Adenosine 5'-O-(3-thio) triphosphate
AZ11645373	3-[1-[[[(3'-Nitro[1,1'-biphenyl]-4-yl)oxy]methyl]-3-(4-pyridinyl)propyl]-2,4-thiazolidinedione
BN-PAGE	Blue native polyacrylamide gel electrophoresis
BX430	1-(2,6-dibromo-4-isopropyl-phenyl)-3-(3-pyridyl) urea
Bz-ATP	2'(3')-O-(4-Benzoylbenzoyl)adenosine-5'-triphosphate triethylammonium salt
cAMP	adenylate cyclase
cDNA	complementary DNA
CNS	Central nervous system
DF	Dorsal fin
DNA	Deoxyribonucleic acid
DRG	Dorsal root ganglion
EB	Ethidium bromide
ECL	Enhanced chemiluminescence reagent
E. Coli	<i>Escherichia coli</i>
EC₅₀	Half maximal effective concentration of agonist

EC₉₀	Concentration of ATP that evoked 90% of the maximal current
EM	Electron microscopy
FRET	Fluorescence resonance energy transfer
FSEC	Fluorescence-detection size exclusion chromatography
GPCR	G-protein coupled receptor
G-protein	Guanosine nucleotide binding protein
HEK	Human embryonic kidney
HIV	Human immunodeficiency virus
HRP	Horseradish peroxidase
IC₅₀	Half maximal effective concentration of antagonist
IP₃	Inositol triphosphate
KO	Knockout
LF	Left flipper
mRNA	messenger RNA
MD	Molecular dynamic
MRS 2220	Cyclic pyridoxine- $\alpha^{4,5}$ -monophosphate-6-azophenyl-2', 5'-disulfonic acid
MRS 2257	Pyridoxal-5'-phosphonate 6-azophenyl 3',5'-bismethylenephosphonate
MRS2365	2-methylthio-ADP
MTS	Methanethiosulfonate
MTSEA	(2-aminoethyl) methanethiosulfonate
MTSEA-biotin	(2-aminoethyl) methanethiosulfonate hydrobromide-biotin
MTSES	Sodium (2-sulfonatoethyl) methanethiosulfonate
MTSET	N,N,N-trimethyl-2-[(methylsulfonyl)thio]-ethanaminium bromide
MTS-TPAE	2-(Tripenylammonium) ethyl Methanethiosulfonate Bromide
MTS-TAMRA	MTS-5(6)-carboxytetramethylrhodamine
NA	Noradrenaline
NANC	Non-adrenergic, non-cholinergic

NF023	8,8'-(Carbonylbis(imino-3,1-phenylene carbonylimino)bis(1,3,5-naphthalenetrisulfonic) acid)
NF279	8,8'-(Carbonylbis(imino-4,1-phenylenecarbonylimino-4,1-phenylenecarbonylimino)) bis(1,3,5-naphthalenetrisulfonic acid)
NF449	4,4',4'',4'''-(Carbonylbis(imino-5,1,3benzenetriylbis (carbonylimino)))
NF770	7,7-(carbonylbis(imino-3,1-phenylenecarbonylimino-3,1-(4-methyl-phenylene)carbonylimino))bis(1-methoxy-naphthalene-3,6-disulfonic acid)
NF776	6,6-(carbonylbis(imino-3,1-(4-methylphenylene)carbonylimino))bis(1-methoxynaphthalene-3,5-disulfonic acid)
NF778	6,6-(carbonylbis(imino-3,1-phenylenecarbonylimino-3,1-(4-methyl-phenylene)carbonylimino))bis(1-methoxy-naphthalene-3,5-disulfonic acid)
NO	Nitric oxide
P2XR	Purinoceptors 2X receptor
P2YR	Purinoceptors 2Y receptor
P5P	Pyridoxal 5'-phosphate
PCR	Polymerase chain reaction
pdP2X7R	panda P2X7 receptor
pD₂	negative log of EC ₅₀
pEC₅₀	Negative logarithm of the EC ₅₀
pIC₅₀	Negative logarithm of the IC ₅₀
PKC	Protein kinase C
PLC	Phospholipase C
PNS	Peripheral nervous system
polyA	Polyadenylated
PPADS	Pyridoxal-phosphate-6-azophenyl-2', 4'-disulfonate
PPNDS	Pyridoxal-5'-phosphate-6-(2'-naphthylazo-6'-nitro-4',8' disulfonate)

PSB-10211	sodium 1-amino-4-[3-(4,6-dichloro[1,3,5]triazine-2-ylamino)phenylamino]-9,10-dioxo-9,10-dihydroanthracene-2-sulfonate
PSB-1011	disodium 1-amino-4-[3-(4,6-dichloro[1,3,5]triazine-2-ylamino)-4-sulfophenylamino]-9,10-dioxo-9,10-dihydroanthracene-2-sulfonate
PSB-12054	N-(benzyloxycarbonyl)phenoxazine
PSB-12062	N-(p-Methylphenylsulfonyl)phenoxazine
RF	Right flipper domain
RNA	Ribonucleic acid
SCAM	Substituted cysteine accessibility method
SDS-PAGE	Sodium dodecyl sulfate polyacrylamide gel electrophoresis
SEM	Standard error of the mean
SNP	Single nucleotide polymorphism
TEVC	Two electrode voltage clamp
TGF	Tubuloglomerular feedback
TM	Transmembrane domain
TNP-ATP	[2'(3')-O-(2,4,6-Trinitrophenyl)adenosine 5'-triphosphate]
UDP	Uridine diphosphate
UTP	Uridine 5'-triphosphate
VCF	Voltage Clamp Fluorometry
WT	Wildtype
zfP2X4R	Zebra fish P2X4 receptor
α,β-meATP	α,β -methylene ATP

Contents

Chapter 1. Introduction	1
1.1 Adenosine 5'- triphosphate (ATP)	1
1.2 Purinergic Receptors	5
1.2.1 P1 receptors	5
1.2.2 P2Y receptors	6
1.2.3 P2X receptors	9
1.3. Properties of recombinant P2X receptors	10
1.3.1 Agonists.....	11
1.3.2 Time-course of the ATP evoked current at P2XRs	14
1.3.3 Properties of hetero-trimeric receptors	16
1.4 Physiological and pathological roles of P2X receptors	18
1.4.1 P2X1 receptors	19
1.4.2 P2X2-P2X7 receptors	21
1.5 Structure of P2X receptors	27
1.5.1 Pre-crystal insights into structure.....	27
1.5.2 The crystal structure of the P2X receptor	30
1.5.3 ATP binding site.....	34
1.5.4 Conformational changes on agonist binding.....	36
1.5.5 Ion access	39
1.5.6 Desensitized state	41
1.5.7 Divalent cation binding sites	46
1.6 Antagonists at P2X receptors	49
1.6.1 Suramin	49
1.6.2 Analogues of suramin.....	51
1.6.3 Mutagenesis studies on suramin and NF449 at the P2X1 receptor..	54
1.6.4 Competitive antagonism of the hP2X3R	56
1.6.5 Structural basis for selective P2X7 antagonism.....	58
1.7 Antagonism of PPADS	63
1.7.1 PPADS actions at P2XRs expressed in native tissues	63

1.7.2 PPADS action at recombinant P2XR subtypes.....	64
1.7.3 PPADS action at P2Y receptors	65
1.7.4 Structure and analogues of PPADS.....	66
1.8 Aims and Objectives.....	68
Chapter 2. Materials and methods.....	70
2.1 Molecular Biology	70
2.1.1 The human P2X1 receptor.....	70
2.1.2 Site-directed mutagenesis	70
2.1.3 Combination of mutants.....	73
2.1.4 Transformation and DNA Extraction	73
2.1.5 DNA Sequencing	74
2.1.6 mRNA synthesis	75
2.2 Expression in <i>Xenopus laevis</i> oocytes.....	75
2.3 Treatment of oocytes and sample preparation for MTSEA- biotinylation	76
2.4 Western blotting.....	77
2.5 Electrophysiological Recordings	78
2.6 Use of MTS compounds to modify cysteine mutants.....	79
2.7 Data analysis.....	80
2.8 Molecular docking	81
Chapter 3. Characterisation of antagonist PPADS and the effect of K249C on the sensitivity of the hP2X1R to PPADS	82
3.1 Introduction.....	82
3.1.1 Previous studies into the molecular basis of PPADS Action at P2XRs	82
3.1.2 Aims.....	85
3.2 Results.....	85
3.2.1 The ATP sensitivity of WT hP2X1Rs	85
3.2.2 The time-course of the ATP evoked response at WT hP2X1Rs	87
3.2.3 Characterisation of PPADS action at WT hP2X1R	87

3.2.4 The effect of K249C on sensitivity of the hP2X1R to ATP and PPADS	90
3.3 Discussion.....	95
3.3.1 PPADS works as a non-competitive and reversible antagonist at the hP2X1R	95
3.3.2 The importance of K249 to the sensitivity of the hP2X1R to PPADS	97
3.3.3 The extracellular loop and the potential PPADS binding area	98
Chapter 4. Effect of PPADS on accessibility of residues in the extracellular loop of the hP2X1R	100
4.1 Introduction.....	100
4.1.1 Substituted cysteine accessibility studies on P2XRs	100
4.1.2 Hypothesis.....	106
4.1.3 Aim	109
4.2 Results.....	109
4.2.1 No free cysteine residue can be detected at WT hP2X1Rs	109
4.2.2 PPADS decreased accessibility of K249C at the hP2X1R.....	111
4.2.3 PPADS does not have an effect on accessibility of residues out of the potential PPADS binding area	111
4.2.4 Effect of PPADS on accessibility of surface cysteine mutants around the ATP binding sites.....	113
4.2.5 Effect of PPADS on accessibility of cysteine mutants deep in the ATP binding sites.....	115
4.2.6 Effect of PPADS on accessibility of the cysteine residues in the upper body of the hP2X1R	117
4.2.7 Effect of PPADS on accessibility of the cysteine residues around the dorsal fin of the hP2X1R.....	117
4.2.8 Effect of PPADS on accessibility of the residues lining the upper vestibule	120
4.2.9 Comparison effects between PPADS and ATP on accessibility of cysteine mutants in the potential PPADS binding area.....	120
4.3 Discussion.....	126
4.3.1 No effect of PPADS on accessibility of cysteine mutants out of the ring	126
4.3.2 The importance of K249 in PPADS binding	126

4.3.3 Residues showing decreased accessibility by PPADS binding in the ring	127
4.3.4 Increased accessibility of the residues by PPADS binding results from PPADS-evoked conformational changes.....	129
4.3.5 Residues showing decreased accessibility by PPADS binding at the allosteric site.....	130
4.3.6 Potential of mutants with no change in accessibility in PPADS binding	130
Chapter 5. Effect of cysteine mutants and Methanethiosulfonate (MTS) Reagents on PPADS sensitivity of hP2X1Rs	138
5.1 Introduction	138
5.1.1 Use of MTS compounds to modify cysteine mutants to investigate the ATP binding site	138
5.1.2 Aim	140
5.2 Results	140
5.2.1 Effect of individual cysteine mutants around the ATP binding site on PPADS sensitivity.....	140
5.2.2 Effect of the cysteine mutants deep in the ATP binding site on PPADS sensitivity	142
5.2.3 Effect of the cysteine mutants opposite to the ATP binding sites on PPADS sensitivity.....	146
5.2.4. Effect of the cysteine mutants in the left flipper (E282-P287) on PPADS sensitivity.....	146
5.2.5 Effect of combinations of cysteine mutants on PPADS sensitivity ..	146
5.2.6 Effect of MTS compounds on PPADS sensitivity	152
5.3 Discussion.....	164
5.3.1 Effect of residues on PPADS potency within and around the orthosteric pocket	164
5.3.2 Residues outside the orthosteric pocket showing no effect on PPADS potency	166
5.3.3 Comparison of effects of cysteine mutants on ATP and PPADS potency	167
Chapter 6 General discussion.....	179
6.1 The contribution of K249 to PPADS binding at P2XRs.....	179

6.2 The contribution of positively charged residues to PPADS binding	181
6.3 PPADS binding quenches fluorescence at MTS-TAMRA labelled cysteine mutants in the antagonist binding pocket	183
6.4 Molecular docking of PPADS	185
6.5 PPADS evoked conformational changes	187
6.6 The contribution of the cysteine rich head region to PPADS sensitivity	189
6.7 Using PPADS as a template to develop specific P2XR subtype antagonists	190
References	192

Chapter 1. Introduction

1.1 Adenosine 5'- triphosphate (ATP)

Discovery and structure

Adenosine 5'-triphosphate (ATP) was discovered in muscle by Lohmann, and by Fiske and Subbarow in 1929 (Fiske and Subbarow 1929, Lohmann 1929). It was initially thought to be a substrate in muscular contraction. Subsequently, ATP was shown to be a vital intracellular energy carrier for all living cells. The structure of ATP was established in 1945 (Lythgoe and Todd 1945). It is composed of a purine base (adenine), a ribose sugar (β -D- ribofuranose) and a 3' phosphate group (Figure 1.1). Energy is stored in the phosphate bonds within phosphate groups. ATP is hydrolysed to adenosine 5'- diphosphate (ADP) when one of the covalent bonds is cleaved, with energy released. ADP can be further hydrolysed to adenosine 5'- monophosphate (AMP) and subsequently adenosine.

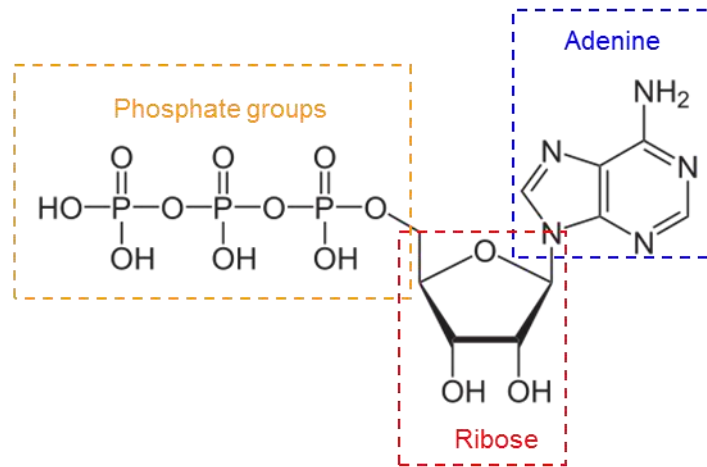
Formation and storage

The synthesis of ATP occurs in all cells. ATP is generated by the processes of glycolysis, the tricarboxylic acid cycle and predominantly oxidative phosphorylation in mitochondria by ATP synthase (Sperlágh and Vizi 1996). ATP is the universal source of energy for cell metabolism. The level of ATP usually reaches the millimolar range within cells (Bonora et al. 2012). Interestingly, a considerable amount of ATP was also found in vesicles in nerve terminals. ATP was found co-stored with the neurotransmitter acetylcholine (Whittaker et al. 1974) and noradrenaline (Schumann 1958) in sympathetic nerves. The degradation products of ATP (ADP, AMP, adenosine) and other nucleotides, such as UTP, can also be stored in the synaptic vesicles (Zimmermann 1994).

ATP as a transmitter

The first hint showing ATP may work extracellularly was in 1929 when adenylic acid was shown to have actions on heart rate and arterial dilatation (Drury and Szent-Gyorgyi 1929). Subsequent studies found intra-arterial injection

(a)



(b)

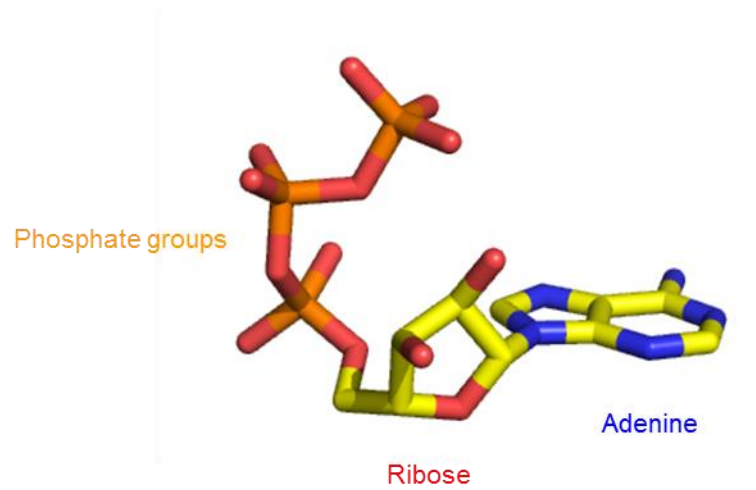


Figure 1.1 Structure of ATP

(a) The molecular structure of ATP consists of an adenine ring, a ribose and three phosphate groups. (b) The structure of ATP is shown as sticks generated by PyMol software.

of ATP potentiated acetylcholine-evoked muscle contraction (Buchthal and Folkow 1948). Intravenous injection of ATP was found to cause complex effects on autonomic ganglia (Emmelin and Feldberg 1948). In 1959, ATP was for the first time shown to be released from the nervous system during stimulation of sensory nerve fibres in the skin of the rabbit's ear and contributed to vasodilatation (Holton 1959). This indicated that ATP may work as a transmitter.

In the early 1960s, Burnstock found stimulation of smooth muscle in guinea-pig taenia coli produced inhibitory junction potentials when the adrenergic and cholinergic nerves were blocked (Burnstock et al. 1963). This was referred to as a non-adrenergic and non-cholinergic (NANC) transmission. Subsequent studies showed purine compounds may be involved in NANC transmission in the gut (Burnstock et al. 1970) and guinea-pig bladder (Burnstock et al. 1972). Among the purine nucleotides tested, ATP was the most potent.

To identify a neurotransmitter, the substance must satisfy several criteria (Eccles 1964). Firstly, the transmitter must be synthesised and stored within the nerve terminals; secondly, the transmitter must be mimicked by exogenous application; thirdly, the processes involved in inactivation or uptake of the transmitter must be present; finally, drugs that affect the nerve-mediated response must have similar actions on the response to the exogenously applied transmitter. ATP was the substance that best satisfied the above criteria for the NANC nerves (Figure 1.2). In 1972, ATP was proposed to be the NANC transmitter (Burnstock 1972). In 1976, ATP was suggested to work as a co-transmitter in sympathetic nerves (Burnstock 1976a). Now, ATP has also been shown to be co-released with various transmitters in parasympathetic, enteric, sensory-motor and central nervous systems (Burnstock 2007). In addition, ATP can be released from non-neuronal cells in response to mechanical stress, hypoxia, inflammation and cytolysis (Bodin and Burnstock 2001). Once released, the extracellular ATP can be rapidly broken down by various ATPases and nucleotidases (Zimmermann 2001).

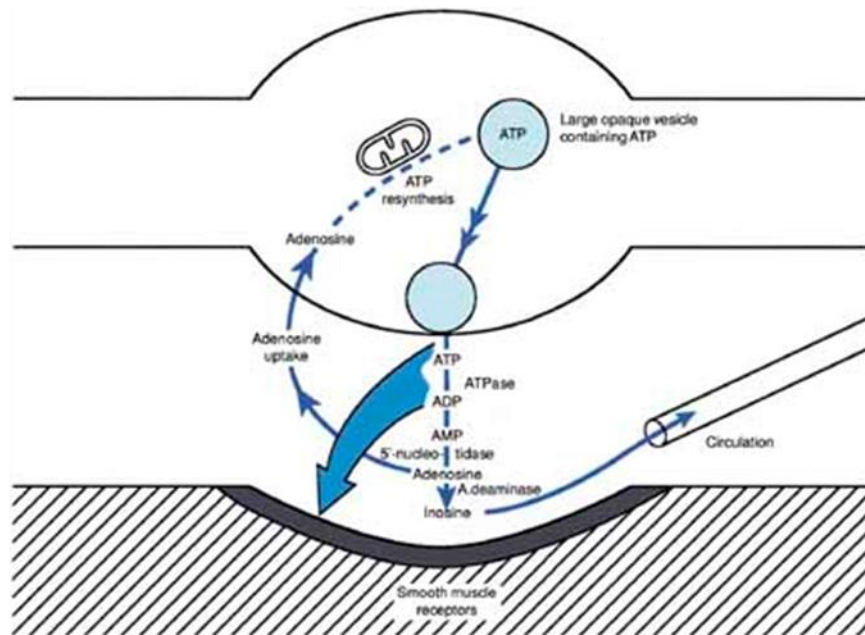


Figure 1.2 The process of ATP synthesis, storage, release and inactivation
 ATP, stored in vesicles in nerve varicosities, is released by exocytosis to act on postjunctional receptors for ATP on smooth muscle. ATP is broken down extracellularly by ATPases and 5'-nucleotidase to adenosine, which is taken up by varicosities to be resynthesized and reincorporated into vesicles. Adenosine is broken down further by adenosine deaminase to inosine and hypoxanthine and removed by the circulation (Image taken from Burnstock 1972).

1.2 Purinergic Receptors

Since the initial idea of purinergic transmission was accepted, the receptors for the purinergic responses needed to be identified. The term purinergic receptors was established in 1976 (Burnstock 1976b). Purinergic receptors were originally divided into two classes, P1 (activated by adenosine) and P2 families (activated by ATP/ADP) (Burnstock 1978). P2 receptors were subsequently separated into two subtypes, namely P2X receptors (P2XRs) and P2Y receptors (P2YRs), based on their pharmacological characteristics (Burnstock and Kennedy 1985). When the first P2XR and P2YRs were cloned in the early 1990s (Lustig et al. 1993, Valera et al. 1994, Webb et al. 1993), P2 receptors were reclassified on the basis of their structures. P2XRs were defined as ligand-gated ion channels and P2YRs as G-protein coupled receptors (Abbracchio and Burnstock 1994).

1.2.1 P1 receptors

P1 receptors are activated by adenosine, therefore they are also termed adenosine receptors (Fredholm et al. 2001). Genes encoding four different adenosine receptor subtypes, A₁, A_{2A}, A_{2B} and A₃, have been cloned and characterised (Libert et al. 1989, Stehle et al. 1992, Zhou et al. 1992).

Signalling

Adenosine receptors are all G protein-coupled receptors. Generally, A₁ and A₃ receptors couple to G_{i/o} proteins and A_{2A} and A_{2B} receptors couple to G_s proteins. After activation of the G proteins, A₁ and A₃ receptors mediate inhibition of adenylate cyclase (cAMP) whereas A_{2A} and A_{2B} receptors potentiate cAMP actions (Fredholm et al. 2001). In addition, all the adenosine receptor subtypes stimulate phospholipase C (PLC) activity (Akbar et al. 1994, Gao et al. 1999, Offermanns and Simon 1995, Palmer et al. 1995).

Distribution and physiological roles

Adenosine receptors are widely distributed in various cell types and mediate diverse physiological and pathological processes. For example, A₁

receptors were suggested to be important in pain stimulation and hypoxia conditions. The A₁ knockout mice were reported to be hyperalgesic and show decreased neuroprotection in hypoxia (Johansson et al. 2001). Studies in A_{2A} receptors (-/-) mice have shown that A_{2A} receptors play a role in mediating pain, inhibiting blood pressure, heart rate and platelet aggregation (Ledent et al. 1997). A₃ receptors were shown to be involved in pro- and anti-inflammatory responses (Salvatore et al. 2000).

Agonists and Antagonists

Some compounds targeting adenosine receptors have been investigated. For example, the A₁ partial agonist GW493838 shows analgesic effects in patients with postherpetic neuralgia or peripheral nerve injury (Fredholm et al. 2011). Caffeine, as an effective adenosine receptor antagonist, was shown to impair preconditioning in humans in vivo (Riksen et al. 2006) and have adverse effects on the fetal neural development in mice (Silva et al. 2013). In addition, caffeine was reported to improve anxiety and depression at low doses and to exacerbate anxiety at high doses in normal healthy patients but enhance anxiety-related symptoms in patients with panic disorders (Yamada et al. 2014). A series of selective A_{2A} antagonists were evaluated for the treatment of Parkinson's disease and for drug addiction, for example istradefylline has been studied in clinical trial phase III studies (Hauser et al. 2008).

1.2.2 P2Y receptors

P2YRs are G-protein-coupled receptors. At present, there are eight subtypes in the human P2YR family, P2Y₁, P2Y₂, P2Y₄, P2Y₆, P2Y₁₁, P2Y₁₂, P2Y₁₃ and P2Y₁₄. The first P2YRs (P2Y₁ and P2Y₂) were cloned in 1993 (Lustig et al. 1993, Webb et al. 1993). After that, P2Y₄, P2Y₆ and P2Y₁₁Rs were isolated by homology cloning and assigned a subscript on the basis of cloning chronology (Chang et al. 1995, Communi et al. 1997, Communi et al. 1995). The P2Y₁₂R was isolated from platelets by expression cloning in 2001 (Hollopeter et al. 2001). P2Y₁₃ and P2Y₁₄Rs were characterized later during a systematic study of orphan receptors (Chambers et al. 2000, Communi et al. 2001). The missing numbers represent either non-mammalian orthologs, or receptors having some

sequence homology to P2YRs, but for which there is no functional evidence of responsiveness to nucleotides.

P2YRs are activated by a range of purine and pyrimidine nucleotides, including ATP, ADP, UTP, UDP or UDP-glucose (Table 1.1). ATP is an agonist for P2Y2 and P2Y11Rs. ATP can work as a partial agonist for P2Y12 and P2Y13Rs. The human P2Y4R is antagonized by ATP but the rat P2Y4R can be activated by ATP.

Receptor	Agonists	G-protein coupling	References
P2Y1	ADP	Gq, G11	(Palmer et al. 1998, Waldo and Harden 2004)
P2Y2	UTP ≥ ATP	Gq	(Abbracchio et al. 2006, Lustig et al. 1993)
P2Y4	UTP(human) ATP=UTP (rat)	Gq	(Bogdanov et al. 1998, Nicholas et al. 1996)
P2Y6	UDP>UTP>>ATP	Gq	(Nicholas et al. 1996)
P2Y11	ATP	Gq, Gs	(Communi et al. 1997, Communi et al. 1999)
P2Y12	ADP>ATP	Gi	(Gachet 2006, Hollopeter et al. 2001)
P2Y13	ADP	Gi	(Marteau et al. 2003)
P2Y14	UDP-glucose	Gi/o	(Chambers et al. 2000)

Table 1.1 Pharmacological profiles of agonists and G-protein coupling for P2YRs

Second Messenger Systems

The eight mammalian P2YRs are divided into two subfamilies on the basis of signal transduction. The first subfamily includes P2Y1, P2Y2, P2Y4, P2Y6 and P2Y11Rs. This group couples to Gq protein to increase inositol triphosphate (IP₃) and cytosolic calcium therefore to stimulate PLC. The second subfamily, consisting of P2Y12, P2Y13 and P2Y14Rs, in contrast, couple to Gi protein to inhibit cAMP (von Kügelgen and Hoffmann 2016). In addition, P2Y11Rs can also couple to Gs proteins to increase cAMP activity (Communi et al. 1997, Communi et al. 1999). (Table 1.1).

Physiological roles

P2YRs are widely expressed and play important roles in physiology and pathophysiology (von Kügelgen and Hoffmann 2016). For example, it has been shown that P2Y1 and P2Y12Rs, together with P2X1Rs, are involved in ADP-induced platelet aggregation (Gachet 2006). In P2Y1R knockout (KO) mice, platelet aggregation in response to ADP (10 µM) was decreased to ~25% and no platelet shape change was reported. More P2Y1R KO mice survived (9 of 10) in thromboembolism models compared to wild type (1 of 10) (Fabre et al. 1999). Similarly, mice deficient in P2Y12R showed loss of platelet aggregation and shape change to ADP (<10 µM) and an increase in bleeding time (~4-fold). The time of thrombus formation and occlusion was also delayed (~2-fold) (Andre et al. 2003).

P2Y2Rs were suggested to be important for immune responses. P2Y2R deficient mice had a reduced pulmonary inflammation after smoke-induced lung injury (Cicko et al. 2010). P2Y4R(-/-) mice showed a loss of nucleotide-regulated chloride responses in intestinal epithelium (Robaye et al. 2003). P2Y6Rs were shown to mediate vasocontraction in human cerebral arteries (Malmsjö et al. 2003).

Agonists and Antagonists

A large number of potent and subtype-selective P2YR agonists have been identified. For example 2-methylthio-ADP (MRS2365) is a selective P2Y1R

agonist, with EC₅₀ of 0.4 nM (Chhatriwala et al. 2004). The UMP analogue PSB-1114 is a potent agonist with more than 50-fold selectivity for P2Y2R versus P2Y4 and P2Y6Rs (El-Tayeb et al. 2011). R (p) isomer of 5-OMe-UDP (α -B) is a selective P2Y6R agonist (EC₅₀ of 8 nM), being 19-fold more potent than UDP and showing no activity at P2Y2 and P2Y4Rs (Ginsburg-Shmuel et al. 2012). The analogue α , β -methylene-2-thio-UDP is a very potent selective P2Y14R agonist (EC₅₀ of 0.92 nM) (Das et al. 2010).

Suramin is a commonly used antagonist for P2YRs except P2Y4 and P2Y6Rs which are insensitive (Charlton et al. 1996b). PPADS is a potent antagonist at P2Y1Rs and inhibited maximal agonist responses of P2Y4, P2Y6 and P2Y13Rs with high concentrations (see detail in 1.7.3). There are also some subtype-selective P2YR antagonists identified and used for treatment (Jacobson and Boeynaems 2010). For example, several antithrombotic drugs targeting P2Y12R including the prodrugs clopidogrel (Savi et al. 2000) and prasugrel (Niitsu et al. 2005) which have been approved for the prevention of stroke and myocardial infarction (see more P2YR antagonists in review (von Kügelgen and Hoffmann 2016). Recently, the crystal structure of human P2Y12R in complex with a non-nucleotide reversible antagonist AZD1283 was published, which provided essential insights for the development of improved P2Y12R ligands and allosteric modulators as drug candidates (Zhang et al. 2014).

1.2.3 P2X receptors

Genes encoding seven mammalian P2XR subunits have been identified, from P2X1 to P2X7. The first P2XRs were cloned from the rat vas deferens and rat pheochromocytoma PC12 cells, termed P2X1R and P2X2Rs (Brake et al. 1994, Valera et al. 1994). Subsequently, five other subunits of receptors were cloned and named in the order they were discovered (Table 1.2). The P2X3R was first isolated from DRG neurons (Chen et al. 1995). The first P2X4R cDNAs were cloned from hippocampus, whole brain, and superior cervical ganglia cDNA libraries (Buell et al. 1996, Soto et al. 1996). The P2X5R was originally isolated from rat celiac cervical ganglia and shortly after also from a rat heart cDNA library (Collo et al. 1996, Garcia-Guzman et al. 1996). The P2X6R was first isolated from

the rat superior ganglion and a rat brain cDNA library (Collo 1996, Soto 1996). The P2X7R was first isolated from a rat brain cDNA library (Surprenant et al. 1996). The P2X subunit proteins are from 379 (P2X6) to 595 (P2X7) amino acids long (Table 1.2). The P2X1 to P2X7Rs show 40-50% amino acid identity. Three P2XR subunits assemble to form functional homo- or hetero-trimeric receptors.

Receptor	Length (amino acids)	First cloning
P2X1	399	rat vas deferens (Valera et al. 1994)
P2X2	472	rat pheochromocytoma PC12 cells (Brake et al. 1994)
P2X3	397	rat dorsal root ganglion (DGR) sensory neurons (Chen et al. 1995, Lewis et al. 1995)
P2X4	388	rat superior cervical ganglion cDNA library (Buell et al. 1996)
P2X5	417	rat celiac ganglia (Collo et al. 1996)
P2X6	379	rat superior cervical ganglion cDNA library (Collo et al. 1996)
P2X7	595	rat brain cDNA library (Surprenant et al. 1996)

Table 1.2 Length and first cloning of homo-trimeric P2XRs.

1.3. Properties of recombinant P2X receptors

Amino acid differences between subunits give rise to different pharmacological profiles for each receptor. Their properties were characterised by recombinant expression of homomeric P2XRs in *Xenopus* oocytes and HEK cells. The characteristic features include sensitivity to different agonists and antagonists and the time-course of the response to ATP.

1.3.1 Agonists

The native agonist for P2XRs is ATP. Agonist potency can be quantified as the concentration needed to give 50% of the maximum response (EC_{50}). The potency of the agonist varies between different P2X subtypes. The P2X1 and P2X3Rs show the highest ATP sensitivity, with EC_{50} value of $\sim 1 \mu\text{M}$ (Chen et al. 1995, Evans et al. 1995). The P2X2R was shown to have an EC_{50} value of $\sim 1\text{-}12 \mu\text{M}$ depending on the expression system (Eickhorst et al. 2002, Evans et al. 1995, Lynch et al. 1999). The EC_{50} value was $\sim 10 \mu\text{M}$ for P2X4, P2X5 and P2X6 (Buell et al. 1996, Collo et al. 1996) and $\sim 100 \mu\text{M}$ for P2X7Rs (Surprenant et al. 1996). Analogs of ATP (Figure 1.3) can also be agonists but vary in potency and efficiency (Table 1.3). These compounds were initially used as important tools for distinguishing different native P2X subtypes following cloning (Table 1.3).

α,β -Methylene-ATP (α,β -meATP): The bridging oxygen atom between the corresponding phosphates is replaced with the methylene group. It is metabolically more stable than ATP. It exhibits high potencies at P2X1Rs ($EC_{50} \sim 2 \mu\text{M}$) (Evans et al. 1995), P2X3Rs (Chen et al. 1995), and heteromeric assemblies, which contain P2X1 or P2X3 subunits. Heteromeric P2X4/6Rs also show α,β -meATP-sensitivity ($EC_{50} \leq 10 \mu\text{M}$). It is a partial agonist for P2X2Rs, P2X4Rs, P2X5Rs and P2X7Rs (Coddou et al. 2011).

Adenosine-5'-O-(3-thiotriphosphate) (ATP γ S): The oxygen atom at the terminal phosphate is replaced by a thio group. It is relatively resistant to breakdown by ectonucleotidases. It can work at all P2XRs.

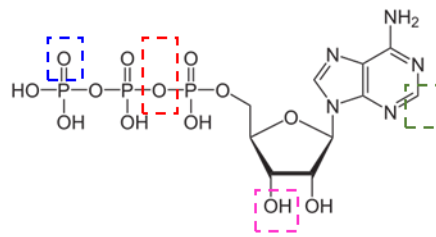
2-methylthio-ATP (2-meSATP): The 2' position at the adenine ring is substituted by the methylthio group. It is a common agonist for P2XRs and shows similar potency to ATP except at P2X7Rs.

2'(3')-O-(4-benzoylbenzoyl)-ATP (BzATP): A hydroxy group at the ribose is modified by a bulky benzoyl group. It is a partial agonist for P2X1Rs and P2X2Rs. It shows much higher potency than ATP at P2X7Rs.

Receptor	Full Agonists	Partial Agonists	ATP (EC ₅₀)	References
P2X1	2-MeSATP ≥ ATP > αβ-meATP	BzATP > ATPγS	~0.7 μM	(Evans et al. 1995, Valera et al. 1994)
P2X2	2MeSATP > ATP	BzATP ≥ ATPγS > αβ-meATP	~8 μM for rP2X2Rs; ~12 μM for mP2X2Rs; ~1 μM hP2X2Rs	(Evans et al. 1995, Lynch et al. 1999) (Eickhorst et al. 2002)
P2X3	2MeSATP > α,β-meATP ≥ ATP	ATPγS	~1.2 μM	(Chen et al. 1995)
P2X4	ATP ≥ 2MeSATP > ATPγS	αβ-meATP	~10 μM	(Buell et al. 1996, Jones et al. 2000)
P2X5	2-MeSATP ≥ ATP	α,β-meATP	~15 μM	(Collo et al. 1996, Wildman et al. 2002)
P2X6	2-MeSATP ≥ ATP	ATPγS	~12 μM	(Collo et al. 1996)
P2X7	BzATP >> ATP (EC ₅₀ ~7 μM)	2-MeSATP > ATPγS > α,β-meATP	~120 μM	(Surprenant et al. 1996)

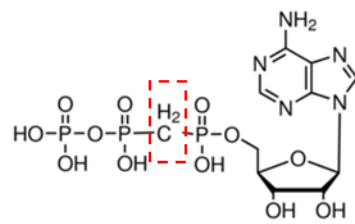
Table 1.3 Pharmacological profile of P2XR subtypes. Agonist EC₅₀ values, including ATP EC₅₀ values at the homo-trimeric P2XRs are given (see review by (Coddou et al. 2011)).

(a)



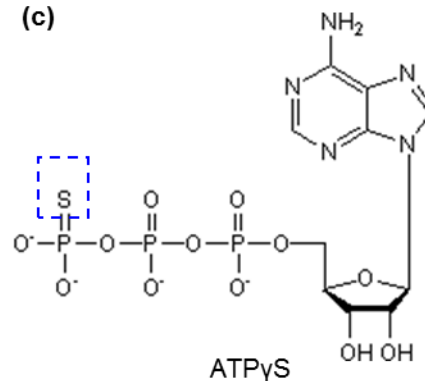
ATP

(b)



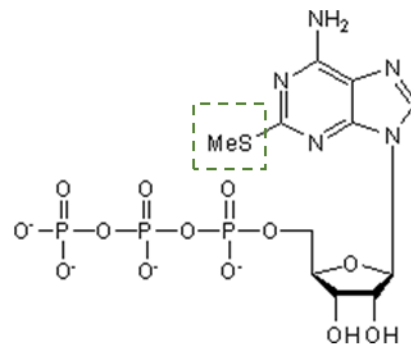
α,β -Methylene-ATP

(c)



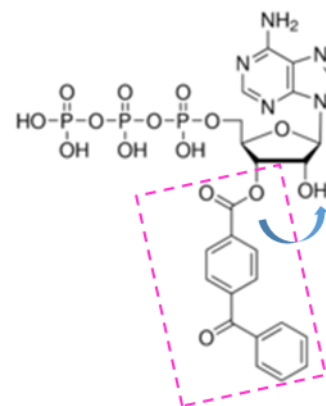
ATP γ S

(d)



2-meSATP

(e)



BzATP

Figure 1.3 Structures of ATP analogs.

(a) ATP (b) α,β -meATP (c) ATP γ S (d) 2-meSATP (e) BzATP (mixture of 2'-O-(4-benzoylbenzoyl)-ATP and 3'-O-(4-benzoylbenzoyl)-ATP) The red box indicates the oxygen atom between corresponding phosphates. The blue box indicates the oxygen atom at the terminal phosphates. The green box indicates the 2' position at the adenine ring. The pink box indicates the hydroxy at the ribose.

1.3.2 Time-course of the ATP evoked current at P2XRs

The P2XR is activated by the binding of extracellular ATP. One of the characteristics of the currents produced from each P2XR subtype is the time-course of the evoked response. Decline in the current evoked by ATP during continuous ATP application was referred to as desensitization. The time-course of P2XR currents in response to continuous ATP application varies between different subtypes. For some P2XRs, the decline occurs in ~100 milliseconds for example P2X1 and P2X3Rs whereas it occurs much more slowly for others for example P2X2 and P2X5Rs (Figure 1.4).

For P2X1Rs, the inward current evoked by high concentrations ($>10 \mu\text{M}$) of agonists has a fast rise time (10-90%, ~7 ms at $10 \mu\text{M}$ in HEK293 cells), followed by a desensitization during the sustained agonist application. The desensitization rates were agonist concentration dependent. Currents were sustained with low agonist concentration (10-30 nM) but desensitized rapidly ($<1\text{s}$) with high concentrations of ATP ($\geq 1 \mu\text{M}$) (Valera et al. 1994). Similarly, the response evoked by high concentrations of ATP ($\geq 3 \mu\text{M}$) at P2X3Rs had a fast rise time and rapid desensitisation (Chen et al. 1995). In contrast, P2X2 and P2X5 channels show relatively slow or non-desensitising currents (Brake et al. 1994, Collo et al. 1996, Surprenant et al. 1996). The P2X4R has an intermediate time-course of desensitisation between these fast desensitising and non-desensitising receptor subtypes (Buell et al. 1996, Garcia-Guzman et al. 1997). ATP evoked currents at P2X6Rs resembled that for the P2X2R, with quick rise time (15 ms) and little desensitization (during 2s) (Collo et al. 1996).

The P2X7R is the longest receptor in P2XR family, with an extended intracellular C terminal domain (Surprenant et al. 1996). The channels are permeable to both small cations and large organic cations. It has been shown that large molecules including the dye YO-PRO-1 (629 daltons) entered HEK293 cells expressing P2X7Rs during prolonged incubation with BzATP (Surprenant et al. 1996). It suggested that the bifunctional permeation properties of the P2X7R reflects a dilation of the pore of the channel. However, this time-dependent pore dilation mechanism is controversial. Recent studies provided evidence that ATP

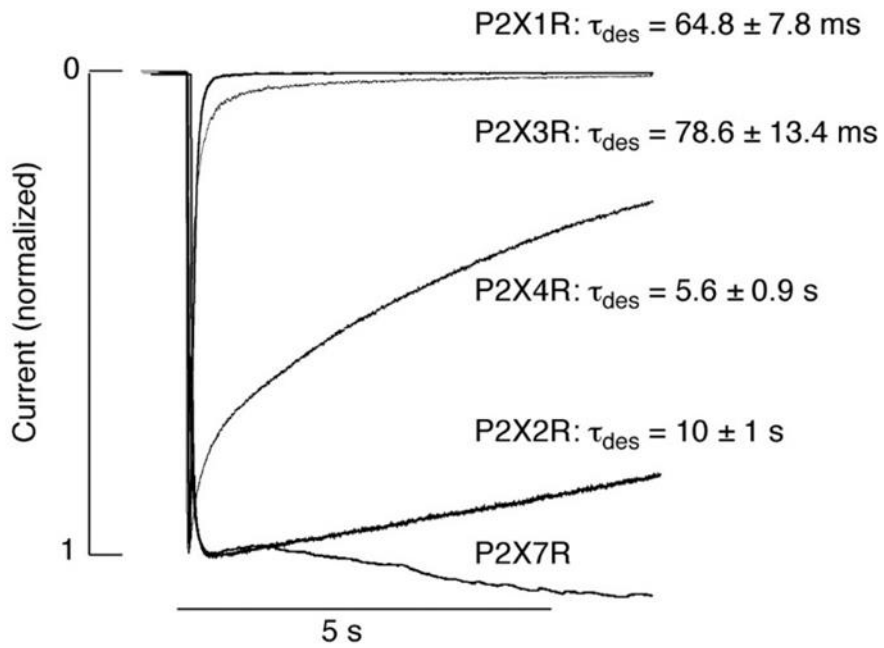


Figure 1.4 Time-course of the ATP evoked current at P2XRs

Profiles of P2XR currents induced by sustained agonist application. Recombinant rat receptors were expressed in HEK293 cells and stimulated with ATP (10 μ M for P2X1R and P2X3R, 100 μ M for P2X2R and P2X4R, and 3 mM for P2X7R). τ_{des} indicates the desensitization time constant derived from monoexponential fitting (mean \pm S.E.M.; values from at least five records per channel) (Image taken from Coddou et al. 2011).

binding opens a large cation permeable channel within milliseconds and that the time-course of the permeability superimposed that of Na⁺. It demonstrated that the molecular motions leading to the permeation of large cations are very similar to those that drive Na⁺ flow. It suggested that the open pore of P2X7R is wide enough to allow the permeation of large cations (Harkat et al. 2017). The pdP2X7R with a truncated C-terminus exhibited no obvious current facilitation (run-up) after repeated ATP applications compared to the hP2X7R and still can mediate YO-PRO-1 uptake (Karasawa and Kawate 2016). This suggests the C terminus of P2X7R may not account for the permeation of large cations.

1.3.3 Properties of hetero-trimeric receptors

Co-expression of two different subunits of P2XR can lead to the formation of functional ion channels distinct from either of the contributing subunits, which suggested the formation of functional hetero-trimeric channels. This was first suggested for sensory neurons that co-expressing P2X2 and P2X3Rs showing different properties from either of P2X2R or P2X3R (Lewis et al. 1995). An extensive study looking at the co-immunoprecipitation of epitope-tagged P2XR subunits provided the benchmark of possible subunit combinations (Torres et al. 1999). The combination of different subunits can potentially give rise to channels with different pharmacological properties compared to the homo-trimeric channels. Hetero-trimeric channels generally have composite properties of the two receptor subunits. The receptor with the slower time-course is dominant in kinetics. The hetero-trimer adopts the agonist sensitivity of the subunit with the highest potency. For example, P2X2/3 heteromer has the time-course of the P2X2 receptor but the P2X3 subunit confers to the channel its agonist sensitivity (Spelta et al. 2002). However, the P2X1/2 heteromer is an exception to this rule, with the fast desensitisation of the hP2X1R (Brown et al. 2002). The properties of known P2X hetero-trimers are discussed below.

Co-expression studies indicated the formation of a heteromeric channel but gave no indication of the subunit stoichiometry. In a stoichiometry study using disulphide bond formation between engineered cysteines, a trimeric P2X2/3R was suggested to form with one P2X2 subunit and two P2X3 subunits (Jiang et

al. 2003). So far, heteromerisation has only been described when two different subunits associate and it remains to be seen whether three different subunits can form a functional channel (Roberts et al. 2006)

P2X1/2 The co-expression of P2X1 and P2X2Rs in oocytes exhibited a pH-sensitivity different from that of both P2X1 and P2X2Rs (Brown et al. 2002), suggesting the formation of heteromeric receptors. Subsequent studies found the hetero-trimeric P2X1/2 receptors expressed at the plasma membrane (Aschrafi et al. 2004).

P2X1/4 The functional P2X1/4R was investigated by co-injection of mRNA in oocytes. The pharmacological profile was similar to homomeric P2X1Rs, with high sensitivity to ATP and α,β -meATP. The kinetic properties resembled homomeric P2X4Rs, with slow desensitization. The agonist-induced current at the end of a 5s application was 65%, 55% and 18% for P2X1/4 (at 10 μ M α,β -meATP), P2X4 (at 10 μ M ATP) and P2X1Rs (at 10 μ M α,β -meATP) (Nicke et al. 2005).

P2X1/5 P2X1 and P2X5 subunits were shown to form a functional heteromeric receptor in cells that co-expressed both subunits (Haines et al. 1999, Lê et al. 1999, Gonzalo E. Torres et al. 1998). Like the P2X1R, the hetero-trimer was sensitive to α,β -meATP with the EC₅₀ value of 5 μ M. The kinetic properties resembled the P2X5R, with a rapid rise to peak and then decayed to a pronounced non-desensitizing plateau in current. The rank order of agonist potency was ATP \geq 2MeSATP > ATP γ S > α,β -meATP. Only ATP and 2MeSATP were full agonists (Haines et al. 1999). The native channel in guinea pig submucosal arterioles is pharmacologically similar to the recombinant P2X1/5R, suggesting its role in autonomic neuroeffector junctions (Surprenant et al. 2000). It was also found expressed and functional in mouse cortical astrocytes (Lalo et al. 2008).

P2X2/3 For the hetero-trimeric P2X2/3 receptors, α,β -meATP-induced (30 μ M) currents activated more slowly and desensitized negligibly (>2s) compared to P2X3Rs (Lewis et al. 1995). The P2X2 subunit is dominant with respect to rise time and desensitization but the P2X3 subunit confers to the channel its agonist

sensitivity. It has been shown that the composition of the hetero-trimeric receptor would be two P2X3 subunits and one P2X2 subunit (Jiang et al. 2003).

P2X2/6 Studies on co-expression of rat P2X2 and P2X6Rs in oocytes have confirmed that they could form functional heteromers. The receptor showed a significantly different phenotype from the rat P2X2R including agonist potency and pH regulation. The sensitivity to ATP was reduced ~2-fold (EC_{50} ~30 μ M) compared to the rP2X2R (EC_{50} ~15 μ M). The ATP response at rP2X2Rs increased over the range of pH 8.0 to 6.3 and was maintained at lower pH whereas that at rP2X2/6Rs initially increased (pH 8.0-6.3) and then decreased in amplitude as pH levels were lowered further (King et al. 2000). The stoichiometry studies showed the composition of P2X2/6R heteromers were dependent on relative subunit expression levels. It was demonstrated that when expression of the P2X2 subunit predominated, the receptors contain primarily two P2X2 subunits and one P2X6 subunit. In contrast, when the P2X6 subunit predominated, the subunits stoichiometry of the receptor was two P2X6 subunits and one P2X2 subunit (Barrera et al. 2007).

P2X4/6 P2X4 and P2X6 subunits have been shown to co-assemble into a heteromeric receptor. The sensitivity to ATP (EC_{50} ~6 μ M) was similar to the homomeric P2X4R (EC_{50} ~4 μ M). The potency of 2MeSATP (EC_{50} ~7 μ M) and α,β -meATP (EC_{50} ~12 μ M) increased about 4 fold compared to the P2X4R. The kinetic profile of the current evoked by 100 μ M ATP was similar to that in oocytes expressing P2X4Rs (Lê et al. 1998).

1.4 Physiological and pathological roles of P2X receptors

P2XRs are distributed in many tissues throughout the body of mammals. In early studies, their expression patterns were evaluated at the mRNA level by using Northern blot, RT-PCR and in situ hybridization analysis. Following the development of P2XR subtype specific antibodies, their distribution was verified at the protein level by Western Blot and immunohistochemistry. In addition, potent and selective antagonists for some P2XR subtypes have been used to identify their existence and functions in native tissues. Each receptor of the P2XR family has a different expression pattern in native tissues.

P2XRs are a class of non-selective cation ion channels. Activation of the receptors by ATP binding allows Na^+ and Ca^{2+} to enter and K^+ to leave the cell. The process results in membrane depolarization and cell excitation. In addition, calcium entry and its impact on calcium sensitive signalling processes such as muscle contraction or exocytosis can also occur. It has been suggested that the P2XR family mediates a wide range of physiological and pathophysiological processes, ranging from synaptic transmission, smooth muscle contraction to pain sensation and inflammation. Many of their functions have been identified and verified by the generation of knockout (KO) and transgenic animals (Kaczmarek-Hajek et al. 2012).

1.4.1 P2X1 receptors

P2X1Rs are highly expressed on smooth muscle cells of various organs, including the vas deferens (Mulryan et al. 2000, Valera et al. 1994), urinary bladder (Valera et al. 1995, Vial and Evans 2000) and arteries (Chan et al. 1998). P2X1Rs were also found on blood cells, including platelets and their progenitor megakaryocytes (Sun et al. 1998, Vial et al. 1997). In addition, studies have shown functional P2X1Rs expressed in immune cells, for example in human lung mast cells (Wareham et al. 2009) and mouse macrophages (Sim et al. 2007). The widespread expression of P2X1Rs indicated their roles in a variety of physiological processes.

Vas deferens – Fertility

P2X1Rs have been found to be highly expressed in vas deferens (Valera et al. 1994). The activation of the receptor in response to sympathetic nerve stimulation was responsible for ~60% of smooth muscle contraction of the vas deferens. The residual contraction was mediated through α_1 adrenoceptors activated by noradrenaline which was co-released with ATP from sympathetic nerves (Burnstock and Verkhatsky 2010, Mulryan et al. 2000). Studies have shown that the fecundity of the P2X1R knockout male mice was reduced by ~90% compared to WT mice (Mulryan et al. 2000). The P2X1R deficient (-/-) mice copulated normally. The spermatogenesis and sperm quality of the -/- mice was similar to that of the WT mice, but the sperm was absent from the ejaculate due

to the lack of P2X1R-mediated contractions in vas deferens smooth cells (Mulryan et al. 2000). Subsequent studies showed knocking out both P2X1Rs and α_{1A} -adrenoceptors in male mice caused 100% infertility without effects on sexual behaviour or function (White et al. 2013). This indicated that a potent P2X1R selective antagonist combined with an α_1 -adrenoceptors antagonist may provide a target for the development of a non-hormonal male contraceptive pill.

Urinary Bladder – Bladder Dysfunction

ATP was shown to be released together with ACh from parasympathetic nerves. P2XRs were shown to contribute to neurogenic smooth muscle contractions of the urinary bladder (Kasakov and Burnstock 1982). *In vitro* and *in vivo* studies on animals showed that ATP acting through P2X1Rs contributed ~50% to the contraction of the bladder whereas the remaining 50% was mediated by muscarinic receptors (Brading and Williams 1990, Hegde et al. 1998). P2X1Rs have been shown in the smooth muscle membranes of the bladder and associated arteries. ATP-mediated bladder responses were absent in P2X1R deficient mice, suggesting that the P2X1R is essential for the expression of functional P2XRs in the smooth muscle of the bladder (Vial and Evans 2000). The contribution of P2X1Rs to neurogenic contractions of the bladder is significantly different in human (Sibley 1984). In the healthy human bladder, the purinergic component is ~2% but it increased to ~40% in pathological conditions, such as outflow obstruction, interstitial cystitis and hypoxia-glucopenia (Elliott et al. 2013, Palea et al. 1993). This suggested that P2X1Rs could play a role in the treatment of bladder disorders.

Renal Arteries – Autoregulation of Renal Blood Flow

Autoregulation of renal blood flow involves myogenic and tubuloglomerular feedback (TGF). Studies have shown that P2X1Rs are widely expressed in smooth muscle cells of afferent arteries in rat kidney (Chan et al. 1998) and play an essential role in TGF-mediated afferent arteriolar vasoconstriction. In P2X1R knockout mice, arteriolar autoregulatory responses were markedly attenuated (Inscho et al. 2003). Accordingly, the regulatory pathway suggested that ATP released from the macula densa in response to changes in tubular fluid osmolarity

activated TGF responses via P2X1Rs to maintain stable renal blood flow and glomerular filtration rate. The importance of P2X1Rs in renal autoregulation was also confirmed *in vivo* by showing that whole kidney autoregulation of renal blood flow in rats was inhibited by P2X1R blockade, PPADS or IP5I (Inscho 2010).

Platelets – Thrombosis

The role of P2X1Rs in platelets has been investigated in P2X1R- deficient mice. *In vitro* studies showed that platelet aggregation in KO mice was reduced in response to a low collagen concentration ($\leq 1.5 \mu\text{g/ml}$). Platelet thrombus formation on a collagen-coated surface was significantly decreased in the P2X1R^{-/-} blood at high shear rate (6000 s^{-1}). The mortality in an *in vivo* model of systemic thromboembolism was reduced and the size of mural thrombi formed after a laser-induced vessel wall injury was decreased in P2X1^{-/-} mice. The bleeding time was normal in most of the P2X1R^{-/-} mice (Hechler et al. 2003). Subsequent studies showed that intravenous injection of a selective P2X1R antagonist NF449 (10 mg/kg) into mice reduced by ~15% intravascular platelet aggregation in a model of systemic thromboembolism but without prolongation of the bleeding time, confirming a role of this receptor in platelet activation induced by collagen (Hechler et al. 2005). Studies about the functions of P2X1Rs in platelets indicated they can be considered as a potential antithrombotic target. It should be noted that there may be some potential side-effects of a P2X1R antagonist, including reduced fecundity and autoregulation of renal blood flow.

1.4.2 P2X2-P2X7 receptors

P2X2Rs

P2X2Rs have been found to be expressed abundantly in both the central and peripheral nervous systems (Nörenberg and Illes 2000). In the central nervous system, high level expression of P2X2Rs was found in olfactory bulb, cerebral cortex, mesencephalon, cerebellum and the dorsal horn area of the spinal cord (Kanjhan et al. 1999, Kidd et al. 1995). In the peripheral nervous system, significant P2X2Rs expression has been described in both sensory and autonomic ganglion neurons (Xiang et al. 1998). P2X2Rs were also found in non-

neuronal tissues, for example in interstitial cells of the vas deferens (Burton et al.) and skeletal muscle (Ryten et al. 2001).

The widespread expression suggests a variety of roles of P2X2Rs in the central nervous system. P2X2Rs have been found to play a role in fast synaptic transmission regulating processes such as learning, memory and sensory integration (Gever et al. 2006). P2X2Rs, together with P2X3Rs, were suggested to contribute to taste responses in the taste nerves (Finger et al. 2005). Taste behaviour and gustatory neural responses were largely abolished in mice lacking P2X2 and P2X3Rs (Huang et al. 2011). P2X2Rs have been shown to be related with age-related hearing loss. P2X2R-null mice developed severe progressive hearing loss and their early exposure to continuous moderated noise led to high-frequency hearing loss in young adulthood (Yan et al. 2013).

P2X2R knockout mice revealed impaired peristalsis in the small intestine, which may result from the absence of P2X2R-mediated synaptic transmission in the myenteric plexus (Ren et al. 2003). The P2X2R^{-/-} mice also showed reduced responses of the carotid sinus nerve to hypoxia and markedly attenuated ventilatory responses to hypoxia (Rong et al. 2003). It indicated the important role of P2X2Rs in normal carotid body function and in ventilator response to hypoxia. In addition, P2X2R knockout mice have demonstrated a role for P2X2R-dependent signalling in the development and maintenance of skeletal neuromuscular junctions (Ryten et al. 2007).

P2X3Rs and P2X2/3Rs

P2X3R expression has been demonstrated mostly on sensory neurons within the DRG as well as nodose and trigeminal ganglia (Vulchanova et al. 1997, Xiang et al. 1998). This pattern of P2X3 subunit distribution has been associated with P2X3R-mediated nociceptive sensory nerve responses to ATP released from inflamed or damaged tissues (North 2004). P2X3Rs have also been reported in intestine (myenteric plexus neurons), urinary bladder (urothelium and suburothelium) and dental pulp (Alavi et al. 2001, Elneil et al. 2001, Tempest et al. 2004).

The important role of the P2X3R in nociceptive signalling was confirmed by P2X3R knockout mice. The P2X3R deficient mice showed reduced pain-related behaviour (Cockayne et al. 2000). In line with an important function in sensory systems, P2X3R-null mice had enhanced thermal hyperalgesia in chronic inflammation and were unable to code the intensity of non-noxious 'warming' stimuli (Souslova et al. 2000). P2X3Rs were also shown to be expressed in the afferent fibres that evoke cough (Weigand et al. 2012). P2X3Rs activation could enhance responsiveness to a range of stimuli, either through the sensory afferent nerve terminals in airways or modulation of activity at the central synapses (Prado et al. 2013, Vulchanova et al. 1997). AF-219, as an oral P2X3R antagonist, has been tested to reduce cough frequency in patients with refractory chronic cough. In the observed case analysis (24 patients), cough frequency was reduced by 75% when patients were allocated to AF-219 compared to when allocated to placebo. It was reported that daytime cough frequency fell from a mean ~37 coughs per hour to ~11 coughs per hour after AF-219 treatment versus ~65 coughs per hour to ~44 coughs per hour after placebo. Six patients withdrew before the end of the study because of taste disturbances, which were reported by all patients taking AF-219 (Abdulqawi et al. 2015). This suggested that antagonists of P2X3Rs are promising new group of antitussives but the serious side effects should also be considered.

In addition, hetero-trimeric P2X2/3Rs were shown to contribute to nociceptive responses and mechanosensory transduction within the urinary bladder (Cockayne et al. 2005). In mice lacking both P2X2 and P2X3 subunits, all ATP currents were lost in DRG and nodose ganglion neurons. The KO mice showed significantly attenuated nociceptive behavioural responses (~30%) and urinary bladder hyporeflexia (Cockayne et al. 2005).

P2X4Rs

Extensive and abundant P2X4R expression has been demonstrated in several regions of central and peripheral nervous systems as well as vital and reproductive organs, skeletal and smooth muscle, epithelial and endothelial cells (Xuenong Bo et al. 2003).

Studies have shown that P2X4Rs are involved in the pathogenesis of chronic neuropathic and inflammatory pain. P2X4R expression significantly increased in the ipsilateral spinal cord after nerve injury. Activation of P2X4Rs in hyperactive microglia is necessary for tactile allodynia after nerve injury (Tsuda 2003). In agreement with this finding, P2X4R^{-/-} mice showed attenuations of pain hypersensitivity to innocuous mechanical stimuli (tactile allodynia) (Tsuda et al. 2009) and a significant reduction in peripheral inflammation-induced pain (Ulmann et al. 2010).

P2X4Rs were also found to be expressed in cardiomyocytes and their activation enhanced cardiac contractility (Mei and Liang 2001). The P2X4R transgenic mice exhibited significantly increased basal cardiac contractility with greater rates of contraction and relaxation, left ventricular developed pressure, and cardiac output (HU et al. 2001). It indicated that P2X4Rs has a role in stimulating cardiac contractility. In heart failure models, transgenic overexpression of P2X4R showed an enhanced cardiac contractile performance after infarction and increased survival. It indicated the P2X4R is a novel target to treat post-myocardial infarction ischemic heart failure (Sonin et al. 2008).

P2X4Rs were demonstrated to be involved in the shear stress-mediated Ca²⁺ influx in human vascular endothelial cells (Yamamoto et al. 2000a, Yamamoto et al. 2000b). P2X4R knockout mice showed abnormal endothelial cell responses to flow, such as influx of Ca²⁺ and production of the potent vasodilator nitric oxide (NO). Moreover, P2X4 KO mice showed no adaptive vascular remodelling, with no decrease in vessel size in response to a chronic decrease in blood flow. Thus, P2X4Rs were suggested to be crucial to flow-sensitive mechanisms that regulate blood pressure and vascular remodelling (Yamamoto et al. 2005). The mutation T315C in P2X4Rs was found to lead to loss of P2X4R function through disruption of the agonist binding site. Humans with this P2X4R mutation showed increased pulse pressure, suggesting reduced large arterial compliance as a result of impaired endothelium-dependent vasodilation in large arteries (Stokes et al. 2011).

P2X5Rs and P2X1/5Rs

P2X5Rs were found in the adrenal gland, kidney, cardiac and skeletal muscle, testis and the central and enteric nervous system (Kaczmarek-Hajek et al. 2012). It has been reported that more than 90% of humans express a splice variant of the P2X5R (P2X5a). The P2X5a encodes a truncated, non-functional P2X5R protein lacking a portion of both the ATP binding site and TM2. This suggested that P2X5Rs do not fulfil an essential physiological function in humans (Kotnis et al. 2010). However, P2X5Rs have been shown to form hetero-trimer with P2X1Rs expressed in cortical astrocytes (Palygin et al. 2010, R. et al. 2010). Activation of the receptors expressed in neuronal afferents in cortical slices triggered astroglial Ca²⁺ signals and the responses were blocked by NF449 (P2X1R selective antagonist). It suggested that P2X1/5Rs may contribute to a specific mechanism for fast neuronal-glia signalling at the synaptic level (Palygin et al. 2010).

P2X6Rs

It is well established that the P2X6 subunit is unable to homo-oligomerize effectively, and the frequent co-localization of P2X6 with P2X4 or P2X2 subunits suggests the formation of heteromeric P2X2/6 and P2X4/6 channels (Barrera et al. 2005). Studies suggested that partial glycosylation was necessary for cell expression and that further glycosylation would yields a functional channel (Jones et al. 2004). Further studies showed an uncharged region at the N terminus of P2X6 inhibited the assembly and export of the receptor from the endoplasmic reticulum to the cell membrane (Ormond et al. 2006).

P2X7Rs

The P2X7R is mainly expressed on cells of hematopoietic origin, including monocytes, macrophages, lymphocytes, dendritic cells and mast cells (Berchtold et al. 1999, Zhang et al.). They are also found on different types of glial cells in the central (microglia, astrocytes, oligodendrocytes, ependymal cell) (Franke et al. 2001, Yu et al. 2008) and peripheral (satellite cells, enteric glial cells) (Chen et al. 2008, Vanderwinden et al. 2003) nervous systems. In addition, they are

widely distributed on various epithelial (Li et al. 2003) and endothelial cells (Ray et al.).

The P2X7R has been shown to play an important role in cytokine production and inflammation. P2X7R^{-/-} mice showed decreased leukocyte function and had less susceptibility to arthritis compared to wild-type mice (Labasi et al. 2002). Moreover, it was demonstrated that the absence of the P2X7R led to an inability of LPS-activated peritoneal macrophages to release IL-1 in response to ATP and initiation of a cytokine cascade (Solle et al. 2001). The similar contribution of P2X7Rs on secretion of IL-1 β was also found in the dorsal horn, which is associated with nociceptive behaviour and microglial activation (Clark et al. 2010).

P2X7Rs were also shown to be involved in bone development and remodelling. The KO mice displayed deficient periosteal bone formation as well as excessive trabecular bone resorption. Thus, the P2X7R represents a novel therapeutic target for the management of skeletal disorders such as osteoporosis (Ke et al. 2003).

P2X7Rs are involved in regulation of cell survival and this has been of interest in the cancer field. Human pancreatic stellate cancer cells were found to highly express P2X7Rs and cell proliferation was reduced by the treatment of an allosteric P2X7R antagonist AZ10606120 (Giannuzzo et al. 2016). P2X7Rs were also found to be up-regulated in breast cancer cell lines and tissues. It was demonstrated that knockdown of P2X7R promoted apoptosis in breast cancer cells through down-regulating Bcl-2 and increasing the cleavage caspase-3 protein level (Zheng et al. 2014).

The gene encoding human P2X7R is located on a locus known to confer the susceptibility to mood disorders (Shink et al. 2005). The P2X7R gene contains a large number of single nucleotide polymorphisms. The polymorphic variant P2X7R with Q460R was reported to be associated with mood disorders. It was shown that heterozygous mice co-expressing the variant and WT P2X7Rs have sleep disturbances and human participants with the heterozygote genotype also

had subtle alterations in their sleep quality, which may increase the risk for developing mood disorders (Metzger et al. 2017, Wei et al. 2018).

A variety of P2X7R antagonist have been in clinical trials but with little success. For example AZD9056 (Keystone et al. 2012) and CE-224535 (Duplantier et al. 2011) have been put into a clinical trial for the treatment of rheumatoid arthritis but did not show any beneficial effect in patients. These results show that although P2X7R antagonists have strong therapeutic potential in rodent experiments, an efficient drug for treating humans has yet to be found. This may be due to the differences in the properties of rodent and human P2X7Rs.

1.5 Structure of P2X receptors

P2XRs comprise a distinct class of ligand gated ion channels, without sharing sequence homology with any other known ion channels. Initially, the structure of the P2XR was determined by biochemical and molecular studies. Subsequently, the crystal structures of P2XRs were obtained, providing a major advance of understanding the receptor.

1.5.1 Pre-crystal insights into structure

Membrane topology

Following the cloning and sequence identification, two hydrophobic regions were identified in each subunit that were sufficiently long to cross the membrane. It was proposed that each subunit consisted of two transmembrane domains. The N terminal lacked a leader signal peptide, suggesting the termini were intracellular (Brake et al. 1994, Valera et al. 1994). The P2XR mass was greater than the predicted mass, suggesting the possibility of glycosylation of the extracellular portion of the receptor (Brake et al. 1994, Valera et al. 1994). The consensus site for glycosylation is known to be an asparagine (N)-any amino acid (X)-serine or threonine (S/T). In the predicted extracellular domain of the P2X2R, there were 3 possible N-linked glycosylation sited in the sequence (Brake, 1994). Subsequent studies also suggested N-linked glycosylation was in the extracellular part of the receptor and important for the channel expression (G. E. Torres et al. 1998). Therefore, the P2XR was predicted to have a topology of two

transmembrane domains, with intracellular N- and C-termini and a large extracellular loop (Figure 1.5). This structure is distinct from existing cys-loop receptors, glutamate and GABA receptors (Ortells and Lunt 1995). This topology is similar to that of the acid-sensing ion channel (ASICs) family (Jasti et al. 2007) but they do not share amino acid sequence homology.

Trimeric assembly of P2X receptors

Co-expression of two distinct P2X subunits (P2X2 and P2X3) were reported to form a novel phenotype with different properties from either of the two subunits. This indicated that at least two subunits assemble to form a receptor (Lewis et al. 1995). To investigate the quaternary structure of the P2XR, a study used chemical cross-linking and blue native polyacrylamide gel electrophoresis (BN-PAGE) (Nicke et al. 1998). The P2X1 and P2X3 subunits were cross-linked by chemical compounds quantitatively to homo-trimers and migrated as non-covalently linked homo-trimers on the gel (Nicke et al. 1998), suggesting P2XRs form as a stable trimer. Cross-linking of P2X2 subunits was also shown to produce high order complexes, consistent with the presence of trimers (Barrera et al. 2005).

Subsequently, the stoichiometry of the P2XR has been supported by direct imaging from atomic force microscopy (AFM) (Barrera et al. 2005), fluorescence resonance energy transfer (FRET) and electron microscopy (EM) methods (Mio et al. 2005, Young et al. 2008). The measurement of the molecular volume of the receptor and the determination of the geometry of the receptors complexed with antibodies by AFM suggested that the P2X2R is a trimer whereas the P2X6R subunits were unable to form stable trimers (Barrera et al. 2005). The first visual evidence on the structure of P2XRs came from EM experiments. The image by EM demonstrated the P2X2R as an inverted three-sided pyramid with a crown-capped extracellular domain (Mio et al. 2005). Another EM study on the hP2X4R showed that the receptor was a globular torpedo-like molecule with a compact propeller-shaped ectodomain (Young et al. 2008). FRET results indicated that the distance between the C-terminal tails of the P2X4R was 5.6 nm, and labelling of

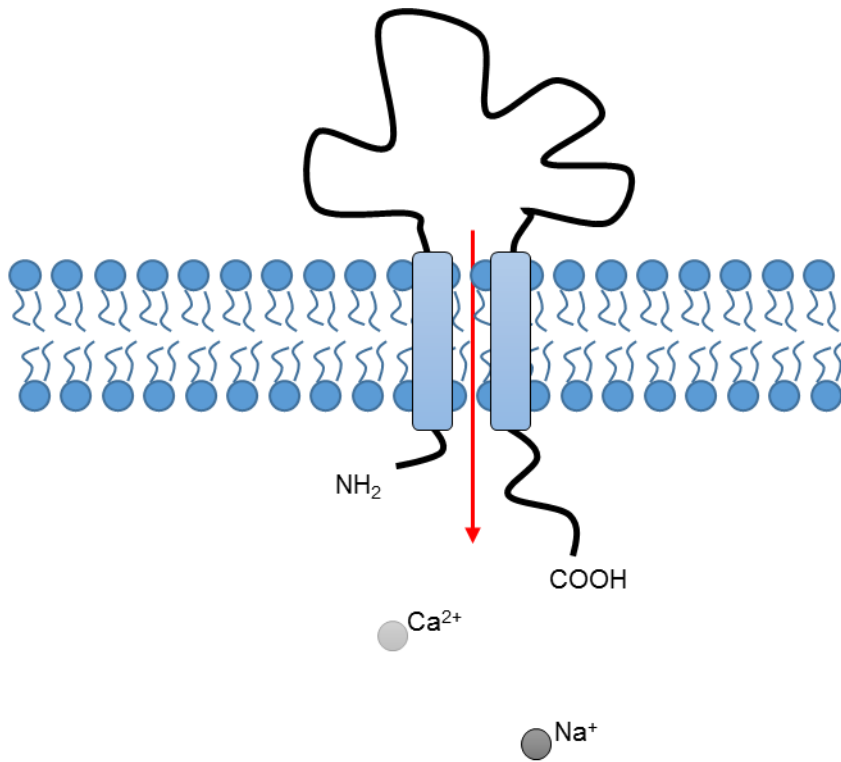


Figure 1.5 Structure of the P2XR Subunit. Basic cartoon representation of an individual subunit, with the intracellular N and C termini, two transmembrane domains and a large extracellular loop.

these termini with gold particles predicted that the distance between them was 6.1 nm (Young et al. 2008), suggesting the accuracy of this technique. The data furthered the understanding of the P2XR.

Before the crystal structure was available, mutagenesis and biochemical experiments contributed to understanding the structure of P2XRs. The studies showed that the extracellular loop harbours the binding sites for agonists (ATP and its analogues), antagonists and modulatory metal ions (Ennion et al. 2000). The TM2 domain lines a non-selective cation ion channel (Browne et al. 2010). The intracellular portions have been shown to play various roles, including the control of receptor time-course, signal transduction and their trafficking (Ennion and Evans 2002c). These predictions were confirmed following the crystallization of the receptor, which are described below.

1.5.2 The crystal structure of the P2X receptor

The first crystal structure of the P2XR was produced in 2009 (Kawate et al. 2009). Fluorescence-detection size exclusion chromatography (FSEC) was used for pre-scanning of construct prior to crystallization. After testing a range of P2X orthologs expressed in HEK293 cells, the zebrafish P2X4R (zfP2X4R) emerged as the most promising P2XR for crystallization, with a sharp and symmetrical elution profile in FSEC. Modifications are often necessary to improve stability of crystallization of ion channels. For the zfP2X4R, it was necessary to make a series of amino acid deletions and point mutations. The zfP2X4R was truncated, with 27 amino acids removed from the N terminus and 8 amino acids from the C terminus. Furthermore, three point mutations (C51F, N78K and N187R) were made (Δ zfP2X4-B) to avoid non-native disulphide bond formation and to reduce heterogeneity resulting from glycosylation. Electrophysiological experiments showed the receptor was still functional, activating by 1 mM ATP but with smaller peak current amplitude compared to full-length receptor (Kawate et al. 2009).

Overall structure

Crystallisation showed the 3D structure of the receptor. The homotrimeric Δ zfP2X4-B has a chalice-like shape, with a large hydrophilic and glycosylated extracellular domain, two transmembrane (TM) domains consisting of 6 α -helices and short intracellular amino and carboxy termini. Each individual subunit was described with reference to a dolphin, with the extracellular domain forming the upper body, and the transmembrane domains forming the fluke (Kawate et al. 2009). The upper body could be further split into the head, body, right flipper, left flipper and dorsal fin sections (Figure 1.6a, b).

Three subunits form one functional receptor, which confirmed biochemical studies indicating P2XR subunit forms as a trimer. The large extracellular domain protruded ~ 70 Å above the membrane. The interfaces between subunits form mainly in the extracellular domain, which are body to body, head to body, and left flipper to dorsal fin. The residues in the body domain are highly conserved, suggesting that the body to body interactions are common to all P2XRs. In contrast, the residues in the head, the left flipper and the dorsal fin are less conserved. This suggested that the interactions between head to body and left flipper to dorsal fin may be responsible for functional differences in P2XRs. Previous mutagenesis studies had predicted that ten conserved cysteine residues formed five disulphide bonds in the extracellular loop (Ennion and Evans 2002b). This was confirmed in the structure, showing three of these bonds were in the head region, one at the bottom of the body and one at the dorsal fin (Kawate et al. 2009, Young 2010).

Transmembrane domain

The transmembrane domains extend ~ 28 Å through the membrane. They twist to the left within the membrane in the unbound state with the second transmembrane domains crossing over one another, allowing a mechanism of closing the pore of the channel (Kawate et al. 2009). The crystal structure of the zfP2X4R in the ATP bound state showed the pore is lined by TM2 with residues Leu340, Ala344, Ala347, Leu351 and Ile355 (Hattori and Gouaux 2012). It is consistent with the predicted ion permeation pathway in previous cysteine-

accessibility studies (Egan et al. 1998). The recent published crystal structure of the hP2X3R showed I323 (L340 for zfP2X4R numbering) defines the extracellular boundary of the gate in the apo state and T330 (A347 for zfP2X4R numbering) defines the cytoplasmic boundary (Mansoor et al. 2016).

The intracellular region

The crystal structures of zfP2X4R provided a major advance in the understanding of P2XRs. The structures were supported by previous mutagenesis and functional studies (Jiang et al. 2013, Young 2010). However, there are still some questions that remain to be solved. For example, the truncated receptor did not provide information on the intracellular termini of the P2XR. The recently published crystal structure of hP2X3R which was less truncated provided more information about the intracellular part (Mansoor et al. 2016). The crystallization construct of the hP2X3R spans residues D6-T364. In addition, three rP2X2R specific amino acid substitutions (T13P, S15V and V16I) were made in the N terminus to induce slow and incomplete desensitization. The hP2X3R in apo resting and ATP-bound open states were similar to previously published crystal structures of P2XRs (Hattori and Gouaux 2012, Kasuya et al. 2016, Kawate et al. 2009). Comparison between the hP2X3R and zfP2X4R structures shows the longer transmembrane and the cytoplasmic domain of the new structure. The open state structure of the hP2X3R visualized the intracellular parts which were truncated in previous published zfP2X4R structures. The cytoplasmic residues form a domain termed the 'cytoplasmic cap' (Mansoor et al. 2016).

The cytoplasmic cap includes two sequential β -strands from the N terminus and a β -strand from the C terminus. Three β -strands sit beneath the transmembrane domain, capping the cytoplasmic surface of the pore. The C-terminal β -strand of each subunit interacts with N-terminal β -strands of the other two subunits, forming a small β -sheet (Figure 1.6c). The cytoplasmic cap was only observed in the open state structure of the hP2X3R. The three mutations (T13P, S15V and V16I) that slow desensitization make key hydrophobic interactions that stabilize the structure of the cap (Mansoor et al. 2016). This

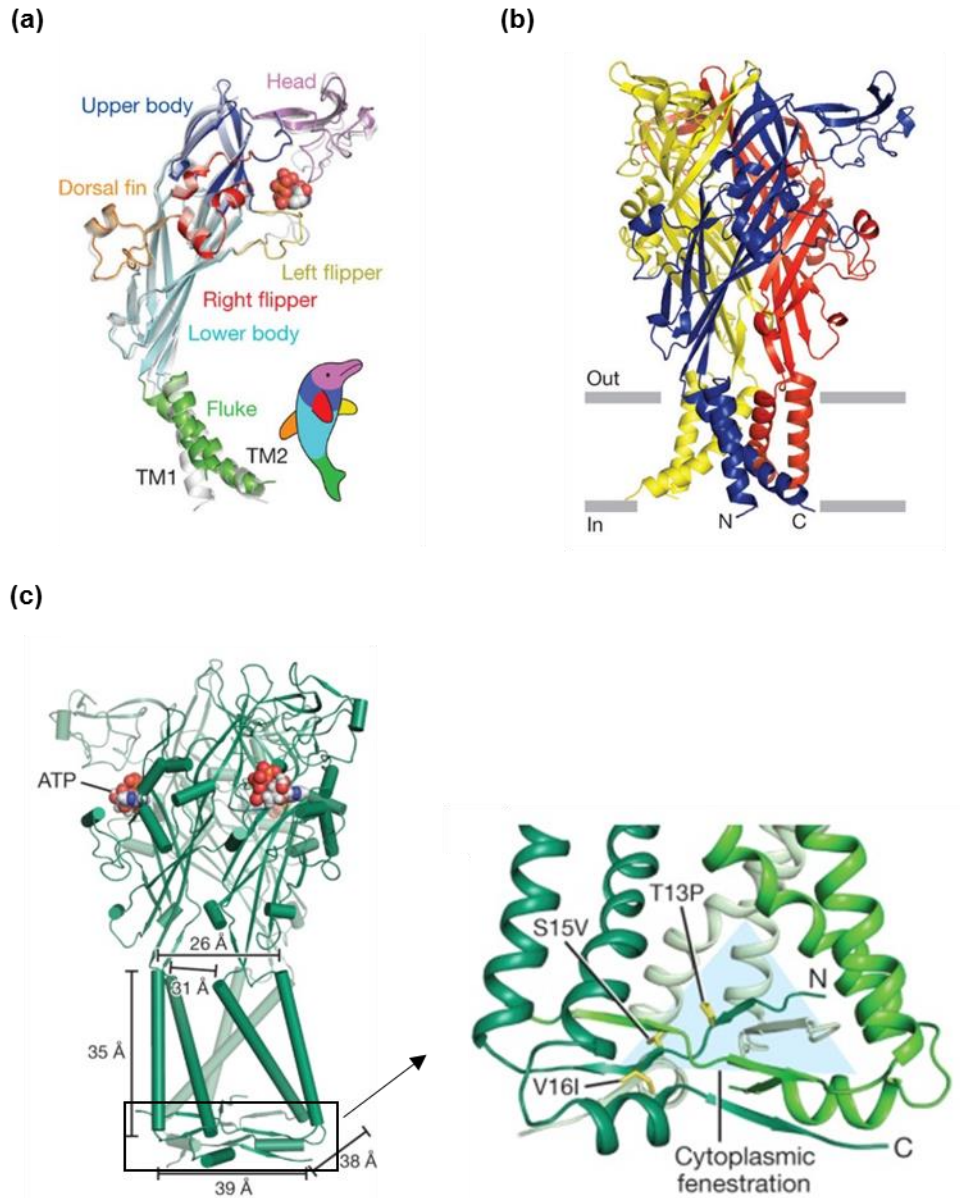


Figure 1.6 The crystal structure of the P2X receptor.

(a) Structure of an individual zfP2X4 subunit. The structure has been compared to a dolphin, with head, body, left flipper, right flipper, dorsal fin and fluke regions. (b) Structure of a trimeric P2X receptor (Images taken from Hattori & Gouaux, 2012).. (c) The structure of hP2X3R in open state (left). The cytoplasmic cap (right) is composed of domain-swapped β-strands from each subunit, above which are triangular-shaped cytoplasmic fenestrations. The T13P, S15V and V16I mutations are shown in one subunit as yellow sticks (Images taken from Mansoor et al. 2016).

suggested the cytoplasmic cap has an important role in channel gating and is likely to be disassembled in the apo and desensitized states.

1.5.3 ATP binding site

Prior to a high-resolution crystal structure of the P2XR in an ATP-bound state, a mutagenesis-based approach was used to determine the site of agonist action. In initial studies, alanine substitution was widely used as this simple amino acid is well tolerated. The mutagenesis studies suggested that (i) conserved positively charged residues (K68, K70, R292 and K309, numbering for P2X1R) bind to the negatively charged phosphate of ATP because they contributed to ATP potency, with the greatest decrease (>1400-fold) in ATP sensitivity for K68A and K309A (Ennion et al. 2000, Jiang et al. 2000). (ii) Aromatic amino acids bind to the aromatic-adenine ring. It demonstrated a contribution of F185 and F291 in ATP action, with ~10- and ~140-fold decreases in ATP potency following alanine replacements respectively (Roberts and Evans 2004). (iii) Polar amino acids also contribute to agonist binding. Studies highlighted the role of T186 and N290, with their alanine mutants showing ~6- and ~60-fold decreases in ATP potency respectively (Roberts and Evans 2006). The mutation of conserved residue (K190A) resulted in a ~5, ~200, and ~2000-fold decreases in ATP potency at P2X1, P2X2 and P2X4Rs respectively (Ennion et al. 2000, Jiang et al. 2000, Yan et al. 2005).

Subsequently, more cysteine-substituted mutations were made to further investigate ATP action at P2XRs. The major advantage of cysteine substitution over alanine is that it can be modified by Methanethiosulfonate (MTS) compounds with different side chains and charges. The modifications gave additional information about contributions of the residues to ligand binding (see detail in 5.1.1). At the P2X1R, the region S286-I329 includes part of the predicted ATP binding site and their adjacent residues. Analysis of the individual cysteine mutants showed that ATP potency was decreased by ~20-fold for N290C and ~50-fold for F291C, R292C and K309C. These results confirmed the role of N290, F291, R292 and K309 in ATP action, which was consistent with the previous alanine mutagenesis studies (Roberts and Evans 2007). The contribution of the

region E181-V200 in the extracellular loop of the hP2X1R was also evaluated by cysteine scanning mutagenesis. T186C, F188C and K190C were shown to have significant effects on agonist action, with EC_{50} of ~ 6.5 , ~ 5.8 and ~ 3.4 μM compared to WT P2X1Rs (EC_{50} of ~ 0.8 μM) (Roberts et al. 2009b). Moreover, cysteine scanning mutagenesis in the region E52-G96 suggested the role of K68 and K70 to ATP potency, with $> \sim 3000$ -fold decrease in ATP potency at K68C and ~ 10 -fold at K70C. The mode of ATP action was also supported by cysteine substitution mutagenesis at equivalent residues in P2X2 and P2X4Rs (Roberts et al. 2008).

The crystal structure of zfP2X4R in the closed state showed the above residues were positioned too far apart for the ATP molecule to interact with all of them (Kawate et al. 2009). However it was thought that agonist binding involves conformational changes in the receptor that bring the residues closer together to enable strong binding. Studies on the P2XRs have indicated that only two of the three binding sites are sufficient for activating by ATP (Stelmashenko et al. 2012).

The first crystal structure of the P2XR (zfP2X4R) in an ATP bound state was published in 2012 (Hattori and Gouaux 2012). The construct of the P2X4R in ATP bound state was $\Delta\text{P2X4-C}$ that starts at S28 and ends at K365 ($\Delta\text{N27}/\Delta\text{C24}/\text{N78K}/\text{N187R}$). The crystal structure of $\Delta\text{P2X4-C}$ in ATP bound state showed three equivalent ATP binding sites located at each of the subunit interfaces in the trimeric receptor. The sites are located ~ 40 Å from the extracellular boundary of the TM domain. Each ATP-binding pocket, lined with multiple positively charged residues, is formed by the head domain (chain A), upper body (chain A), lower body (chain B), left flipper (chain A) and the dorsal fin (chain B). ATP is recognized by the upper (chain A) and lower (chain B) body domains through extensive hydrophilic interactions (Hattori and Gouaux 2012) (Figure 1.7a).

The bound ATP molecule adopts a U-shaped structure with the β - and γ -phosphates folded toward the adenine ring. The negative charged phosphate groups bond with a cluster of highly conserved polar residues in two adjacent body domains through salt bridges and hydrogen interactions (Hattori and

Gouaux 2012). Lys70 (zfP2X4 numbering) (Lys68 in hP2X1R numbering) is a crucial residue in the ATP binding sites because its ammonium group resides at the centre of the triphosphate 'U'. It interacted with oxygen atoms on α , β and γ phosphate groups of ATP. It is consistent with the observation that mutating this residue led to a significant decrease in ATP sensitivity of P2XRs (Ennion et al. 2000). N296 and K316 (N290 and K309 in hP2X1R numbering) (chain A) mediate additional contacts with β -phosphate groups. K72 (K70 in hP2X1R numbering) (chain B), R298 and K316 (R292 and K309 in hP2X1R numbering) (chain A) form interactions with the γ -phosphate. The adenine base of ATP is deeply buried in the ATP binding pocket. It interacts with the side chain of T189 (T186 in hP2X1R numbering) and the main chain carbonyl oxygen atoms of K70 and T189 in the lower body through three hydrogen bonds. L191 in the lower body and I232 in the dorsal fin also have hydrophobic interactions with the adenine base (Hattori and Gouaux 2012). The ATP binding site present in the crystal structures of the P2XR were consistent with the mutagenesis results. The crystallisation demonstrated mutagenesis as a successful technique in understanding molecule binding.

1.5.4 Conformational changes on agonist binding

A comparison of the ATP-bound and unbound crystal structures demonstrated substantial conformational changes on activation (Hattori and Gouaux 2012). In general, ATP binding induces cleft closure of the nucleotide binding pocket, flexing of the lower body β -sheet and a radial expansion of the extracellular vestibule (Hattori and Gouaux 2012) (Figure 1.7b, 1.12). The conformational changes in the different domains of the receptor are discussed below.

Head domain The head domain of the P2XR subunit consists of residues 111-167 (zfP2X4 numbering). The ATP-bound open structure showed that ATP binding promotes downward movement of the head domain, with cleft closure between the head and dorsal fin domains (Hattori and Gouaux 2012). Molecular dynamic (MD) simulations studies revealed the downward motion of the head domain may result from its inherent dynamics (Zhao et al. 2014). The movements

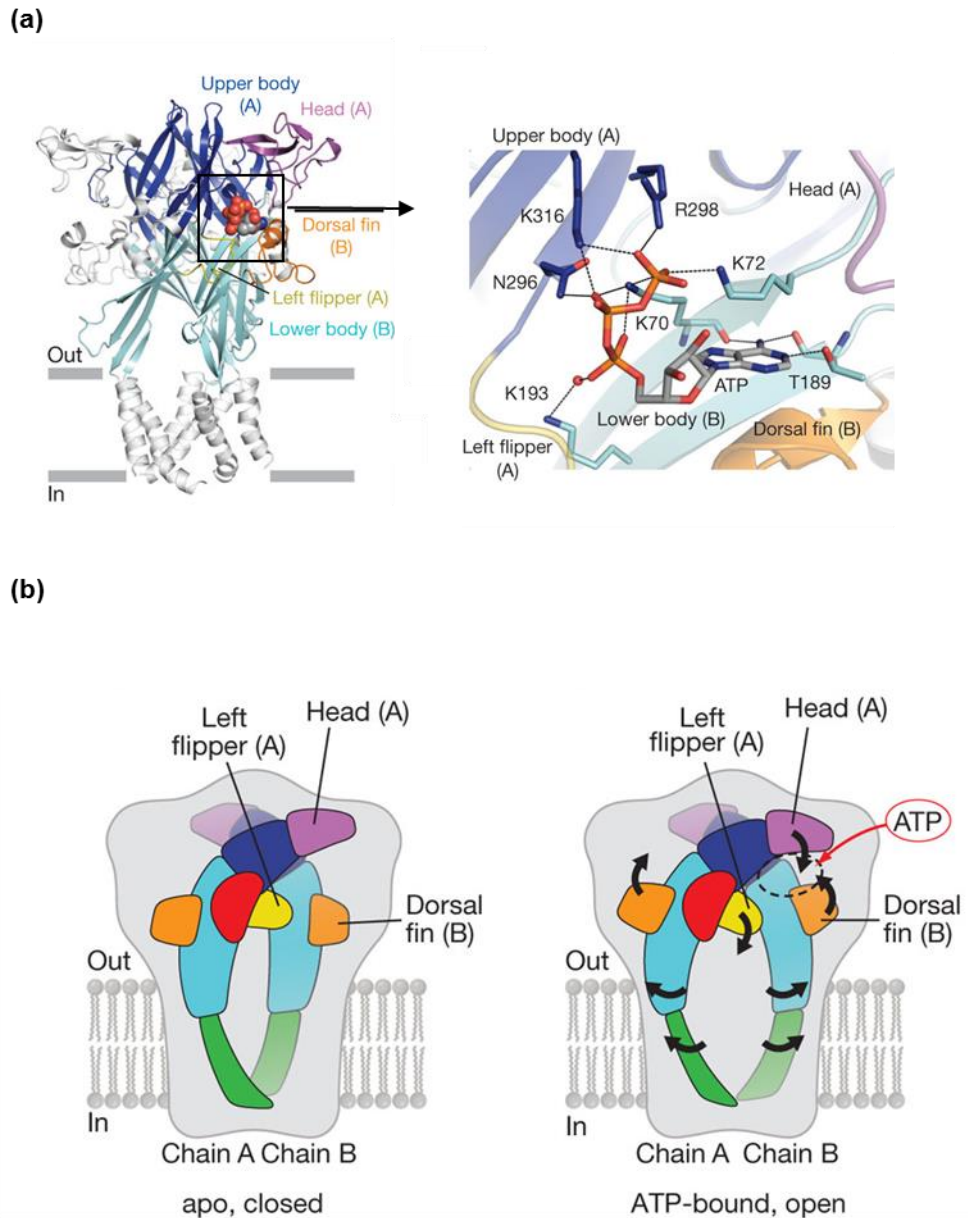


Figure 1.7 The ATP binding sites and conformational changes during activation. (a) The zFP2X4R is shown in ATP-bound open state. The ATP molecule is shown in sphere representation (left). The ATP is shown in sticks and the interactions between the residues and ATP are shown in dashed lines. (b) A cartoon model of the ATP-dependent activation mechanism. The black arrows denote the movement from the closed state to the ATP-bound open state (Images taken from Hattori and Gouaux 2012).

were consistent with the conformational changes demonstrated by ATP binding and are pivotal for the channel gating of P2XRs. K138 (P2X1 numbering) in the head domain was suggested to be involved in the binding of the antagonist suramin and its analog NF449. The antagonists were suggested to bind at a site below the head domain of the P2X1R and therefore impede the downward movement of this domain (El-Ajouz et al. 2012a, Farmer et al. 2015). In addition, it was reported that for P2X7Rs, ADP-ribosylation at R125 located in the cysteine-rich head region at the interface of the subunits gated the channel (Adriouch et al. 2008).

Dorsal fin domain The dorsal fin (DF) domain is composed of residues 206-234 (zfP2X4 numbering). The upward motion of the DF domain is another allosteric change for P2XR action. Disulphide crosslinking or zinc bridges between the LF and DF domains that constrain their relative motions significantly reduced P2X4 channel gating (Zhao et al. 2014). Moreover, it has been suggested that small molecules interrupting this motion may effectively block the activation of P2XRs. Mutagenesis studies suggested residues A197 and T202 (hP2X3R numbering) located in the DF domain are responsible for the reduced sensitivity of the antagonist TNP-ATP and RO-51 at hP2X3Rs which showed ~200-fold higher potency at rP2X3Rs (Serrano et al. 2012).

Left flipper domain The left flipper (LF) domain corresponds to residues 281-296 (zfP2X4 numbering). The LF was pushed out from the ATP binding pocket during ATP binding to open the channel (Hattori and Gouaux 2012). Previous studies showed that alteration in interactions among I208, L217, V291 and K193 (zfP2X4R numbering) were induced by ATP binding (Zhao et al. 2014), suggesting that the proper interactions between the DF and LF domains are indispensable for channel gating of P2XRs.

Right flipper domain (RF) This domain is composed of residues 178-189 and 235-254 (zfP2X4 numbering). **The upper body domain** This domain is composed of residues 75-92, 105-113 and 294-319 (zfP2X4 numbering). Based on the two snapshots of the structure in closed and open states, ATP does not cause significant conformational changes at these two domains.

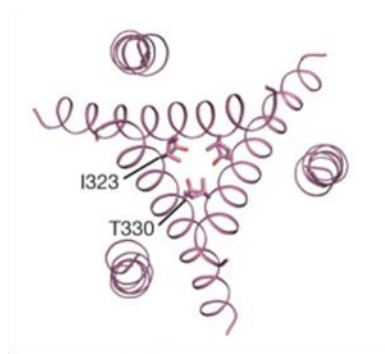
Lower body domain The domain is composed residues 56-74, 93-104, 188-207, 254-281 and 320-330 (zfP2X4 numbering). As the lower body domain is coupled with DF and LF, the upward motion of DF and outward motion of LF result in a concomitant outward flexing of the lower body and substantial expansion of the extracellular vestibule (Hattori and Gouaux 2012).

TM domains In zfP2X4R, the helices rearrange in an iris-like movement in going from the closed to open state. TM1 and TM2 rotated by $\sim 10^\circ$ and $\sim 55^\circ$ counterclockwise perpendicularly and by $\sim 8^\circ$ and $\sim 2^\circ$ horizontally respectively (Hattori and Gouaux 2012). This resulted in the helices moving away from the central axis by $\sim 3 \text{ \AA}$, which provides a pathway for ion permeation (Kawate et al. 2011). In the hP2X3R, the outward rotation of TM2 promotes the translation of I323 (the residue defining the extracellular gate of the apo state) upward by $\sim 6.3 \text{ \AA}$ towards the extracellular surface and reorients it away from the pore centre. T330 (the residue defining the cytoplasmic gate of the apo state) also moves upward by $\sim 5.3 \text{ \AA}$ and rotates away from the pore centre. In addition to a rigid-body translation described in zfP2X4, there is a transition in TM2 from an α -helix to a 3_{10} -helix. It is suggested that the formation of the cytoplasmic cap fixes the cytoplasmic portion of TM2 in place, forcing the α -helix to 'stretch' to a 3_{10} -helix. The change of helical pitch stabilized pore opening (Mansoor et al. 2016) (Figure 1.8).

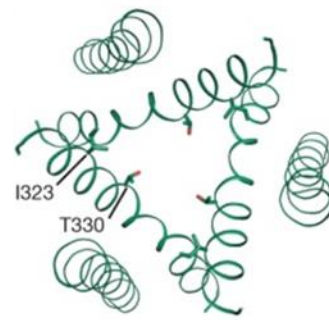
1.5.5 Ion access

The crystal structure of the zfP2X4R in the closed state indicated two possible pathways by which cations might access the ion channel. One was a central pathway by which ions went through three fold axis of symmetry. The other one was a lateral pathway through the fenestration located immediately above the ion channel pore (Kawate et al. 2009). The crystal structure of zfP2X4R and hP2X3R in open state suggested that the central pathway was too small to allow for ion permeation (Hattori and Gouaux 2012, Mansoor et al. 2016) (Figure 1.9). In contrast, the lateral pathway was wide enough for ions pass through. Previous cysteine-accessibility and cysteine-based cross-linking studies also supported this prediction, providing three evidence that (i) lateral fenestrations

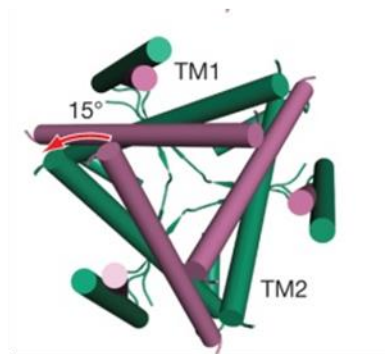
(a)



(b)



(c)



(d)

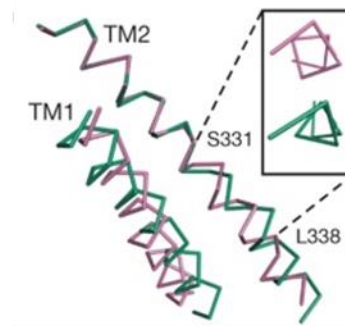


Figure 1.8 Apo to open transition in TM domains Top-down view of the pore comparing (a) the apo state to (b) the open state. (c) Relative conformational changes in the pore, shown from the extracellular surface, between the apo (red-purple) and open (green) states after aligning the upper body domain of the trimer, demonstrate pore opening. (d) Alignment of TM2 in apo versus open states reveals a change in helical pitch to a 3_{10} -helix in the open state. The inset shows the view along the axis of the TM2 helix, observed from the cytoplasmic surface. (Images taken from Mansoor et al. 2016).

were energetically favourable for monovalent cations; (ii) MTS reagents permeated in the lateral fenestration and the region became larger after ATP binding; and (iii) disulphide bridges that constrain movement in the vestibules within the central pathway did not prevent ion conduction (Kawate et al. 2011). The crystal structure of the hP2X3R showed that the cytoplasmic cap and TM2 helices from adjacent subunits form the borders of a triangular-shaped cytoplasmic fenestration. MD simulations revealed that Na⁺ passed through all three cytoplasmic fenestrations, suggesting that ions enter the receptor through the lateral extracellular fenestrations and exit through lateral cytoplasmic fenestrations (Mansoor et al. 2016). (Figure 1.10).

1.5.6 Desensitized state

The P2XR in the desensitized state has been recently presented based on the crystal structure of the hP2X3R (Mansoor et al. 2016). The crystallized structure has ATP in the pocket but a closed pore (Figure 1.11a, 1.12). The extracellular domains of the structures in open and desensitized state are similar, but there are striking differences in the transmembrane domains and the gate.

During the transition from the open state to the desensitized state, the cytoplasmic portion of TM2 rotated by ~9° and the short 3₁₀-helix formed in the open state reverts to an α-helix, resulting in the upward translation towards the extracellular surface (4.4Å) and inward rotation of V334. This movement allowed the pore to close at a new constriction site, located deeper within the membrane bilayer than the constriction site for the apo state (Figure 1.11b, c).

The N terminus in the desensitized state is directed away from the pore, in the opposite direction of the backbone. This suggested that a transient cytoplasmic cap forms in the open state but unfolds or disassembles during receptor desensitization. This finding was consistent with previous studies showing residues in both termini of P2XRs have been implicated in modulation of desensitization (Koshimizu et al. 1998).

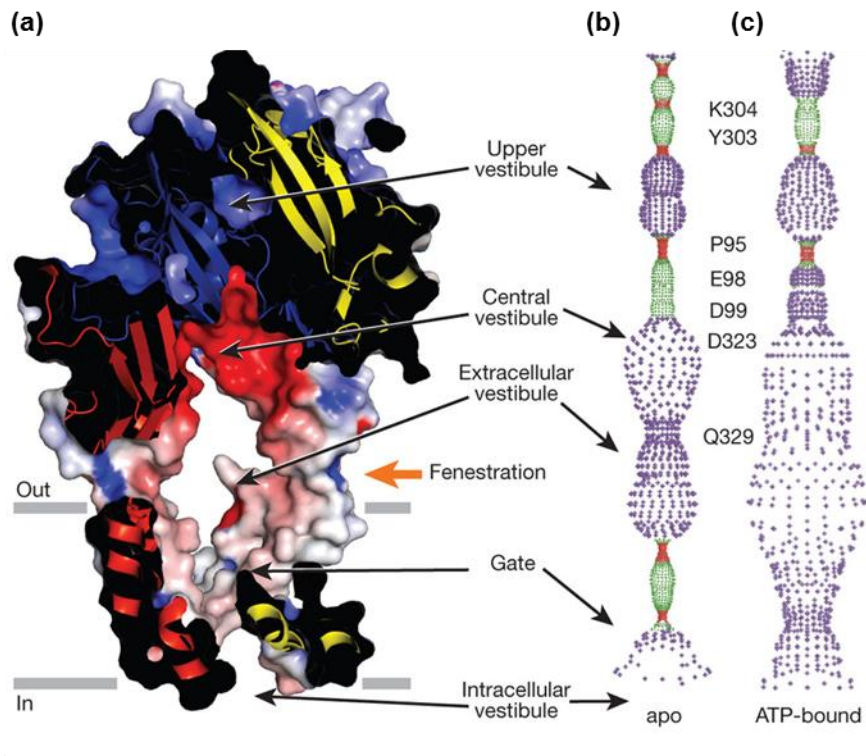


Figure 1.9 The vestibules in the zfP2X4R.

(a) A section of an electrostatic potential surface of $\Delta P2X_4-C$. (b) Pore-lining surfaces of the zfP2X4R in closed state (c) and ATP-bound state. Each colour indicates a different radius range from the pore centre (red: <1.15 Å, green: 1.15–2.3 Å, and purple: >2.3 Å) (Images taken from Hattori & Gouaux, 2012).

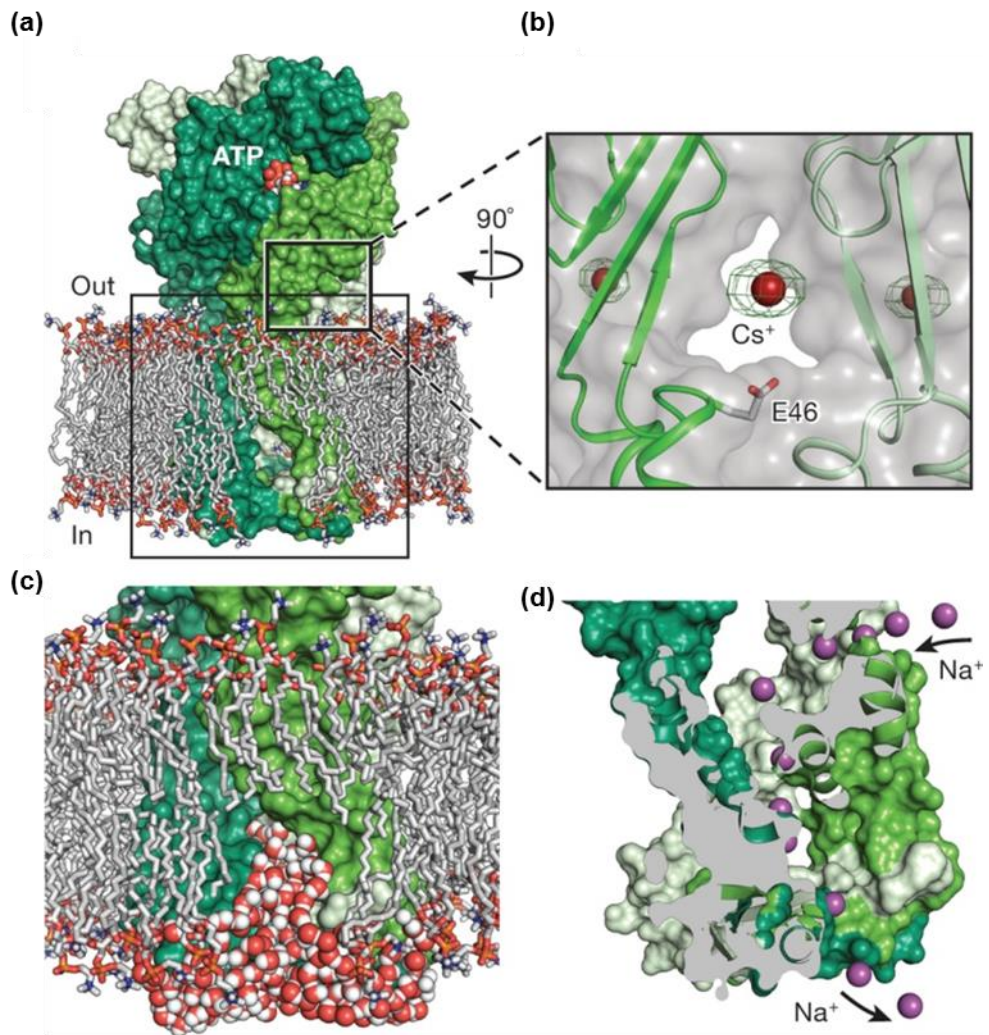


Figure 1.10 Extracellular and cytoplasmic fenestrations.

(a) The equilibrated, membrane-bound model of the open state of hP2X₃ with the protein shown in surface representation and each subunit in a different shade of green. POPC lipid tails are silver. For the head groups, oxygen is in red, nitrogen in blue, and phosphorus in orange. (b) a Cs⁺ ion at the entrance of the extracellular vestibule. (c) Cytoplasmic fenestrations enable water-filled rivulets, juxtaposed between the protein and lipid membrane, to function as pathways for ion egress into the cytoplasm. (d) Simulation snapshot of an independent Na⁺ ion permeation event as Na⁺ enters through the extracellular fenestrations and egresses through the cytoplasmic fenestrations. Na⁺ ions are shown as purple spheres. (Images taken from Mansoor et al. 2016).

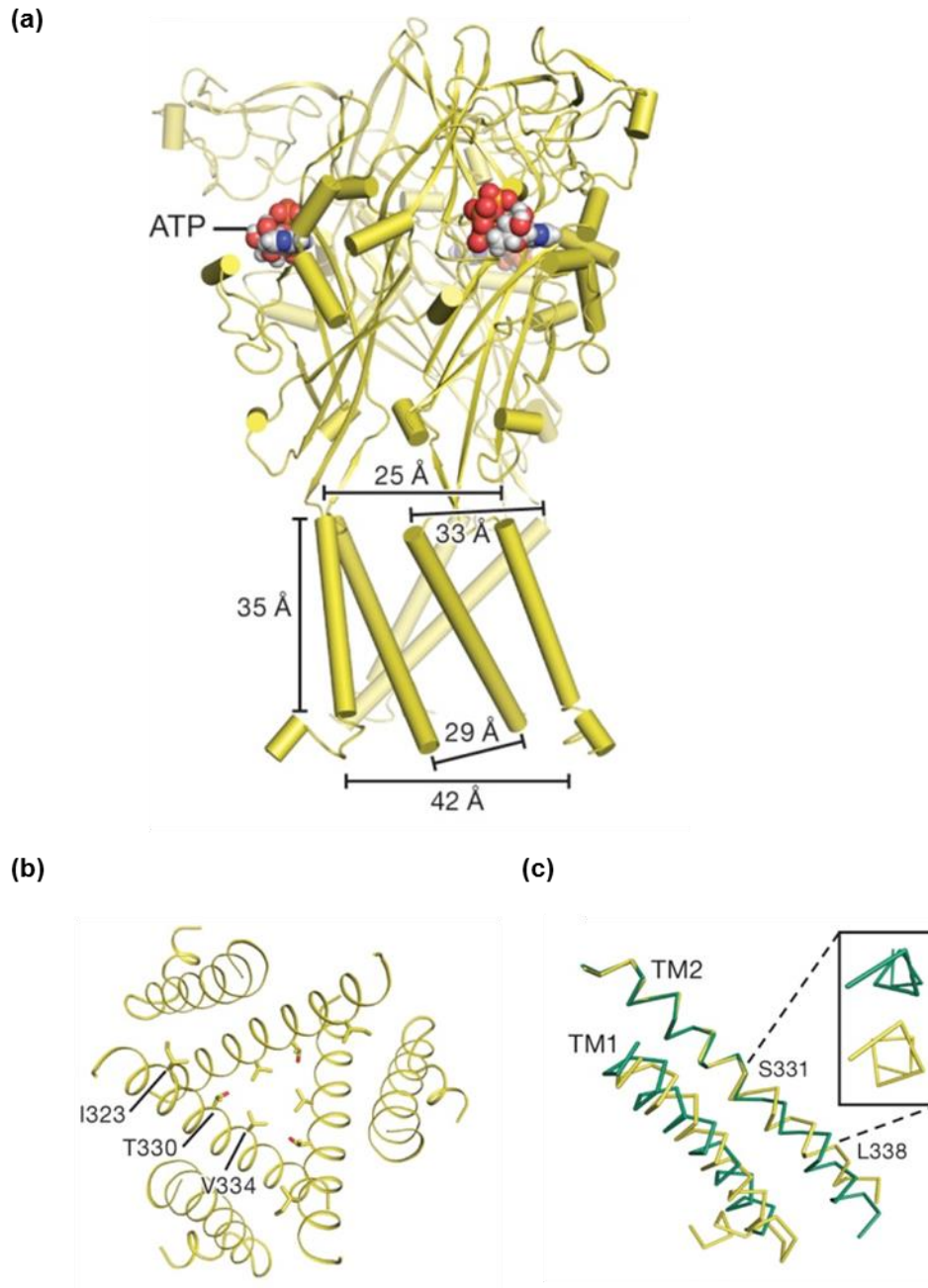


Figure 1.11 The crystal structure of the hP2X3R in desensitized state.

(a) Structure of the desensitized state shown parallel to the membrane. (b) Top-down view of the pore in the desensitized state. (c) Alignment of TM2 in open (green) versus desensitized states (yellow) reveals that the 3_{10} -helix in the open state reverts to an α -helix in the desensitized state (Images taken from Mansoor et al. 2016).

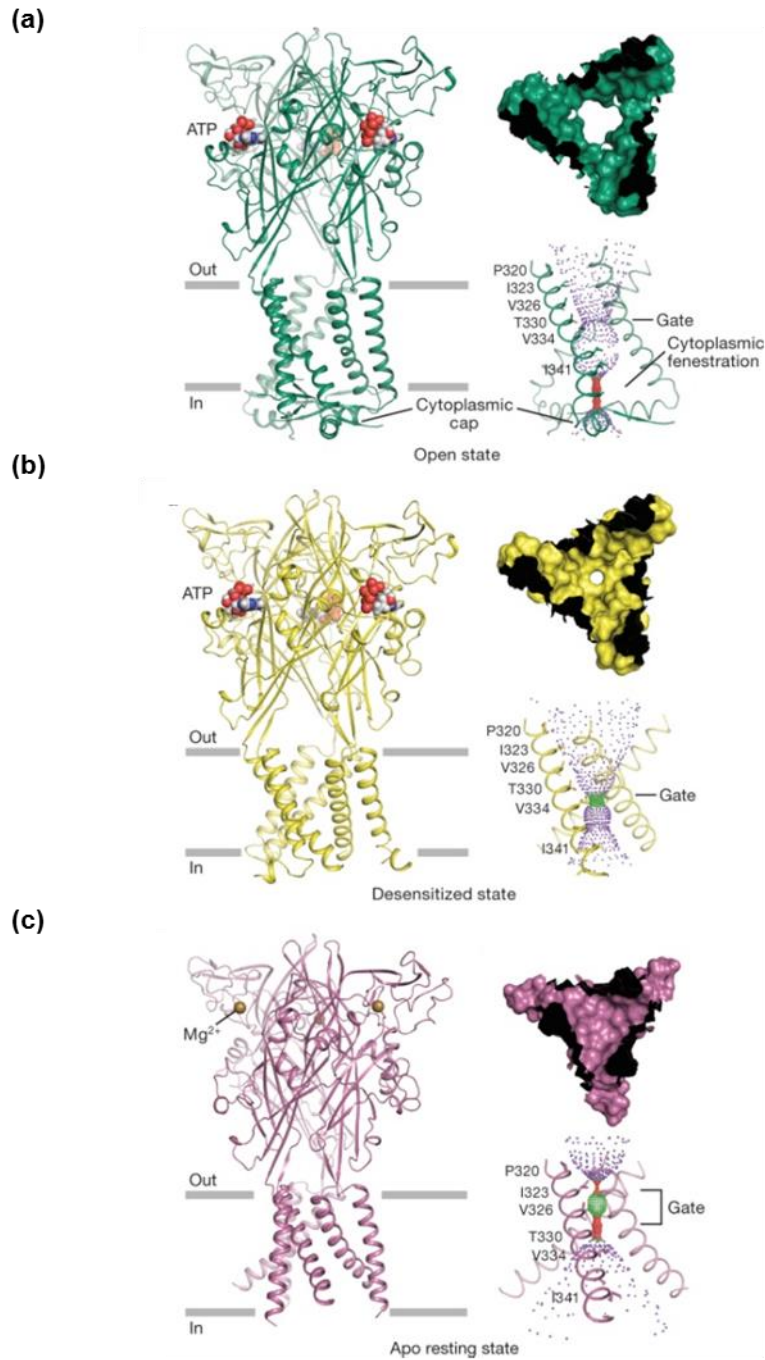


Figure 1.12 Architecture and pore structure for three states of hP2X₃. Cartoon representation of each hP2X₃ structure shown parallel to the membrane as a side view, perpendicular to the membrane from the extracellular side as a surface representation, and the ion permeation pathway, respectively, are drawn for (a) open state, (b) desensitized state and (c) apo state. Each conformational state is colour-coded unless otherwise noted: open state in green, desensitized state in yellow, and apo state in red-purple. (Images taken from Mansoor et al. 2016).

1.5.7 Divalent cation binding sites

Divalent cations are important regulatory factors in the P2XR family. For example, extracellular Zn^{2+} inhibited ATP evoked responses at the rP2X1R in a time-dependent manner. It was shown that 20 min pre-incubation was optimal, with an IC_{50} value of $\sim 1 \mu M$. In contrast, Zn^{2+} potentiated ATP sensitivity at the rP2X3R, with an EC_{50} value of $\sim 11 \mu M$ (Wildman et al. 1999). At P2X2Rs, Zn^{2+} (10-130 μM) reversibly potentiated ATP induced responses ($EC_{50} \sim 20 \mu M$). At P2X4Rs, Zn^{2+} (0.5 to 20 μM) enhanced currents with an EC_{50} value of $\sim 2.5 \mu M$ (Xiong et al. 1999). Another trace metal, Mg^{2+} , has also been shown to work as a regulator at P2XRs. As ATP contains four negative charges, the free anionic form of ATP is ATP^{4-} . Mg^{2+} can bind to free ATP, forming $MgATP^{2-}$. In the presence of Mg^{2+} (5 mM), the activity of P2X2Rs and P2X4Rs were inhibited (<10% of maximum activation) whereas P2X1Rs and P2X3Rs were strongly activated by $MgATP^{2-}$ (>90% of maximum activation) (Li et al. 2013).

The molecular mechanism of the divalent cation modulation of the P2XRs was obtained when the crystal structure of an invertebrate P2XR from the Gulf Coast tick *Amblyomma maculatum* (AmP2X) in the presence of ATP and Zn^{2+} ion was published (Kasuya et al. 2016). The amino acid sequence of AmP2X is most closely related to that of P2X4Rs among the mammalian P2XR family. In order to be crystalized, the AmP2XR was truncated 23 residues at N-terminal and 7 residues at C-terminal respectively and with mutations of Asn171 and Cys374 (Kasuya et al. 2016). The overall crystal structure and the ATP binding site of AmP2XR were consistent with the crystal structure of the zfP2X4R (Hattori and Gouaux 2012). Two distinct metal binding sites in the extracellular domain of AmP2XR were identified, named the M1 and M2 sites.

M1 site

The M1 site is located at the subunit interface at the centre of the upper body domain. It is surrounded by the side chains of E105 in one subunit and E106 in the neighbouring subunit (Figure 1.13a). The corresponding residues at the M1 site are strictly conserved as Q and E residues among the P2X4Rs. The M1 site is responsible for Zn^{2+} potentiation by allosterically facilitating the structural

change of the body domain in the extracellular region for pore opening. Mutagenesis studies on the rP2X4R showed the mutation E95A (corresponding to E106 in AmP2X) at the site abolished the potentiation effect of Zn^{2+} ion. It confirmed the M1 site for Zn^{2+} binding.

The comparison between the structures in the absence and presence of Zn^{2+} ion revealed its site of action. Zn^{2+} binding brings two glutamate residues (E105 and E106) toward each other by electrostatic attraction. The movement of the two residues induces a small counterclockwise rotation ($\sim 2^\circ$) of the lower body. The rotation is magnified into the larger movement in transmembrane ($\sim 10^\circ$) to open the pore (Kasuya et al. 2016).

However, previous studies revealed that Zn^{2+} may allosterically bind to histidine residues (H120 and H213) (P2X2 numbering) at P2X2Rs (Nagaya et al. 2005). These two residues are located at the head of the subunit and dorsal fin of the neighbouring subunit respectively. It suggested that tightening of the ATP binding pocket induced the channel open. (Jiang et al. 2012). Therefore, interactions between Zn^{2+} and the residues may induce the cleft closure motion in the ATP binding pocket to potentiate ATP induced responses at P2X2Rs. These two histidine residues are not conserved among the P2X4Rs. Therefore, the molecular mechanism of Zn^{2+} modulation at P2X2Rs may be different from that in P2X4Rs.

M2 site

The M2 site is coupled with the ATP binding site. It is coordinated by the side chain of D188 and the γ -phosphate group of ATP (Figure 1.13b). The corresponding residue D188 is conserved among the P2X1R and P2X3Rs. The M2 site may contribute to $MgATP^{2-}$ sensitivity among P2XRs. Mutations at the M2 site, D170A (corresponding to D188) and neighbouring D171A in the hP2X1R caused a 5-fold reduction in ATP affinity at high concentrations of Mg^{2+} (5 mM) compared to that at a low concentration of Mg^{2+} (0.5 mM). In contrast, WT hP2X1Rs exhibited similar sensitivity to ATP at different concentrations of Mg^{2+} (Kasuya et al. 2016). This suggested the M2 site may be responsible for various sensitivities to $MgATP^{2-}$ among subtypes of P2XRs.

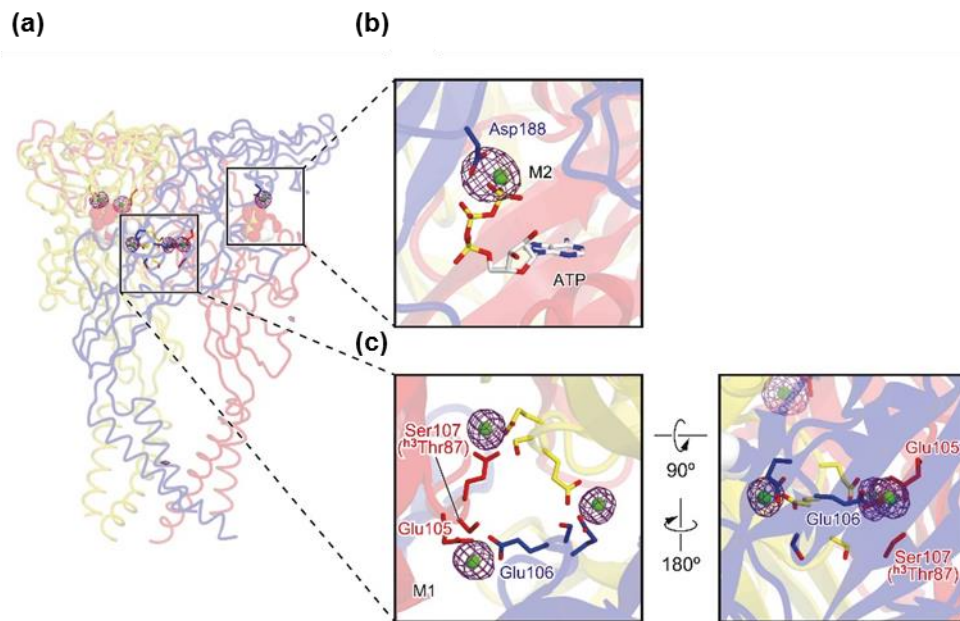


Figure 1.13 Divalent cation binding sites

(a) Overall view of the metal binding sites in the AmP2X structure. **(b)** The M2 (Mg^{2+} binding site). **(c)** The M1 (Zn^{2+} binding site). (Images taken from Kasuya et al. 2016)

1.6 Antagonists at P2X receptors

There is a lot of evidence showing that activation of P2XRs is involved in various pathological conditions. For example, P2XR1s contribute to the formation of thrombus. P2X7Rs respond to 'danger signals' such as inflammation and cellular damage. Therefore, the antagonists of P2XRs are promising to provide important novel therapeutics. A range of antagonists of P2X receptors have been identified (Table 1.4). The most commonly used non-selective antagonists are suramin and PPADS. In order to improve the potency and selectivity of the antagonists, their analogues were generated. For example, NF449, the analogue of suramin, is selective for P2X1Rs. The properties of the antagonists at different P2XR subtypes were discussed below.

Understanding the molecular basis of the antagonism would accelerate the development of potent and selective P2XR antagonists. Mutagenesis was widely used to predict the antagonists binding site, for example for suramin and NF449. Recently, the crystal structures of the hP2X3R in a competitive antagonist (TNP-ATP) bound state (Mansoor et al. 2016) and that of the pdP2X7R in selective antagonists bound states (Karasawa and Kawate 2016) have provided a major advance for understanding the antagonism of P2XRs.

1.6.1 Suramin

Suramin (8-[[4-methyl-3-[[3-[[3-[[2-methyl-5-[(4,6,8-trisulfonaphthalen-1-yl)carbamoyl]phenyl]carbamoyl]phenyl]carbamoylamino]benzoyl]amino]benzoyl]amino]naphthalene-1,3,5-trisulfonic acid) was originally found to inhibit trypanocidal activity. It has been widely used for treatment of human trypanosomiasis in Africa since the 1920s (Voogd et al. 1993). Subsequent studies showed suramin was a competitive inhibitor of the reverse transcriptase of RNA tumour viruses (De Clercq 1979). Then suramin was demonstrated to block the infectivity and cytopathic effect of HIV *in vitro* at doses that are clinically attainable in human beings (Mitsuya et al. 1984). Suramin was entered into clinical trials as a treatment for AIDS (Broder 1985, Cheson 1987). As suramin was shown to have adrenal toxicity in the AIDS trials, it was tested as an anticancer drug for adrenocortical cancer (Allolio et al. 1989). Unfortunately, the

pharmacological properties of suramin appear to be highly nonspecific, which results in many side effects and a complex toxicological profile. Therapeutic prospects were restricted by many toxicities (Kaur et al. 2002).

The interest in the relationship between suramin and P2XRs was after it was shown to be a potent inhibitor of various hydrolytic and oxidative enzymes (Wills and Wormall 1950), including Na-K-ATPase (Fortes et al. 1973) and Mg²⁺-ATPase (Smolen and Weissmann 1978). It suggested that its inhibition was possibly by interfering with the binding of ATP. As P2XRs are activated by ATP, the action of suramin at the receptors was investigated. Suramin was first identified as a P2XR antagonist in 1988 when it was found to inhibit P2XR mediated contractions in the mouse vas deferens (Dunn and Blakeley 1988). Subsequently, suramin was found to display an antagonistic activity at both P2XRs and P2YRs at concentrations higher than 10 µM (Hoyle et al. 1990). Suramin was used as a potent P2XR antagonist when P2XRs were cloned from the native tissues, including rat vas deference (Valera et al. 1994) and vagus nerve (Trezise et al. 1994).

Suramin has been useful for identifying and characterising P2XRs at recombinant P2XRs. Suramin acted effectively at most subtypes but had little action at P2X4Rs and P2X7Rs. It was most effective at P2X1Rs, with IC₅₀ values of ~1 µM (Evans et al. 1995). P2X2Rs are 10-fold less sensitive than P2X1Rs (IC₅₀ ~10 µM) (North and Surprenant 2000). The potency of suramin at P2X3Rs and P2X5Rs were similar, with IC₅₀ values of ~3 µM (Lewis et al. 1995, Wildman et al. 2002). P2X4Rs and P2X7Rs showed insensitivity to suramin (IC₅₀ >300 µM) (Buell et al. 1996, Surprenant et al. 1996) (Table 1.4). Sensitivity to suramin also varies among the same P2XR but from different species, for example the mouse P2X1R is insensitive to 10 µM suramin while the human variant is nearly completely inhibited by this concentration (Sim et al. 2008).

In terms of the structure of suramin, it is a symmetrical molecule with urea at the centre. Two arms extend from this urea, each containing 4 benzene rings, of which two are fused together to form a naphthyl ring containing 3 negative charged polysulphonates on each arm (Figure 1.14a). The structure has been

used as the starting point for a series of suramin derivatives with the P2X1R antagonist properties.

1.6.2 Analogues of suramin

Suramin is an effective but non-selective P2XR antagonist. Various suramin derivatives have been synthesized to try to find more potent and selective P2XR antagonists (Lambrecht et al. 2002). Some representative suramin derivatives with high potency and selectivity at P2XR subtype are described below (Table 1.4).

NF023 (8,8'-[carbonylbis(imino-3,1-phenylenecarbonylimino)]bis-1,3,5-naphthalene-trisulphonic acid), is a truncated form of suramin (Figure 1.14b). It showed highest potency at P2X1Rs with an IC₅₀ value of ~0.2 μM, ~5-fold more potent than suramin. P2X3Rs have an intermediate sensitivity with IC₅₀ value of ~8.5 and 28.9 μM for rat and human subtypes respectively. It has been used as a useful discriminating ligand between P2X1 and P2X3Rs. P2X2Rs showed reduced sensitivity with an IC₅₀ value >50 μM. P2X4Rs were insensitive to NF023 at concentrations up to 100 μM (Soto et al. 1999).

NF279 (8,8'-[Carbonylbis(imino-4,1-phenylenecarbonylimino-4,1-phenylenecarbonylimino)]bis-1,3,5-naphthalenetrisulfonic acid), has similar structure to suramin, with two methyl groups removed (Figure 1.14c). It exhibited higher potency than suramin and NF023 at P2X1Rs, with an IC₅₀ value of ~20 nM with 10s preincubation before ATP application and 2 μM without preincubation. NF279 showed IC₅₀ values of ~0.76 μM and ~1 μM at rP2X2Rs and rP2X3Rs. At hP2X7Rs, NF249 showed IC₅₀ value of ~2.8 μM. P2X4Rs were insensitive to NF279 (IC₅₀ >300 μM). The antagonism was competitive and fully reversible at all P2XR subtypes (Klapperstück et al. 2000, Rettinger et al. 2000).

NF449 (4, 4', 4'', 4'''-[Carbonylbis (imino-5,1,3-benzenetriyl-bis(carbonylimino))] tetrakis-1, 3-benzenedisulfonic acid) showed the highest affinity and selectivity at P2X1Rs among the analogues of suramin, with an IC₅₀ value of ~0.3 nM (Braun et al. 2001). Compared with suramin, the structure of NF449 has eight negative charges, two more than suramin, which are spread around the

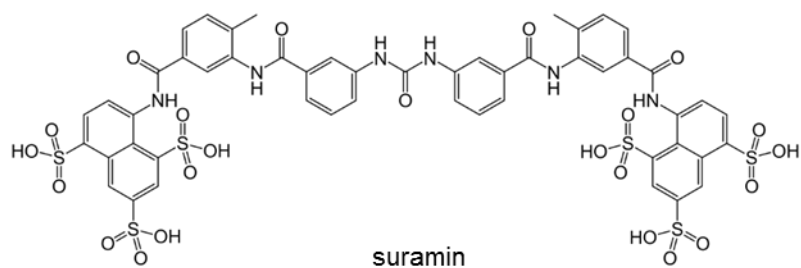
molecule (Figure 1.14d). This could account for the increased potency at the P2X1R compared to the parent molecule. It acts as a reversible competitive antagonist with much higher potency at P2X1 than P2X2 (IC₅₀ value of ~47 μM), P2X3 (IC₅₀ value of ~1.8 μM), and P2X7Rs (IC₅₀ value of ~40 μM) with least potency at P2X4Rs (IC₅₀ value >300 μM) (Hulsmann et al. 2003, Rettinger et al. 2005).

	P2X1R	P2X2R	P2X3R& P2X2/3R	P2X4R	P2X7R
Antagonists & IC ₅₀ values	Suramin (IC ₅₀ 1-2 μM)	Suramin (IC ₅₀ ~10 μM)	Suramin (IC ₅₀ ~3 μM)	Suramin (IC ₅₀ >300 μM)	Suramin (IC ₅₀ >300 μM)
	NF449 (IC ₅₀ ~0.5 nM)	PPADS (IC ₅₀ ~1-3 μM)	PPADS (IC ₅₀ ~1.5 μM)	PPADS (IC ₅₀ >300 μM)	PPADS (IC ₅₀ 10-45 μM)
	PPADS (IC ₅₀ ~1 μM)	TNP-ATP (IC ₅₀ ~2 μM)	TNP-ATP (IC ₅₀ ~1 nM)	TNP-ATP (IC ₅₀ ~15 μM)	PPNDS (IC ₅₀ 1-10 μM)
	PPNDS (IC ₅₀ ~15 nM)	PSB-1011 (IC ₅₀ ~79 nM)	A-317491 (P2X3R: IC ₅₀ ~97 nM P2X2/3R: ~169 nM)	5-BDBD (IC ₅₀ ~0.5 μM)	MRS2159 (IC ₅₀ ~5 μM)
	TNP-ATP (IC ₅₀ ~6 nM)	PBS-10211 (IC ₅₀ ~86 nM)	RO-4 (IC ₅₀ ~13 nM)	Paroxetine (IC ₅₀ ~2 μM)	A-740003 (rat: IC ₅₀ ~18 nM human: IC ₅₀ ~40 nM)
		NF770 (IC ₅₀ ~19 nM)	RO-51 (IC ₅₀ ~10 nM)	BX430 (IC ₅₀ ~0.5 μM)	A-804598 (IC ₅₀ ~10 nM)
		NF776 (IC ₅₀ ~97 nM)	RO-85 (P2X3R: IC ₅₀ ~30 nM P2X2/3R: ~400 nM)	PSB-12054 (IC ₅₀ ~0.2 μM)	AZ11645373 (human: IC ₅₀ ~90 nM rat: >45 μM)
		NF778 (IC ₅₀ ~140 nM)	Antibody 12D4 (IC ₅₀ ~16 nM)	PSB-12062 (IC ₅₀ ~0.9 μM)	

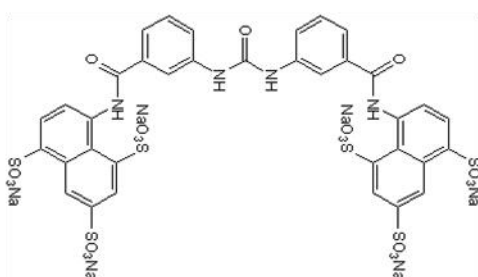
Table 1.4 Antagonists of P2XR subtypes and their IC₅₀ values

References: (Ase et al. 2015, Balázs et al. 2013, Baqi et al. 2011, Brotherton-Pleiss et al. 2010, Buell et al. 1996, Casati et al. 2011, Coddou et al. 2011, Fisher R 2005, Garcia-Guzman et al. 1997, Hernandez-Olmos et al. 2012, Jahangir et al. 2009, Kwon 2012, Lewis et al. 1998, Michel et al. 1997, Nagata et al. 2009, Norenberg et al. 2012, Shcherbatko et al. 2016, Sim and North 2010, Surprenant et al. 1996, Wolf et al. 2011, Wu et al. 2011)

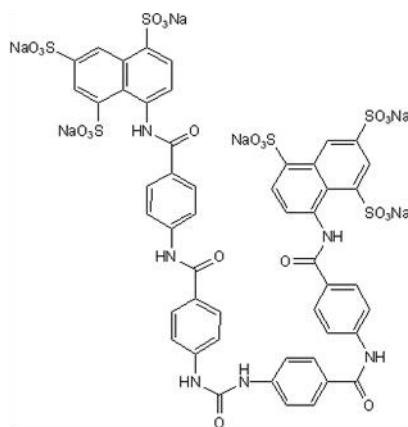
(a)



(b)



(c)



(d)

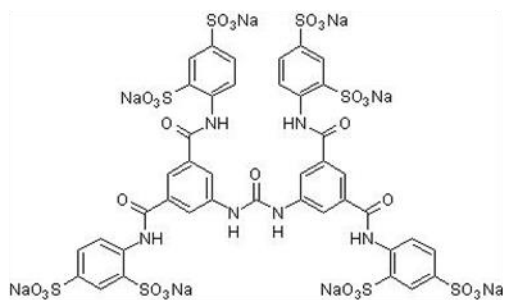


Figure 1.14 Structures of Suramin analogs.
(a) Suramin (b) NF023 (c) NF279 (d) NF449

1.6.3 Mutagenesis studies on suramin and NF449 at the P2X1 receptor

Suramin appears to be a competitive antagonist, and insights into the binding site have come from differences in potency between species variants of P2XR subunits. In initial studies, it was found that the antagonist suramin blocked the hP2X4R (IC_{50} ~178 μ M) with much higher efficiency than the rP2X4R (IC_{50} >500 μ M). A lysine at position 78 was highlighted to be responsible for the different apparent efficiency for suramin. The single-point mutation (Q78K) at the rP2X4R enhanced the suramin affinity by >50-fold without affecting the ATP binding affinity (Garcia-Guzman et al. 1997). However, this was still >100-fold lower than suramin affinity at the hP2X1R (Roberts, 2004), suggesting that other residues also contribute substantially to sensitivity.

Different suramin sensitivity was also found between the mouse and human P2X1Rs. Suramin, at concentration of 10 μ M, had little effect on the response to ATP (10 μ M) at the mouse P2X1R (mP2X1R) while it showed almost complete inhibition at the hP2X1R (Ikeda , Sim et al. 2007). Suramin is a polysulfonate, with six negative charges. Four lysines in the human sequence (K111, K127, K138 and K148) were replaced by neutral or negatively charged residues in the corresponding mouse sequence. It was hypothesized that species differences might result from differences in positive residues presented by the large receptor extracellular domain. The hypothesis was tested by substituting each of the four lysines in the human sequence by their equivalent residues in the mouse and vice versa. Suramin (10 μ M) had little or no effect on the response evoked by 10 μ M ATP at the mP2X1R but it significantly decreased the ATP concentration curve (~40-fold) with the introduction of a lysine at position 138 (E138K). The effect of suramin was similar whether the lysine was introduced alone or in combination with three others. Conversely, suramin caused a 25-fold decrease in ATP potency at the hP2X1R but only 10-fold in the receptor when K138 was replaced by glutamate (K138E) (Sim et al. 2008). These results indicated that the lysine in the cysteine rich head region (K138) was an important contributor to the effectiveness of suramin.

NF449 is an analog of suramin, a polysulfonate with eight negative charges. It is highly selective for the P2X1R subtype ($IC_{50} \sim 0.3$ nM) (Rettinger et al. 2005). The contribution of the positively charged residue (K138) to NF449 inhibition at P2X1Rs were also investigated. Similarly, NF449 had a very small effect at 3 nM ($pEC_{50} \sim 6.4$) at the mP2X1R but it was much more potent to the receptor with E138K ($pEC_{50} \ll 4$). In addition, replacement of the glutamic acid at position 138 with aspartic acid at the mP2X1R resulted in a receptor insensitive to NF449. Conversely, 300 nM NF449 strongly blocked the hP2X1R but had much less effect on the receptor with mutation K138E (Sim et al. 2008). The results indicated that K138 also played an important role in NF449 action at P2X1Rs. However, the full extent of the suramin-binding site is unclear, as is the molecular basis for the high selectivity of NF449 for P2X1Rs. Other residues must also contribute to the antagonist sensitivity.

A further clue to the binding sites of suramin and NF449 came from studies on the *Dictyostelium* P2XRs that are insensitive to suramin. In *Dictyostelium* P2XRs, a cysteine-rich head region of >40 amino acids, including conserved cysteine residues 2-5, is absent, compared to the antagonist sensitive P2X1Rs (El-Ajouz et al. 2012a). Subsequently, a chimeric approach was used to study the contribution of the head region. NF449 was effective in the nanomolar range at the P2X1R but >1000-fold less effective at P2X2Rs (Rettinger et al. 2005). Chimeric receptors where portions of the cysteine-rich loop region of the hP2X1R were replaced by the corresponding regions from the insensitive hP2X2R were generated. The NF449 sensitivity of the P2X1R with the whole head region of the P2X2R decreased ~300-fold compared to that of P2X1Rs. Sub-chimeras made within this region showed that swapping residues between the third and fourth conserved cysteine residues caused a ~1700-fold decrease in NF449 sensitivity. The following site-directed mutagenesis identified a cluster of positively charged amino acids (K136, K138, R139 and K140) that are essential for NF449 sensitivity of P2X1Rs. Mutating these residues to the equivalent residues of the P2X2R (KAKEK-ELDML) caused ~700-fold reduction of NF449 compared to WT P2X1Rs (El-Ajouz et al. 2012a). Similarly, the same mutants at P2X1Rs also caused a ~35-fold decrease in suramin sensitivity ($IC_{50} \sim 70$ μ M) compared to the WT receptor ($IC_{50} \sim 2$ μ M). However, the reciprocal chimera and mutants in the

P2X2R did not show significant increase suramin and NF449 sensitivity. This suggested that the four positively charged residues are important for sensitivity to suramin and NF449 but other variant residues in the binding site remain to be identified.

Chimeras between the hP2X1R and the rP2X4R suggested the contribution of the extracellular ligand binding loop to the action of antagonists (Allsopp et al. 2013). The hP2X1R showed high sensitivity to the antagonists PPADS, suramin and NF449 (IC_{50} ~1 μ M, ~2 μ M and ~1 nM respectively) while the rP2X4R is insensitive to these antagonists (IC_{50} >300 μ M). Chimeras in the extracellular loop between these two P2X subtypes were generated to investigate the antagonist binding sites. There was little or no effect on sensitivity to suramin and PPADS in chimeric P2X1/4Rs (Farmer et al. 2015). However, NF449 sensitivity of the hP2X1R decreased by ~60-fold and ~135-fold in chimeras replacing the cysteine-rich head (133-184) and the dorsal fin region (185-261). Point mutations in these two regions showed that positive charges at the base of the cysteine-rich head region (K136, K138, R139, and K140) and residues T216 and Q231 (P2X1 numbering) are important in NF449 action, which is consistent with previous mutagenesis-based research (El-Ajouz et al. 2012b). The six important residues were used for molecular docking of NF449 at the hP2X1R. The four best potential poses all occupy the cavity under the cysteine-rich head region close to the ATP binding sites. It could prevent the downward motion of the head region to close the ATP binding pocket which is necessary for channel opening (Hattori and Gouaux 2012) (Figure 1.15).

1.6.4 Competitive antagonism of the hP2X3R

TNP-ATP strongly inhibited rP2X3Rs with an IC_{50} value of ~1 nM. Some analogues of TNP-ATP also act as potent antagonists at P2X3Rs (Dal Ben et al. 2017). A-317491 was the first reported P2X3R selective antagonist, with an IC_{50} value of ~97 nM. This compound also inhibited heteromeric P2X2/3Rs (IC_{50} value ~169 nM) but is ineffective at other P2XR subtypes. A-317491 was shown to be potent in attenuating both thermal hyperalgesia and mechanical allodynia after chronic nerve constriction injury (Jarvis et al. 2002).

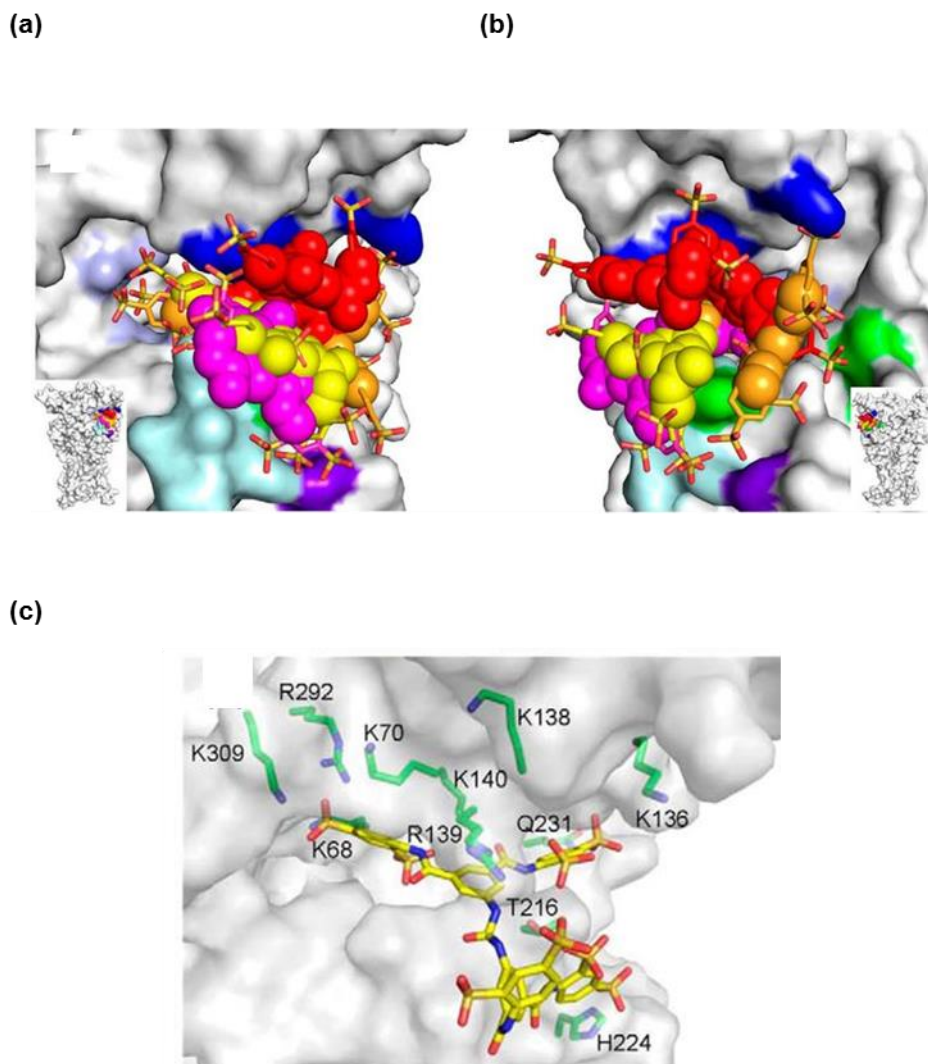


Figure 1.15 Docking poses for the NF449-P2X1 complex.

(a) and (b), overlay of the four docking poses A–D on the P2X1R shown from different angles. The P2X1R is shown in surface representation, highlighting the positively charged residues of the ATP-binding site (K68, K70, R292, and K309) in light blue, the positively charged residues of the cysteine-rich head region (K136, K138, R139, and K140) in dark blue, NF449 poses A (*red*), B (*orange*), C (*pink*), and D (*yellow*) are shown as a mixture of sphere representation (for the core of the poses) and stick representation (for the arms of the poses). All four poses bind to the cleft between the cysteine-rich head region, ATP-binding site, and dorsal fin. (c) snapshot of NF449 from the pose C trajectory. NF449 and residues Lys-68, Lys-70, Lys-136, Lys-138, Arg-139, Lys-140, Thr-216, His-224, Gln-231, Arg-292, and Lys-309 are shown in stick representation. (Images taken from Farmer et al. 2015).

The crystallized hP2X3R in complex with two high affinity P2XR competitive antagonists (TNP-ATP and A317491) has been published recently. In the structure of the antagonist-bound state, both ATP and the antagonists occupy the orthosteric ligand-binding pocket located at the interface between two subunits. The ion channel pore is in the closed state. Compared to ATP, the antagonist sits deeper in the binding cleft. Both TNP-ATP and A-317491 bind in a Y-shape, with the trinitrophenyl moiety of TNP-ATP and the phenoxy-benzyl moiety of A-317491 acting as the 'trunk'. The trunk from the antagonist forms hydrophobic interactions with F174. TNP-ATP makes important interaction with K65, D158, T172, F174, N279, R281 and K299. D158 and F174, which are not conserved among all P2XR family members but both are present in P2X1Rs and P2X3Rs (Mansoor et al. 2016) (Figure 1.16), suggesting they may account for its high potency at P2X1 and P2X3Rs.

By occupying the space in the cleft between the two subunits, the antagonists prevents ATP-induced upward movement of the dorsal fin to close the binding cleft, precluding the conformational changes necessary for channel opening. The structure is nearly identical to the apo state structure.

1.6.5 Structural basis for selective P2X7 antagonism

Several new compounds have been introduced as potent P2X7R antagonists. A-740003 (N-(1-[[[(cyanoimino) (5-quinolinylamino) methyl] amino-2, 2-dimethylpropyl)-2-(3, 4-dimethoxyphenyl)aceta-mide) had an IC₅₀ value of ~40 nM for human and ~18 nM for rat. It showed weak or no activity (IC₅₀ >10 μM) at other P2XRs. This selective blockade of P2X7Rs has been demonstrated to produce significant antinociception in an animal model of neuropathic and inflammatory pain. A-804598 (2-cyano-1-[(1S)-1-phenylethyl]-3-quinolin-5-ylguanidine) represents a structurally novel, competitive and selective antagonist that has equivalent high affinity at P2X7Rs (IC₅₀ ~10 nM) (Donnelly-Roberts et al. 2009). It is important to note that these antagonists are not selective between rat, mouse and human P2XRs. A selective and potent antagonist of hP2X7R was characterized, AZ11645373 (3-[1-[[[(3'-Nitro [1, 1'-biphenyl]-4-yl) oxy] methyl]-3-(4-pyridinyl) propyl]-2, 4-thiazolidinedione). It inhibited the hP2X7R with IC₅₀

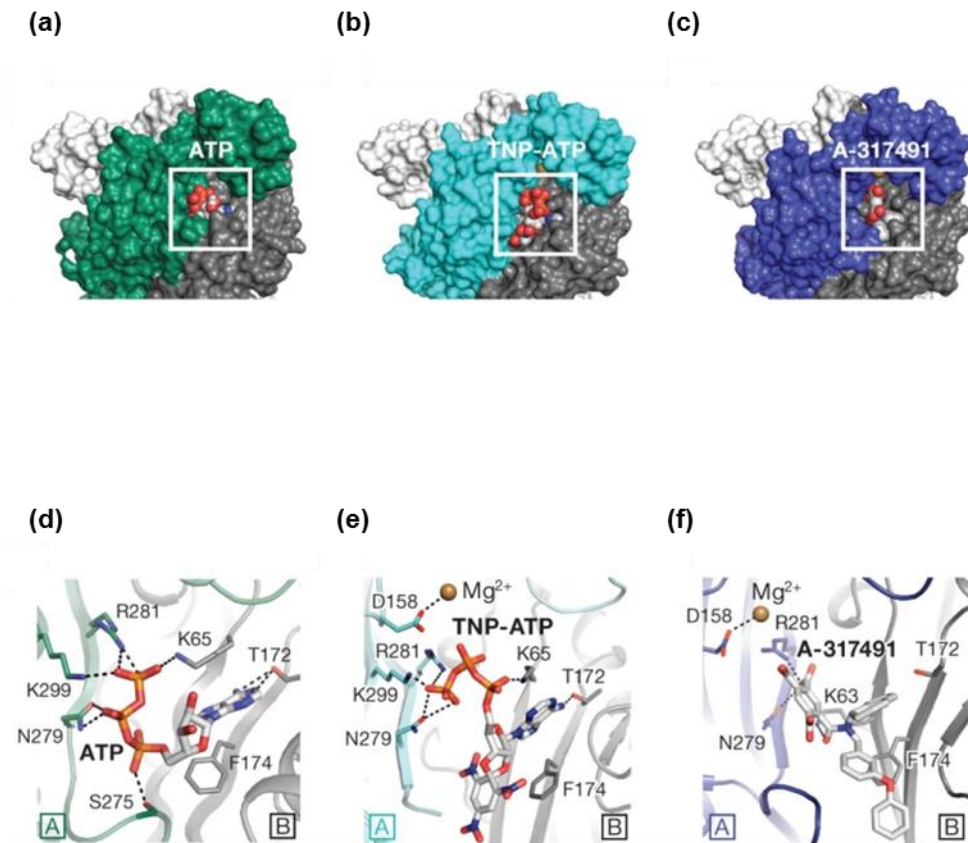


Figure 1.16 The competitive antagonist binding site at the hP2X3R.

a–c, Surface representation of the binding pocket for **(a)** the ATP-bound, open state, **(b)** the TNP-ATP-bound, closed state, and **(c)** the A-317491-bound, closed state of hP2X₃. **d–f,** The binding pocket showing key interactions made by **(d)** ATP, **(e)** TNP-ATP, and **(f)** A-317491. ATP-binding residues make interactions with TNP-ATP and A-317491 (Images taken from Mansoor et al. 2016).

value of ~90 nM but was >500-fold less effective at inhibiting rP2X7Rs with less than 50% inhibition occurring at 10 μ M (Stokes et al. 2006). Recently, it was reported that nanobodies (small, single-domain antibody fragments) highly selectively and effectively blocked mP2X7Rs. The small molecule P2X7 antagonist is currently in clinical development (Danquah et al. 2016).

The crystal structure of the panda P2X7R (pdP2X7R) in the antagonist bound state was published. In order to optimize the crystallization, the pdP2X7R was truncated, with deletions of 1-21 amino acids in N-terminal, 360-600 amino acids in C-terminal and five mutations (N241S/N284S/V35A/R125A/E174K). A single subunit of the P2X7R resembles that of zfP2X4 (45% identical to pdP2X7) (Hattori and Gouaux 2012, Kawate et al. 2009) and the hP2X3R (38% identical to pdP2X7) (Mansoor et al. 2016). The truncated pdP2X7R exhibited slower deactivation and no obvious current facilitation (run-up) after repeated ATP applications. The pdP2X7R in the apo state represents a closed conformation but with a larger allosteric pocket and larger central vestibule. The transmembrane helices are similar and the channel gate is at residues G338, S339 and S342, compared to the closed state structure of zfP2X4. The antagonist-bound P2X7R structures represent the same closed conformation, indicating these drugs likely stabilize a resting closed state. The binding site for P2X7R specific inhibitors were demonstrated that those inhibitors bind at an allosteric site at the subunit interface behind the ATP binding site to stop conformational changes associated with P2X7R activation (Karasawa and Kawate 2016).

The drug binding pocket

The five structurally distinct antagonists they used were A740003 (Honore et al. 2006), A804598 (Donnelly-Roberts et al. 2009), AZ10606120 (Michel et al. 2007), GW791343 (Michel et al. 2008a, Michel et al. 2008b), and JNJ47965567 (Bhattacharya et al. 2013). It was shown that all five tested drugs are allosteric and non-competitive inhibitors. Interestingly, the structure showed that all five structurally unrelated compounds bind in the same pocket formed between neighbouring subunits, which is behind the ATP-binding pocket (Figure 1. 17a). This drug-binding pocket is surrounded by thirteen residues mainly from β -

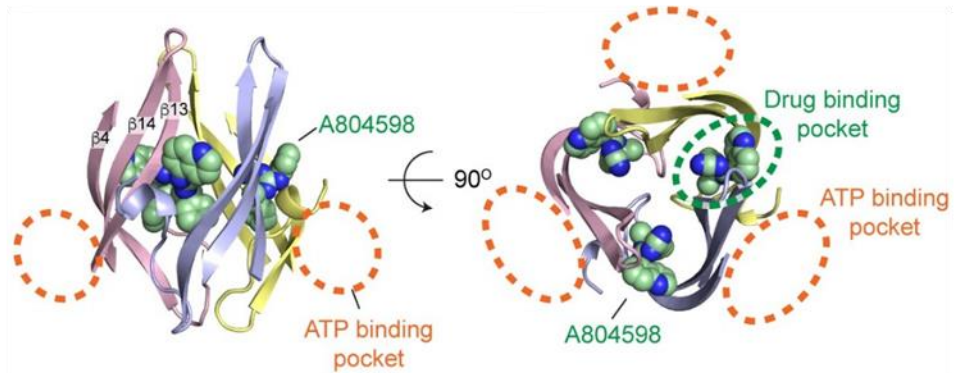
strands (β 4, β 13 and β 14) in the upper body domains of the neighbouring subunits. Drug binding seems to be mediated mainly by hydrophobic interactions, especially at positions deep within the cavity, involving F95, F103, M105, F293 and V312 (Karasawa and Kawate 2016).

The equivalent pocket in the P2X4R is too narrow to accommodate the smallest P2X7 antagonist, A804598, even though it is similarly hydrophobic to that of the pdP2X7R. It suggested that the differences in the size of the inter-subunit hydrophobic pocket is the major factor that confers P2X7 specific binding of the inhibitors. Consistent with the crystal structure, the mutants, F88A, F95A, F103A, M105A, F108A and V312A showed increased IC_{50} values, supporting that these residues play important roles in drug binding. In particular, interaction with F103 is crucial for the inhibitory action of all five drugs (Karasawa and Kawate 2016).

Conformational changes

Compared to the zfP2X4R and hP2X3R, the inter-subunit cavity formed by β 13 and β 14 in the upper body domain is much wider in the pdP2X7R (Mansoor et al. 2016). In their studies, cysteine mutagenesis and a large cysteine-reactive agent MTS-TPAE (Mw: 447) were used to investigate the involvement of the inter-subunit cavity. It was hypothesized that modification of a cysteine residue with a bulky moiety should interfere with the conformational changes necessary for channel opening, thereby resulting in diminished channel activity. When MTS-TPAE was applied in the absence of ATP, four cysteine mutants (F103C, K110C, T308C and I310C) showed irreversible current reduction. It suggested that the covalently bound MTS-TPAE at these positions hinders the conformational changes required for channel opening. When MTS-TPAE was applied in the presence of ATP, none of the cysteine mutants presented significant current reduction. It suggested that at least the four residues in the drug-binding pocket are more accessible to MTS-TPAE in the closed state than in the open state. It indicated that the drug-binding pocket narrows upon ATP binding. MTS-TPAE application either in the presence or absence of ATP did not exhibit current reduction for cysteine mutants of the counterpart residues

(a)



(b)

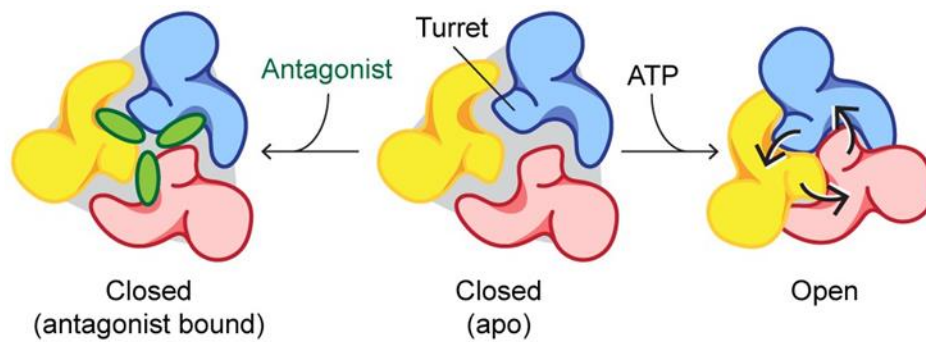


Figure 1.17 The binding sites for selective P2X7 antagonists and the conformational changes in different states (a) Side view of the upper body domains exhibiting A804598 binding sites with respect to the ATP-binding pockets (orange dashed lines) (left). Top view of the apo pdP2X7 structure with respect to the ATP-binding pockets (orange dashed lines) and one of the drug-binding pockets (green dashed line) (right) **(b)** Schematic representations of the P2X7R viewed from the top. Each color represents a different subunit. The drug-binding pocket and the allosteric binding pocket narrow during channel activation. (Image taken from Karasawa and Kawate 2016)

in the P2X4R, suggesting that narrowing of the inter-subunit space seems unique to the P2X7R (Karasawa and Kawate 2016). This also explained the mechanism of the P2X7 subtype-specific antagonism.

It was proposed that the narrowing of the allosteric binding pocket in body domain of the P2X7R shrinks during activation. This motion allows the lower body domain to widen further. In the antagonist-bound state, the allosteric binding pocket was locked without shrinking. The accompanying movement of the pore-lining transmembrane helices was stopped and insufficient for channel opening. Therefore, the narrowing of the allosteric pocket seems to be crucial for full-widening of the lower body domain, which is necessary for channel opening (Figure 1.17b).

This finding was consistent with chimeras and mutagenesis studies which also suggested that AZ10606120 works in allosteric binding sites because mutations of individual residues around the orthosteric site did not destroy AZ10606120 binding. Both studies identified a new, largely hydrophobic allosteric binding site in the P2X7R. The proposed mechanism for allosteric inhibition, the shrinking of the allosteric pocket required for activation can be blocked by binding of AZ10606120 is in full agreement with the X-ray structures (Allsopp et al. 2017). It suggested that a combination of mutagenesis and modelling is able to make accurate predictions on the site of drug action supported by crystal structures.

1.7 Antagonism of PPADS

1.7.1 PPADS actions at P2XRs expressed in native tissues

Pyridoxal-phosphate-6-azophenyl-2', 4'-disulfonate (PPADS) is one of the most commonly used P2XR antagonists. PPADS was first proposed as a P2XR antagonist in 1992. It was found that PPADS (1-10 μM) inhibited contractile responses to α , β -MeATP in the rabbit vas deferens, with no antagonist action at α_1 -adrenoceptors, muscarinic M2 and M3 receptors, histamine H1 and adenosine A1 receptors (Lambrecht et al. 1992). Subsequent studies described the antagonistic action of PPADS in other native smooth muscles. In the rabbit urinary bladder detrusor muscle, PPADS (1-30 μM) caused concentration-

dependent inhibition to P2XR-mediated contractions without affecting contractions mediated via muscarinic receptors. The pD_2 value (negative log EC_{50}) for α , β -MeATP was ~ 6.5 . In the presence of PPADS at concentrations of 1, 3, 10, 30 μM , the pD_2 values were significantly different from control, being respectively ~ 6.2 , ~ 5.2 , ~ 4.8 (Ziganshin et al. 1993). In rabbit isolated ear and saphenous artery, contractions evoked by α , β -MeATP were concentration-dependently inhibited by PPADS (1-30 μM) without influence on the contractile responses to noradrenaline and histamine (Ziganshin et al. 1994). In guinea-pig isolated vas deferens, PPADS (30 μM) inhibited the contractions 50% evoked by sympathetic nerve stimulation and exogenous α , β -MeATP, without affecting the responses to exogenous noradrenaline, carbachol or histamine (McLaren et al. 1994). As P2XRs are widely expressed, the actions of PPADS at other native tissues were investigated. For example, in the central nervous system, PPADS (0.5-10 μM) inhibited ATP-activated current in bullfrog dorsal root ganglion (DRG) neurons ($IC_{50} \sim 2.5 \mu M$) (Li 2000).

1.7.2 PPADS action at recombinant P2XR subtypes

P2XRs antagonised by PPADS in initial studies were on native receptors in smooth muscles, which we now know correspond to P2X1Rs. Studies on recombinant P2XRs (P2X1-P2X7) showed that PPADS antagonism was dependent on subtypes (Table 1.4). PPADS was most effective at P2X1Rs, with an IC_{50} value $\sim 1 \mu M$ (Evans et al. 1995). PPADS antagonized recombinant P2X2, P2X3 and P2X5Rs with an $IC_{50} \sim 3 \mu M$ (Evans et al. 1995, Lewis et al. 1995, Wildman et al. 2002) whereas it was less effective at P2X6Rs ($IC_{50} \sim 30 \mu M$) (Jones et al. 2004) and P2X7Rs ($IC_{50} \sim 45 \mu M$) (Surprenant et al. 1996). The rP2X4R was insensitive to PPADS with an $IC_{50} > 500 \mu M$ (Buell et al. 1996). It was found that PPADS, at high concentration of 100 μM , inhibited $\sim 20\%$ of the current at rP2X4Rs and the inhibition developed (30s) and washed out (2 min) rapidly (Buell et al. 1996). It was strikingly different from the PPADS antagonistic action at P2X1 and P2X2Rs, with a slower time course of onset (5-10 min) and reversal (15-20 min) (Evans et al. 1995). Interestingly, the hP2X4R showed intermediate sensitivity to PPADS ($IC_{50} < 30 \mu M$) (Garcia-Guzman et al. 1997). Use of chimeras and point mutants identified some important regions contributing

to the differences in PPADS effects between different P2X4R species, which are discussed in detail in Chapter 4.

1.7.3 PPADS action at P2Y receptors

In initial studies, PPADS (30 μM) was shown to have an effect on P2YR mediated responses in native tissues, for example in vascular smooth muscles (Ziganshin et al. 1994). PPADS, at high concentrations (3-100 μM), inhibited P2YR mediated responses in bovine aortic endothelial cells (Brown et al. 1995) and in guinea-pig taenia coli and rat duodenum (Windscheif et al. 1995). The different inhibitory actions of PPADS to P2YRs may result from various species or different P2YR subtypes. After the different human P2YR subtypes were cloned, PPADS was used to investigate their pharmacological profile. PPADS showed high potency on P2Y1Rs, with IC_{50} value of 4-12 μM . It can also partially inhibit P2Y4, P2Y6 and P2Y13Rs (Table 1.5) (von K ugelgen and Hoffmann 2016).

Receptor	PPADS (IC_{50})	References
P2Y1R	4-12 μM	(Windscheif et al. 1995)
P2Y2R	-(30 μM)	(Charlton et al. 1996b)
P2Y4R	30% (100 μM)	(Charlton et al. 1996a)
P2Y6R	69%(100 μM)	(Robaye et al. 1997)
P2Y11R	-(100 μM)	(Communi et al. 1999)
P2Y12R	-(100 μM)	(von Kugelgen and Harden 2011)
P2Y13R	50% (10 μM)	(Marteau et al. 2003)

Table 1.5 IC_{50} values of PPADS at P2YRs.

1.7.4 Structure and analogues of PPADS

The PPADS molecule consists of a phosphate moiety and two polysulfonates. It contains four negative charges, two on the phosphate moiety and one on each of the two polysulfonates (Figure 1.18a). Some analogues of PPADS have been investigated to evaluate the importance of structural elements for inhibition. In order to develop more potent and selective antagonists for P2XR subtypes, a series of PPADS analogues have been synthesized based on its structure.

Iso-PPADS is an isomer of PPADS with the sulphonic acid group at the 5'- instead of the 4'- position on 6-azophenylpyridoxal 5-phosphate (Figure 1.18b). IsoPPADS (10 μ M) significantly depressed depolarizations of rat superior cervical ganglion (by $43 \pm 6\%$) evoked by α , β -Me-ATP (100 μ M), which showed a similar degree of antagonism with PPADS. It suggested that the position of the sulphonic acid group is not particularly critical for the antagonistic activity of PPADS (Connolly 1995).

Pyridoxal-5'-phosphate (P5P) is a precursor of PPADS, with 6-azophenyl disulphonic acid removed (Figure 1.18c). P5P still had antagonistic activity at P2XRs but the potency was ~ 10 -fold weaker compared to PPADS (Connolly 1995). This indicated that the pyridoxal-5'-phosphate moiety is partly responsible for PPADS antagonism but the addition of the 6-azophenyl-disulphonic acid moiety markedly enhanced its potency.

MRS 2220 (Cyclic pyridoxine- α^4 , 5'-monophosphate-6-azophenyl-2', 5'-disulfonic acid) (Figure 1.18d), in which the phosphate group was cyclized by esterification to a CH₂OH group at the 4-position, was found to be ~ 10 -fold less potent ($IC_{50} \sim 10\mu$ M) than PPADS at P2X1Rs (Jacobson et al. 1998) but more selective to P2X1Rs. MRS 2220 showed less efficiency on rP2X3Rs ($IC_{50} \sim 58\mu$ M) and no effect on rP2X2Ps, P2X4Rs, P2YRs and adenosine receptors (Jacobson et al. 1998). It suggested the aldehyde group is not necessarily required for the inhibitive action of PPADS.

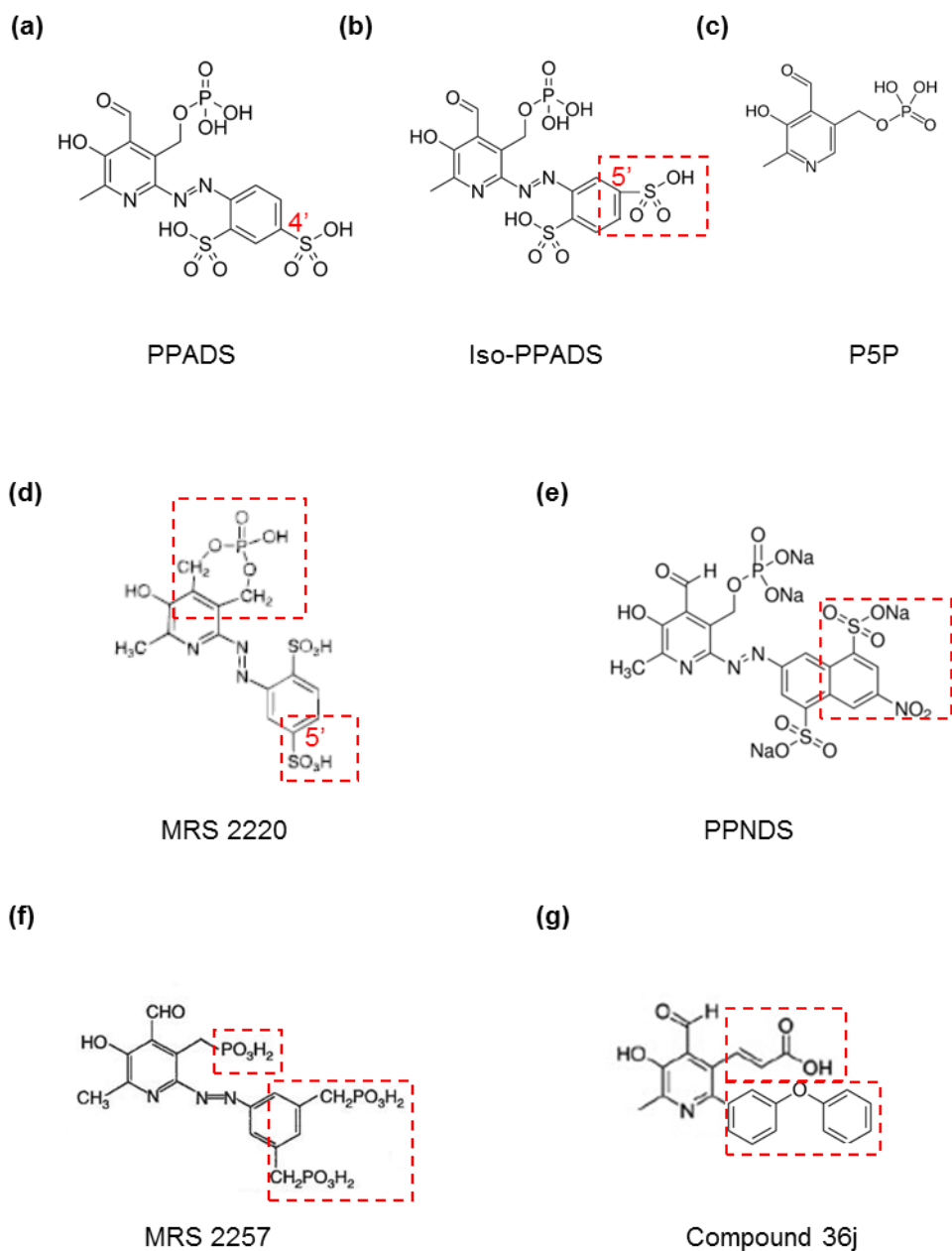


Figure 1.18 Chemical structure of PPADS and a series of analogues
(a) PPADS (b) Iso-PPADS (Connolly 1995) **(c) P5P** (Connolly 1995) **(d) MRS 2220** (Jacobson et al. 1998) **(e) PPNDS** (Lambrecht et al. 2000) **(f) MRS 2257** (Brown et al. 2001) **(g) Compound 36j** (Cho et al. 2013) Red boxes indicate structural changes compared to PPADS.

PPNDS (Pyridoxal-5'-phosphate-6-(2'-naphthylazo-6'-nitro-4', 8'-disulfonate), made with modifications on sulfophenyl ring based on PPADS (Figure 1.18e), was shown to be a more (~6-fold) potent than PPADS at P2X1Rs (Lambrecht et al. 2000). It was selective for P2Rs, especially for P2X1Rs (vs. P2Y1 ~52 fold) (Lambrecht et al. 2000) but its potency at other P2R subtypes is unknown.

MRS 2257 (Pyridoxal-5'-phosphonate 6-azophenyl 3',5'-bismethylenephosphonate), with a 5'-phosphate group replaced with 5'-phosphonate group and the disulfonate groups removed from azophenyl moiety (Figure 1.18f), showed ~14-fold (IC_{50} ~5 nM) and ~10-fold (IC_{50} ~22nM) more potency than PPADS at P2X1 and P2X3Rs respectively (Brown et al. 2001).

Another optimized compound modified by the replacement of the unstable azo (-N=N-) linker with stable carbon-carbon linkers and substitutions with 4-carboxaldehyde, 3-propenoic acid and bulky hydrophobic aromatic groups at the 2-position (Figure 1.18g) was more potent (IC_{50} ~60 nM) and selective to hP2X3Rs. The antagonist was also shown to significantly inhibited pain signalling in the rat dorsal horn, suggesting that it may be developed as a potential pain modulator targeting P2X3Rs (Cho et al. 2013). These effective PPADS analogues suggested that PPADS can be used as a template to design a series of P2XR selective antagonists.

1.8 Aims and Objectives

The aim of the thesis was to determine the molecular basis of antagonism of PPADS at the hP2X1R. The contribution of residues in the extracellular loop to PPADS binding at the receptor was investigated. Cysteine scanning mutagenesis and following accessibility and sensitivity tests were used to explore the PPADS binding site. (i) Accessibility changes following PPADS binding gave prediction of residues involved in PPADS binding or and/or conformational changes during PPADS. (ii) PPADS sensitivity tests on these residues where access was PPADS sensitive distinguished those directly contributing to PPADS binding from those involved in conformational changes. Furthermore, combinations of mutants and modifications on mutants were used to further

characterize PPADS binding pocket. At last, molecular docking was used to predict the promising PPADS binding poses at the hP2X1R.

PPADS is a general antagonist which can work at most P2XR subtypes. Defining PPADS binding site at the hP2X1R would help docking of PPADS to other P2XR subtypes. By comparing differences of side chains of the residues in PPADS binding site in each P2XR subtypes, a series of PPADS analogues can be generated by modifying chemical groups of the PPADS molecule. Therefore, understanding the nonselective antagonism of PPADS would help develop novel P2XR subtype selective antagonists with potential treatment for various diseases.

Chapter 2. Materials and methods

2.1 Molecular Biology

2.1.1 The human P2X1 receptor

The Wild Type (WT) hP2X1R complementary DNA (cDNA) had previously been used in the laboratory. The hP2X1 cDNA was originally cloned from the human bladder (Ennion et al. 2000). The cDNA was used as a template in Polymerase Chain Reactions (PCR) and the PCR product was cloned into a pcDNA3.1 plasmid (Figure 2.1, Invitrogen, Paisley, UK). The plasmid contains an Ampicillin resistance gene, T7 promoter and a *MluI* restriction enzyme site. The Ampicillin resistance gene allows for selection of this plasmid in *E.coli*. The T7 promoter facilitates the formation of RNA. T7 RNA polymerase is very active enzyme, which synthesizes RNA at a rate several times that *E. coli* RNA polymerase and it terminates transcription less frequently. T7 promoter is highly selective for initiation of RNA polymerase at its own promoter sequences and the transcription can circumnavigate a plasmid, resulting in RNA several times the plasmid length in size (Tabor 1990). The *MluI* site linearizes the plasmid to increase the yield of messenger RNA (mRNA) for injecting into *Xenopus laevis* oocytes. The vector had been modified to contain a poly (A) tail adjacent to the 3'-untranslated region of the cloned P2X1 cDNA (Ennion and Evans 2002a). The poly (A) tail protects the resulting mRNA from exonucleases.

2.1.2 Site-directed mutagenesis

Many of the cysteine point mutations were made in the lab previously using the hP2X1R plasmid as the template (Ennion et al. 2000, Jonathan A Roberts et al. 2012, Roberts et al. 2009a). For those not available, they were generated using oligonucleotide primers. Primers were designed to substitute the original amino acid with cysteine using the program PrimerX (www.Bioinformatics.org/primerx). The program optimized primer design and provided the melting temperature (T_m), the GC base content, and the primer length. An example shown below is the mutant Q237C.

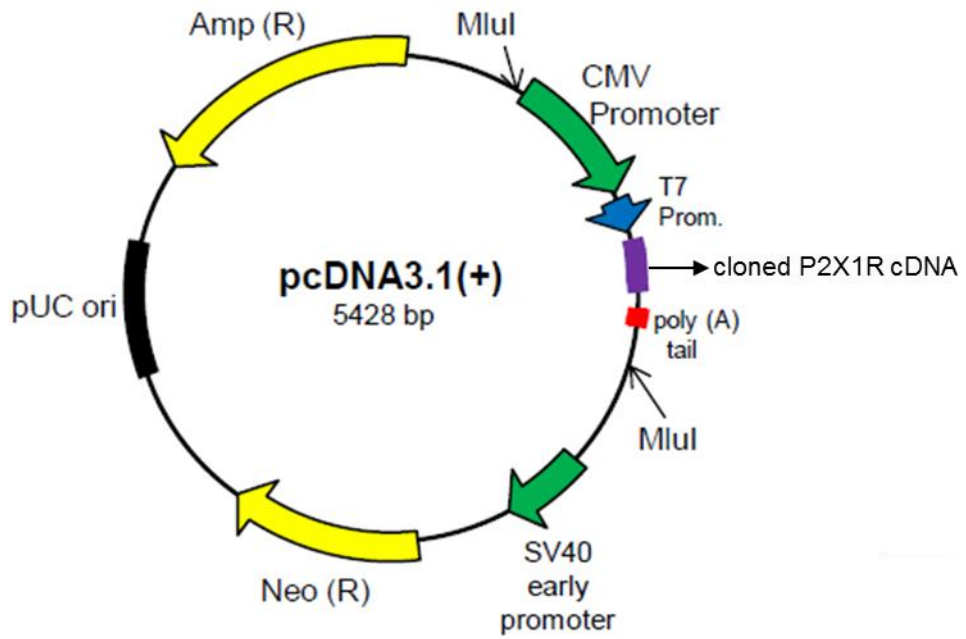


Figure 2.1 Map of the pcDNA3.1 Plasmid.

The Ampicillin resistance gene is for selection of the plasmid in *E.coli*; The T7 promoter is for efficient protein expression; The *MluI* site is for linearizing the plasmid; The poly (A) tail is for protecting the mRNA from exonucleases (Image taken from El-Ajouz,2002).

Q (CAA/CAG) → C (TGT/TGC):

Forward primer for Q237C:

5' CTTGGCTACGTGGTGTGTGAGTCAGGCCAGAAC 3'

The bases in the red box indicates the coding of the cysteine.

Reverse primer for Q237C:

5' GTTCTGGCCTGACTCACACACCACGTAGCCAAG 3'

The bases in the red box indicates the complementary coding of the cysteine.

GC content: 57.58% Location: 694-726

Melting temp: 75.8°C Mismatched bases: 3

Length: 33 bp Mutation: Substitution

The primers were ordered from Sigma and were reconstituted to a stock concentration of 1 nmol/μl. Then they were diluted to a working concentration of 10 pmol/μl with sterile milliQ water. The point mutations were introduced into the hP2X1R plasmid using the QuikChange™ mutagenesis kit (Stratagene, La Jolle, CA, USA). The PCR reaction came to a final volume of 50 μl as follow:

40.5 μl nuclease free water

5 μl of 10X Pfu reaction buffer

1 μl of template (50 ng/μl)

1 μl of Forward primer (125 ng)

1 μl of Reverse primer (125 ng)

0.5 μl of NTP mix

1μl of Pfu Turbo DNA polymerase (2.5 U/μl)

The reactions were carried out in a Techne Genius thermocycler with the following parameters:

Denaturation 95°C for 3 minutes

Denaturation 95°C for 30 seconds

Annealing 55°C for 60 seconds

Extension 68°C for 16 minutes

4°C on hold

} 16 cycles

The PCR products were run on a 1% agarose gel (50 ml TAE buffer, 0.5 g agarose) to check the molecular weight of the PCR products. The gel was

stained using 2 µl ethidium bromide (EB). EB can intercalate between DNA pair bases with a fluorescent tag, which enables the DNA fragments to be seen with a UV light. 6 µl of the products were loaded onto the gel with 2 µl of loading buffer (5X blue juice, Bionline Ltd., U.K.) and run at 80 V for 30 minutes. The molecular weight marker used to quantify the bands was the DNA ladder Hyperladder™ I (Bionline Ltd., U.K.). The gel was visualised on a UV light box to see the molecular weight of the PCR products. If the PCR failed, only the primer dimer bands would be detectable.

In order to remove the hP2X1R plasmid template, 1 µl Dpn1 (Stratagene, Agilent Technologies) was added to each PCR product for digestion and incubated for 1 hour at 37°C. The restriction enzyme Dpn1 specifically digests methylated DNA but not the new mutant synthetic DNA generated which is not methylated. The plasmid DNA was then ready to be transformed into supercompetent cells. Then the DNA was isolated, which is shown in detail in section 2.1.4.

2.1.3 Combination of mutants

For the generation of double cysteine mutants, the DNA of the hP2X1R with a single mutant was used as the template and then a second mutant was added by PCR. For example, the generation of the double mutants K249C+G123C, the template used was the DNA of hP2X1R with G123C mutant and Primer used was the DNA with K249C mutant. For the triple mutants, the template used was the DNA with the double mutants and Primer for the additional single mutant. The PCR was set up as for the single mutant, which is described in section 2.1.2.

2.1.4 Transformation and DNA Extraction

The mutated DNA was transformed into XL-1 Blue supercompetent cells (Stratagene, Agilent Technologies). 1 µl of DpnI treated PCR product was added to 25 µl of XL-1 Blue supercompetent cells in a cooled Falcon tube and mixed by gentle flicking and incubated on ice for 30 minutes. The cells were then heat shocked in a 42°C water bath for 45 seconds and then incubated on ice for 2

minutes. 0.25 ml of Super Optimal broth with Catabolite repression (SOC) medium (Invitrogen®) was added to each tube of the cells in sterile conditions. The tubes were then incubated at 37°C in a shaking incubator at 250 rotations per minute (rpm) for 1 hour. 50 µl of cells in the SOC medium were then spread onto LB agar (LB, Broth with agar (Lennox), SIGMA, Dorset, UK) plates (1 tablet per 50 ml) containing 50 µg/ml Ampicillin. The plates were incubated overnight in a 37°C incubator. Only cells containing the pcDNA3.1 vector with the ampicillin resistance gene could grow.

The next day two distinct colonies were picked from each plate using a sterile pipette tip and each colony was placed into an individual 30 ml tube (Sterilin Ltd., U.K.) containing 6 ml of LB broth and 100 µg/ml of ampicillin. These were incubated overnight in a shaking incubator at 37°C, 250 rpm.

The following day, if there was evidence of growth (cloudy solution), 0.5 ml of the culture was placed into an Eppendorf tube and was spun down for 2 minutes at 13000 rpm. Then the supernatant was removed and 0.5 ml of LB/glycerol mix (0.5 ml of LB broth and 0.125 ml of glycerol) was added into the tube. The glycerol stocks were then stored in the -80°C freezer for future use.

The remainder of the culture was centrifuged for 7 minutes at 4000 rpm at 4°C. The pellet was processed using a miniprep kit (Wizard plus SV miniprep kit, Promega®), which isolated the plasmid DNA from other genomic DNA and bacterial proteins. The final product was dissolved in 100 µl of nuclease free water. The DNA was quantified using a nanodrop spectrophotometer (Labtech International). The concentration of the DNA was normally between 100 to 300 ng/µl.

2.1.5 DNA Sequencing

The DNA was sent for sequencing to check the correct mutations and absence of coding errors in the P2X1 mutant constructs. The sequencing was performed by the Protein and Nucleic Acid Chemistry Laboratory (PNACL), University of Leicester. The sequence was analysed using Seqman II software (DNASTAR).

2.1.6 mRNA synthesis

Once the DNA was correctly sequenced, the incorporation of the mutant and lack of other changes was confirmed. The DNA was linearized in a digest containing 86 μ l of DNA, 10 μ l of buffer H and 4 μ l of *Mlu*-1 enzyme at 37°C for 4 hours. 5 μ l of 10% SDS and 1 μ l of proteinase (20 mg/ml) were added into the linearized product and incubated at 50°C for 1 hour to remove any residual RNAs and transcription inhibitors. DNA was extracted with Phenol/Chloroform/Isoamyl (25:24:1) and precipitated overnight at -20°C in 2X volume of 100% ethanol. The following day this was centrifuged at 13000 rpm for 1 hour at 4°C and washed with 1 ml of 70% ethanol. Ethanol was removed from the pellet and dried at 50°C for 2 minutes to completely evaporate ethanol. The DNA was resuspended in 6 μ l DNAase free water.

The mMessage mMachine T7 kit (Ambion) was used to synthesise mRNA. 10 μ l of 2X ribonucleic mix (2X NTP CAP), 2 μ l of Reaction Buffer and 2 μ l of T7 polymerase enzyme mix were added to 6 μ l of the linear DNA and incubated at 37°C for 2 hours. 1 μ l of Turbo DNaseI was added and incubated at 37°C for 15 minutes to remove residual template DNA. 30 μ l of lithium chloride was added and stored overnight at -20°C to precipitate RNA and remove any residual nucleotides and proteins. The following day the mRNA pellet was centrifuged at 13000 rpm at 4°C for 1 hour and washed with 1 ml of 70% ethanol. Ethanol was removed and the pellet was dried at 50°C for 1-2 minutes until all the ethanol was removed. The mRNA was resuspended in 2-4 μ l of nuclease free water and quantified using a nanodrop spectrophotometer. RNA was finally diluted to a final concentration of 1 μ g/ μ l.

2.2 Expression in *Xenopus laevis* oocytes

Xenopus laevis oocytes are a convenient expression system for robust screening of ion channels with both electrophysiological and biochemical methods. They allow efficient translation of RNA, resulting in the expression of many P2XRs and the detection of large currents (Buckingham et al. 2006). *Xenopus laevis* should be housed in a temperature-controlled environment at approximately 20°C. In addition, the frogs should be maintained in a constant

light-dark cycle of 12 hour each. *Xenopus* are freshwater frogs that prefer stationary water. The water need to be purified as the frogs are sensitive to both chlorine and chloramine in tap water (Goldin 1992).

According to UK home office regulations and in compliance with Animals Scientific Procedures Act 1986, the frogs were humanely killed using a schedule 1 method, which is by overdose of the anesthetic agent MS222 (1 g/l) followed by destruction of the brain before return to consciousness. Stage V oocytes were extracted from *Xenopus laevis* frogs. They can be easily identified at this stage as they are clearly split into a dark brown animal half and a yellow vegetal half (Rasar and Hammes 2006). Lobes of oocytes were cut into small clumps and digested with 1 mg/ml collagenase in OR2- solution (82.5 mM NaCl, 2.5 mM KCl, 1 mM MgCl₂, 5 mM HEPES) for 20-30 minutes until manual defolliculation was easy. Oocytes were washed with OR2- solution for oocyte isolation and then washed with Barth's solution (88 mM NaCl, 1 mM KCl, 0.41 mM CaCl₂, 0.33 mM Ca(NO₃)₂, 1 mM MgSO₄, 2.4 mM NaHCO₃, 10 mM HEPES). Oocytes were kept in Super Barth's solution which is Barth's solution with added Na pyruvate (100 mM), gentamycin (50 mg/ml) and tetracycline hydrochloride (50 mg/l). An Inject + Matic microinjector (J. Alejandro Gaby, Geneva, Switzerland) was used to inject 50 ng of cRNA into the oocytes. Oocytes were used 3-7 days later. The Super Barth's solution was changed daily.

2.3 Treatment of oocytes and sample preparation for MTSEA-biotinylation

Oocytes injected with WT or mutant receptor mRNA were divided into two equivalent groups (7-10 oocytes in each group) labelled as apyrase or PPADS group respectively. Oocytes in the apyrase group were pre-incubated in 0.5 ml of ND96 (96 mM NaCl, 2 mM KCl, 5 mM Na pyruvate, 1 mM MgCl₂, 1.8 mM CaCl₂, 5 mM HEPES, pH7.6) with added 15 U/ml apyrase (SIGMA, Poole, UK) and those in the PPADS group were pre-incubated in ND96 with 100 µM PPADS (Cayman, MI, USA) for 10 minutes. 100 µM MTSEA-biotin (BIOTIUM, Cambridge, UK) was applied to the oocytes in the two conditions for 90 seconds. After the oocytes were washed 3 times with the preincubation solutions, they were placed in 1.5 ml Eppendorf tubes and the excess liquid was removed. Oocytes were lysed with

100 µl Buffer H (100 mM NaCl, 20 mM TrisCl, 1% Triton-100, pH7.4, 10 µl/ml, Proteinase Inhibitor Cocktail was added before use) per tube and pipetting with a 200 µl pipette. After vortexing, the samples were left on the ice for 10 minutes and then were centrifuged at 4 °C for 5 minutes at 13000 rpm. The supernatant samples were pipetted to new Eppendorf tubes and 15 µl was removed, to act as the total sample, and placed in the freezer. 200 µl Buffer H and 50 µl Streptavidin agarose beads (Life Technologies, Paisley, UK) were added to the remaining samples labelled as biotin sample and were rolled at 4°C overnight to allow the protein bound by MTSEA-Biotin to bind to the beads. The next day, the beads were washed 5 times with 0.5 ml Buffer H per wash and spun for 5 minutes between each wash to isolate the proteins bound by MTSEA-Biotin. Both total and biotin samples had 25 µl and 15 µl SDS sample buffer (0.18 M Trisbase, 5.7% SDS, 29% Glycerol, 0.003% Bromophenol Blue, pH 6.8, 5% β-mercaptoethanol added immediately prior to use) added respectively and were heated at 95°C for 5 minutes. Samples were vortexed and spun down for 5 minutes 13000 rpm and they were then loaded on gels.

2.4 Western blotting

Samples (15 µl for each lane) were loaded on the Stacking Gel (5% Acrylamide, 375 mM Tris (pH 6.8), 0.1% (w:v) SDS, 0.1% (w:v) Ammonium persulfate (APS), 0.07% TEMED) and run through the Resolving Gel (10% Acrylamide, 125 mM Tris (pH 8.8), 0.1% (w:v) SDS, 0.1% (w:v) APS, 0.2% TEMED) at 120V for 100 minutes in running buffer (12.2 mM Tris base, 125 mM Glycine, 10% SDS). The samples on the gel were then transferred to nitrocellulose membranes. Two blotting papers were placed on the top and bottom of the membrane and two pads were placed on both sides of the blotting papers. The entire stack was placed in Transfer Buffer (25 mM Trizma Base, 192 mM Glycine, 20% Methanol) and then transferred at 100V for 1h. Nitrocellulose membranes were then incubated with 5% non-fat milk powder in TBS-T buffer (20 mM Tris Base, 137 mM NaCl, 0.1% Tween-20, pH 7.6) for 1h as a blocking step. After 2X5 minute washes with TBS-T, the blots were then incubated in anti-P2X1R antibody (1:2000) (Alomone, Jerusalem, Israel) overnight at 4°C. The next day, the blots were washed 3X5 minutes in TBS-T and then were incubated

with anti-rabbit secondary antibody (1:2000) (SIGMA, Poole, UK) for 1h. After another 3X5 minute washes in TBS-T, blots were incubated in the enhanced chemiluminescence reagent (ECL) (GE Healthcare, Buckinghamshire, UK) (mix of equal volumes of Enhanced Luminol Enhancer Solution and the Peroxide Solution) for 5 minutes. ECL was used to develop the blots. As the protein of interest was complexed with horseradish peroxidase (HRP) conjugated secondary antibodies and HRP catalysed the oxidation of luminol into a reagent which emits light, the amount and location of light is directly correlated with the location and amount of protein on the membrane. Finally, the blots were exposed on film or scanned by a Typhoon Scanner. The exposure time on film was chosen from 10 s, 1 min or 5 min to make sure no saturation. The exposure time on the Typhoon Scanner was chosen automatically. Densitometry was used for quantification and the intensities of samples were calculated using Image J software (see detail in 4.2.2 and figure 4.4).

2.5 Electrophysiological Recordings

Two-electrode voltage clamp (TEVC) was used to record currents from RNA-injected oocytes. In general, the method allows ion flow across a cell membrane to be measured as electric current, whilst the membrane voltage is held under experimental control with a feedback amplifier. Oocytes were held in a 2 ml bath which was perfused at ~3 ml/min with ND96 solution with 1.8 mM BaCl₂ replacing the 1.8 mM CaCl₂ to prevent activation of endogenous calcium sensitive chloride channels (Valera et al. 1994). Microelectrodes made from capillary glass (TW150F-4 World Precision Instruments Inc) were pulled using a two-stage puller (Narishige, Japan). They were filled with 3 M KCl and the resistance was between 0.1 and 0.4 MΩ. The two electrodes were inserted into the oocytes, one sensing clamped voltage at -60 mV and the other injecting current. Membrane currents were recorded using a Digidata 1322A analog digital converter with pClamp 8.2 acquisition software (Axon Instruments, CA, USA), which had a sampling frequency 2kHz and filtering frequency of 10Hz. Current readings can be used to analyse the electrical response of the oocyte to different applications. ATP was applied from a U-tube perfusion system for 3 seconds whereas different concentrations of the antagonist PPADS were bath-perfused

for 5 minutes because PPADS was characterised as a slowly-equilibrating and slowly-reversible antagonist (Ziganshin et al. 1993, Ziganshin et al. 1994), and co-applied with ATP. Each application was separated by 5-10 minutes for receptors to recover from desensitization.

The ion channel activity of the receptor was recorded by measuring the peak current. The responses of the receptor to various concentrations of ATP were plotted on ATP-concentration curves. The concentration curves of the cysteine mutated hP2X1Rs were generated in the same way and the EC_{50} was used to compare the effect of the mutant on the potency to ATP. In the figures, concentration-response curves were fitted to the mean normalised data, which showed the peak amplitude as the maximum response (100%). pEC_{50} , the $-\log_{10}$ of the EC_{50} value, was used to calculate the significant changes of the mutants compared to WT.

In order to test the effects of cysteine mutants on PPADS sensitivity of hP2X1Rs, the EC_{90} (the concentration of ATP that evoked 90% of the maximal current (100 μ M ATP for WT receptors) was used to standardize the ATP concentration when different concentrations of PPADS (0.1-30 μ M) were applied. The peak currents generated by PPADS based on EC_{90} of ATP were normalized by the current evoked by the EC_{90} of ATP in the absence of PPADS. The PPADS concentration curves were generated by plotting the normalized peak currents of each application. pIC_{50} values were used to evaluate the effects of different mutants.

2.6 Use of MTS compounds to modify cysteine mutants

Three different MTS compounds, MTSES (Sodium (2-Sulfonatoethyl) methanethiosulfonate), MTSEA (2-Aminoethyl Methanethiosulfonate Hydrobromide) (Toronto Research Chemicals, Toronto, Canada) and MTS-TPAE (2-(Tripropylammonium) ethyl Methanethiosulfonate Bromide) (Santa Cruz Biotechnology, Inc.) were used to modify cysteine mutants. MTS reagents (100 μ M) were prepared immediately before use. To test the effect of MTS compounds on ATP action at the WT and cysteine mutants, an EC_{50} concentration of ATP was used because it is the most sensitive part of the concentration-response

curve. Either MTSEA or MTSES were bath-perfused for 5 minutes and co-applied with ATP to the oocytes. This allowed the MTS compounds to react with the introduced cysteine residue if it is accessible in either the closed or open states. 5-minute recovery time was required between each application.

For the cysteine mutants showing no change in the response to an EC₅₀ concentration of ATP in the presence of MTS compounds, the effect of MTS compounds to PPADS sensitivity were investigated. It is known the MTS compounds form covalent bounds with cysteine residues and this action is irreversible (Roberts et al. 2009b). In previous studies, the concentration response curves generated with MTS reagents in the bath or after longer term treatment followed by washout of the MTS reagents give the same results for a range of P2X1R cysteine mutants (Roberts and Evans 2007). In this study, the oocytes were pre-treated with 100 µM MTS reagents for more than 1 hour to modify the cysteine mutants. Then PPADS concentration response curves were generated as above following by washout of MTS reagents.

2.7 Data analysis

MTSEA-biotinylation between apyrase, ATP and PPADS treatment was measured by densitometry (Image J software) and corrected for any differences in the total amount of P2X1R protein in the samples. Differences in biotinylation levels were compared with a paired student's t test. The t-test was used to p>0.05.

Concentration response curves were fitted with the Hill equation: $Y = \frac{[(X)^H \times M]}{[(X)^H + (EC_{50})^H]}$, Y is the response, X is the agonist concentration, H is the Hill coefficient, M is the maximum response. EC₅₀ is the concentration of ATP that evokes 50% of the maximum response and IC₅₀ is the concentration of antagonist inhibiting of the EC₉₀ of ATP by 50%. Inhibition curves were fitted with the same formula, with IC₅₀ values instead of EC₅₀ values.

In the figures, concentration-response curves were fitted to the mean normalised data, which showed the peak amplitudes as the maximum response. Individual curves generating from each oocyte were fitted. EC₅₀ or IC₅₀ values

were then calculated and the pEC_{50} is the $-\log_{10}$ of the EC_{50} values and pIC_{50} is the $-\log_{10}$ of the IC_{50} values. All experiments were repeated ≥ 3 times. Data are reported as the mean \pm standard error of the mean (SEM). The analysis software used was Prism 6 (GraphPad Software Inc.). Significant differences between WT and the mutant hP2XR1s (current amplitudes, rise and decay time, hillslope, pEC_{50} and pIC_{50}) were calculated by one-way ANOVA followed by Dunnett's test.

2.8 Molecular docking

The homology models of the hP2X1R in closed and ATP bound state were constructed by Dr. Ralf Schmid (Department of Molecular and Cell biology, University of Leicester). The trimeric assembly of the hP2X1R (residues 33-352) was modelled in Modeller 9v14 software based on the zfP2X4R structure as the template (PDBid: 4DW1 and 4DW0 (Hattori and Gouaux 2012)). The reason of using zfP2X4R instead of recent published hP2X3R as the template is because it shares more similarity with the hP2X1R. Ten representative hP2X1R model for each state were selected as receptors for ligand docking.

The homology model of the hP2X1R was then used as the starting structure for ligand docking with PPADS (also carried out by Dr Ralf Schmid). PPADS was docked into the hP2X1R models using RosettaLigand (Davis and Baker 2009). The docking area was centred at the orthosteric site. For both states 10000 docking poses were generated. Of these the best scoring 10% docked complexes were clustered using cpptraj (Roe and Cheatham 2013). From the resulting clusters representative poses were visualised in PyMol and further analysed in the context of the experimental data.

Chapter 3. Characterisation of antagonist PPADS and the effect of K249C on the sensitivity of the hP2X1R to PPADS

3.1 Introduction

P2XRs are widely expressed throughout the human body and mediate various physiological and pathological processes. They represent a class of therapeutic targets and their antagonists have potentials for novel treatments for a range of diseases. PPADS has been commonly used as a P2XR antagonist. It is generally considered as a non-selective antagonist at P2XR subtypes however selectivity has been introduced with some PPADS analogues. This suggested PPADS can be used as a template to design more selective P2XR antagonists. Understanding the molecular basis of antagonism PPADS will contribute to the development of novel drugs targeting P2XRs.

3.1.1 Previous studies into the molecular basis of PPADS Action at P2XRs

PPADS inhibits at most subtypes of P2XRs (IC_{50} 1-45 μ M) except the rP2X4R which is considered insensitive to PPADS (Buell et al. 1996). Analysis of the amino acid sequence identified a conserved lysine at position 249 (K249) in the P2X1&2R that is replaced by glutamic acid (E) in the rP2X4R. This led to a hypothesis that an aldehyde group on position 4 in PPADS may form a Schiff base with a lysine residue in P2XRs, which contributes to the antagonist action (Buell et al. 1996). With an introduced lysine mutant in the position (E249K), the sensitivity of the P2X4R to PPADS was introduced (IC_{50} ~2.6 μ M) and the PPADS inhibition was slowly reversible (20 min) (Buell et al. 1996), which was similar to PPADS action at P2X1 and P2X2Rs. This finding supported the Schiff base theory.

However, the reciprocal mutation (K249E) in the P2X2R did not significantly decrease the sensitivity to PPADS (Buell et al. 1996). In addition, the K249 is not conserved in all PPADS-sensitive P2XRs. For example, the P2X3R that has a Threonine (T) in the equivalent position showed PPADS sensitivity with an IC_{50} value of 1-3 μ M. Also, it was found that an analogue of PPADS (MRS 2220) that lacks the aldehyde group was more potent and selective at P2X1Rs (Jacobson et al. 1998). These data indicated that Schiff base formation with lysine

249 is not necessary for PPADS antagonism. Therefore, it suggested that the lysine residue at 249 is important for the antagonism of PPADS at the P2X4R but that other residues are also involved.

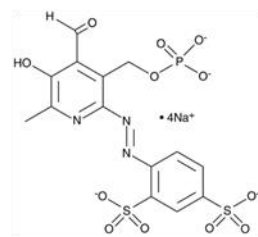
The cloning and characterization of the hP2X4R provided further clues regarding PPADS action. It was found that the hP2X4R showed a notably higher sensitivity to PPADS ($IC_{50} \sim 27 \mu M$) than the rP2X4R ($IC_{50} > 300 \mu M$). The hP2X4R and rP2X4R have the same glutamic acid (E) at position 249, indicating other variations are also important for PPADS antagonism. In order to investigate the structural determinants of PPADS sensitivity, several chimeric receptors and point mutations between the two species were made. The domain 81-183 located in the extracellular loop was found to determine the higher PPADS sensitivity for the hP2X4R (Garcia-Guzman et al. 1997). Within this domain, there are 22 amino acids differing between the rat and human receptors and only one lysine residue exclusively present in the human sequence (K127) but replaced by asparagine (N127) in the rat homologue. The mutation (N127K) in the rP2X4R did not confer its human-like PPADS sensitivity (Garcia-Guzman et al. 1997), suggesting K127 is not responsible for the difference in PPADS binding. Therefore, an exact mechanism of PPADS binding at P2XRs remains to be determined.

As PPADS contains four negative charges, positively charged residues in PPADS-sensitive P2XRs may play important roles in PPADS action. The positively charged lysine 249 (numbering for rP2X4) is conserved at PPADS-sensitive P2X1 and P2X2Rs but replaced by negatively charged glutamic acid (E) in the rP2X4R (Figure 3.1a, b). The strong evidence provided in previous studies (Buell et al. 1996) for the contribution of K249 to PPADS antagonism at P2X4RS suggested the residue (K249) may be in or close to the PPADS binding site. Following crystallization of zfP2X4R, it became apparent that K249 was close to the ATP binding site. It raised the possibility that PPADS binding at K249 would interfere with ATP access to the agonist pocket (Figure 3.1c). The E249 at P2X4Rs may repel PPADS whereas the K249 at P2X1Rs may attract PPADS. However, one residue is not enough for binding the multiple negative charges of PPADS. Other residues involved in PPADS action remain to be identified.

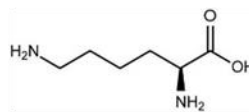
(a)

	244	245	246	247	248	249	250	251	252	253	254
hP2X1	S	T	L	A	E	K	G	G	V	V	G
hP2X2	T	E	L	A	H	K	G	G	V	I	G
hP2X3	A	K	L	A	R	T	G	G	V	L	G
rP2X4	Q	E	M	A	V	E	G	G	I	M	G
hP2X4	Q	D	M	A	V	E	G	G	I	M	G
rP2X5	Q	D	I	A	L	K	G	G	V	I	G
hP2X6	E	D	L	A	L	L	G	G	S	V	G
hP2X7	S	D	V	A	I	Q	G	G	I	M	G

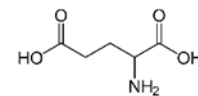
(b)



PPADS



Lysine (K)



Glutamic acid (E)

(c)

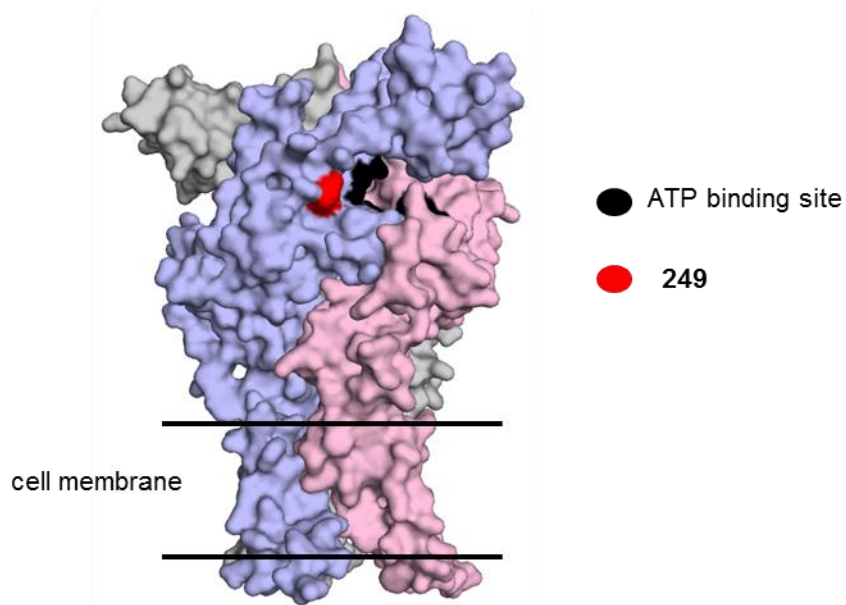


Figure 3.1 Amino acid sequences around 249 at P2XRs and the location of Lysine 249 at the hP2X1R (a) Alignment of the P2XR subtypes amino acid sequences around 249 (numbering for hP2X1). Grey boxes indicate conserved amino acids. (b) Molecular structure of PPADS, Lysine and Glutamic acid. (c) Homology model of the hP2X1R is shown in closed state. Three subunits are shown in blue, pink and grey surface respectively. ATP binding pocket is shown in black and the 249 residue is labelled in red. Two black lines indicate cell membrane.

If charge around the agonist binding pocket was important for PPADS action, K249 may contribute to PPADS sensitivity of hP2X1Rs. The starting point of this thesis was to determine whether K249 contributed to PPADS sensitivity at the hP2X1R. To do this, the cysteine substitution mutant K249C was made and tested to see whether PPADS sensitivity of the hP2X1R was changed with the mutation. Mutating a residue to cysteine is a useful tool because (i) there are no free cysteine residues in the extracellular loop of the WT P2XRs, and (ii) the cysteine side chains can be modified by MTS compounds with different side chains and charges. For example, MTSEA-biotin assay can be used to measure accessibility of the residues. The further use of cysteine mutants to investigate PPADS action are described in Chapter 4 and 5.

3.1.2 Aims

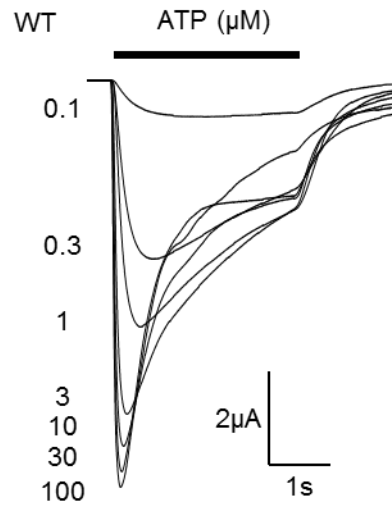
The aim of this chapter was to understand the basic pharmacology of the antagonist PPADS acting at the hP2X1R and determine whether the lysine at position 249 contributes to PPADS potency.

3.2 Results

3.2.1 The ATP sensitivity of WT hP2X1Rs

WT hP2X1Rs were expressed in *Xenopus Laevis* oocytes and TEVC recordings were used to characterise their properties. ATP (100 μ M) had no effect on non-injected oocytes, suggesting no endogenous P2XRs are expressed in native oocytes. ATP evoked concentration-dependent responses at WT hP2X1Rs (Figure 3.2a). The maximal response was reached at 100 μ M ATP (ATP_{max}). Once reproducible responses to ATP_{max} were obtained, different concentrations of ATP were applied to the receptor and a concentration response curve was generated. The EC_{50} value which is the concentration of ATP that generates 50% of the maximal response was used as the measure of ATP potency. The EC_{50} value of the response evoked by ATP at WT hP2X1R was ~ 0.8 μ M (Figure 3.2b), which is consistent with previous research (Ennion et al. 2000).

(a)



(b)

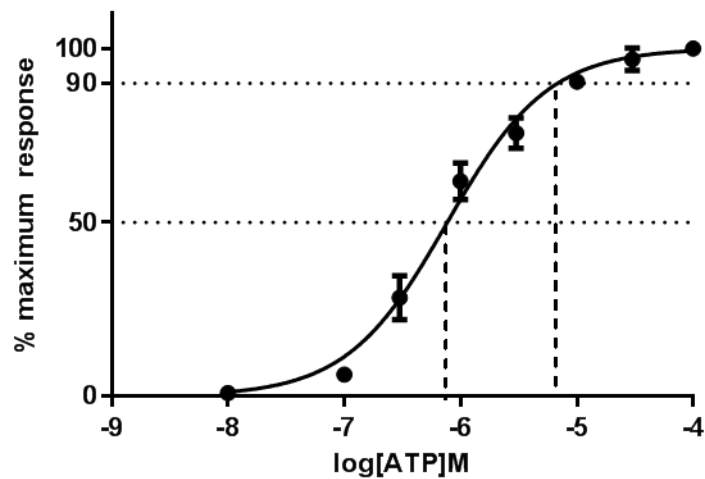


Figure 3.2 ATP-evoked currents at the hP2X1R

(a) Representative traces of different concentrations of ATP (0.1-100 μM) applied for 3 seconds with 5 minutes intervals between each application to an oocyte expressing WT hP2X1Rs. Black bar indicates 3 second application of ATP. (b) Average ATP concentration curve for WT hP2X1Rs. The EC_{50} and EC_{90} values are shown by dashed lines. The data are plotted as mean \pm SEM (n=4).

3.2.2 The time-course of the ATP evoked response at WT hP2X1Rs

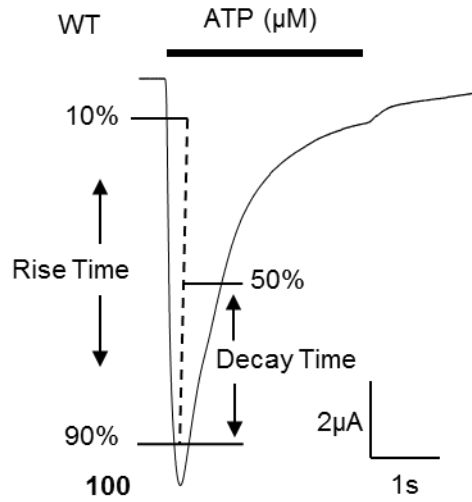
Application of ATP (100 μM) to oocytes expressing the WT hP2X1Rs caused a transient inward current that decayed back to the baseline during continued ATP application (Figure 3.3a). This decay with continued agonist application is referred to as desensitisation. The time it takes the current to increase from 10% to 90% of the peak amplitude was defined as the rise time and the time for the peak current to decay from 90% to 50% as the decay time (Figure 3.3a). The time-course of the ATP-evoked response was concentration dependent (Figure 3.3b, c). At ATP_{max}, the WT hP2X1R showed almost complete and very quick desensitisation within 3s, which is consistent with previous studies (Ennion et al. 2000). The rise time of the maximum response was 174 ± 14 ms and the decay time was 987 ± 92 ms. Lower concentrations of ATP had slower rise-times and desensitisation.

3.2.3 Characterisation of PPADS action at WT hP2X1R

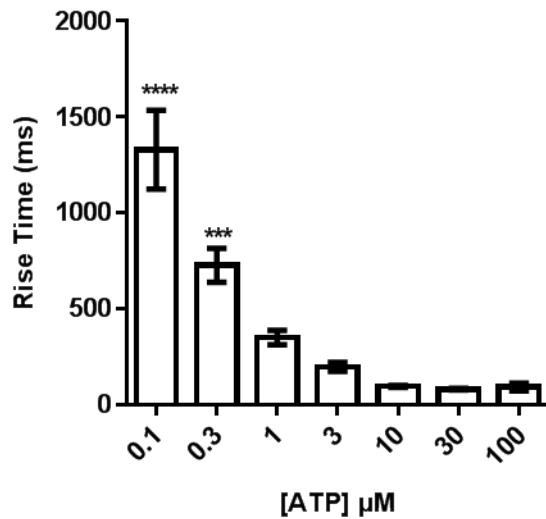
Based on the ATP dose response curve, the EC₉₀ value was used to standardise the ATP concentration for antagonist studies. The EC₉₀ value of ATP at the WT hP2X1R was ~ 10 μM (Figure 3.2b). Once the response to ATP (EC₉₀) was reproducible, individual concentrations of PPADS were pre-perfused and then co-applied with ATP (EC₉₀). Repeat applications of PPADS at 5-minute intervals showed that the antagonist equilibrated within the 5 minutes. The inhibition of the ATP-evoked response by PPADS at WT hP2X1R was concentration dependent (Figure 3.4). In the presence of 1 μM PPADS, the current evoked by ATP (EC₉₀) decreased by 80%. In the presence of 10 μM PPADS, the response decreased by 95%. PPADS, at a concentration of 30 μM , completely inhibited the response. A high concentration of PPADS (100 μM) was applied on its own at the WT P2X1Rs and showed no effect on the holding current, demonstrating that PPADS does not act as a partial agonist. The response inhibited by PPADS recovered by $\sim 90\%$ after a 5-minute wash-off period (Figure 3.4a).

The IC₅₀ value of PPADS at WT hP2X1R was ~ 0.7 μM and the average Hill slope was ~ 1.4 (Figure 3.4c). The ATP potency of WT hP2X1R in the

(a)



(b)



(c)

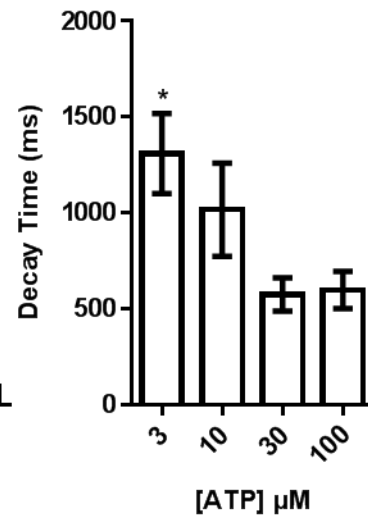


Figure 3.3 Time-course of the ATP-evoked currents at the hP2X1R

(a) Representative trace of the WT hP2X1R in response to 100 μM ATP and the calculation of the time-course (rise and decay times) (b) The Rise Time (10% - 90%) and (c) Decay Time (90% - 50%) of the currents evoked by individual concentration of ATP. Significant differences were compared with the rise and decay time of the current produced with 100 μM ATP by one-way ANOVA ($*p < 0.05$, $***p < 0.001$, $****p < 0.0001$, $n > 3$). The data are plotted as mean \pm SEM ($n = 7$).

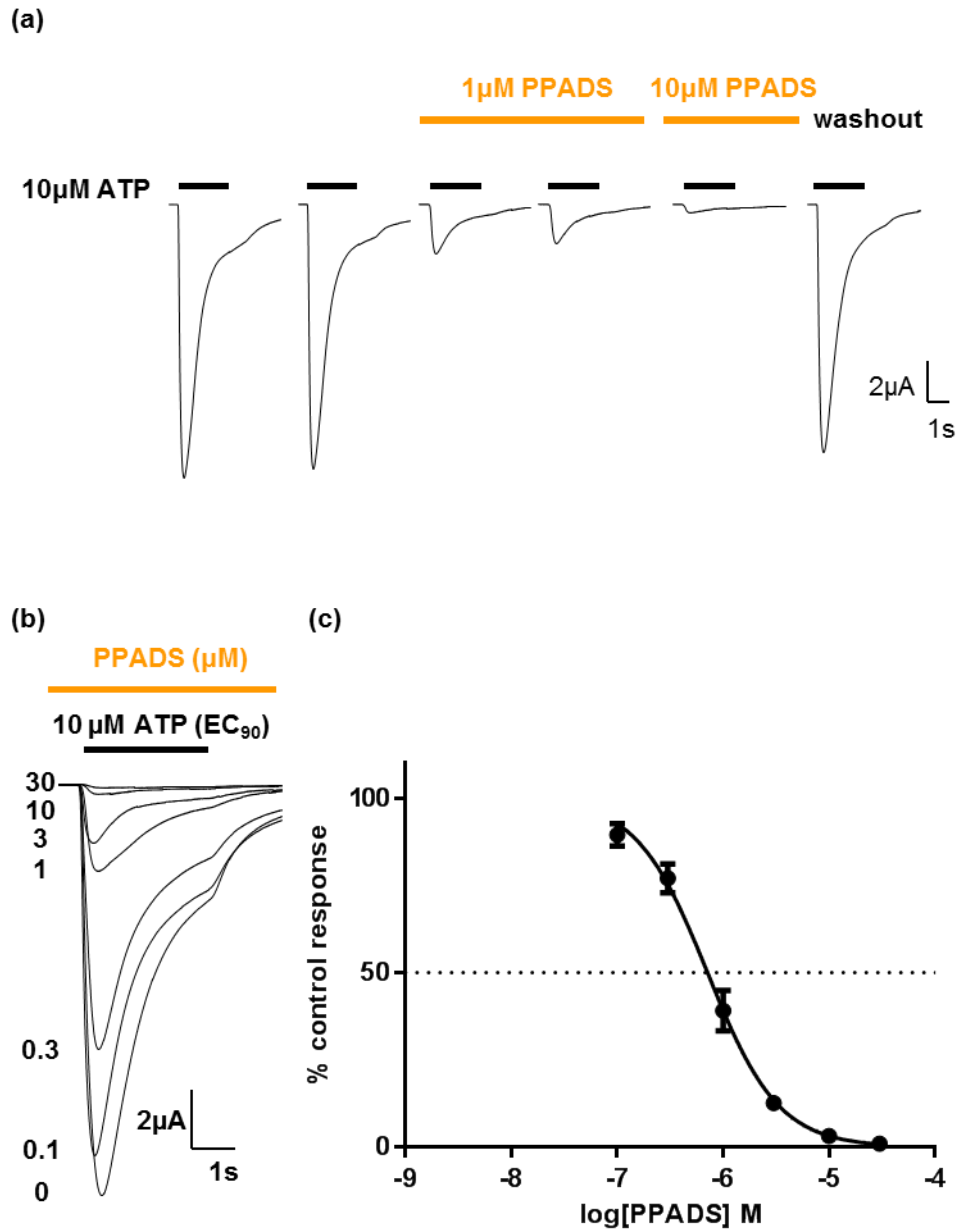


Figure 3.4 Inhibition by PPADS of ATP-evoked currents at the hP2X1R
(a) Representative traces of 10 μM ATP (EC₉₀), co-applied with 1 μM and 10 μM PPADS, and then with 5-minute washout. PPADS (1, 10 μM) was perfused with 5 minutes before co-application with ATP. Each application last for 3 seconds, with a 5-minute interval between each application. Orange bar indicates application of PPADS and black bar indicates application of ATP. **(b)** Representative traces of 10 μM ATP (EC₉₀), co-applied with different concentrations of PPADS (0.1-30 μM). PPADS (0.1-30 μM) was perfused for 5 minutes between each application. **(c)** Average of PPADS concentration curve for WT hP2X1Rs. The IC₅₀ value is shown by a dashed line. The data are plotted as mean ± SEM (n=8). The Hill Slope is ~1.4.

presence of 1 μM PPADS (EC_{50} value of $\sim 0.85 \mu\text{M}$) was similar to that in the absence of PPADS. The response inhibited by PPADS reached a maximum at 10 μM ATP. Increasing the concentration of ATP did not overcome the inhibition by PPADS (Figure 3.5). It indicates that PPADS may work as a non-competitive antagonist at the hP2X1R.

PPADS decreased peak current amplitude but had no effect on the time-course, except the rise-time in the presence of the high concentrations of PPADS ($\geq 10 \mu\text{M}$) (Figure 3.6a). The increased rise-time at the concentration of 10 and 30 μM may be because with the small amplitude it was difficult to calculate the time course (not shown in figures). The decay time of the current inhibited by individual concentration of PPADS showed no significant change compared to that without PPADS (Figure 3.6b).

3.2.4 The effect of K249C on sensitivity of the hP2X1R to ATP and PPADS

In order to test the contribution of K249 to PPADS sensitivity of the hP2X1R, a cysteine mutant was made at this position (K249C). Initially, the ATP potency of the hP2X1R was tested. The peak current amplitudes at ATP_{max} (100 μM) ($-10063 \pm 588 \text{ nA}$) for K249C was not significantly different from that of WT receptors ($-11867 \pm 932 \text{ nA}$) (Figure 3.7a). The EC_{50} value of this mutant was $\sim 0.7 \mu\text{M}$, which was not significantly changed compared to the WT receptor (EC_{50} value of $\sim 0.8 \mu\text{M}$) (Figure 3.7b). This indicates that K249 is not an important residue for ATP potency.

Based on the EC_{90} value of ATP ($\sim 10 \mu\text{M}$), PPADS potency was tested at K249C by generating a PPADS concentration response curve. The sensitivity to inhibition by PPADS of the receptor with K249C (IC_{50} value of $\sim 2.49 \mu\text{M}$) was reduced ~ 3 fold compared to the WT receptor (IC_{50} value of $\sim 0.71 \mu\text{M}$) (Figure 3.8). The pIC_{50} values ($= -\log(\text{IC}_{50} \text{ values})$) were used to measure statistical significance. The mutant K249C significantly decreased PPADS sensitivity at the hP2X1R ($***p < 0.001$). The results showed that K249 contributes to the sensitivity of the hP2X1R to PPADS.

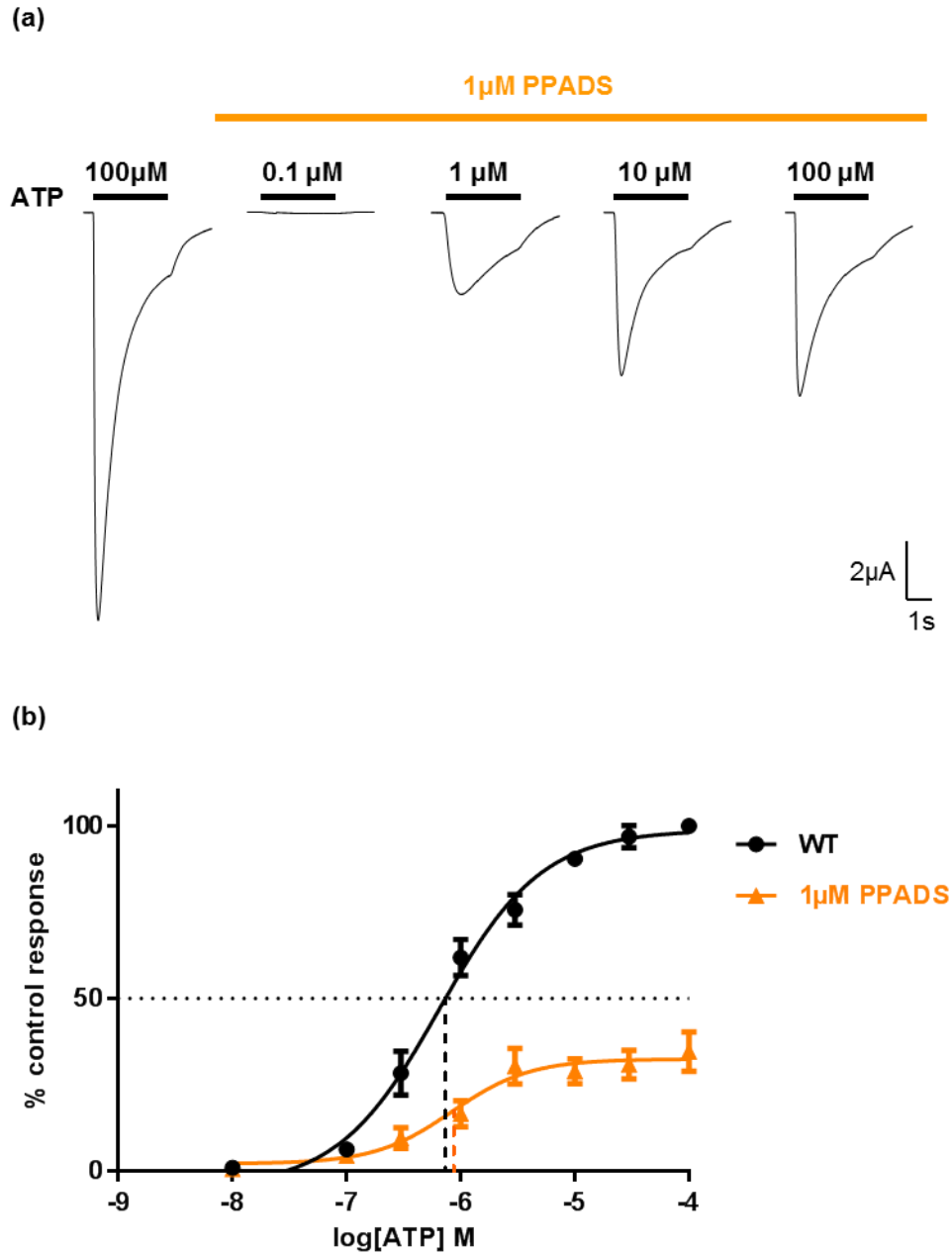
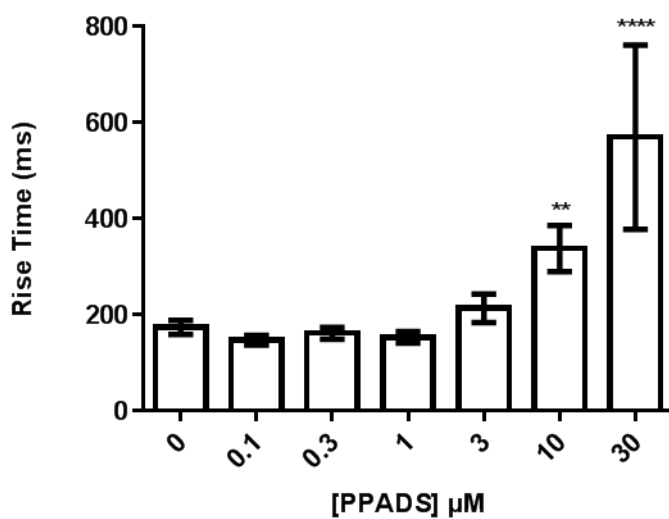


Figure 3.5 Effect of PPADS on ATP potency at WT hP2X1Rs

(a) Representative traces of different concentrations of ATP in the presence of 1 μ M PPADS. PPADS was continuously perfused. Each ATP application lasted for 3 seconds, with a 5-minute interval between each application. Orange bar indicates application of PPADS and black bar indicates application of ATP. (b) Concentration-dependent responses to ATP in the absence and presence of 1 μ M PPADS. The data are plotted as mean \pm SEM ($n=4$). The horizontal dashed line indicates the IC_{50} value in the absence of PPADS. The black and orange vertical dashed lines indicate the IC_{50} values of the concentration curves in the absence or presence of PPADS.

(a)



(b)

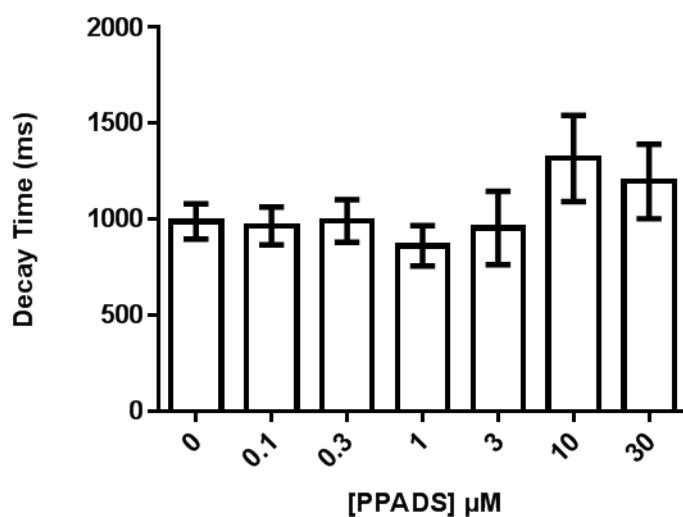


Figure 3.6 Effect of PPADS on the time-course of the currents evoked by 10 μM ATP at the hP2X1R (a) The rise-time (10%-90% of the current amplitude) and (b) the decay-time (90%-50% of the current amplitude) of 10 μM ATP in the absence and presence of different concentrations of PPADS. Significant differences were compared with the rise and decay time of the current produced by 10 μM ATP in the absence of PPADS (** $p < 0.01$, **** $p < 0.0001$, $n > 3$). The data are plotted as mean \pm SEM ($n = 6$).

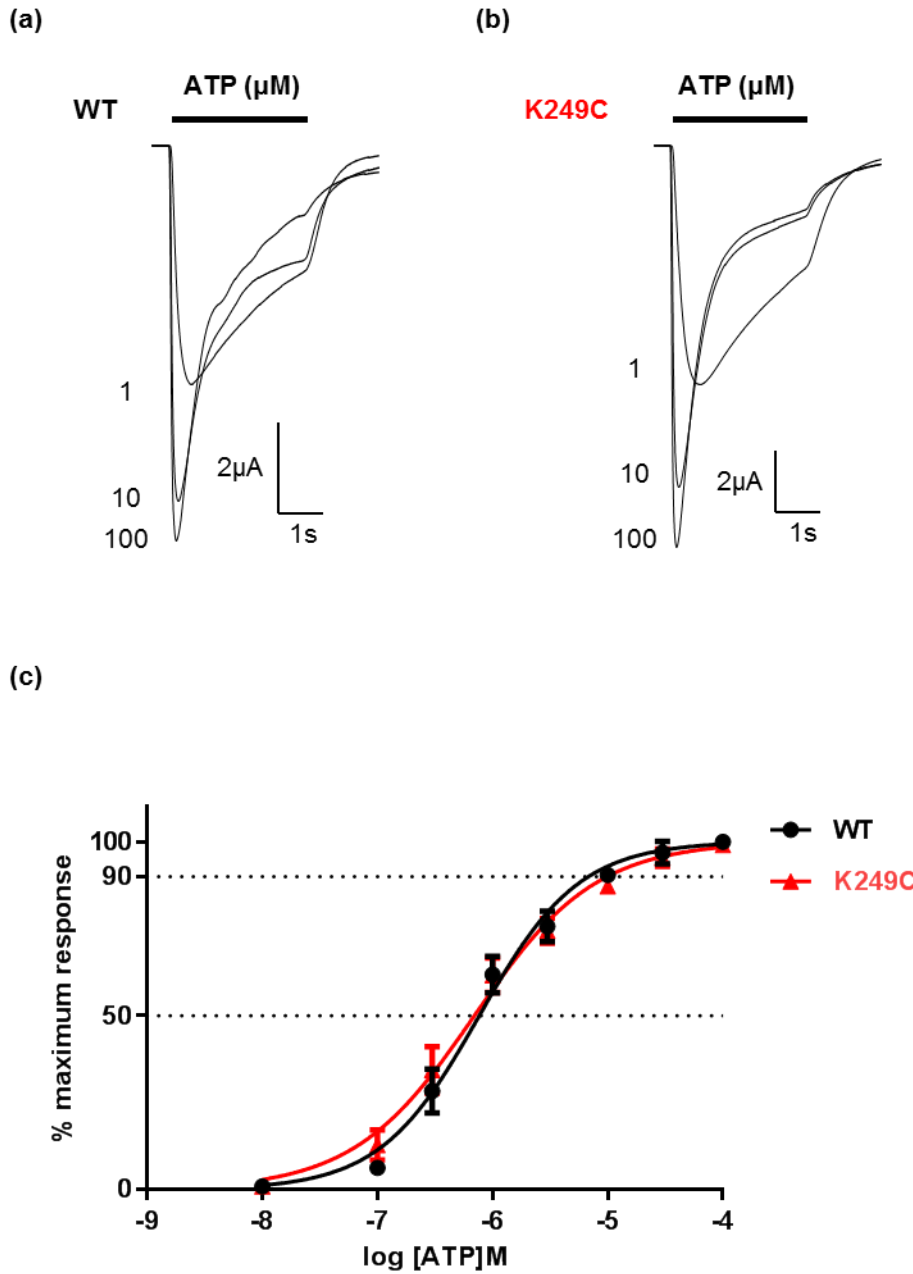


Figure 3.7 Comparison of ATP sensitivity between WT and K249C mutant hP2X1Rs (a) Representative traces of different ATP concentrations (1, 10, 100 μM) at the WT hP2X1R. (b) Representative traces of different ATP concentrations (1, 10, 100 μM) at the K249C mutated hP2X1R. (c) Average of ATP concentration curves for the WT and K249C mutated hP2X1Rs. The EC₅₀ and EC₉₀ values are shown by dashed lines. The data are plotted as mean ± SEM (n=4).

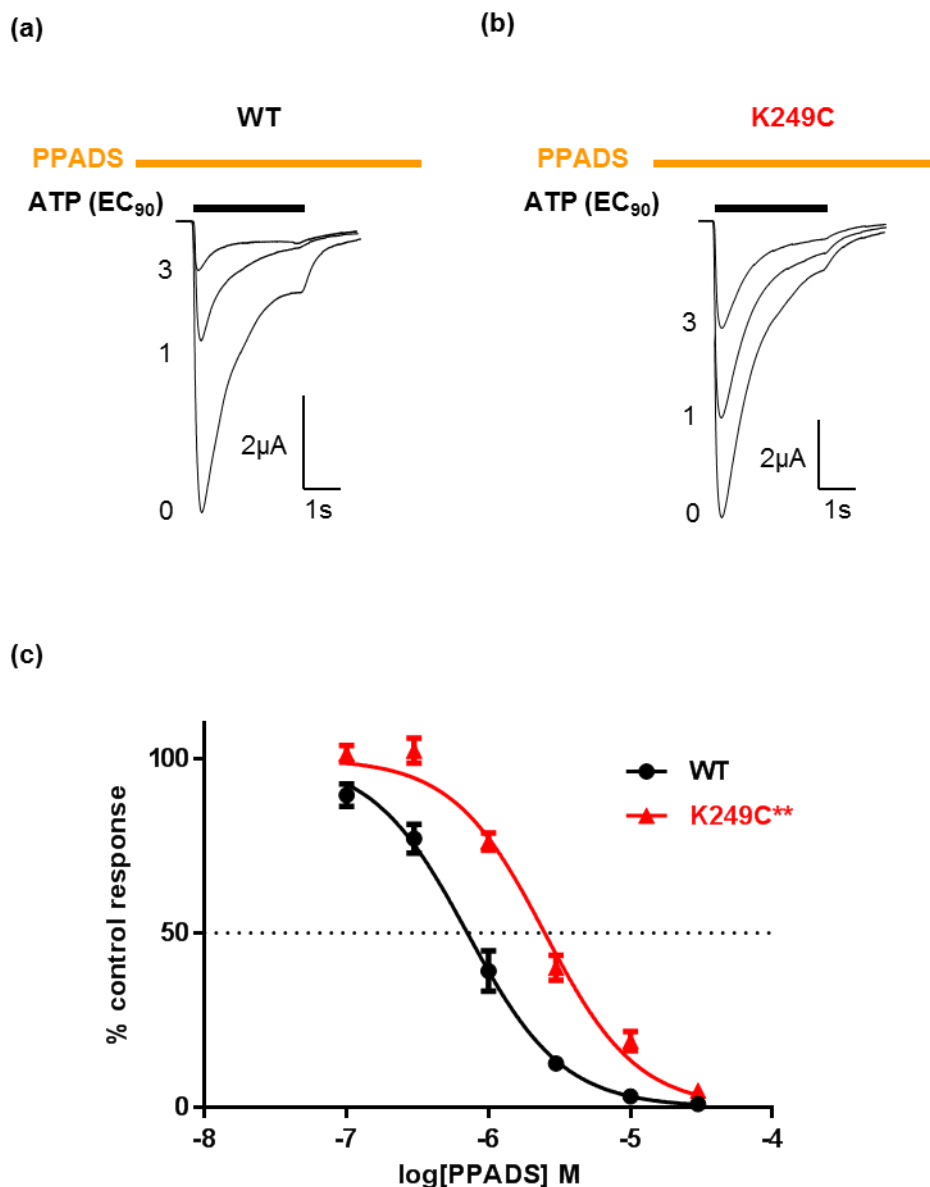


Figure 3.8 Comparison of PPADS sensitivity between WT and K249C mutated hP2X1Rs (a) Representative traces of 1 and 3 μM PPADS co-applied with EC_{90} ATP for 3 seconds with 5 minutes intervals between each application. PPADS was perfused for 5 minutes before the co-application. Orange bar indicates application of PPADS and black bar indicated application of ATP. (b) Representative traces of 1 and 3 μM PPADS co-applied with EC_{90} ATP to the K249C mutated hP2X1R. (c) Average of PPADS concentration curves for the WT and K249C mutated hP2X1Rs. The IC_{50} values are shown by the dashed line (** $p < 0.01$, $n > 3$). The data are plotted as mean \pm SEM ($n = 7$).

3.3 Discussion

This chapter initially characterized ATP action at the hP2X1R. ATP activated the hP2X1R in a concentration dependent manner, with an EC₅₀ of ~0.8 μM. The current evoked by 100 μM ATP (maximum response) peaked and desensitized quickly. The desensitization rate of the current was concentration dependent. These results are consistent with previous studies of the basic pharmacological properties of the hP2X1R (Ennion et al. 2000, Evans et al. 1995, Roberts and Evans 2004, Valera et al. 1994).

PPADS inhibited ATP evoked currents at the hP2X1R in a concentration dependent manner. The hP2X1R showed high sensitivity to PPADS (IC₅₀ of ~0.7 μM), which is consistent with previous studies (Evans et al. 1995). The cysteine mutant K249C decreased PPADS by ~3-fold, suggesting the importance of the residue to PPADS action.

3.3.1 PPADS works as a non-competitive and reversible antagonist at the hP2X1R

In pharmacology, antagonists have affinity but no efficacy. They can be classified into competitive and non-competitive antagonists based on their binding sites and have different pharmacological profiles. The ATP concentration response curve in the presence of PPADS (1 μM) showed a collapse in the maximum current with no significant effect on ATP potency (EC₅₀). It indicates PPADS worked as a non-competitive antagonist. As the time-course of the response was concentration dependent, it was predicted that if PPADS shifted ATP sensitivity, there would be changes in the time-course. In this study, there were no significant changes in the time-course of the currents in the presence of PPADS, suggesting PPADS did not change ATP sensitivity. It also supports a non-competitive manner of the antagonist. In contrast, previous studies in the lab showed that suramin antagonised the ATP-evoked response with a parallel rightward shift in the concentration response curve and that had no change in the maximum response. Increasing concentrations of suramin on a defined concentration of ATP not only reduced the ATP-evoked current but also slowed

the time-course of the response. This suggests PPADS has a different molecular basis of action from another non-selective antagonist suramin.

The competitive or non-competitive nature of PPADS is controversial in previous studies. Some studies showing PPADS non-competitively inhibited P2XRs expressed in native tissues, including smooth muscle (Lambrecht et al. 1992) and bullfrog dorsal root ganglion (DRG) neurons (Li 2000) and also for recombinant P2XRs (El-Ajouz et al. 2012a), with a decrease in the amplitude of the maximum response to ATP (30 μ M) in the presence of PPADS. There are also some studies reporting PPADS showed competitive antagonist patterns in concentration-response curves to P2XRs expressed in native tissues. For example, the PPADS-induced inhibition of contractions evoked by α , β -methylene ATP in guinea-pig vas deferens was overcome by increasing the concentration of agonist (McLaren et al. 1994). However, the inhibition by PPADS in contraction is different from that in ATP evoked current. The contractile response may be saturated at less than full current. Therefore, the competitive or non-competitive nature of PPADS may depend on the cell types expressing P2XRs and output that is being measured. In this study, the hP2X1Rs were expressed in oocytes, which provides a direct way to look at channel in the state of activation, desensitization and deactivation. It is commonly used to test recombinant P2XRs properties.

The inhibition by PPADS at the hP2X1R in this thesis was reversible. The ATP evoked current recovered by ~90% after 5-minute wash-off. It is consistent with previous studies in native bullfrog DRG neurons showing that ATP-activated current fully recovered after 8 minutes (Li 2000). Previous studies showed PPADS antagonistic action at recombinant P2X1Rs was reversible with 15-20 minutes (Evans et al. 1995). However, for some studies on native smooth muscles, the effect of PPADS was not shown to be readily reversible. For example, it took 90 min to recover to the control level for the responses evoked by α , β -MeATP in rabbit vas deferens (Lambrecht et al. 1992) and 1 h in guinea-pig vas deferens (McLaren et al. 1994). In rabbit urinary bladder, the responses recovered by 15-20% after >2h wash-out (Ziganshin et al. 1993). Buel *et al* (Buell et al. 1996) suggested the formation of the Schiff base between the lysine 249 in

P2X1Rs and P2X2Rs with PPADS may account for the slower reversible time of PPADS. But this theory is not applicable to all P2XR subtypes because K249 is not conserved in all P2XRs. The reversibility of PPADS inhibition may also depend on the concentration of PPADS and the incubation time before applying the agonist.

The differences in reversibility of PPADS action may be due to the various tissues expressing P2XRs and/or the subtypes of P2XRs. For example, the studies mentioned above were carried out in isolated native tissues. There may be additional non-specific effects e.g. that lead to long term regulation of P2XRs which is independent on the ligand binding to the receptor. In oocytes, there may be a rapid turnover of the hP2X1Rs and antagonist-unbound P2X1Rs could be recycling to the surface in the 5-minute wash-off period.

3.3.2 The importance of K249 to the sensitivity of the hP2X1R to PPADS

According to the homology model of the hP2X1R based on the crystal structure of zfP2X4R, lysine 249 is close to the ATP binding pocket. Interestingly, the cysteine mutant (K249C) did not significantly affect ATP potency. This shows that the residue is not involved in ATP binding. In contrast, the PPADS sensitivity of the hP2X1R was significantly reduced (~3 fold), suggesting that K249 contributes to PPADS binding. This is the first time that the contribution of K249 to PPADS action at the hP2X1R has been demonstrated. This result is in agreement with previous observations by Buell et al. who reported that K249 is essential for PPADS sensitivity of rP2X4Rs (Buell et al. 1996).

The equivalent 249 residue in PPADS-insensitive rP2X4R ($IC_{50} > 500 \mu M$) is glutamic acid. Previous studies showed the mutation E249K introduced rP2X4R sensitivity to PPADS ($IC_{50} \sim 10 \mu M$) (Buell et al. 1996). As PPADS contains negative charges, the positively charged lysine may play an important role in PPADS sensitivity. The PPADS-sensitive P2X5R ($IC_{50} \sim 3 \mu M$) (Wildman et al. 2002) also has a lysine at the equivalent position. However, the hP2X4R that also has a glutamic acid at position 249 has an $IC_{50} \sim 30 \mu M$. PPADS-sensitive P2X3 ($IC_{50} 1-5 \mu M$) have Threonine at the equivalent position which is not charged. In addition, it was shown that the corresponding mutation (K249E)

in the rP2X2R did not remove its sensitivity to PPADS (Buell et al. 1996). This suggested that the relative contribution of the lysine at position 249 (numbering for P2X1&4) was dependent on the species and background. These results suggest that positive charge at position 249 can contribute to the action of PPADS but that other residues must also be involved. In the future work, it would be interesting to make other substitutions at the residue 249 to see whether PPADS sensitivity is modified or not, for example, K249E, K249T and K249Q. By comparing PPADS sensitivity of these mutations at the P2X1R with P2X4R, P2X3R and P2X7Rs, it would further confirm the importance of the residue to PPADS antagonism.

3.3.3 The extracellular loop and the potential PPADS binding area

PPADS is hypothesized to bind to the extracellular loop of the P2XR because it is unable to cross the cell membrane. Some previous studies also suggested PPADS worked extracellularly at P2XRs. It was found that an intracellular application of PPADS (~10 μ M) in neurons expressing P2XRs did not alter the ATP-evoked responses. However, PPADS produced nearly maximal inhibition at the same concentration when applied extracellularly (Li 2000). Therefore, the focus of this thesis was on the residues in the extracellular loop of the hP2X1R. As the results suggested the importance of the lysine 249 to PPADS action. Residues involved in PPADS action are hypothesized to be included in the ring which centres on 249 with the radius of the length of PPADS (Figure 3.9). The contribution of the residues to PPADS action in the ring were evaluated in the next chapters.

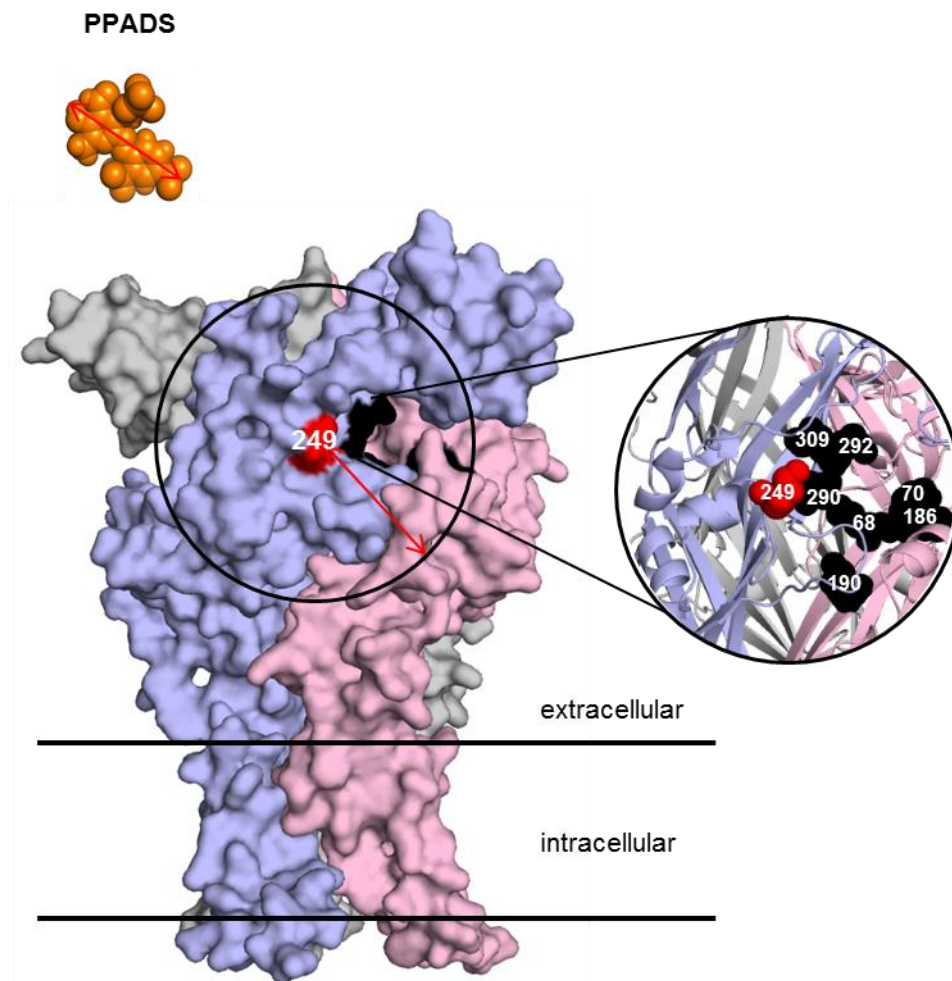


Figure 3.9 Molecular structure of PPADS and lysine and homology model of the hP2X1R. Homology model of the hP2X1R is shown in the apo state. Three subunits are shown in blue, pink and grey respectively. The ATP binding sites are shown in black and the 249 residue is labelled in red. PPADS is shown as orange spheres and its max dimension is shown with a red arrow. The black ring centres on 249 and its radius is the length of PPADS. The right part shows enlarged view of the location of 249 (red) and residues (black) forming ATP binding pockets in apo state of the hP2X1R shown in cartoon.

Chapter 4. Effect of PPADS on accessibility of residues in the extracellular loop of the hP2X1R

4.1 Introduction

The properties of recombinant P2XRs are dependent on the amino acid sequence composition. Mutagenesis has been used as an effective approach to investigate the contribution of defined amino acids in ligand action and function of receptors. Cysteine has been widely used in site directed mutagenesis studies to look at the role of particular amino acids as it is generally well tolerated. In addition, the sulfhydryl group of cysteine is useful as it can (i) be probed with MTSEA-biotin to measure accessibility (J. A. Roberts et al. 2012), (ii) be modified with different charges and sizes of side chains, e.g. by positively charged MTSEA or negatively charged MTSES (Roberts et al. 2008) (see detail in Chapter 5), and (iii) labelled with fluorescence, for example by MTS-TAMRA (Fryatt and Evans 2014).

4.1.1 Substituted cysteine accessibility studies on P2XRs

4.1.1.1 Early accessibility studies

The substituted cysteine accessibility method (SCAM) was introduced by Akabas for identifying pore-lining domains of the nicotinic acetylcholine receptor (Akabas et al. 1992). The unique property of the cysteine residue sulfhydryl group provides an approach to measure its accessibility. The method involved two steps: (1) mutating individual residues to cysteine and then (2) testing the accessibility of the side-chains of the substituted residues by a water-soluble sulfhydryl reagent. The commonly used sulfhydryl specific reagents are silver and MTS derivatives. It was assumed that residues exposed to the water environment lining the ion pathway would be accessible and an addition of the charged group by MTS compounds would alter ion conduction and that residues in the membrane-spanning segment but not exposed in the channel are inaccessible.

In the study on nicotinic acetylcholine receptors, consecutive nine residues (246 to 254) in M2 (membrane-spanning segment) of the mouse muscle α subunit were mutated to cysteines. Among the mutants, S248C, L250C, S252C and

T254C were accessible by MTSEA and irreversibly inhibited by MTSEA in the absence and presence of ACh whereas L251C was not affected by MTSEA in the absence of ACh but irreversibly inhibited by MTSEA in the presence of Ach. It suggested these residues are exposed in the channel and flexibility is required in the channel structure around L251 (Akabas et al. 1992). The results were substantiated by a high-resolution structure of an Ach receptor showing these residues all face to the ion channel of the receptor (Karlin 2002). SCAM therefore is an effective method to explore the structure of ion channels.

SCAM has also been used to identify amino acids contributing to the pore of P2XRs (Egan et al. 1998, François Rassendren et al. 1997). Rassendren *et al.* (François Rassendren et al. 1997) used different sized MTS reagents to determine the location of the pore and the channel gate. Amino acids preceding and throughout the second hydrophobic domain (TM2) (316-354) were mutated individually to cysteines. For three of these mutants (I328C, N333C, and T336C), currents evoked by ATP were inhibited by extracellular application of either positively or negatively charged MTS compounds, suggesting they lie in the outer vestibule of the pore. For L338C and D349C, only the smaller MTS compound inhibited the current at the P2X2R. L338C was accessible to cysteine modification in the absence and presence of ATP, but D349C was inhibited by MTS compounds only when the channel was open by ATP (François Rassendren et al. 1997). The results indicated that TM2 forms the ionic pore and that the channel gate was suggested to be between L338 and D349. Using a similar approach, another study also suggested that TM2 lines pore of the P2X2R but G242 was indicated to be the part of the gate (Egan et al. 1998). TM2 has now been confirmed to line the ion conduction pore of the P2XR by the crystal structure of the zfP2X4R (Kawate et al. 2009).

A subsequent study by SCAM gave a clearer picture of the location of the pore-forming and gate regions in the P2XR. The ability of MTSET and silver to access residue T336C and below was greatly affected by the presence of ATP at the P2X2R, suggesting that T336 may be part of the gate of the receptor (Li et al. 2008). T336 corresponds to A344 in the zfP2X4 receptor and this residue was suggested to be the centre of the gate and the narrowest section of the pore

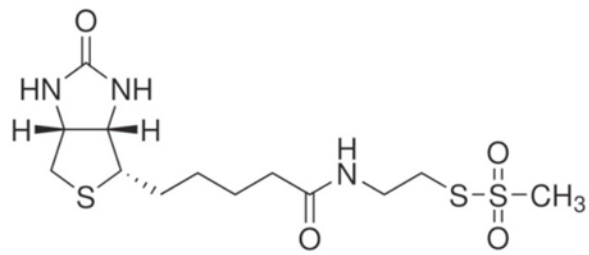
(Kawate et al. 2009). The findings by SCAM and the crystal structure are consistent with each other.

4.1.1.2 Use of MTSEA-biotinylation to investigate P2XRs

MTSEA-biotin ((2-aminoethyl) methanethiosulfonate hydrobromide-biotin) is another commonly used sulfhydryl specific reagent. The molecule contains a reactive disulphide, which can bind to the sulfhydryl group of the free cysteine residue and determine the accessibility of surface exposed cysteine residues (Figure 4.1). Exposed cysteines can be differentiated from protein buried ones by MTSEA-biotin because only exposed cysteines can react at an appreciable rate.

MTSEA-biotinylation was used in a variety of applications to investigate structure and ligand action of P2XRs in the pre-crystallization era. The first use of MTSEA-Biotin assay to P2XRs was for investigating whether the 10 conserved cysteine residues in the extracellular domain of the receptor could form disulphide bonds and constrain the receptor structure. Cysteine reactive MTSEA-biotin was unable to bind to WT P2X1Rs, suggesting that no free cysteine residues in the extracellular domain. A cysteine-alanine point mutation of a residue that normally forms a disulphide bond would result in the bond being unable to form and potentially providing an available free cysteine. Studies showed biotinylation was detected when individual cysteine residues were mutated, suggesting that point mutations removed these disulphide bonds and exposed the free cysteines. It was considered unlikely that the mutation to remove a cysteine resulted in major structural changes in the protein as these mutations resulted only in small 2- to 5-fold changes in ATP potency (Ennion and Evans 2002b). Therefore, biotin detection indicated a disulphide bond that had been broken. It indicated that at least three disulphide bonds were formed in the native receptor. Single cysteine mutants changed P2XR pharmacological properties, with similar effects for pairs of cysteine mutants at both P2X1Rs (Ennion and Evans 2002b) and P2X2Rs (Clyne et al. 2002). It was concluded that the ten conserved cysteine residues in the extracellular loop of mammalian P2XRs formed five disulphide bonds (Clyne et al. 2002, Ennion and Evans 2002b). Cysteine mutagenesis studies were

(a)



MTSEA-Biotin

(b)

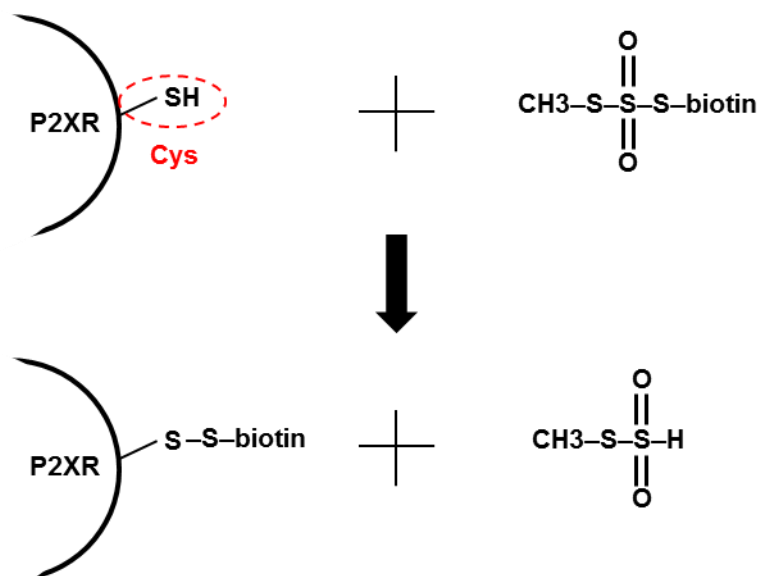


Figure 4.1 The chemical reaction between a free cysteine residue and the MTSEA-biotin assay (a) The molecular structure of MTSEA-biotin. (b) Cysteine sulfhydryl is converted to a disulfide coupled to biotin.

therefore useful in providing the first insight into P2XRs structural constraints and molecular distances between residues. This pairing pattern was confirmed in the crystal structure of the zfP2X4R, showing disulphide pairs 1-6, 2-4 and 3-5 located within the head region, disulphide 7-8 in the dorsal fin region and 9-10 towards the TM domains at the bottom of the body region of the receptor (Kawate et al. 2009, Young 2010).

In subsequent studies, SCAM coupled with MTSEA-biotin has also been successfully used to determine whether a cysteine residue was (i) accessible at the receptor extracellular surface and (ii) whether this is sensitive to receptor activation (Roberts and Evans 2007) (J. A. Roberts et al. 2012, Roberts et al. 2009b) to evaluate their contributions to ATP binding and/or conformational changes. Using the hP2X1R as a model, mutagenesis data suggested N290, F291, R292 and K309 were important for ATP binding. To address the role of these residues and adjacent non-conserved residues, substituted cysteine-scanning mutagenesis coupled with MTSEA-biotin were undertaken in the region S286-I329 (Roberts and Evans 2007). The majority of substituted cysteine residues showed MTSEA-biotinylation with relative levels giving an indication of relative accessibility. Of the MTSEA-biotinylated cysteine residues, only the N290F291R292 and K309 cysteine mutants showed changes in ATP potency after MTS application. MTSEA-biotinylation at these residues was also reduced by ATP application. This was consistent with ATP competing with MTSEA-biotin for occupation of the agonist binding site and further supported the close association of the NFR motif and K309 with the ATP binding site (Roberts and Evans 2007). The result was consistent with the crystal structure showing that N290, R292 and K309 form interacting with phosphates of the ATP (Hattori and Gouaux 2012). However, F291 is not in the ATP binding site from the crystal structure. Because F291 is adjacent to the binding pocket, ATP binding may also decrease its accessibility. This suggests that SCAM coupled with MTSEA-biotin can predict the approximate ligand binding site but other techniques are also needed to identify the residues involved.

The MTSEA-biotinylation assay was also used to map the surface accessibility of the cysteine substituted Glu181-Val200 region and to determine

whether it is sensitive to ATP (Roberts, 2009). It was shown that Thr186-Ser194 alternative residues were MTSEA-biotinylated, which was consistent with bioinformatics predictions that this region of the receptor forms a beta sheet (Digby et al. 2005). Thr186, Phe188 and Lys190 mutants showed decreases in ATP potency. The results suggested that these residues face the ATP binding pocket. The biotinylation of the face of the beta sheet was sensitive to the application of ATP indicating that the accessibility of the beta sheet is either blocked by ATP binding or closure of the agonist binding pocket (Roberts et al. 2009b). It was now known that T186 and K190 are both involved in ATP binding to the receptor (Hattori and Gouaux 2012).

As the crystal structure of zfP2X4R only provided a snapshot of the receptor, MTSEA-biotin was also used to address ATP-induced conformational changes during activation. MTSEA-biotin was used to show ATP-sensitive accessibility of cysteine mutants in the extracellular domain of the hP2X1R. These mutants (E52-G96) stretch from the first transmembrane segment to the receptor apex, and incorporate residues lining the upper, central, and extracellular vestibules and part of the ligand binding site (J. A. Roberts et al. 2012). Mapping all the residues onto a P2X1R homology model, inaccessible residues are predominately buried within the receptor. Cysteine mutants that were biotinylated can be divided into three groups: (i) those on the receptor surface around the mouth of the lateral portal, and at the apex of the receptor that are accessible in the presence/absence of ATP; (ii) residues around the agonist binding site, where MTSEA-biotinylation was generally reduced by ATP consistent with an allosteric reduction in accessibility and (iii) residues that line, or are at the interface between, subunits that form the upper and central vestibules, where ATP reduced MTSEA-biotinylation. Combining the results of electron microscopy and introducing disulphide bonds between adjacent subunits, it was proposed a model whereby agonist binding leads to movement of the head region and right flipper to close the ATP binding pocket and restricts access to the upper vestibule (J. A. Roberts et al. 2012). The motions have been confirmed by comparison the crystal structures of P2XR in close and open states (Hattori and Gouaux 2012, Kawate et al. 2009). Therefore, cysteine mutagenesis

and MTSEA-biotinylation have been proved to be a useful and successful approach to investigate ligand binding to P2XRs.

4.1.2 Hypothesis

The ligand binding site of a receptor comprises a number of specific residues. For example, the high affinity ATP binding of the P2XR is dependent on several key residues (K68, K70, T186, K190, N290, R292 and K309) (numbering for the hP2X1R) (Hattori and Gouaux 2012). The results in Chapter 3 suggested the importance of K249 to PPADS action at the hP2X1R. However, other residues involved in PPADS binding remain to be identified. Based on the molecular dimensions of the antagonist, it was hypothesised that residues involved in PPADS binding would be included in a ring with the radius of the length of PPADS (13 Å) which centres on K249.

Residues on the surface of the hP2X1R in the ring can be predicted from the homology model. It has previously been shown that accessibility of cysteine residues can be modified by ATP binding. This can result from direct blocking of access by ATP or agonist-evolved conformational changes (away from the ATP binding site). Therefore, the effect of PPADS on the accessibility of cysteine mutants on the receptor surface within this area would give indications of their contribution to the PPADS binding site. It was hypothesized that if PPADS had no effect on accessibility, it would not be part of the binding site for the antagonist. PPADS induced changes in accessibility would indicate antagonist binding site and/or conformational changes (Figure 4.2).

In order to map the PPADS binding sites and investigate the relationship of that with the ATP binding sites, residues in the predicted PPADS binding area were divided into three parts, residues around the ATP binding pocket, residues opposite to the ATP binding pocket around the dorsal fin and those in the upper body (Figure 4.3). Residues lining the surface of these sections were mutated into individual cysteine mutants by mutagenesis. Their access to MTSES-biotin and whether sensitive to PPADS or ATP were determined.

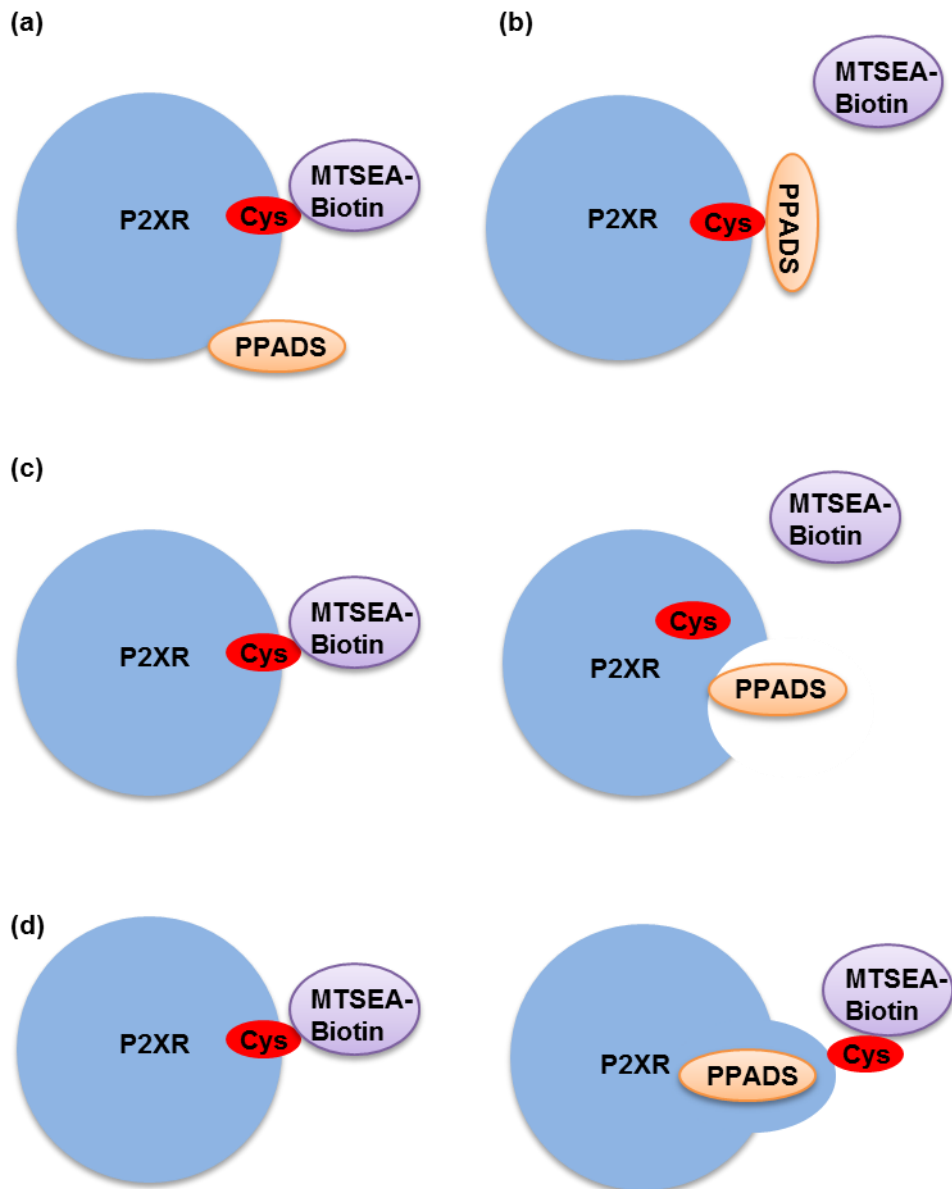
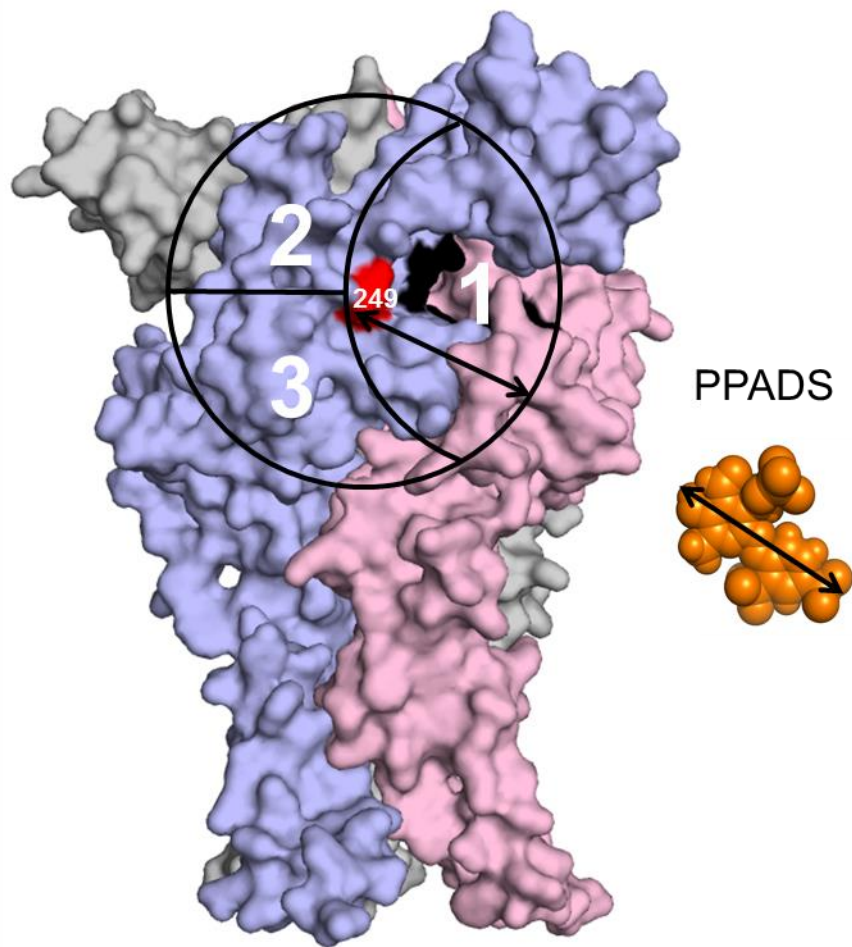


Figure 4.2 Potential effects of PPADS on the level of MTSEA-biotinylation
(a) MTSEA-biotin binds to a surface free cysteine mutant that was introduced to the hP2X1R by mutagenesis. There would be no significant change in accessibility of the cysteine mutant following PPADS binding if it is far from the antagonist binding sites. **(b)** Accessibility of the cysteine mutants would be decreased by PPADS binding if PPADS binds to this residue. **(c)** PPADS-induced conformational changes may decrease accessibility of the cysteine mutant. **(d)** PPADS-induced conformational changes may increase accessibility of the cysteine mutant.



Group 1: Residues around the ATP binding pocket
Group 2: Residues in the upper body
Group 3: Residues around dorsal fin

Figure 4.3 Division of residues in the predict ring which centres on 249. Homology model of the hp2X1R based on the crystal structure of zfP2X4R is shown in the apo state. Three subunits are shown in blue, pink and grey respectively. The conserved residues for ATP binding are shown in black and the 249 residue is labelled in red. PPADS is shown as an orange sphere and its max dimension is shown with a black arrow. The black ring centres on 249 and its radius is the length of PPADS. Residues are divided into three different groups according to their locations.

4.1.3 Aim

The aim of this chapter was to test whether PPADS has an effect on accessibility of individual cysteine mutants in the predicted PPADS binding ring. In addition, it was determined the extent to which changes in accessibility were similar to those evoked by ATP binding.

4.2 Results

4.2.1 No free cysteine residue can be detected at WT hP2X1Rs

Oocytes expressing hP2X1Rs were incubated with apyrase (15 U/ml) or PPADS (100 μ M). The hP2X1Rs were highly expressed as shown in the total sample. WT hP2X1Rs were detected at ~55KDa (Figure 4.4a). The hP2X1Rs run as monomers following heating and with SDS sample buffer plus β -mercaptoethanol (5%) added before loading to the western blotting gel. This molecular weight was ~6KDa higher than predicted from molecular weight of the sequence (~49KDa). The results were consistent with previous studies showing WT hP2X1Rs are glycosylated as demonstrated by reduction in molecular weight following Endo H or PNGase treatment (Roberts and Evans 2006).

Following MTSEA-biotin treatment (100 μ M, 10 min) with apyrase to break down any endogenous ATP released from the oocytes, Streptavidin beads were used to pull down the biotinylated protein. When the lysate was processed to isolate biotinylated protein and run on a gel and probed with anti-P2X1R antibody, the receptor was not detected in either apyrase or PPADS condition (Figure 4.4a), which means no free cysteine residues were available for labelling. This finding is consistent with the 10 conserved native cysteine residues in the extracellular loop of the receptor forming 5 disulphide bonds first suggested by cysteine mutagenesis and MTSEA-Biotin assay (Ennion and Evans 2002b) and confirmed by crystal structures (Kawate et al. 2009). For non-injected oocytes, no hP2X1Rs were detected by the anti-P2X1R antibody, suggesting no endogenous P2X1Rs were expressed in oocytes or cross-reactivity of the antibody with any native oocyte protein (Figure 4.4a).

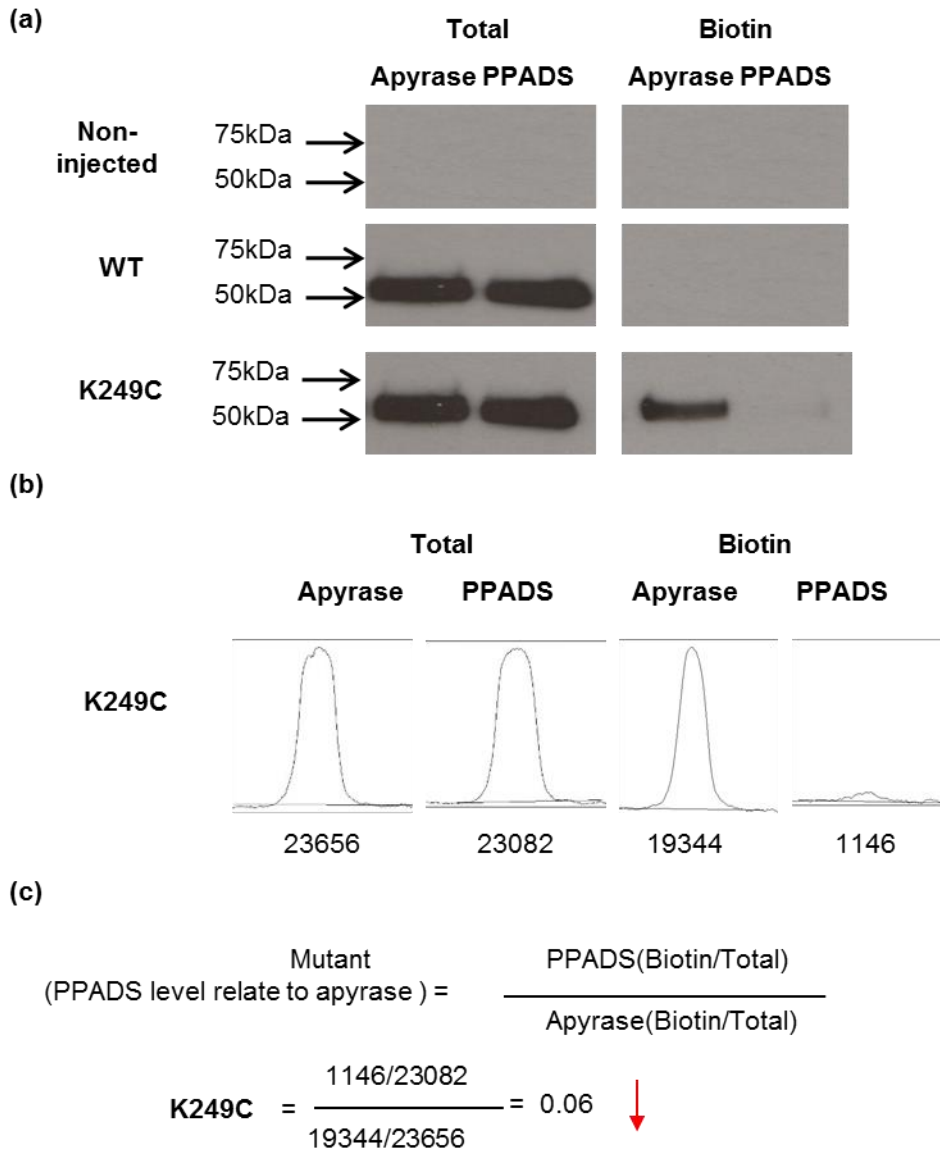


Figure 4.4 Validation of MTSEA-Biotin assay for measuring the effects of PPADS on accessibility of cysteine mutants. (a) Oocytes were pre-incubated with apyrase (15 U/ml) or PPADS (100 μ M) for 10 min and then with MTSEA-biotin (100 μ M, 10 min), then lysed in a fraction kept for detection of total sample. Biotinylated proteins were isolated with Streptavidin beads from total samples. All the samples were run on the gel and blotted with anti-P2X1R antibody (1:2000). Blots showed no hP2X1Rs labelling from non-injected oocytes; hP2X1Rs were detected in total samples of WT and K249C at ~55kDa; No biotinylation was detected for WT hP2X1s; Biotinylation was apparent for K249C receptors and significantly decreased following PPADS treatment. (b) The intensities of apyrase and PPADS bands were derived from the area shown in the square by using ImageJ software, shown by the number under the square. (c) Calculation of the relative intensity of bands and worked examples for K249C.

4.2.2 PPADS decreased accessibility of K249C at the hP2X1R

The cysteine mutant K249C showed a significant decrease (~3-fold) in PPADS potency at the hP2X1R (Chapter 3), suggesting this lysine may be involved in PPADS binding to the receptor. It was hypothesized that if the residue was in the PPADS binding site, it should be on the surface accessible by MTSEA-biotin in the resting state of the receptor and its accessibility would be reduced by PPADS binding. For K249C, the total sample showed the receptors were highly expressed at the cell surface (Figure 4.4a). With this mutant, the receptor was biotinylated in the presence of apyrase, suggesting the introduced K249C provided a free cysteine residue available for MTSEA-biotin. The biotinylated P2X1Rs were observed and the level was markedly decreased following PPADS treatment (Figure 4.4a).

Densitometry was used to quantify the level of biotinylation for each cysteine mutant. The intensities of apyrase and PPADS bands in total and biotin samples were calculated using Image J software (Figure 4.4b). In order to correct for any differences in expression, the bands of biotinylated proteins (biotin sample) were divided by those in the corresponding total sample. The level of biotinylation with PPADS was calculated relative to that with apyrase. An example of a biotinylated protein is shown (Figure 4.4c). The fraction of biotinylation with PPADS labelling compared to that with Apyrase was ~0.06 (Figure 4.4c), showing that in this experiment accessibility of the mutant was reduced by ~94% by PPADS. The mean decrease in biotinylation by PPADS of K249C was ~90% (Figure 4.6). This result showed that PPADS binding reduced accessibility of K249C. This suggests lysine 249 may be an important residue contributing to PPADS binding, which supports the results in Chapter 3.

4.2.3 PPADS does not have an effect on accessibility of residues out of the potential PPADS binding area

As the biotinylation of K249C decreased when the receptors were treated with PPADS, it was necessary to make sure PPADS did not make any chemical modifications affecting the activity of MTSEA-biotin to bind to cysteine residues. As a control the effects of PPADS on biotinylation of three cysteine mutants out

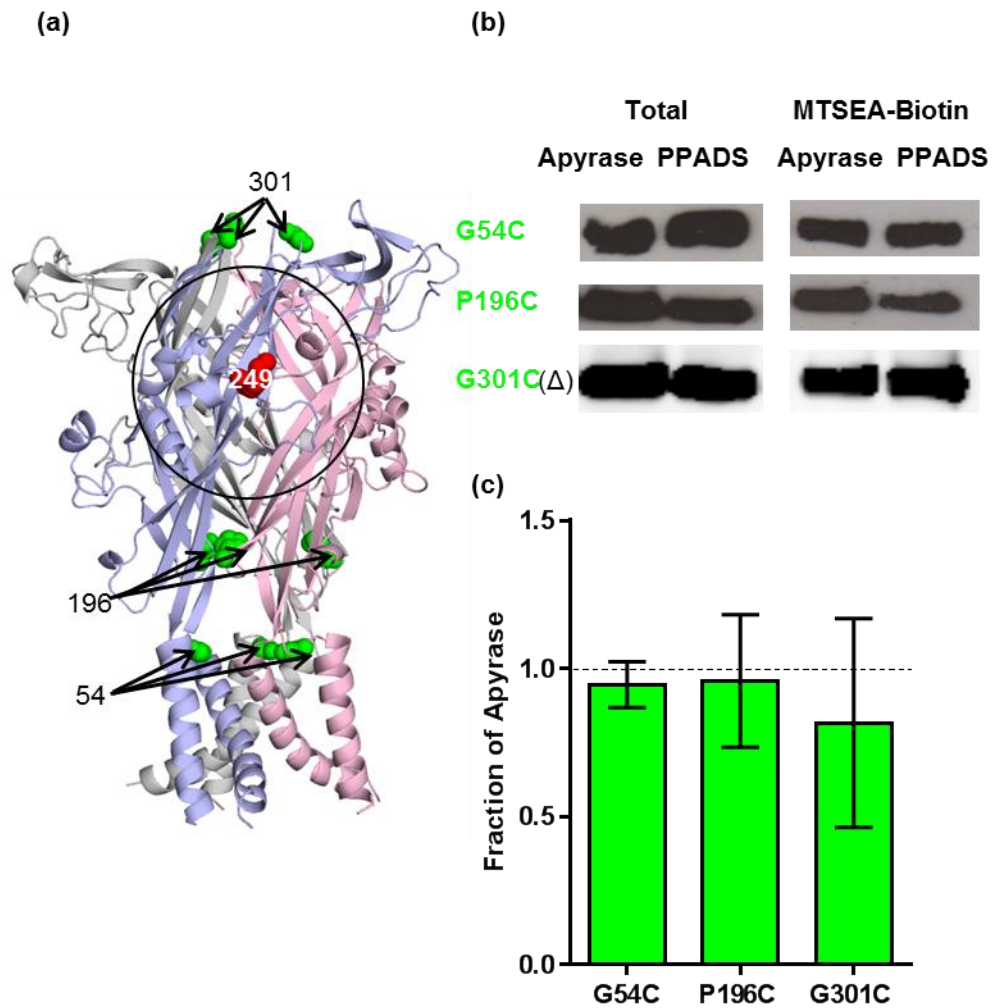


Figure 4.5 No effect of PPADS binding on accessibility of cysteine mutants outside the potential PPADS binding ring. (a) Three residues out of the potential PPADS binding ring are shown as green spheres in the homology model of hP2X1R in the closed state. The receptor is shown as a cartoon. Residue 249 is shown as a red sphere. The black ring centres on 249 and its radius is the length of PPADS. (b) Representative blots of total and biotinylated hP2X1Rs treated with 15 U/ml apyrase or 100 μ M PPADS. (c) Densitometric analysis using ImageJ calculated any change in MTSEA-Biotin accessibility at the cysteine mutants following PPADS treatment ($n \geq 3$). Images were captured by films except Δ by Typhoon scanner.

of the predicted PPADS binding area was tested. P196, G54 and G301 are located at the lower body, the membrane interface and apex of the receptor respectively (Figure 4.5a). Previous studies have shown that their cysteine mutants were accessible by MTSE-biotin and the biotinylation was not changed by ATP binding (J. A. Roberts et al. 2012, Roberts and Evans 2007, Roberts et al. 2009b).

The three mutants were labelled by MTSEA-Biotin (Figure 4.5b,c), confirming previous work (J. A. Roberts et al. 2012, Roberts and Evans 2007, Roberts et al. 2009b). The level of biotinylation was not significantly changed by PPADS treatment (Figure 4.5b, c). These results support the fact that the decreased biotinylation seen for K249C did not result from a direct chemical reaction between PPADS and MTSEA-biotin but from reduced accessibility of the residue. Therefore, the MTSEA-biotin assay can be used to measure changes in accessibility of cysteine mutants in response to PPADS binding.

4.2.4 Effect of PPADS on accessibility of surface cysteine mutants around the ATP binding sites

As PPADS blocks ATP action, the effects of PPADS on accessibility of residues around the ATP binding pocket were investigated first. A range of residues around the ATP binding pocket were selected (Figure 4.6a). Blots of the selected residues (K249, D170, G123, K138, R139, K215, A211, N284 and G288) are shown. All of these cysteine mutants were expressed at the cell surface (Figure 4.6b).

MTSEA-biotinylation was detected for all the cysteine mutants except A211C. The lack of biotinylation at A211C indicates the residue is not accessible. PPADS had no significant effect on the accessibility of cysteine mutants N284C and G288C (at the tip and connection of the left flipper to the body) (Figure 4.6b, c), suggesting they may be not directly involved in PPADS binding and further supports that PPADS does not directly interfere with the ability of MTSEA-biotin to bind to the reactive cysteines. For cysteine mutants K249C and D170C, biotinylation was almost abolished by PPADS (decreased by >90%). For the mutants G123C and K139C, MTSEA-biotinylation was reduced by ~55% and

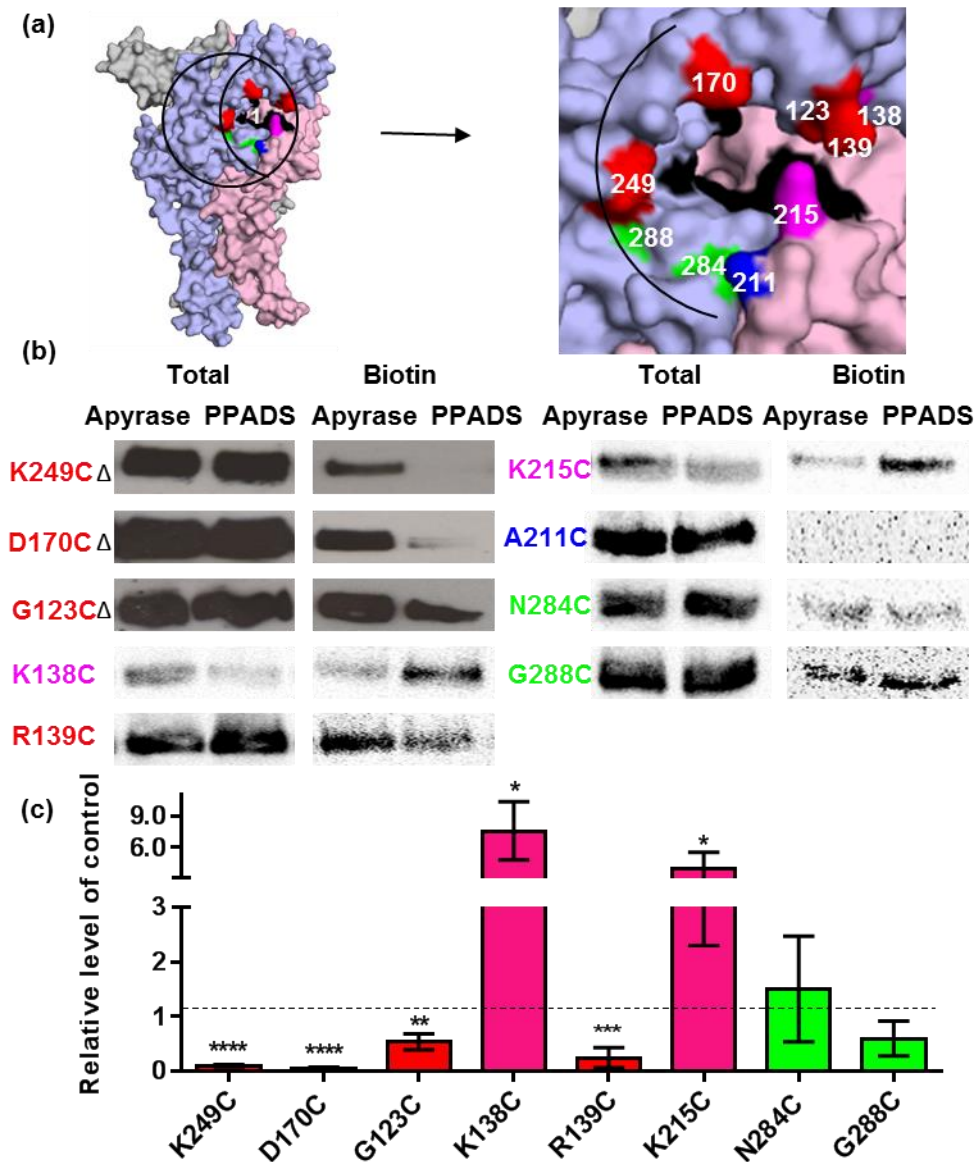


Figure 4.6 Effect of PPADS binding on accessibility of the cysteine mutants around the ATP binding pocket. (a) Selected residues around the ATP binding sites are labelled in the homology model of the hP2X1R in the closed state. The receptor is shown as surface representation. The residues involved in ATP binding are shown in black. The ring centres on 249 and its radius is the width of PPADS. Residues showing decreased accessibility following PPADS treatment are labelled in red, increased in pink, no significant change in green and inaccessible in blue. (b) Representative bands of total and biotinylated hP2X1Rs treated with 15 U/ml apyrase or 100 μ M PPADS. (c) Densitometric analysis using ImageJ calculated any change in MTESA-Biotin accessibility at the cysteine mutants following PPADS treatment. Images were captured by typhoon scanner except those indicated by Δ using by films. Significant differences between biotinylation levels following treatment of apyrase and PPADS were performed by paired t test (* p <0.05, ** p <0.01, *** p <0.001, **** p <0.0001). The data were plotted as mean \pm SEM ($n \geq 3$).

~73% respectively in the presence of PPADS. The decreased accessibility following PPADS binding indicated that these residues may be involved in PPADS binding or result from PPADS-induced conformational changes.

At mutants K138C and K215C, MTEA-biotinylation increased ~8-fold and ~4-fold respectively in the presence of PPADS. This increase demonstrates that PPADS binding results in conformational changes in the P2X1R increasing accessibility at these positions and that PPADS binding may evoke significant changes in accessibility around the ATP binding pocket.

The quality of some images captured by the Typhoon Scanner was not as good as those exposed in films. The noise background in the images were shown as the baselines in analysis using Image J. In addition, the data was generated by comparing the densitometry between samples in different conditions, which were in the same gel. Therefore, some images with poor quality still can be quantified effectively.

4.2.5 Effect of PPADS on accessibility of cysteine mutants deep in the ATP binding sites

Three conserved lysines (K68, K70 and K190) in the first beta strand (β 1) of the extracellular loop of the P2XR contribute to the ATP binding sites (Hattori and Gouaux 2012). Negatively charged PPADS can non-selectively inhibit most P2XR subtypes. We therefore tested whether accessibility to these positively charged lysines was modified by PPADS. Previous studies have shown that alternate cysteine mutants on the strand incorporating K68 and K70 correspond to those facing the agonist pocket and were accessible (J. A. Roberts et al. 2012, Roberts et al. 2009b). The three cysteine mutants (K68C, K70C and K190C) in the ATP binding pocket and another two residues adjacent to them (S64 and S66) showed decreased accessibility by ATP binding in previous studies (J. A. Roberts et al. 2012). Their accessibility changes by PPADS binding were investigated here (Figure 4.7a).

The mutants were all biotinylated, which was consistent with previous studies. For K68C and K190C, biotinylation was reduced by ~40% and ~50%

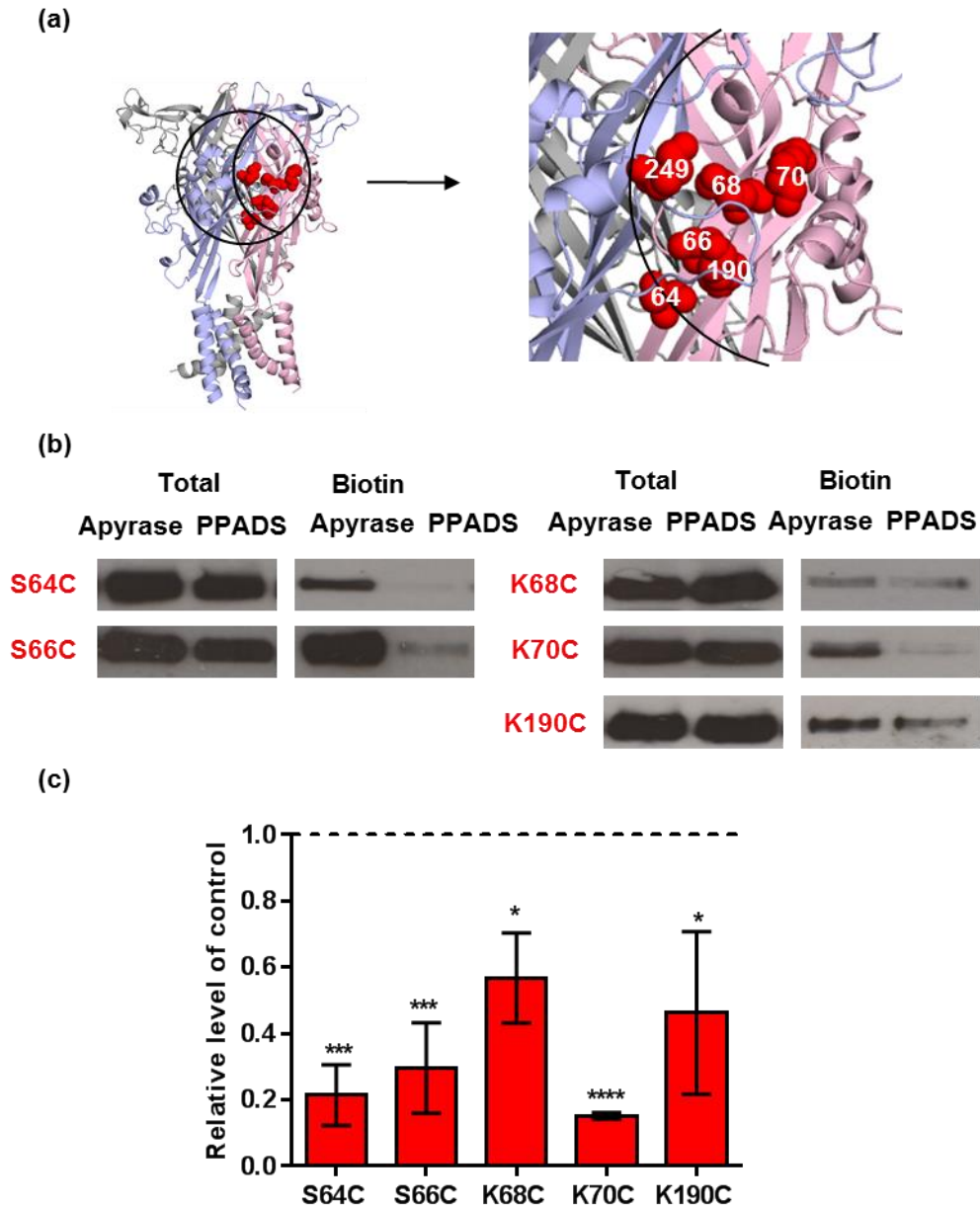


Figure 4.7 Effect of PPADS binding on accessibility of cysteine mutants deep in the ATP binding pocket. (a) The location of selected residues in the ATP binding pocket are shown in red (decreased accessibility) sphere. The receptor is shown as a cartoon. The ring centres on 249 and its radius is the width of PPADS. (b) Representative bands of total and biotinylated hP2X1Rs treated with 15 U/ml apyrase or 100 μ M PPADS. (c) Densitometric analysis using ImageJ calculated any change in MTESA-Biotin accessibility at the cysteine mutants following PPADS treatment. Images were captured by film. Significant differences between biotinylation levels following treatment of apyrase and PPADS were performed by paired t test ($*p < 0.05$, $***p < 0.001$, $****p < 0.0001$). The data were plotted as mean \pm SEM ($n \geq 3$).

respectively following PPADS treatment. Biotinylation of K70C was decreased by ~85%. MTSEA-biotinylation at S64C and S66C was detected and reduced by ~80% and ~70% respectively in the presence of PPADS (Figure 4.7b, c).

4.2.6 Effect of PPADS on accessibility of the cysteine residues in the upper body of the hP2X1R

The section of the potential PPADS binding area opposite to the ATP binding sites was divided into two parts, the upper body and the flipper of the receptor subunit (Figure 4.8a). In the upper body, a range of residues were selected and divided into three regions: (i) top (74-78), (ii) middle 175, (iii) bottom 247-248. In the top region, all the cysteine mutants (V74C-P78C) were surface accessible by MTSEA-biotin, which is consistent with previous studies (J. A. Roberts et al. 2012). Biotinylation of V74C and T75C was almost abolished by PPADS binding (decreased by >95%) and that of L77C was reduced by ~60%. However, at two residues (Q76C, Q78C), there was no significant change in biotinylation following PPADS treatment. The mutant S175C, which is located in the middle region, was also accessible and there was no significant change in biotinylation following PPADS treatment. In the bottom area, the biotinylation level of the mutant A247C was below the limit of detection. E248C was accessible and the biotinylation was reduced by ~85% by PPADS. (Figure 4.8b, c).

4.2.7 Effect of PPADS on accessibility of the cysteine residues around the dorsal fin of the hP2X1R

The final section of the potential PPADS binding area to be tested comprises the flipper of the subunit. A group of residues (A182, R203, L279 and Q237) along the edge of the ring were selected (Figure 4.9a). Their cysteine substitutions were all accessible as measured by MTSEA-biotinylation. For cysteine mutants A182C and L279C, MTSEA-biotinylation was reduced by ~90% and ~65% respectively following PPADS treatment. No significant change was detected for R203C and Q237C in the biotinylation level (Figure 4.9b, c).

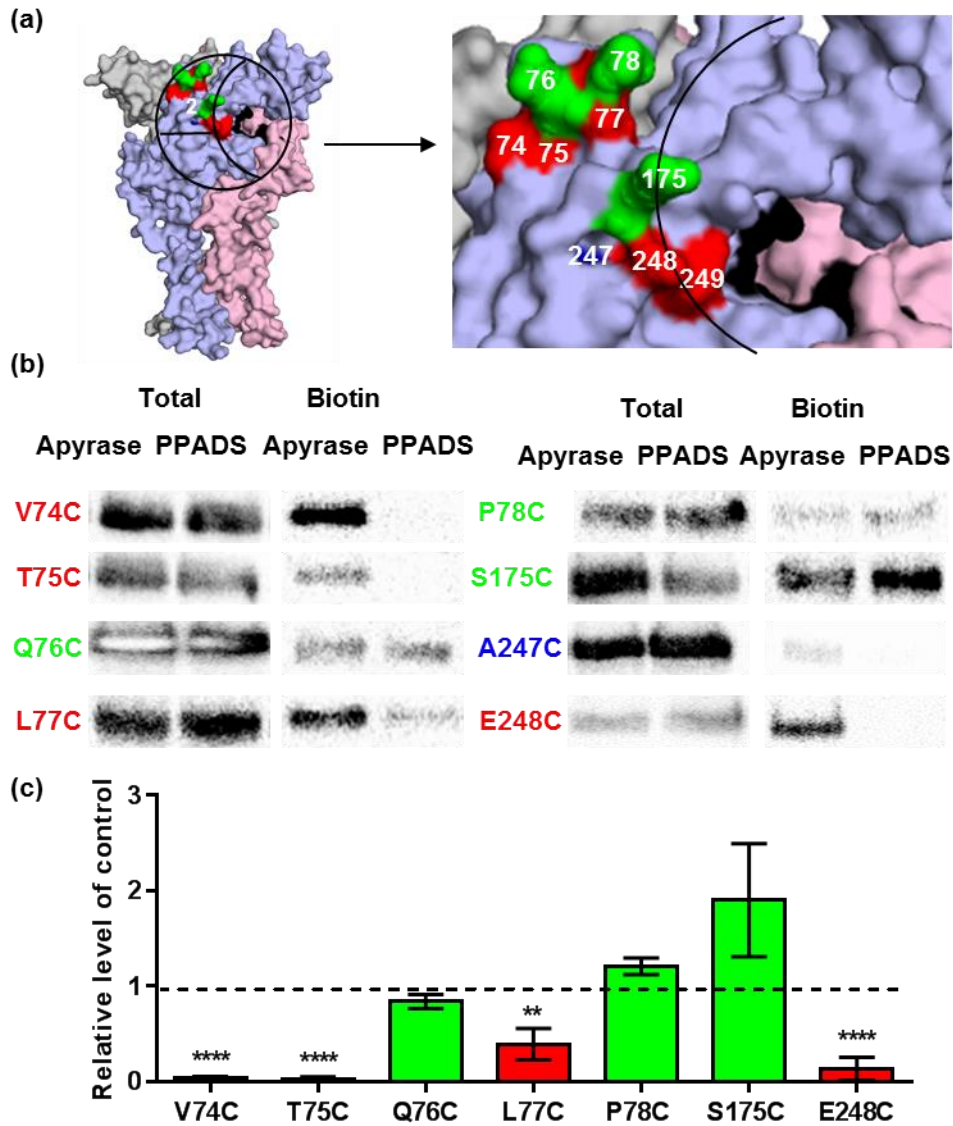


Figure 4.8 Effect of PPADS binding on accessibility of the cysteine mutants opposite to the ATP binding pocket in the upper body. (a) Selected residues opposite to the ATP binding site are labelled in the homology model of the hP2X1R in the closed state. The receptor is shown as surface representation. The residues involved in ATP binding are shown in black. The ring centres on 249 and its radius is the width of PPADS. Residues showing decreased accessibility following PPADS treatment are labelled in red, no significant change in green and inaccessible in blue. **(b)** Representative bands of total and biotinylated hP2X1Rs treated with 15 U/ml apyrase or 100 μ M PPADS. **(c)** Densitometric analysis using ImageJ calculated any change in MTESA-Biotin accessibility at the cysteine mutants following PPADS treatment. Images were captured by typhoon scanner. Significant differences between biotinylation levels following treatment of apyrase and PPADS were performed by paired t test (** $p < 0.01$, **** $p < 0.0001$). The data were plotted as mean \pm SEM ($n \geq 3$).

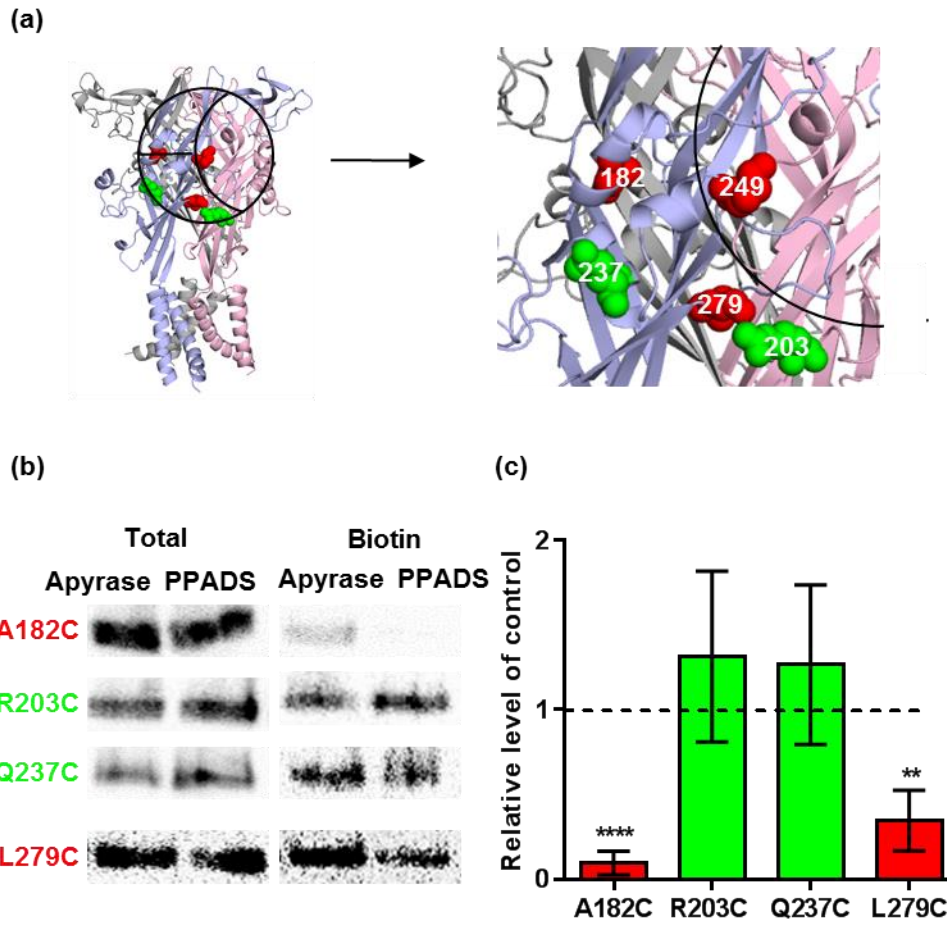


Figure 4.9 Effect of PPADS binding on accessibility of the cysteine mutants opposite to the ATP binding pocket in the flippers. (a) The homology model of the hP2X1R in the closed state is shown in cartoon. The location of selected residues opposite to the ATP binding pocket in the flippers are shown in red (decreased accessibility) and green (no change in accessibility) sphere. The ring centres on 249 and its radius is the width of PPADS. (b) Representative bands of total and biotinylated hP2X1Rs treated with 15 U/ml apyrase or 100 μ M PPADS. (c) Densitometric analysis using ImageJ calculated any change in MTESA-Biotin accessibility at the cysteine mutants following PPADS treatment. Images were captured by typhoon scanner. Significant differences between biotinylation levels following treatment of apyrase and PPADS were performed by paired t test (** $p < 0.01$, **** $p < 0.0001$). The data were plotted as mean \pm SEM ($n \geq 3$).

4.2.8 Effect of PPADS on accessibility of the residues lining the upper vestibule

Previous studies have shown ATP binding leads to conformational changes and reduced MTSEA-biotin access to the upper vestibule of the hP2X1R (J. A. Roberts et al. 2012). In order to see if conformational changes by PPADS extended to the upper vestibule, biotinylation at P93C, A94C, H95C, and G96C lining the upper vestibular was tested (Figure 4.10a, b). The mutants were all accessible by MTSEA-biotin. PPADS binding almost abolished biotinylation of A94C and H95C (decreased by ~95%). The biotinylation of G96C was decreased by ~80%. No significant change in biotinylation was found at P93C (Figure 4.10c, d).

4.2.9 Comparison effects between PPADS and ATP on accessibility of cysteine mutants in the potential PPADS binding area

ATP has been shown to lead to decreased biotinylation both due to direct block and conformational change (J. A. Roberts et al. 2012). Therefore, we determined the effects of PPADS and ATP on accessibility of cysteine mutants in the potential PPADS binding area to allow comparisons between the agonist and the antagonist. For the residues out of the ring, there was no significant change in biotinylation at P196C and G301C (Figure S4.1), which are consistent with previous studies (Roberts and Evans 2007, Roberts et al. 2009b). It shows neither PPADS nor ATP has an effect on accessibility of these two positions. However, ATP treatment resulted in a modest increase (~1.5-fold) in biotinylation of cysteine residue G54C where PPADS showed no significant effect (Figure S4.1).

At the orthosteric site, ATP reduced MTSEA-biotinylation of cysteine mutants K249C, D170C and G123C, by ~75%, ~90% and ~80% respectively (Figure S4.2). No significant change in biotinylation was found at N284C by ATP binding. The effects of ATP on accessibility of these cysteine mutants were similar with those of PPADS (Figure 4.6). The accessibility of G288C was decreased in the presence of ATP by ~50%, which is consistent with previous studies (Roberts and Evans 2007). But there was no change in biotinylation by

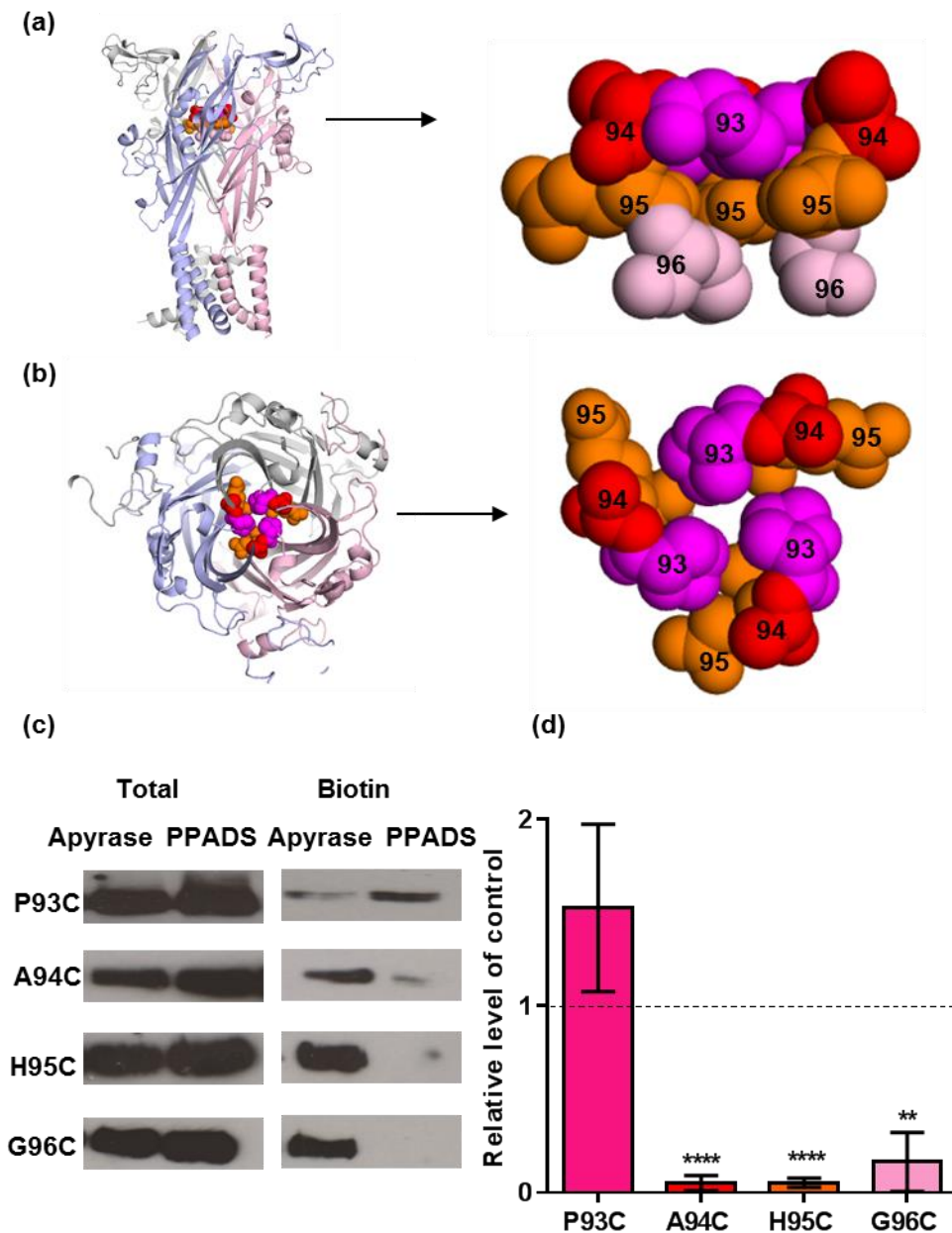


Figure 4.10 Effects of PPADS binding on accessibility of cysteine mutants lining the upper vestibule. (a) Selected residues (93-96) lining the upper vestibule are labelled with different colours in the homology model of the hP2X1R in the closed state. Three subunits of the receptor are shown as cartoon. (b) The top view of the receptor. (c) Representative bands of total and biotinylated hP2X1Rs treated with 15 U/ml apyrase or 100 μM PPADS. (d) Densitometric analysis using ImageJ calculated any change in MTESA-Biotin accessibility at the cysteine mutants following PPADS treatment. Images were captured by typhoon scanner. Significant differences between biotinylation levels following treatment of apyrase and PPADS were performed by paired t test (** $p < 0.01$, **** $p < 0.0001$). The data were plotted as mean \pm SEM ($n \geq 3$).

PPADS binding. More importantly, for three positively charged lysines (K138, R139 and K215), ATP did not show significant effect on MTSEA-biotinylation of their cysteine substitutes (Figure S4.2) but PPADS caused significant changes on their accessibility, with increase at K138 (~8-fold) and K215 (~4-fold) and decrease (by ~85%) at R139. For the lysines in the ATP binding pocket, ATP did not cause significant change in biotinylation of K68C and K70C and modest decrease at K190C (~50%) (Figure S4.3), which is consistent with previous studies (J. A. Roberts et al. 2012, Roberts et al. 2009b). These cysteine mutants have a major effect on ATP potency and the lack of biotinylation by ATP is likely to reflect that marked decrease in ATP binding as shown from radiolabelling (Roberts and Evans 2007). However, PPADS caused significant decreased accessibility of these lysines. For another two residues adjacent to them (S64C and S66C), ATP significantly decreased their biotinylation by ~90% (Figure S4.3), which is the similar effect of PPADS. Different effects of ATP and PPADS on accessibility of cysteine mutants at the orthosteric site suggested these residues play different roles between ATP binding and PPADS binding.

For the residues outside the ATP binding pocket, there was no significant difference in biotinylation of Q76C, Q78C, S175C, R203C, Q237C and L279C following ATP treatment. ATP binding significantly decreased biotinylation of cysteine mutants of V74C, T75C by ~90%. The accessibility of L77C was decreased by ~50% following ATP binding. For A182C and E248C, ATP caused ~80% decreased accessibility. (Figure S4.4, S4.5). The biotinylation change profiles for these cysteine mutants were similar to those seen for PPADS (Figure 4.11).

For the residues lining the upper vestibule, there was no difference of biotinylation at P93C following ATP binding. However, biotinylation of A94C and H95C was reduced by ~85% and that of G96C decreased by ~40% (Figure S4.6), suggesting the decreased accessibility of the upper vestibule. It was consistent with previous studies (Roberts, 2012). The similar accessibility changes of these residues were also shown following PPADS binding.

In summary, most of the cysteine mutants showed similar accessibility changes following either ATP or PPADS treatment only except G54, K138 and R139 (Figure 4.11). Previous studies showed no significant change in accessibility by ATP at G54 (J. A. Roberts et al. 2012). However, accessibility G54C increased ~1.5-fold by ATP but no change by PPADS in the study. Accessibility of K138C significantly increased by PPADS and that of R139C significantly decreased by PPADS but not by ATP. The difference suggests PPADS may cause different conformational changes at head region from those by ATP.

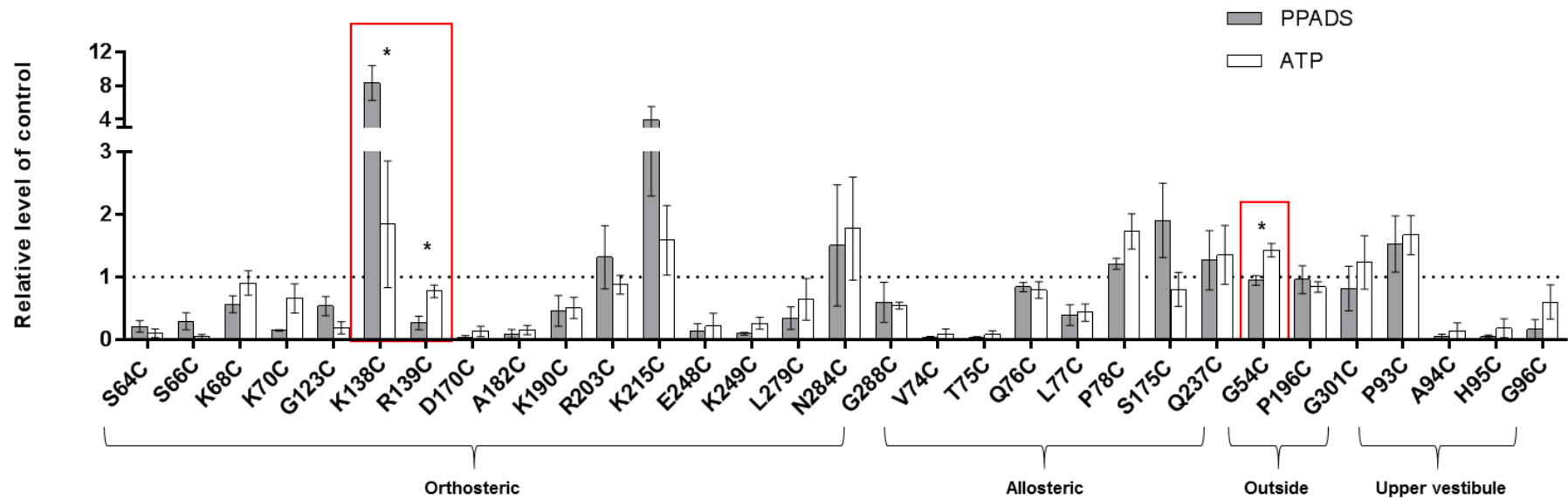


Figure 4.11 Comparison of MTSEA-biotinylation levels at the selected surface cysteine mutants following PPADS or ATP treatment. hP2X1Rs were expressed in oocytes. Individual mutants treated with PPADS (100 μ M) or ATP (1 mM) for 10 min. Densitometric analysis using ImageJ calculated any change in MTSEA-biotin accessibility at the cysteine mutants following PPADS or ATP treatment. For each mutant, the intensity bar of PPADS and ATP has been related to the biotinylation level determined in the presence of apyrase. Significant differences between biotinylation levels following treatment by PPADS or ATP were performed by paired t test ($*p < 0.05$). The data were plotted as mean \pm SEM ($n \geq 3$). Mutation with a significant difference between PPADS and ATP treatment are highlighted with red boxes.

Mutants	PPADS			ATP		
	Mean	S.E.M	n	Mean	S.E.M	n
S64C	0.21***	0.09	3	0.10****	0.07	3
S66C	0.30***	0.14	4	0.06****	0.03	5
K68C	0.57*	0.14	5	0.91	0.19	5
K70C	0.15****	0.01	3	0.66	0.23	3
G123C	0.54**	0.15	3	0.19****	0.10	3
K138C	8.31*	2.06	3	1.84	1.01	3
R139C	0.27***	0.11	3	0.77	0.10	3
D170C	0.04****	0.03	3	0.14****	0.08	3
A182C	0.10****	0.07	3	0.16****	0.07	3
K190C	0.46*	0.25	4	0.51*	0.17	4
R203C	1.31	0.50	3	0.88	0.15	3
K215C	3.90*	1.60	3	1.59	0.56	3
E248C	0.14****	0.12	3	0.22**	0.20	3
K249C	0.10****	0.02	4	0.26****	0.10	4
L279C	0.35**	0.18	3	0.64	0.33	3
N284C	1.50	0.97	3	1.77	0.82	3
G288C	0.60	0.32	3	0.55****	0.05	3
V74C	0.04****	0.02	3	0.09***	0.09	3
T75C	0.03****	0.02	3	0.08***	0.06	3
Q76C	0.84	0.07	3	0.79	0.13	3
L77C	0.40**	0.17	3	0.43**	0.14	3
Q78C	1.21	0.09	3	1.73	0.28	3
S175C	1.90	0.59	3	0.80	0.27	3
Q237C	1.27	0.47	4	1.35	0.47	4
G54C	0.95	0.08	3	1.43**	0.11	3
P196C	0.96	0.22	4	0.84	0.08	4
G301C	0.82	0.35	4	1.23	0.43	5
P93C	1.53	0.45	3	1.67	0.31	3
A94C	0.05****	0.04	3	0.15****	0.13	3
H95C	0.05****	0.02	5	0.19***	0.15	5
G96C	0.17**	0.16	3	0.60*	0.27	3

Table 4.1 Summary of effect of PPADS and ATP on biotinylation of cysteine mutants. The level of biotinylation at individual cysteine mutants following PPADS (100 μ M) or ATP (1 mM) treatment was calculated relative to that with treatment with apyrase (15 U/ml). The average of biotinylation and standard error of the mean is shown. n represents the times of experiments repeat. Significant differences between biotinylation levels following treatment of apyrase and PPADS/ATP were performed by paired t test (* $p < 0.05$, ** $p < 0.01$, *** $p < 0.001$, **** $p < 0.0001$).

4.3 Discussion

This chapter mapped the effects of PPADS on accessibility of residues in the potential PPADS binding ring which centres on residue 249. 33 cysteine mutants were expressed and their accessibility changes by PPADS binding were tested, including 3 mutants out of the ring and 30 mutants in the ring. These studies showed that PPADS can be used to classify residues into those with (i) no change in accessibility following PPADS binding (ii) decreased accessibility following PPADS binding, and (iii) increased accessibility following PPADS binding. They highlight that PPADS is likely to bind in the potential ring and in addition binding leads to significant conformational changes. These results highlight that MTSEA-biotinylation can be used to classify residues into distinct classes.

4.3.1 No effect of PPADS on accessibility of cysteine mutants out of the ring

In order to establish that the MTSEA-biotin assay would be useful, two control experiments were done first to show (i) no background, and (ii) no interference. The first control experiment was done on WT hP2X1Rs. No biotinylation was detected, which is consistent with previous studies showing the 10 conserved cysteines form 5 disulphide bounds in the extracellular loop of the P2XR (Kawate et al. 2009, Young 2010). No free cysteine residue was available for MTSEA-biotin to bind to. The second control experiment was done on residues outside of the potential PPADS binding ring. PPADS binding did not cause any change in the accessibility of the three cysteine mutants (G54C, P196C and G301C) out of the ring. It suggests they are not essential residues for PPADS binding. In addition, it indicates that PPADS has no effect on ability of MTSEA-biotin to bind to cysteines.

4.3.2 The importance of K249 in PPADS binding

Lysine 249 has been shown to be important for PPADS binding at the rP2X4R (Buell et al. 1996). The cysteine mutant K249C was shown to have a significant effect on PPADS sensitivity (~3-fold decrease) of the hP2X1R in

chapter 3. The role of this residue in antagonist action is further supported in this chapter by showing that PPADS decreased accessibility of K249C by ~90%. The decreased accessibility at K249 probably results from direct blocking by PPADS binding. This finding was consistent with previous studies suggesting K249 was involved in PPADS binding at P2XRs (Buell et al. 1996). Therefore, positively charged lysine at position 249 can contribute to the action of PPADS at hP2X1Rs.

4.3.3 Residues showing decreased accessibility by PPADS binding in the ring

The 30 cysteine mutants in the ring included 15 mutants that have been shown to be accessible in previous studies (J. A. Roberts et al. 2012, Roberts and Evans 2007, Roberts et al. 2009b) and 14 additional new mutants (G123C, K138C, R139C, D170C, S175C, K190C, R203C, A211C, K215C, Q237C, A247C, E248C, K249C, L279C, N284C). Most of the cysteine mutants were on the surface and accessible by MTSEA-biotin except A211C and A247C. A number of cysteine mutants where their biotinylation levels were decreased following PPADS treatment were identified. On the homology model of the hP2X1R, the residues showing decreased accessibility are widely spread in the potential PPADS binding area (Figure 4.12). In terms of the molecular size of PPADS, one molecule PPADS is unlikely to bind to all the residues. There are two possibilities to explain the results, one is that there may be multiple PPADS binding sites or poses in one receptor; the other possibility is that PPADS binding induces conformational changes in the receptor in the area other than the binding site and some of the residues showing decreased accessibility may be in the region that shows conformational changes.

The favoured hypothesis was that PPADS could bind at the orthosteric site. It mechanistically makes sense and a cluster of positive charges provides the electrostatic environment. In addition to K249, most of the residues showing decreased accessibility by PPADS binding are also originally positively charged, including three conserved positively charged residues (K68, K70 and K190) in the ATP binding pocket and one in the cysteine rich head (R139). Accessibility changes at these positions may result from direct blocking by PPADS binding or

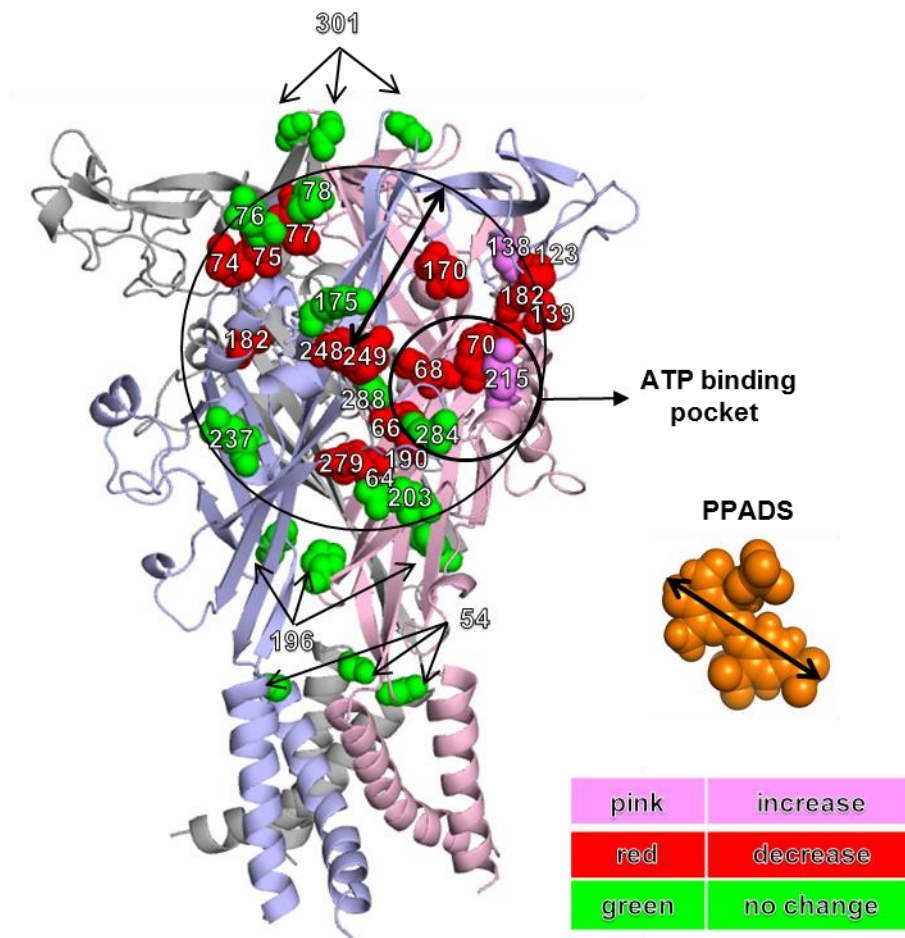


Figure 4.12 Effect of PPADS binding on accessibility of the selected cysteine mutants at the hP2X1R. The selected residues are labelled in the homology model of the hP2X1R in closed state. Residues showing decreased accessibility in the presence of PPADS are labelled in red, increased in pink and no significant change in green. The receptor is shown as a cartoon. The ATP binding pocket is shown as smaller black circle. The molecular structure of PPADS shown in orange sphere is in the same size as the hP2X1R model. The larger black ring centres on 249 and its radius is the width of PPADS.

PPADS-evoked conformational changes. As PPADS is a highly negatively charged compound, it is not surprising that these positively charged residues may interact with PPADS action. Accessibility of D170C, which is a negatively charged residue, also significantly decreased by PPADS, suggesting it may also have a role in PPADS action. Therefore, the electrostatic environment is important for PPADS binding to the receptor.

Accessibility changes of residues at the orthosteric site by PPADS suggests PPADS has a significant effect on the ATP binding site, which may block the ability of ATP to get access to the binding pocket. Two cysteine mutants (S64C and S66C) deep in the ATP binding pocket further support this idea. In addition, the effects of PPADS on the conserved residues can account for this non-selective action between each P2X subtype (Evans et al. 1995, Lambrecht et al. 1992).

4.3.4 Increased accessibility of the residues by PPADS binding results from PPADS-evoked conformational changes

Two cysteine mutants (K215C and K138C) showed increased accessibility following PPADS binding. One is close to the ATP binding pocket (K215C) and the other is in the head of the receptor (K138C). It suggests PPADS caused conformational changes at these positions. The crystal structure of zfp2X4 has suggested the head of the receptor has a downward motion when ATP binding (Hattori and Gouaux 2012). But the accessibility of K138C and R139C was not changed by ATP binding (Figure 4.12). Therefore, PPADS binding probably causes extended movements in the head region to make the positively charged residues cooperate with the residues around the orthosteric site to attract PPADS binding.

Previous studies showed the cluster of positively charged residues (K138-K140) at the cysteine rich head played a very important role in suramin and NF449 sensitivity of P2X1Rs. The K138D P2X1R mutant showed ~3-fold and ~10-fold reduction in suramin and NF449 sensitivity respectively. However, chimera P2X1R with head region (133-184) of the P2X4R showed ~3.5-fold decrease in PPADS inhibition. The effect of a single mutant 138 on PPADS

sensitivity was not shown (Farmer et al. 2015). Increased accessibility (~8-fold) of K138C by PPADS binding suggests PPADS may not directly bind to it but cause significant conformational changes at the position.

4.3.5 Residues showing decreased accessibility by PPADS binding at the allosteric site

Another cluster of residues (V74, T75, L77 and A182) showing decreased accessibility by PPADS was opposite to the ATP binding pocket. Accessibility changes of the cysteine mutants by PPADS at the allosteric site were various. PPADS binding nearly abolished accessibility of some mutants (V74, T75, A182 and E248), modestly decreased accessibility of some mutants (L77 and L279) and showed no effect on some others (Q76C, Q78C, S175C and Q237C). Interestingly, ATP binding also caused similar accessibility changes of these mutants in previous studies (J. A. Roberts et al. 2012). Studies have shown that the accessibility changes of residues at the allosteric site result from ATP-induced conformational changes. But whether these accessibility changes by PPADS binding result from similar conformational changes induced by PPADS or direct binding by PPADS will be discussed in the next chapter.

4.3.6 Potential of mutants with no change in accessibility in PPADS binding

For the residues showing no change in accessibility by PPADS binding, there are two possible reasons: (1) these residues are not directly involved in PPADS binding and PPADS-evoked conformational changes did not affect their accessibility; (2) these residues may be essential for PPADS binding. Cysteine substitution on them may destroy the PPADS binding site and make PPADS no longer bind to the receptor.

Previous studies showed K68C and K70C are key component of the ATP binding site and their cysteine substituted mutants reduced ATP affinity >1000-fold (J. A. Roberts et al. 2012). Therefore ATP would not be expected to effectively modify MTSEA-biotin binding. In order to investigate whether residues

showing no change in accessibility by PPADS binding are directly involved in PPADS binding, their effect on PPADS sensitivity were tested in Chapter 5.

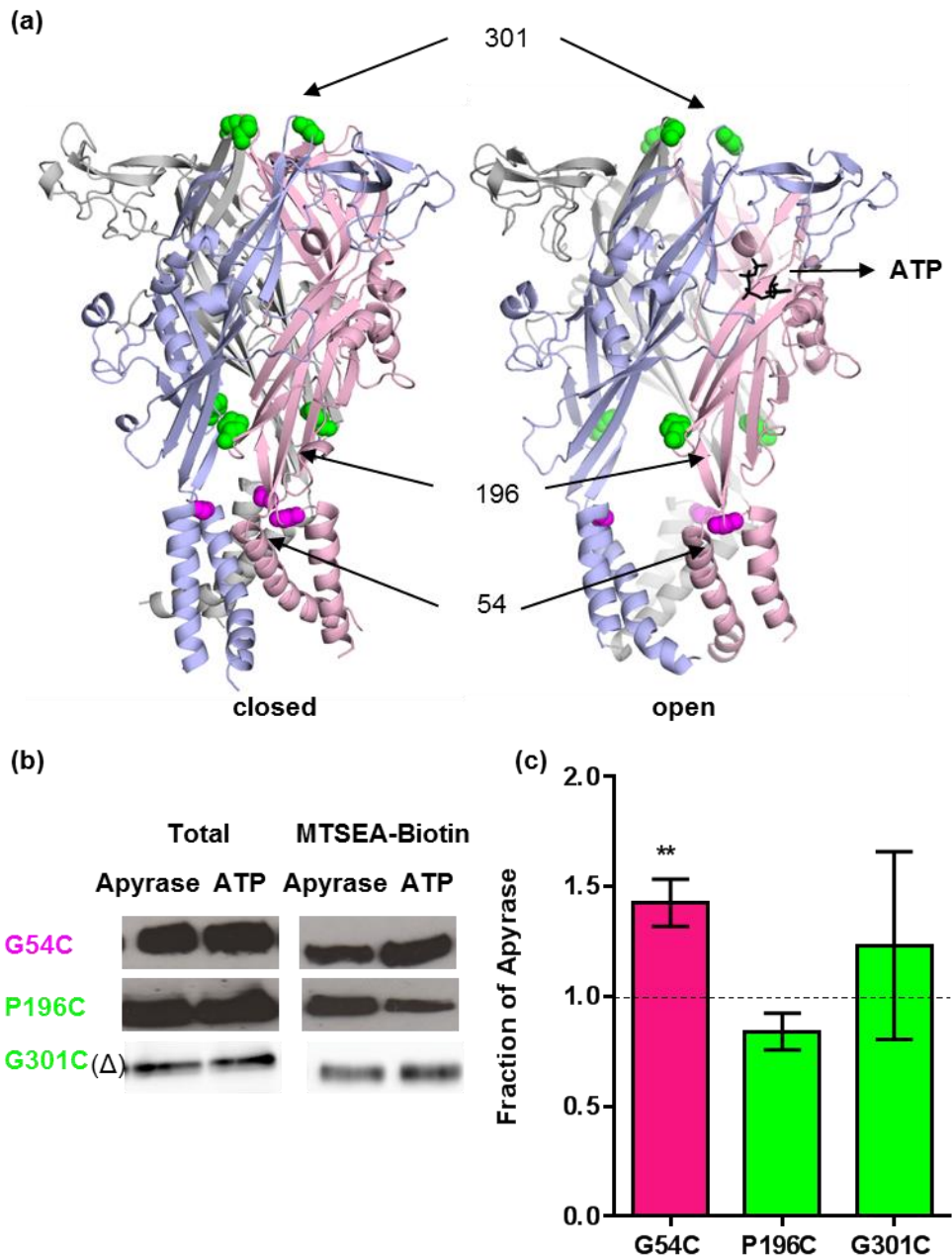


Figure S4.1 Effect of ATP binding on accessibility at the selected residues outside the potential PPADS binding ring. (a) Three residues out of the potential PPADS binding ring are shown in green (no change in accessibility) and pink (increased accessibility) at the homology model of hP2X1R in the closed and open states respectively. The receptor is shown as a cartoon. (b) Representative bands of total and biotinylated hP2X1Rs treated with 15 U/ml apyrase or 1 mM ATP for 10 minutes. (c) Densitometry results of the cysteine mutants response to ATP. Images were captured by film except Δ by Typhoon scanner. Significant differences were compared with the apyrase by t test (** $p < 0.01$). The data were plotted as mean \pm SEM ($n=4$).

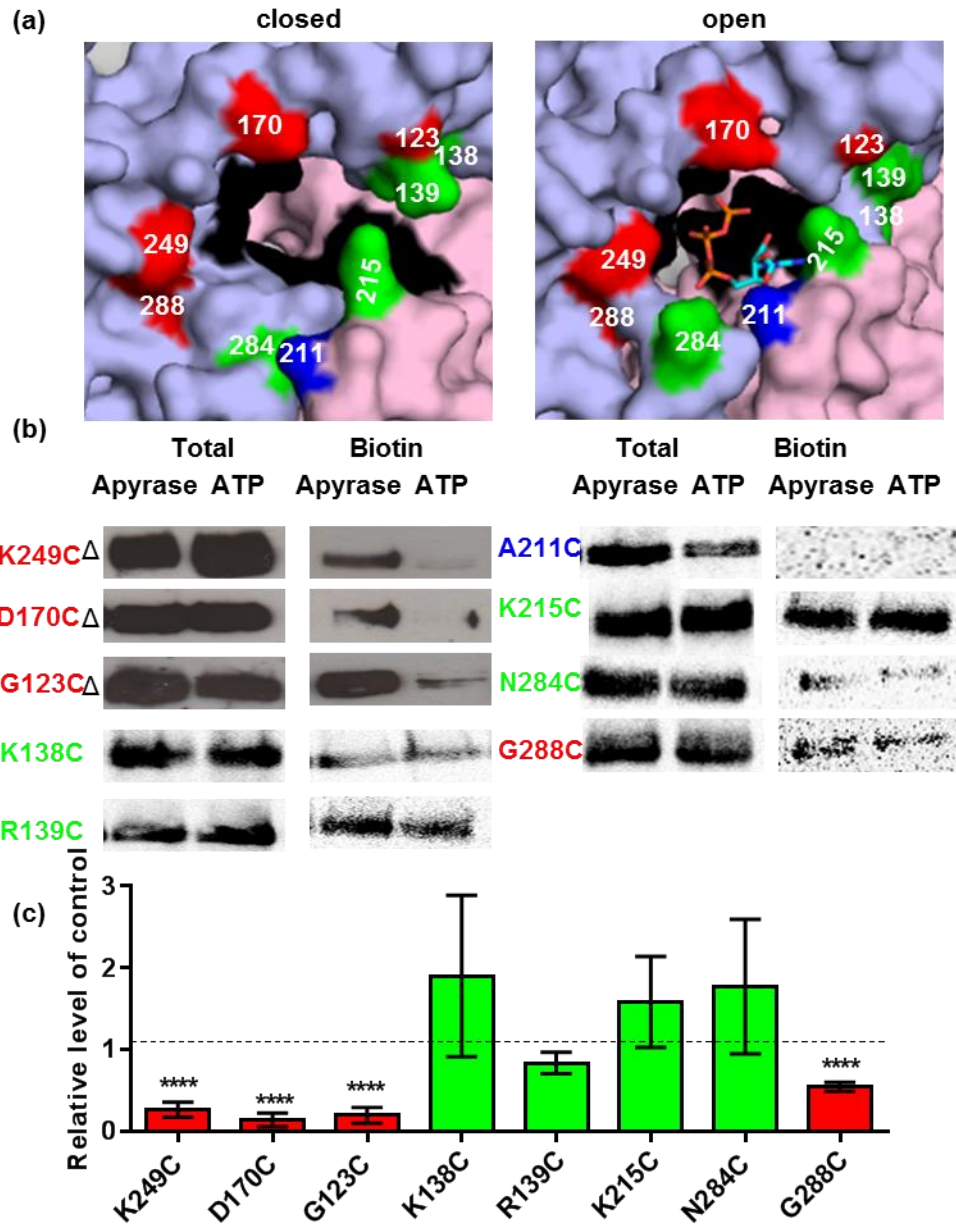


Figure S4.2 Effect of ATP binding on accessibility of the selected cysteine mutants around the ATP binding site. (a) The location of the selected residues are shown in red (decreased accessibility) and green (no change in accessibility) in the homology model of the hP2X1R in the closed and open states. The receptor is shown as surface representation. The residues included in ATP binding are shown in black. ATP is shown as sticks in open state of the receptor **(b)** Representative bands of total and biotinylated hP2X1Rs treated with 15 U/ml apyrase or 1 mM ATP. **(c)** Densitometric analysis using ImageJ calculated any change in MTESA-Biotin accessibility of the cysteine mutants following ATP treatment. Images were captured by typhoon scanner except those indicated by Δ using by film. Significant differences between biotinylation levels following treatment of apyrase and ATP were performed by paired t test (**** $p < 0.0001$). The data were plotted as mean \pm SEM ($n \geq 3$).

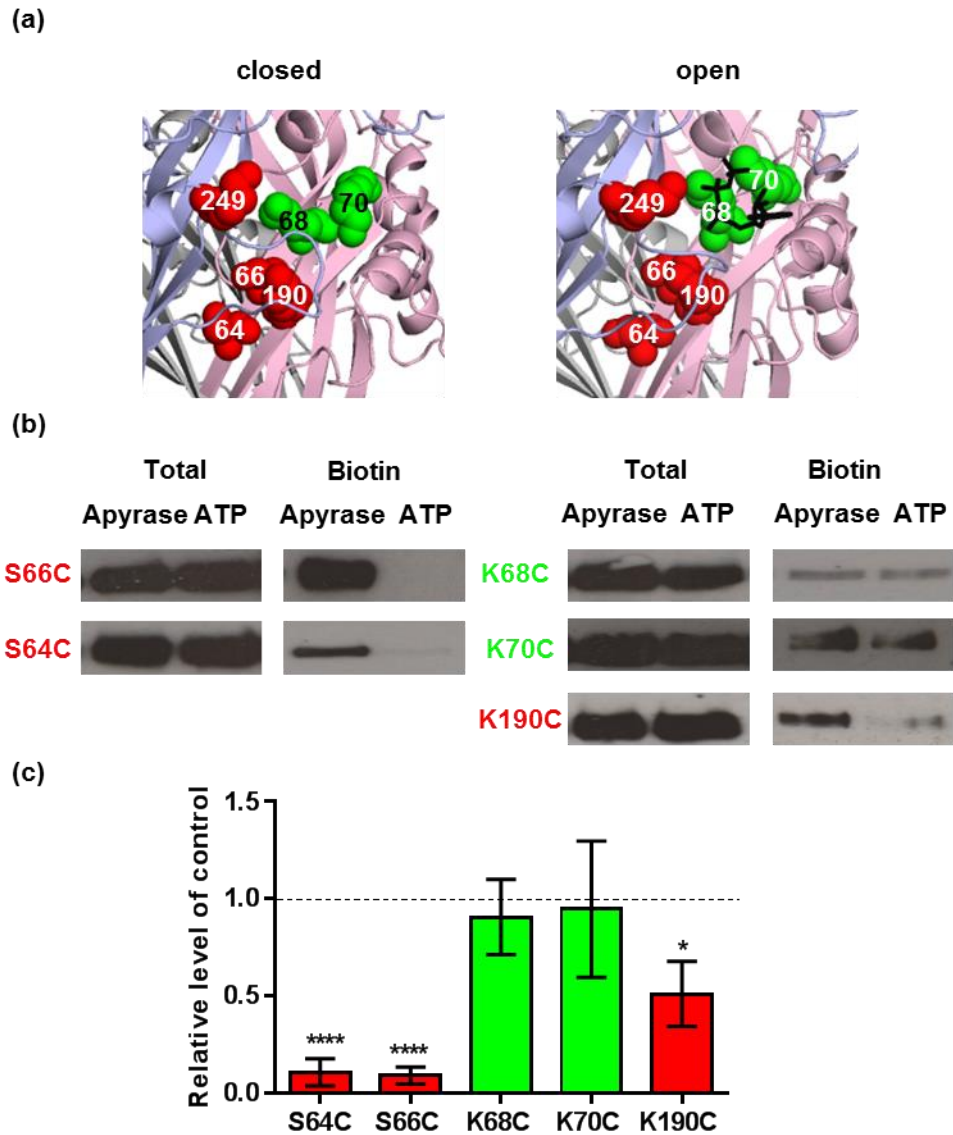


Figure S4.3 Effect of ATP binding on accessibility of the selected cysteine mutants inside the ATP binding site. (a) The location of selected residues inside ATP binding site are labelled in red (decreased accessibility) and green (no change in accessibility) sphere in the homology model of hP2X1R in the closed and open states respectively. The receptor is shown in cartoon. ATP is shown in black sticks in the open state of the receptor. (b) Representative bands of total and biotinylated hP2X1Rs treated with 15U/ml apyrase or 1mM ATP. (c) Densitometric analysis using ImageJ calculated any change in MTESA-Biotin accessibility the cysteine mutants following ATP treatment. Images were captured by film. Significant differences between biotinylation levels following treatment of apyrase and ATP were performed by paired t test (* $p < 0.05$, **** $p < 0.0001$). The data were plotted as mean \pm SEM ($n \geq 3$).

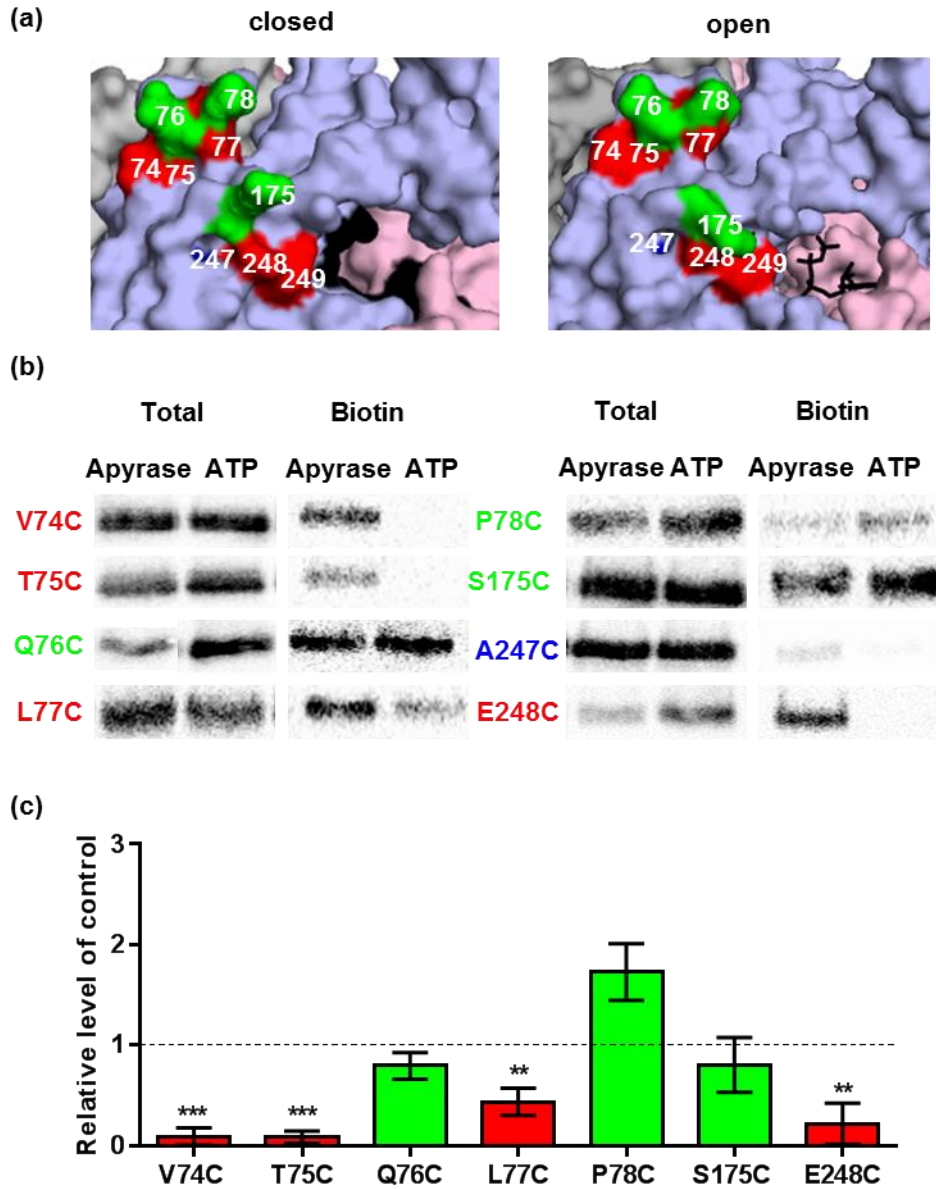


Figure S4.4 Effect of ATP binding on accessibility of the selected cysteine mutants in the upper body. (a) The location of the selected residues are shown in red (decreased accessibility) and green (no change in accessibility) in the homology model of the hP2X1R in the closed and open states. The receptor is shown as surface representation. The residues involved in ATP binding are shown in black. ATP is shown as sticks in open state of the receptor. **(b)** Representative bands of total and biotinylated hP2X1Rs treated with 15 U/ml apyrase or 1 mM ATP. **(c)** Densitometric analysis using ImageJ calculated any change in MTESA-Biotin accessibility of the cysteine mutants following ATP treatment. Images were captured by typhoon scanner. Significant differences between biotinylation levels following treatment of Apyrase and ATP were performed by paired t test (** $p < 0.01$, *** $p < 0.001$). The data were plotted as mean \pm SEM ($n \geq 3$).

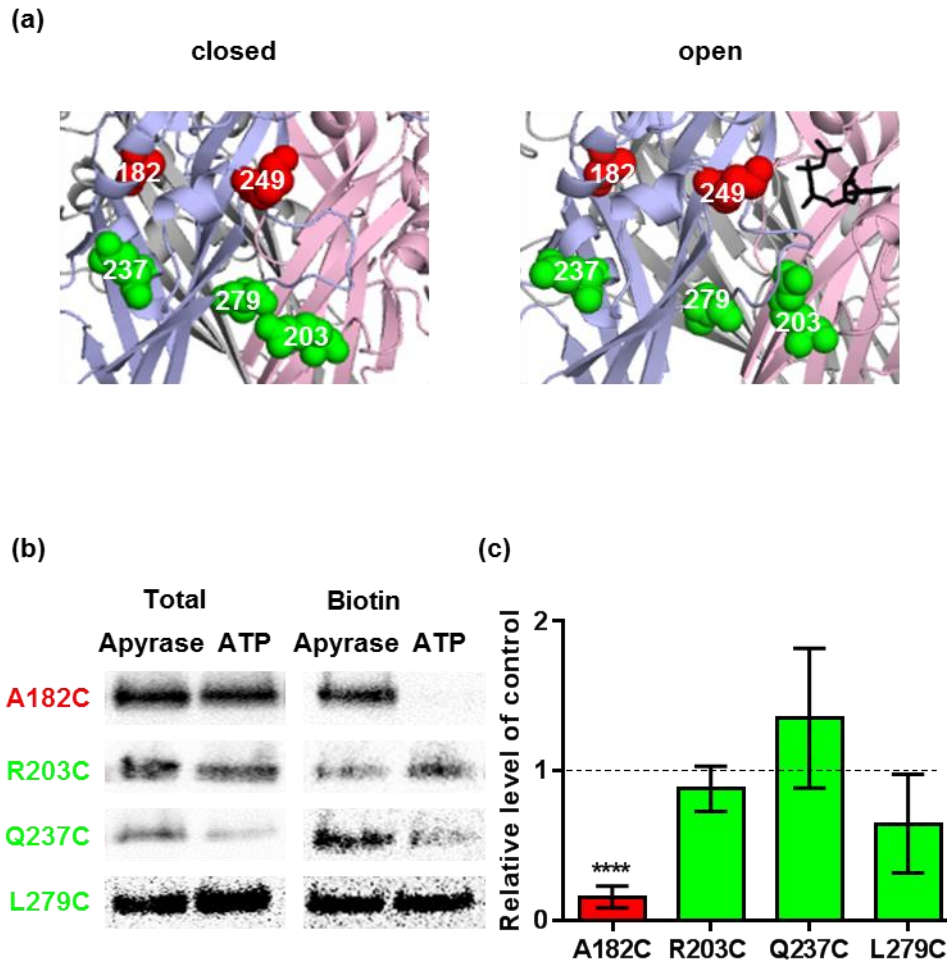
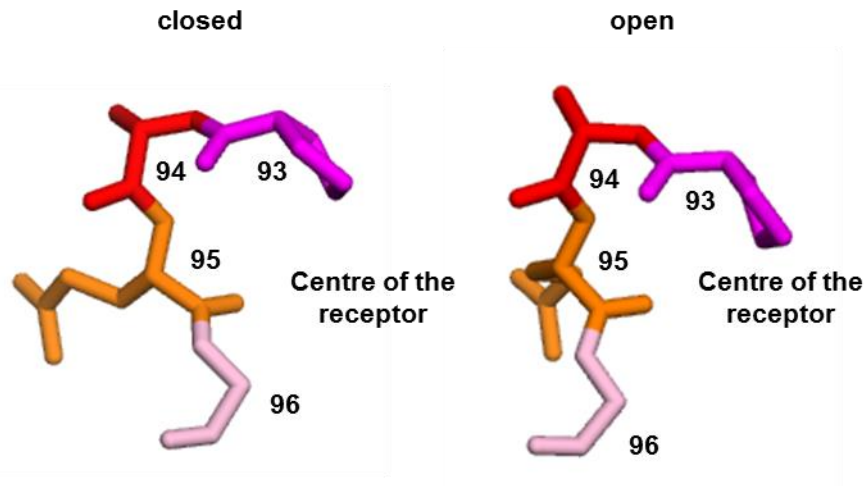
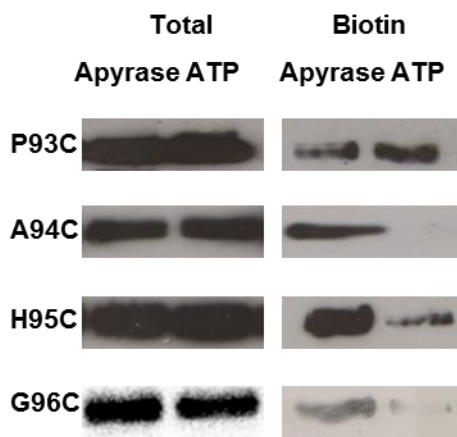


Figure S4.5 Effect of ATP binding on accessibility of the selected cysteine mutants in the flippers. (a) The location of selected residues opposite to the ATP binding pocket in the flippers are labelled in red (decreased accessibility) and green (no change in accessibility) sphere in the homology model of hP2X1R in the closed and open states respectively. The receptor is shown in cartoon. ATP is showed in black sticks in the open state of the receptor. (b) Representative bands of total and biotinylated hP2X1Rs treated with 15 U/ml apyrase or 1 mM ATP. (c) Densitometric analysis using ImageJ calculated any change in MTESA-Biotin accessibility of the cysteine mutants following ATP treatment. Images were captured by typhoon scanner. Significant differences between biotinylation levels following treatment of apyrase and ATP were performed by paired t test (**** $p < 0.0001$). The data were plotted as mean \pm SEM ($n \geq 3$).

(a)



(b)



(c)

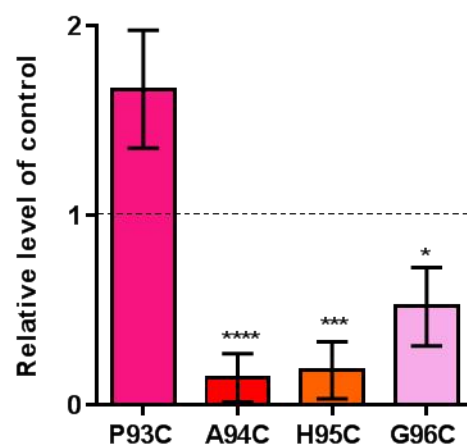


Figure S4.6 Effect of ATP binding on accessibility of the selected cysteine mutants lining the upper vestibule of the hP2X1R. (a) Selected residues (93-96) lining the upper vestibule are shown as sticks with different colours in the homology model of the hP2X1R in the closed and open states respectively. (b) Representative bands of total and biotinylated hP2X1Rs treated with 15 U/ml apyrase or 1 mM ATP. (c) Densitometric analysis using ImageJ calculated any change in MTESA-Biotin accessibility of the cysteine mutants following ATP treatment. Images were captured by typhoon scanner. Significant differences between biotinylation levels following treatment of apyrase and ATP were performed by paired t test (* $p < 0.05$, *** $p < 0.001$, **** $p < 0.0001$). The data were plotted as mean \pm SEM ($n \geq 3$).

Chapter 5. Effect of cysteine mutants and Methanethiosulfonate (MTS) Reagents on PPADS sensitivity of hP2X1Rs

5.1 Introduction

Based on the results in chapter 4, residues showing a decrease in accessibility by PPADS binding can be classified into two groups, (i) those directly involved in PPADS binding, and (ii) those where PPADS binding evokes conformational changes resulting in reduced accessibility. It was hypothesized that if the residue was directly involved in PPADS binding, the mutation of the residue would affect PPADS sensitivity. Whereas if the residue was not in the PPADS binding site (but showing decreased accessibility by conformational changes), then it would not affect PPADS sensitivity. This hypothesis led to the research in Chapter 5.

5.1.1 Use of MTS compounds to modify cysteine mutants to investigate the ATP binding site

As ATP contains negative charges and is complexed with magnesium in physiological solutions, the ability to introduce charges at accessible substituted cysteine using MTS reagents is a useful tool to investigate contributions of the specific residues to the ATP binding site. The commonly used MTS compounds with various charges and sizes includes 2-aminoethyl methanethiosulfonate (MTSEA, small positively charged), N,N,N-trimethyl-2-[(methylsulfonyl)thio]ethanaminium bromide (MTSET, larger positively charged) and sodium (2-sulfonatoethyl) methanethiosulfonate (MTSES, intermediate size, negatively charged). In previous studies, the effects of MTS reagents on the amplitude of ATP-evoked responses and ATP potency at the cysteine mutants P2XRs were tested.

At the majority of cysteine mutants in the region (E52-G96, E181-V200 and S286-I329), MTS compounds had no effect on the amplitude of response and/or ATP potency (Allsopp et al. 2011, Roberts and Evans 2007, Roberts et al. 2009b). For residues involved in the ATP binding site. There were additional shifts by MTS reagents in ATP potency. The effect of MTS compounds on ATP potency at accessible cysteine mutants can be classified into the following three types.

(i) The effects were dependent on the charge of the MTS reagent. For example at K309C, ATP potency was increased ~20-fold after application of positively charged MTSEA but responses even to a maximal concentration of ATP (10 mM) were abolished by negatively charged MTSES (Roberts and Evans 2007). Similarly for K190C, ATP potency was increased ~3-fold by MTSEA whilst MTSES decreased ATP potency ~3-fold and the maximal response was decreased by ~35% (Roberts et al. 2009b). The similar effect of MTS compounds at these two mutations was also found in P2X2 and P2X4Rs (Roberts et al. 2008). The MTSEA-modified cysteine residue is of similar size and charge to the lysine residue. It suggested that the positively charged lysines at these positions play an important role in coordinating the binding of the negatively charged phosphate group of the ATP molecule, which now has been confirmed by the crystal structure of the zfp2X4R (Hattori and Gouaux 2012).

(ii) The effect was dependent on the size of the MTS compounds. For example at T186C, MTSEA and MTSES treatment decreased ATP potency ~10-fold and ~5-fold. The sensitivity of T186C to MTS was independent of the charge and appeared to result from the bulk of the substitution (Roberts et al. 2009b). The crystal structure showed T186 interacts with the adenine base of ATP through hydrogen bonds (Hattori and Gouaux 2012).

(iii) The effect was dependent on both the charge and size of MTS reagents. For example at K70C, MTSES reduced ATP potency by ~14-fold whereas MTSET had no effect on ATP potency but reduced the amplitude of responses even to a maximal concentration of ATP by ~55%. At K68C, MTSES and MTSET abolished responses to the maximal concentration of ATP (10 mM) (Allsopp et al. 2011). The mutation to replace K68 with the larger positively charged Arg also abolished ATP evoked responses (Ennion et al. 2000). MTSEA potentiated ATP-evoked responses at K68C mutant, and this was associated with an increase in ATP sensitivity (Allsopp et al. 2011). It suggested it is not just the positive charge but also the size of the side group that is important for determining ATP potency at K68 and K70. This is consistent with the crystal structure that shows they are key residues in the ATP binding site, interacting with phosphates and the adenine base of ATP at P2XRs (Hattori and Gouaux 2012).

5.1.2 Aim

All cysteine residues showing decreased accessibility in the presence of PPADS have the potential to be involved in antagonist binding. In order to distinguish residues involved in PPADS binding from antagonist induced conformation changes, the effect of cysteine mutants on PPADS sensitivity were explored in this chapter. As the PPADS molecule contains four negative charges, charged MTS compounds were used to modify cysteine mutants to investigate the effect of charge and size of side chains on PPADS sensitivity.

5.2 Results

5.2.1 Effect of individual cysteine mutants around the ATP binding site on PPADS sensitivity

The cysteine mutant hP2X1Rs were expressed in *Xenopus laevis* oocytes. TEVCR was used to investigate the effect of these cysteine mutants on PPADS sensitivity. In order to standardise comparisons between each mutant, EC₉₀ values of ATP (the value of ATP generating 90% of the maximum response) were used for testing the antagonist sensitivity. The pIC₅₀ values (-log₁₀IC₅₀ values) were used to compare significant differences in PPADS sensitivity of WT hP2X1Rs and mutants. The pIC₅₀ value of WT was 6.12±0.07 (see detail in Chapter 3).

Around the ATP binding pocket, residues showing decreased accessibility with PPADS labelling were K249C, D170C, G123C and R139C (Chapter 4) (Figure 5.1a). The EC₉₀ values of ATP for G123C was ~30 μM, ~3-fold less than that for WT. For the other three mutants, the EC₉₀ value was similar to WT (~10 μM) (Figure S5.1). Based on the EC₉₀ values, PPADS potency on these cysteine mutants was tested. K249C decreased PPADS sensitivity of the hP2X1R ~3-fold whereas D170C increased it ~3-fold. The role of positively charged lysine at 249 was discussed in Chapter 3. The removal of negative charge at D170 supported

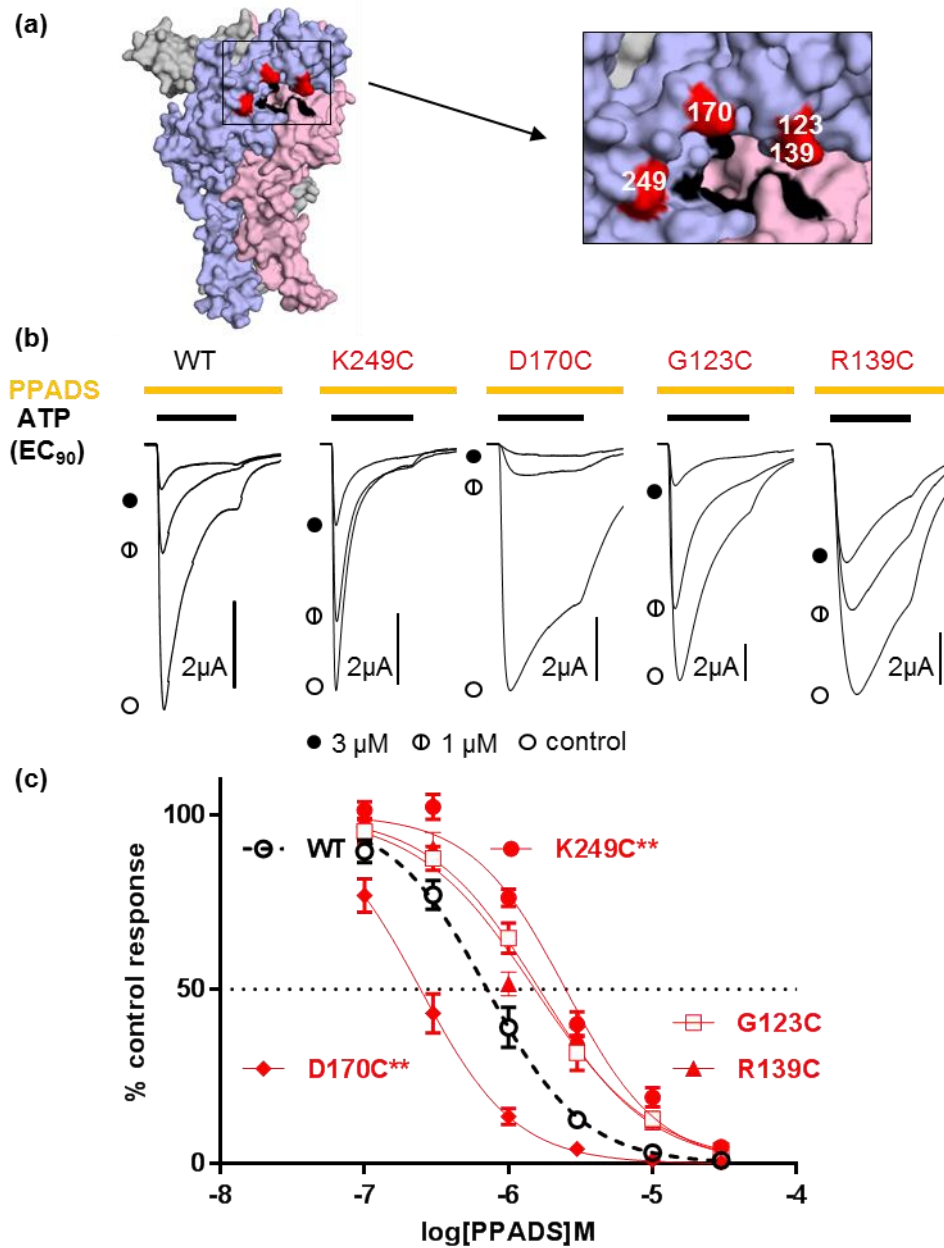


Figure 5.1 Effect of mutants at the hP2X1R showing decreased accessibility by PPADS binding around the ATP binding site on sensitivity to the antagonist (a) Homology model of the hP2X1R in the closed state showing the location of cysteine mutants showing decreased accessibility by PPADS binding. Residues consisting of the ATP binding site are labelled in black. (b) Representative traces of inhibition of ATP-evoked currents in the absence (control) and presence of PPADS. Different concentrations of PPADS were applied 5 min before the co-application with ATP (EC_{90}). Orange bar indicates application of PPADS and black bar indicates application of ATP. (c) PPADS concentration response curves for WT and mutants. The IC_{50} values are shown by the dashed line. Data are plotted on mean \pm SEM ($n=3$). Significant differences in pIC_{50} compared with WT are indicated (** $p<0.01$).

the importance of positive charge to PPADS binding. Removal of positive charge at 139 (R139C) did not significantly affect PPADS sensitivity. The adjacent cysteine mutant G123C also showed no significant effect on PPADS sensitivity (Figure 5.1b, c).

The two cysteine mutants (K138C and K215C) around the ATP binding site showed increased accessibility following PPADS binding. However, they decreased PPADS sensitivity ~3-fold (Figure 5.2). This suggests the importance of positive charges around the antagonist PPADS binding pocket. These two residues may also contribute to the conformational changes associated with binding of the antagonist. At the inaccessible cysteine mutant (A211C), there was no change in PPADS sensitivity (Figure 5.2), suggesting this residue is not on the surface and not directly involved in PPADS binding. For the cysteine mutants (N284C and G288C) showing no change in accessibility, PPADS sensitivity was also not affected (Figure 5.3). It suggests they do not directly contribute to PPADS binding.

5.2.2 Effect of the cysteine mutants deep in the ATP binding site on PPADS sensitivity

Five cysteine mutants (S64, S66, K68 K70C and K190C) within the ATP binding site showed decreased accessibility following PPADS binding. Interestingly, two mutants (S64C and S66C) deep in the ATP binding site did not modify PPADS potency (Figure 5.4). Previous studies showed that a cysteine mutant at a key residue K68 for ATP binding significantly decreased ATP potency but not that for PPADS (Allsopp et al. 2011). This suggests this residue may not be directly involved in PPADS binding. The decreased accessibility may result from PPADS-evoked conformational changes or PPADS binding higher in the pocket and blocking access to the residues. Two cysteine mutants at conserved lysines (K70 and K190) decreased PPADS sensitivity ~3-fold (Figure 5.4), suggesting they may be involved in PPADS binding. Therefore, PPADS and ATP binding sites have at least have two residues in common.

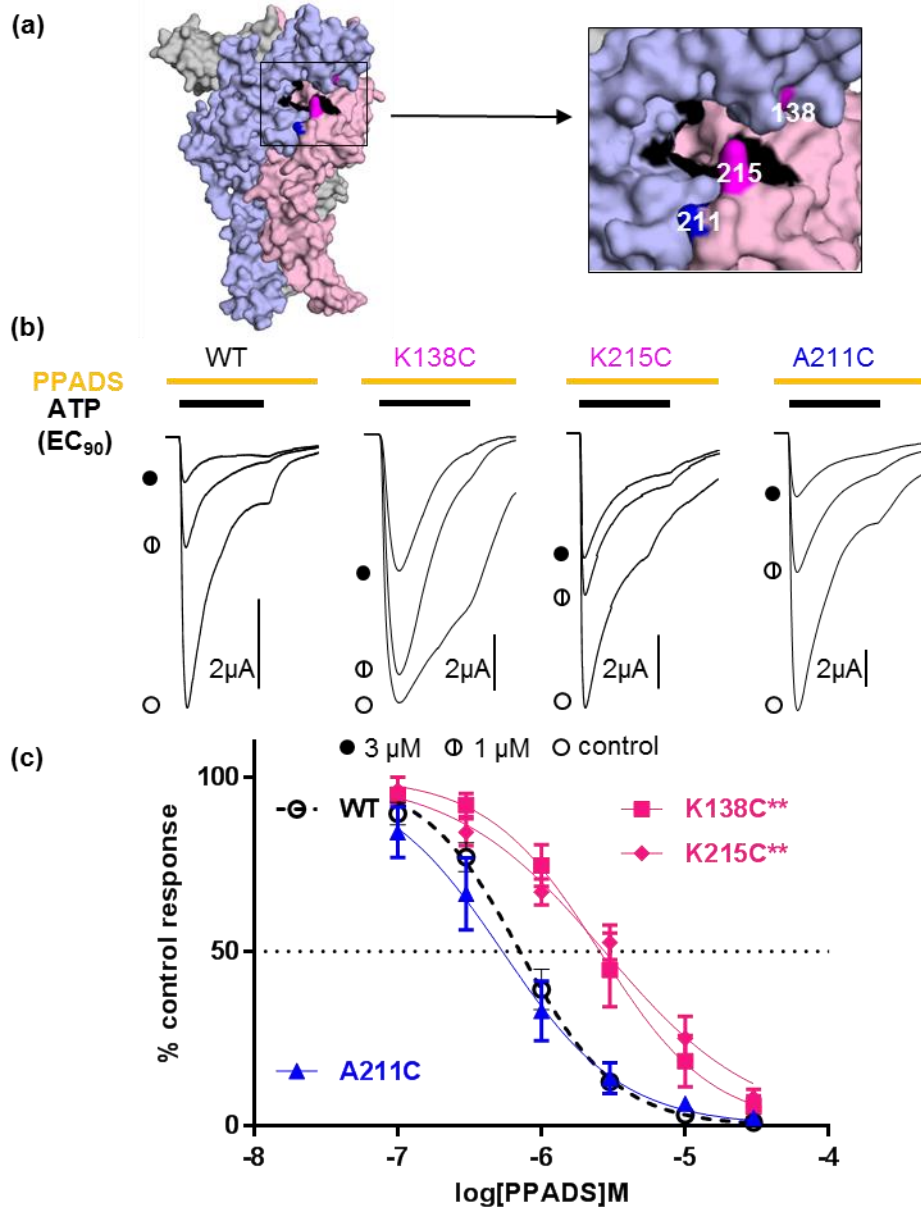


Figure 5.2 Effect of the mutants showing increased accessibility by PPADS binding or inaccessibility around the ATP binding sites on PPADS sensitivity of the hP2X1R (a) Homology model of the hP2X1R showing the location of cysteine mutants showing increased accessibility by PPADS binding (pink) and those were inaccessible (blue). Residues consisting of the ATP binding site are labelled in black. (b) Representative traces of inhibition of ATP-evoked currents in the absence (control) and presence of PPADS. Different concentrations of PPADS were applied 5 min before the co-application with ATP (EC_{90}). Orange bar indicates application of PPADS and black bar indicates application of ATP. (c) PPADS concentration response curves for WT and mutants showing increased accessibility (pink) by PPADS binding and that were inaccessible (blue). The IC_{50} values are shown by the dashed line. Data are plotted on mean \pm SEM ($n=3$). Significant differences in pIC_{50} compared with WT are indicated (** $p < 0.01$).

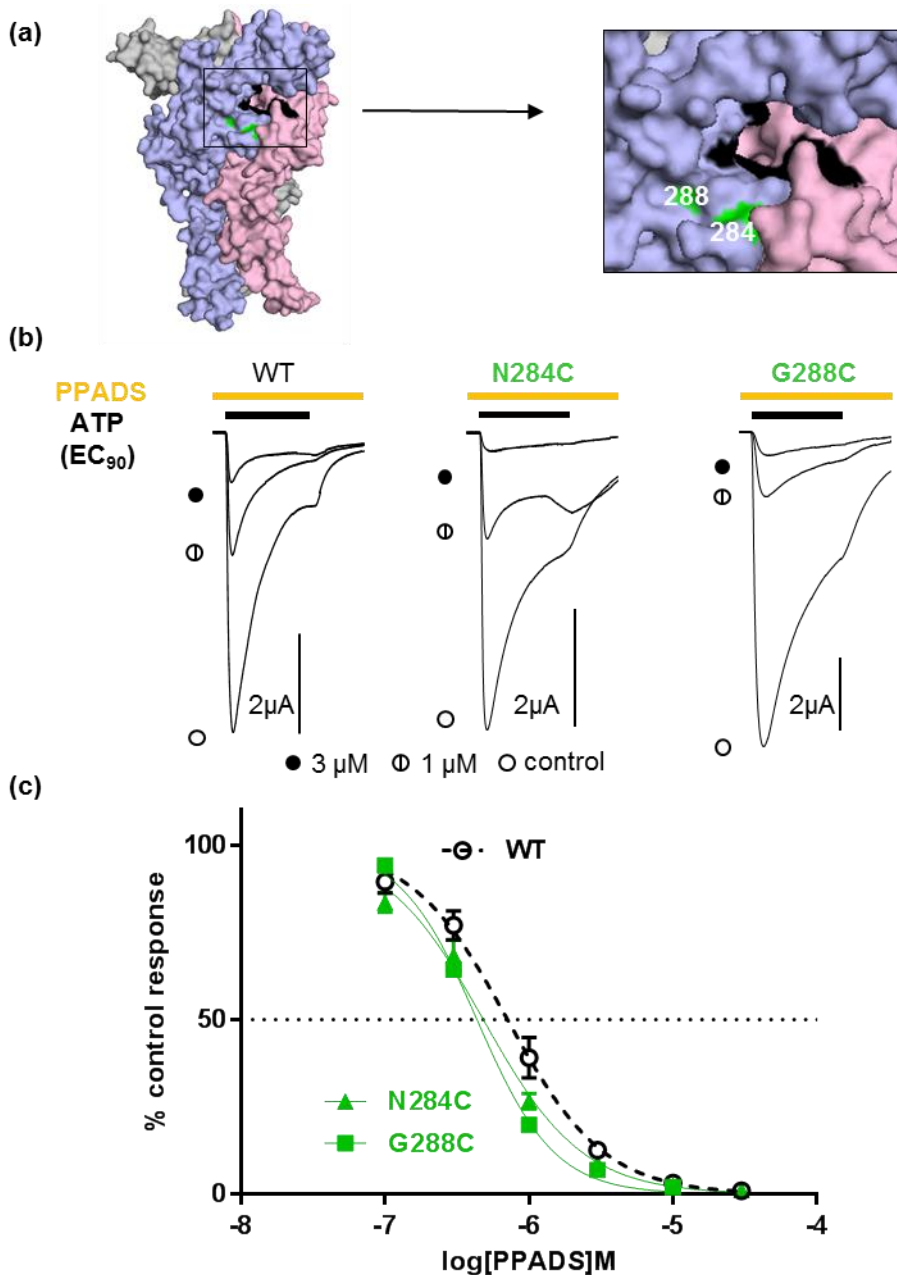


Figure 5.3 Effect of the mutants showing no change in accessibility following PPADS treatment around the ATP binding sites on PPADS sensitivity of the hP2X1R (a) Homology model of the hP2X1R showing the location of cysteine mutants showing on change in accessibility by PPADS binding. Residues consisting of the ATP binding site are labeled in black. (b) Representative traces of inhibition of ATP-evoked currents in the absence (control) and presence of PPADS. Different concentrations of PPADS were applied 5 min before the co-application with ATP (EC_{90}). Orange bar indicates application of PPADS and black bar indicates application of ATP. (c) PPADS concentration response curves for WT and mutants showing no change in accessibility (green) following PPADS treatment. The IC_{50} values are shown by the dashed line. Data are plotted on mean \pm SEM (n=3).

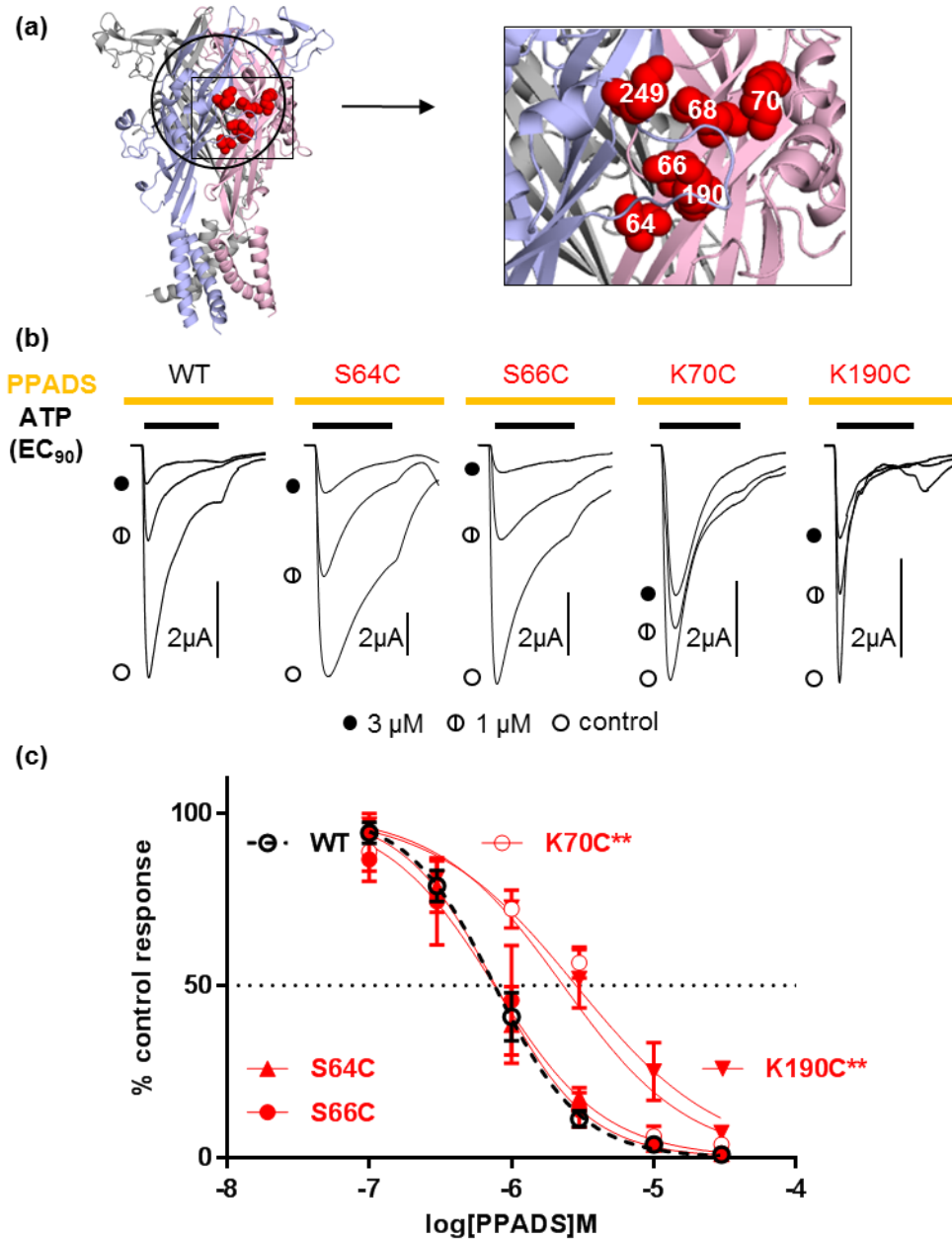


Figure 5.4 Effect of the mutants showing decreased accessibility following PPADS treatment within the ATP binding site on PPADS sensitivity of the hP2X1R (a) Homology model of the hP2X1R in the closed state showing the location of individual cysteine mutants showing decreased accessibility by PPADS binding. (b) Representative traces of inhibition of ATP-evoked currents in the absence (control) and presence of PPADS. Different concentrations of PPADS were applied 5 min before the co-application with ATP (EC₉₀). Orange bar indicates application of PPADS and black bar indicates application of ATP. (c) PPADS concentration response curves for WT and mutants. The IC₅₀ values are shown by the dashed line. Data are plotted on mean ± SEM (n=3). Significant differences in pIC₅₀ compared with WT are indicated (**p<0.01).

5.2.3 Effect of the cysteine mutants opposite to the ATP binding sites on PPADS sensitivity

The cluster of residues in the upper body (V74C, T75C and L77C) and those around the dorsal fin (A182C, E248C and L279C) opposite to the ATP binding site showed decreased accessibility following PPADS binding. However, these cysteine mutants showed no significant change in PPADS sensitivity (Figure 5.5 & Figure 5.6). These results suggest that they do not make a significant contribution to PPADS binding. The decreased accessibility may result from conformational changes induced by PPADS binding rather than direct steric block of access by PPADS.

Five cysteine mutants (Q76C, P78C, S175C, R203C, and Q237C) showed no change in accessibility following PPADS treatment. Previous studies showed Q76C and P78C had no significant effect on PPADS sensitivity (Allsopp et al. 2011). In this study, S175C and Q237C also showed no effect on PPADS sensitivity (Figure 5.7). Cysteine substitution of the positively charged R203 decreased PPADS ~3-fold (Figure 5.7).

5.2.4. Effect of the cysteine mutants in the left flipper (E282-P287) on PPADS sensitivity

Mapping all the selected residues showing decreased accessibility and PPADS potency on the homology model of the hP2X1R showed they are around the orthosteric site (Figure 5.8). In the middle of the cluster of residues, there is a flexible loop located in the left flipper. In order to investigate whether it contributes to PPADS binding, seven cysteine mutants (E282C-G288C) on the loop were made and their effect on PPADS sensitivity was tested. Two of them (N284C and G288C) have shown no effect on PPADS sensitivity (Figure 5.3). Among the other mutants, only E282C showed a significant effect on PPADS potency, increasing ~3-fold (Figure 5.8).

5.2.5 Effect of combinations of cysteine mutants on PPADS sensitivity

In summary, the mutants that decreased PPADS sensitivity are K249, K138, K215, K70, K190 and R203. However, each of the individual cysteine

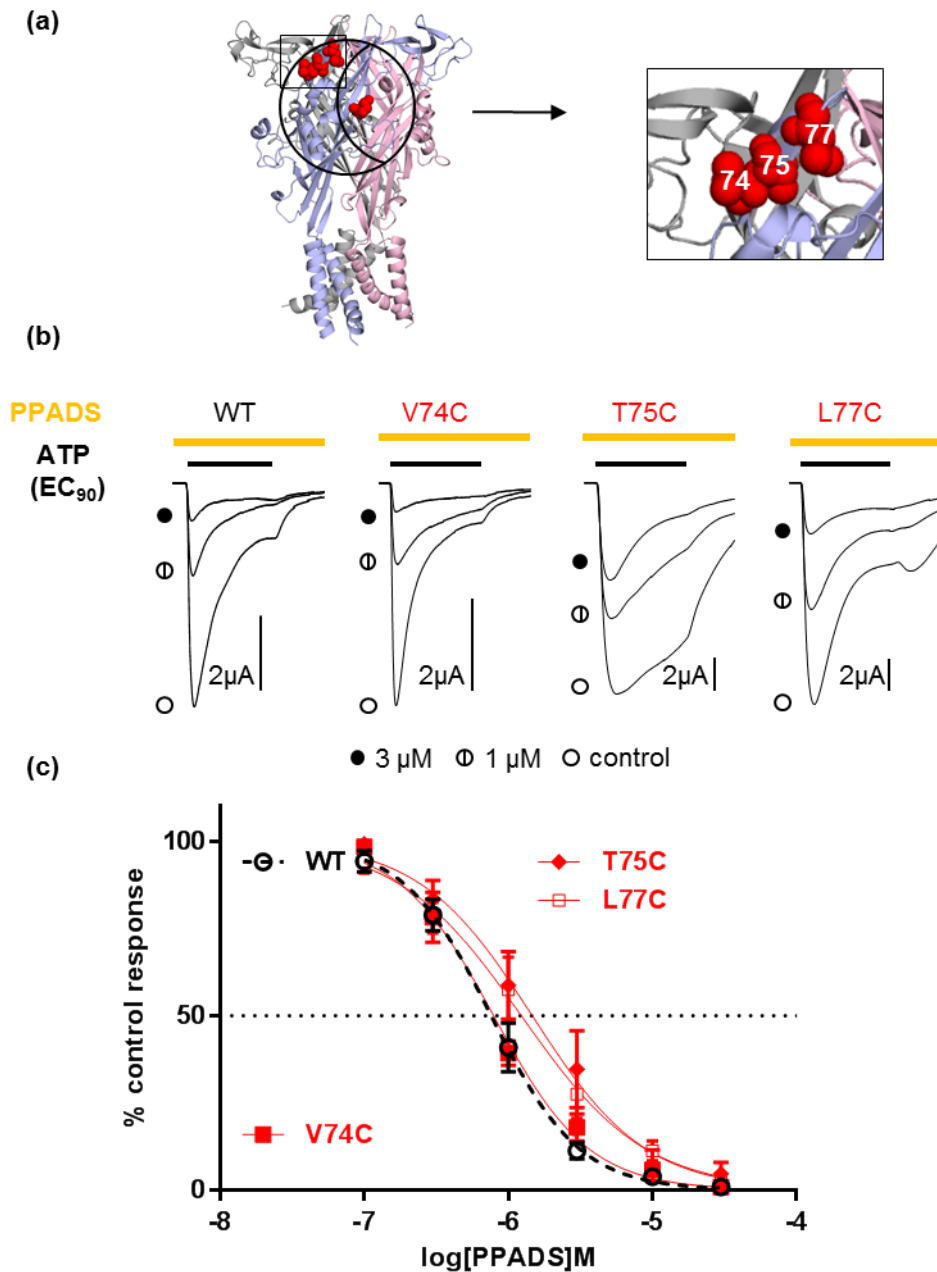


Figure 5.5 Effect of the mutants showing decreased accessibility by PPADS binding on the upper body opposite to the ATP binding sites on the PPADS sensitivity of the hP2X1R (a) Homology model of the hP2X1R in the closed state showing the location of individual cysteine mutants showing decreased accessibility by PPADS binding. (b) Representative traces of inhibition of ATP-evoked currents in the absence (control) and presence of PPADS. Different concentrations of PPADS were applied 5 min before the co-application with ATP (EC₉₀). Orange bar indicates application of PPADS and black bar indicates application of ATP. (c) PPADS concentration response curves for WT and mutants showing decreased accessibility (red). The IC₅₀ values are shown by the dashed line. Data are plotted on mean ± SEM (n=3).

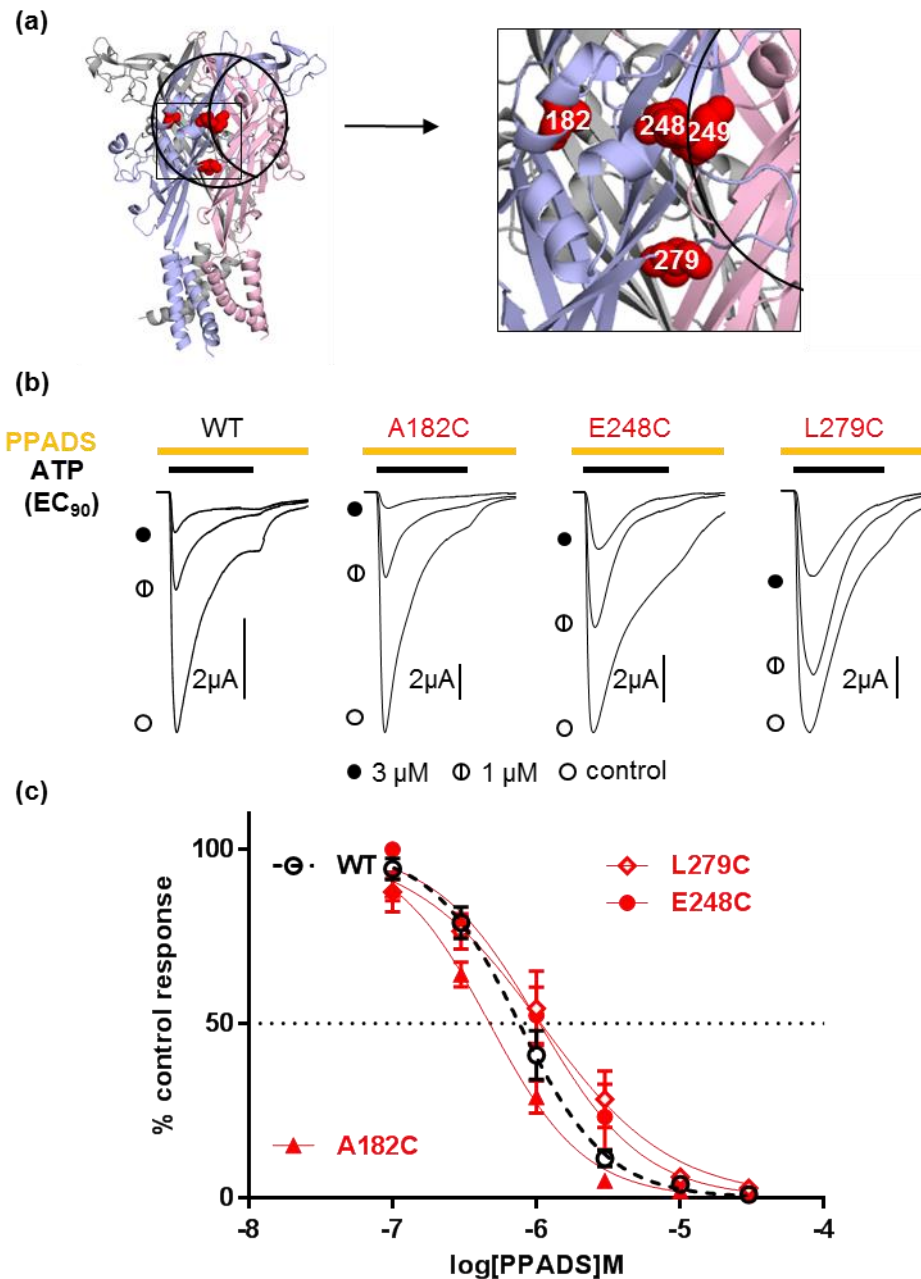
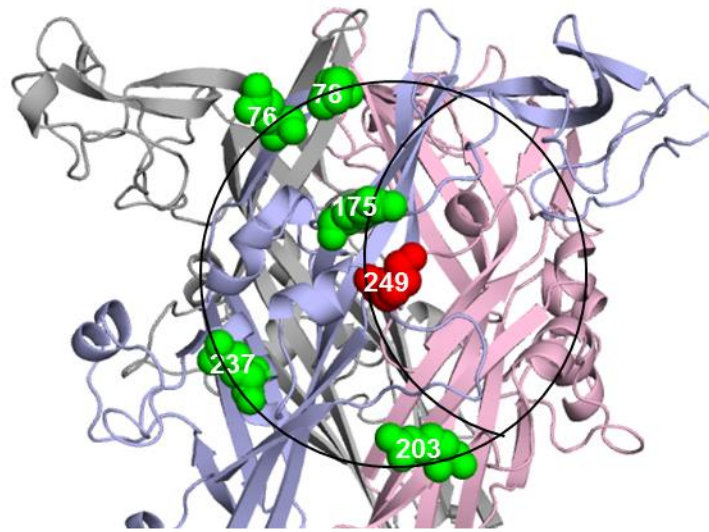


Figure 5.6 Effect of the mutants showing decreased accessibility by PPADS binding around dorsal fin opposite to the ATP binding sites on PPADS sensitivity of the hP2X1R (a) Homology model of the hP2X1R in the closed state showing the location of individual cysteine mutants showing decreased accessibility by PPADS binding. (b) Representative traces of inhibition of ATP-evoked currents in the absence (control) and presence of PPADS. Different concentrations of PPADS were applied 5 min before the co-application with ATP (EC_{90}). Orange bar indicates application of PPADS and black bar indicates application of ATP. (c) PPADS concentration response curves for WT and mutants showing decreased accessibility (red). The IC_{50} values are shown by the dashed line. Data are plotted on mean \pm SEM ($n=3$).

(a)



(b)

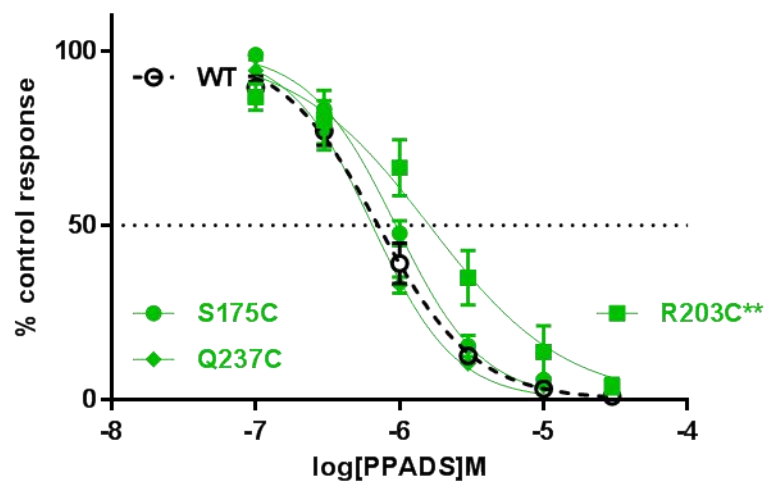
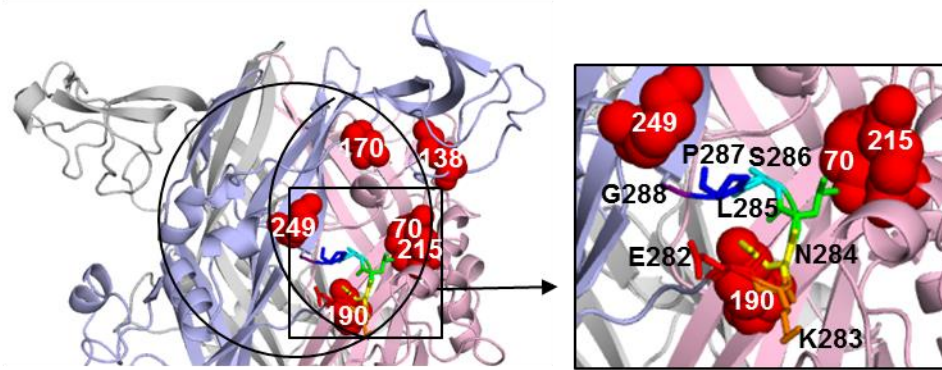


Figure 5.7 Effect of the mutants showing no change in accessibility by PPADS binding opposite to the ATP binding sites on PPADS sensitivity of the hP2X1R (a) Homology model of the hP2X1R in the closed state showing the location of individual cysteine mutants showing no change in accessibility by PPADS binding. (b) PPADS concentration response curves for WT and mutants showing no change in accessibility (green). The IC_{50} values are shown by the dashed line. Data are plotted on mean \pm SEM ($n=3$). Significant differences in pIC_{50} compared with WT are indicated (** $p<0.01$).

(a)



(b)

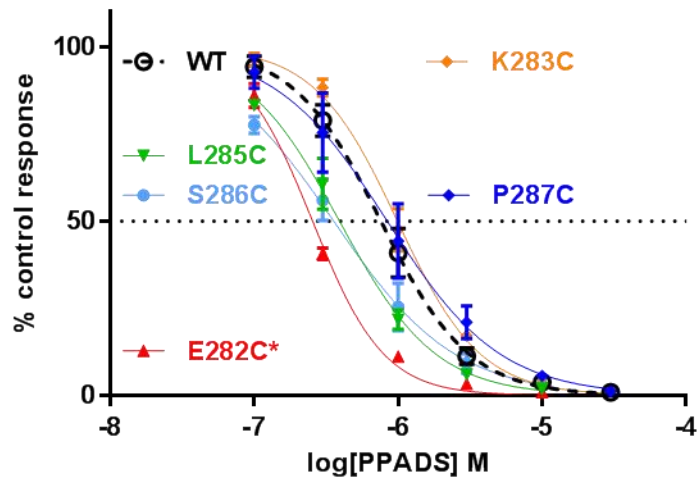
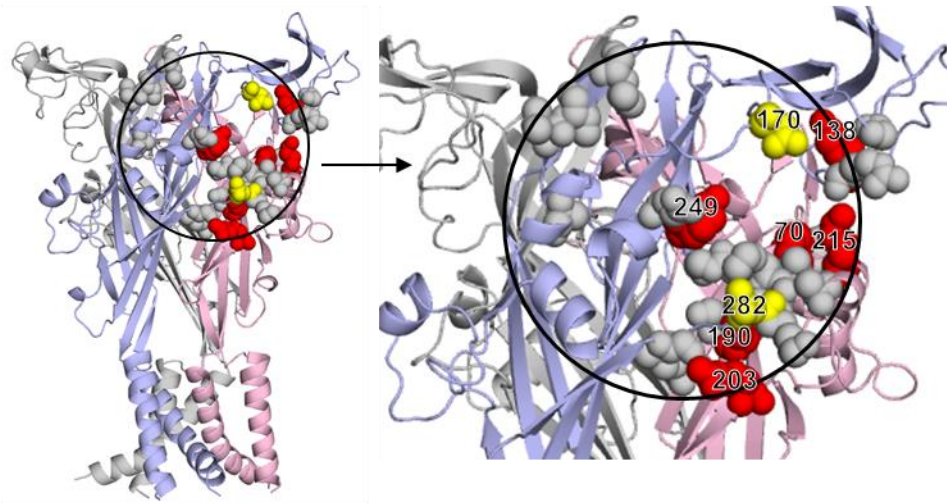


Figure 5.8 Effect of the mutants in the left flipper on PPADS sensitivity (a) Homology model of the hP2X1R in the closed state showing the location of individual cysteine mutants in the left flipper (E282-G288) as sticks. **(b)** PPADS concentration response curves for WT and mutants. The IC_{50} values are shown by the dashed line. Data are plotted on mean \pm SEM ($n=3$). Significant differences in pIC_{50} compared with WT are indicated ($*p<0.05$).

(a)



(b)

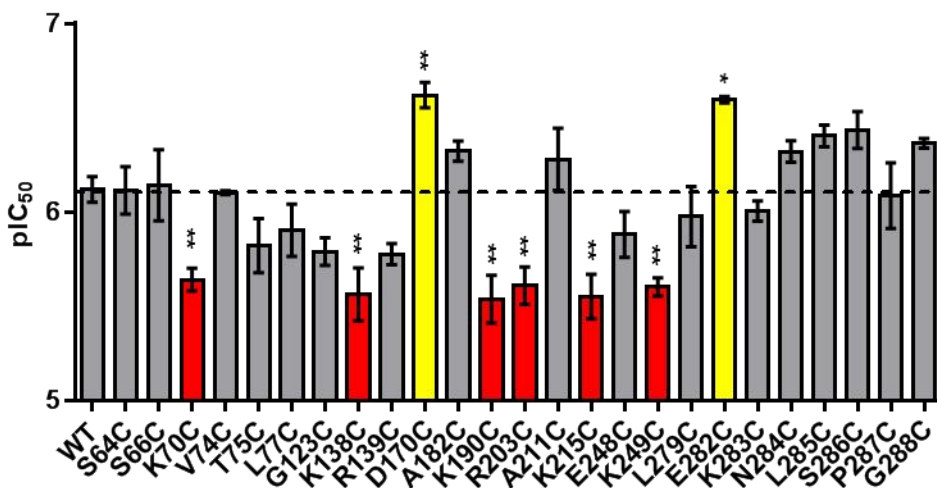


Figure 5.9 Summary of the effect of the mutants on PPADS sensitivity (a) Residues showing decreased accessibility in the presence of PPADS were shown as sphere at homology model of the hP2X1R. Grey spheres indicate decreased accessibility but no change in PPADS potency, red spheres indicate decreased accessibility and PPADS potency and yellow spheres indicate decreased accessibility and increased PPADS potency. **(b)** Comparison of PPADS potency (pIC₅₀ values) between WT and mutant hP2X1Rs. Statistical analysis was performed by one-way ANOVA. Data are plotted on mean \pm SEM (n=3). Significant differences in pIC₅₀ compared with WT are indicated (* $p < 0.05$, ** $p < 0.01$).

mutant only showed ~3-fold change on PPADS potency (Figure 5.9). It suggests there is no single dominant residue for PPADS binding and there may be multiple residues involved, which is consistent with multiple charges on the antagonist. In order to see whether they can work together to cause a larger effect on PPADS sensitivity, four double mutants were generated. As the importance of K249 in PPADS binding has been confirmed in previous studies, all the double mutants made were combined with K249C. The double mutants K249C + K138C and K249C + K190C did not further change PPADS sensitivity compared to the single mutant (Figure 5.10). When K249C combined with K215C, there was a further decrease (~10-fold) in PPADS potency compared to the single cysteine mutant (Figure 5.10). Interestingly, G123C alone did not significantly affect PPADS sensitivity but when it was combined with K249C PPADS potency was further reduced (~10-fold) compared with each of the single mutants (~3-fold) (Figure 5.10).

Based on these results, a triple mutant (K249C+G123C+K215C) was made. However, PPADS sensitivity of the receptor was not further decreased compared to the double mutants (Figure 5.11). It seems there may be another PPADS binding site in the hP2X1R but residues in other area of the extracellular loop did not show evidence involved in PPADS binding in accessibility and sensitivity tests. Another reason causing this may be that the triple mutations destroyed the PPADS binding site at the receptor to some extent but the nearby positively charged residues and other residues in the cysteine rich head region may come to compensate the binding pocket of PPADS by some conformational changes.

5.2.6 Effect of MTS compounds on PPADS sensitivity

A range of residues have been suggested to be involved in PPADS binding. Interestingly, they are all charged. In order to investigate the importance of charge at these positions, MTS compounds were used to modify the charge of these individual cysteine mutants, including negatively charged MTSES and positively charged MTSEA (Figure 5.12). In addition, in order to investigate the effect of the side chain of the residue on PPADS binding, MTS-TPAE (Figure

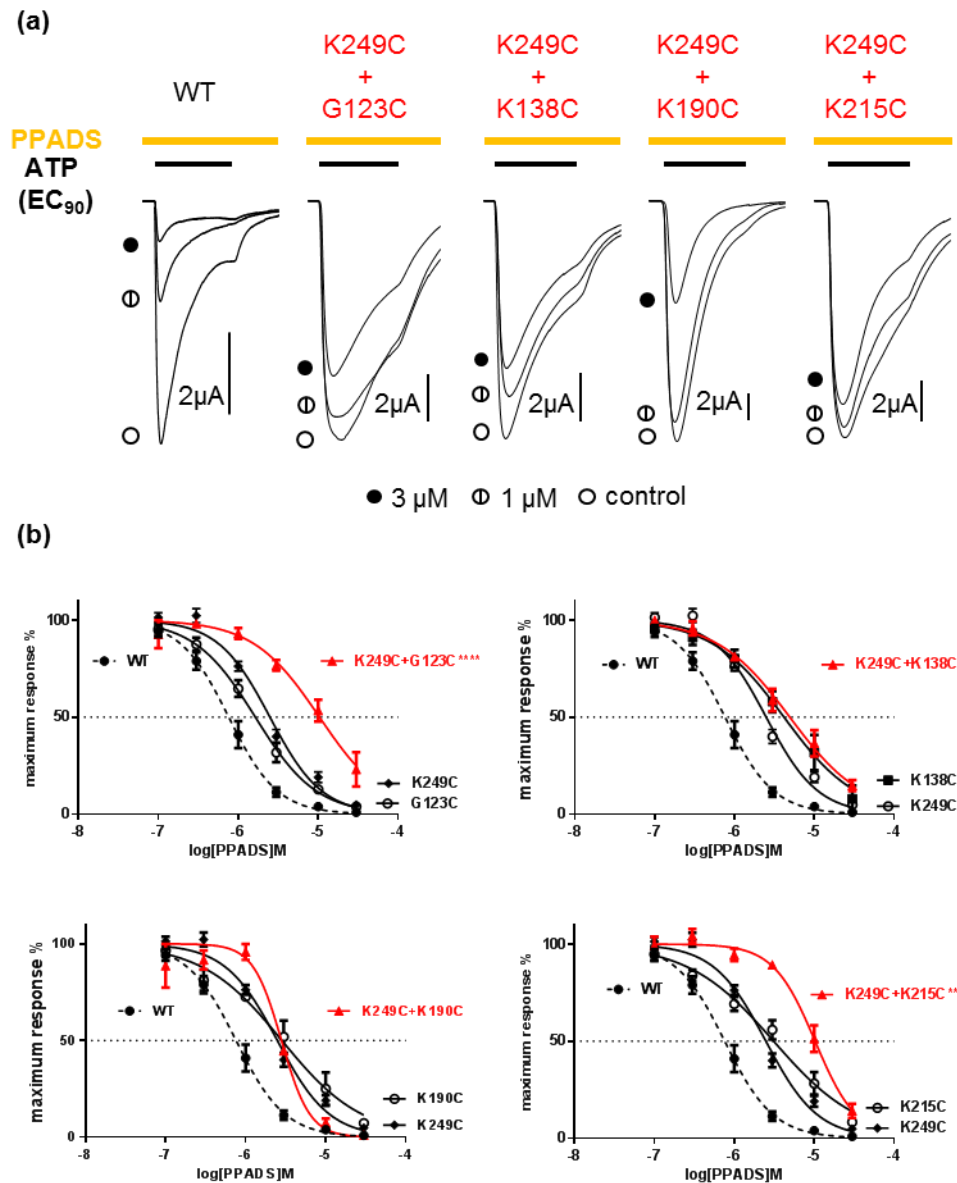
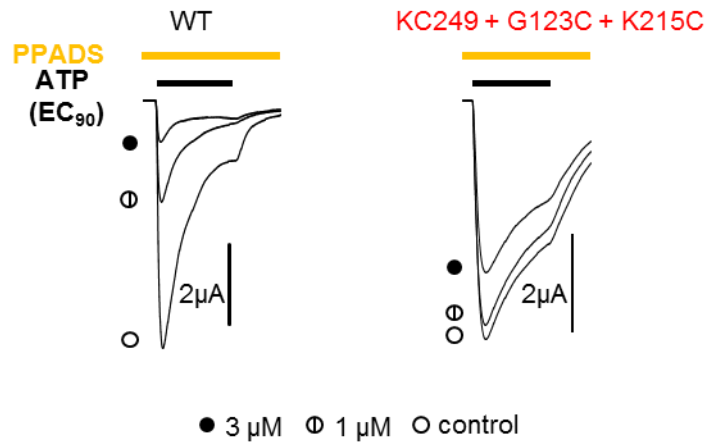


Figure 5.10 Effect of the double mutants on the sensitivity to PPADS

(a) Representative concentration responses to PPADS (1, 3 μ M) of WT hP2X1R and the double mutants based on their EC₉₀. The upper orange bar indicates the 5-minute perfused with PPADS and the application of PPADS throughout the recording. The lower black bar indicates 3 second co-application of ATP and PPADS. (b) PPADS concentration response curves for WT, single mutant and the double mutants (red). The IC₅₀ values are shown by the dashed line. Data are plotted on mean \pm SEM (n=3). Significant differences in pIC₅₀ compared with WT are indicated (** p <0.01, **** p <0.0001).

(a)



(b)

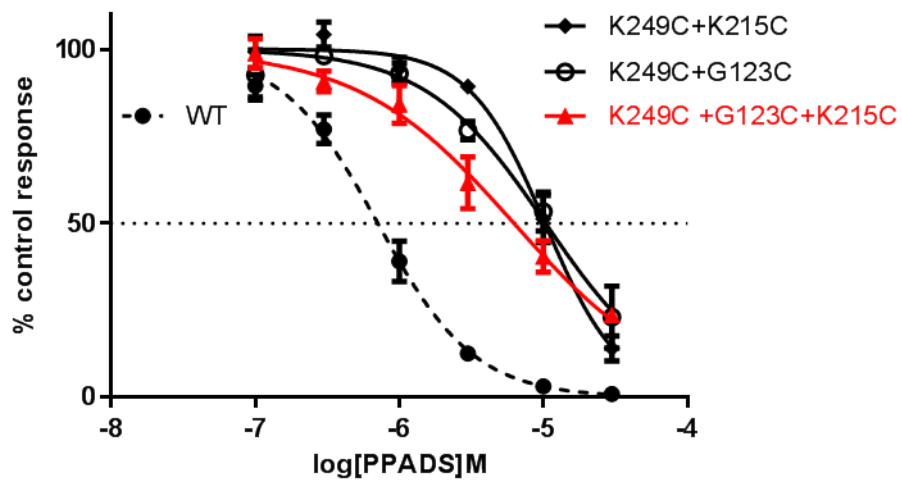


Figure 5.11 Effect of the triple mutants on the sensitivity of hP2X1 receptor to ATP and PPADS (a) Representative concentration responses to PPADS of WT hP2X1R and the triple mutant based on their EC_{90} . The upper orange bar indicates the 5-minute perfused with PPADS and the application of PPADS throughout the recording. The lower black bar indicates 3 second co-application of ATP and PPADS. **(b)** PPADS concentration response curves for WT, double mutants and the triple mutant. The IC_{50} values are shown by the dashed line. Data are plotted on mean \pm SEM ($n=3$).

5.12) was used to insert into the individual cysteine mutant to test whether the bulk will affect PPADS sensitivity.

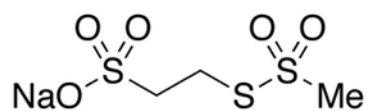
Effect of MTSES on PPADS sensitivity

Firstly, the effect of MTS compounds on ATP potency was tested. An EC_{50} concentration of ATP was used as this would show the greatest sensitivity to any modification (Roberts et al. 2009b). MTSES (100 μ M) was applied for 5 min between ATP applications as well as being co-applied with an EC_{50} of ATP. This should allow the effects of MTS reagents at any accessible cysteine residues either in the absence of ATP or ATP-bound (MTS reagent in the presence of ATP) receptors to be determined (Roberts and Evans 2007).

At WT hP2X1Rs, negatively charged MTSES (100 μ M) had no effect on currents in response to an EC_{50} concentration of ATP (Figure 5.13) as reported previously (Roberts and Evans 2007, Roberts et al. 2009b). It is consistent with a lack of free cysteine residues in the native receptor. For the majority of the individual cysteine mutants (G123C, K138C, D170C, K215C, K249C and N284C), MTSES had no significant effect on their response to an EC_{50} concentration of ATP. However, at K190C there was a significant decrease to ~60% of control (Figure 5.13). Following 5-min washout of MTSES, the responses were still significantly inhibited by ~50%, which is consistent with previous studies (Roberts et al. 2009b).

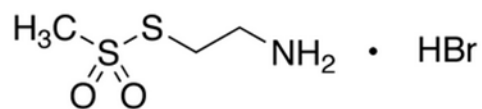
For those individual cysteine mutants where MTSES had no effect on response on an EC_{50} concentration of ATP, the effect of MTSES on their PPADS sensitivity was tested. For majority of the mutants, MTSES did not have significant effect on PPADS sensitivity (Figure 5.14). However, for K138C and K249C, MTSES further decreased the PPADS sensitivity (~10-fold) compared to those without incubation of MTSES (~3-fold) (Figure 5.14). This supports other findings indicating the positive residues at these two positions have important roles in PPADS binding to the receptor.

(a)



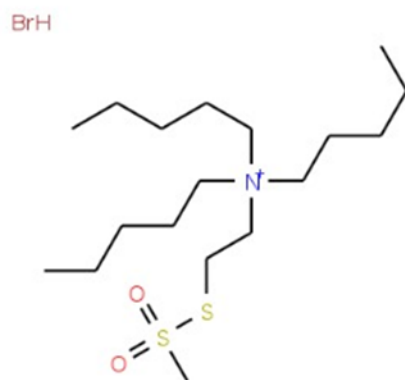
MTSES

(b)



MTSEA

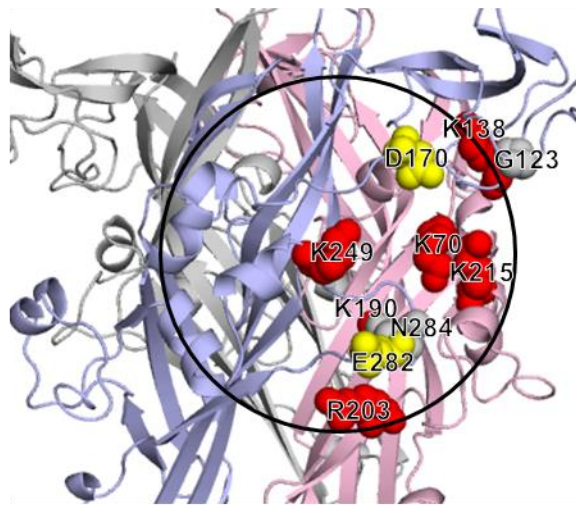
(c)



MTS-TPAE

Figure 5.12 Molecular structure of MTS compounds (a) molecular structure of MTSES (negatively charged) (b) molecular structure of MTSEA (positively charged) (c) molecular structure of MTS-TPAE (no charge)

(a)



(b)

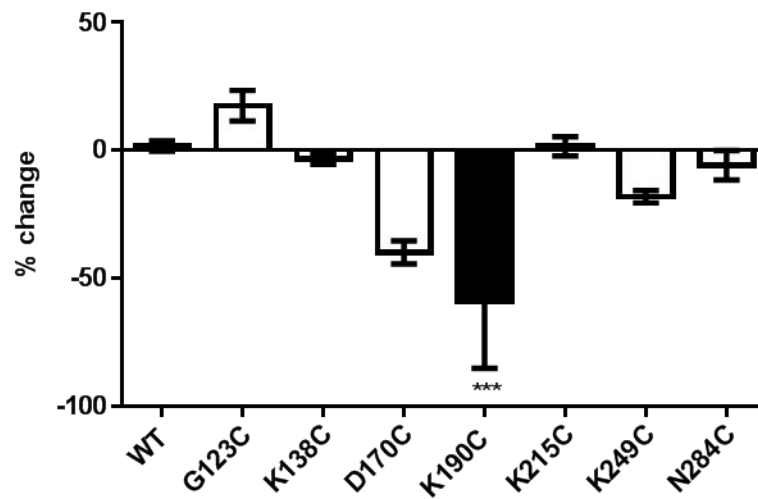


Figure 5.13 Effect of MTSES on ATP evoked responses at cysteine mutants of the hP2X1R (a) Homology model of the hP2X1R in the closed state showing the location of individual cysteine mutants. Red spheres indicate decreased accessibility and PPADS potency, yellow spheres indicate decreased accessibility and increased PPADS potency and grey spheres indicate no change in accessibility and PPADS potency **(b)** Summary of the effects of MTSES on WT and mutant hP2X1Rs of responses to EC₅₀ concentration of ATP, Data are expressed as % (0% indicates no change), significant differences from AT are shown by black bars, *** $p < 0.001$ (n=3).

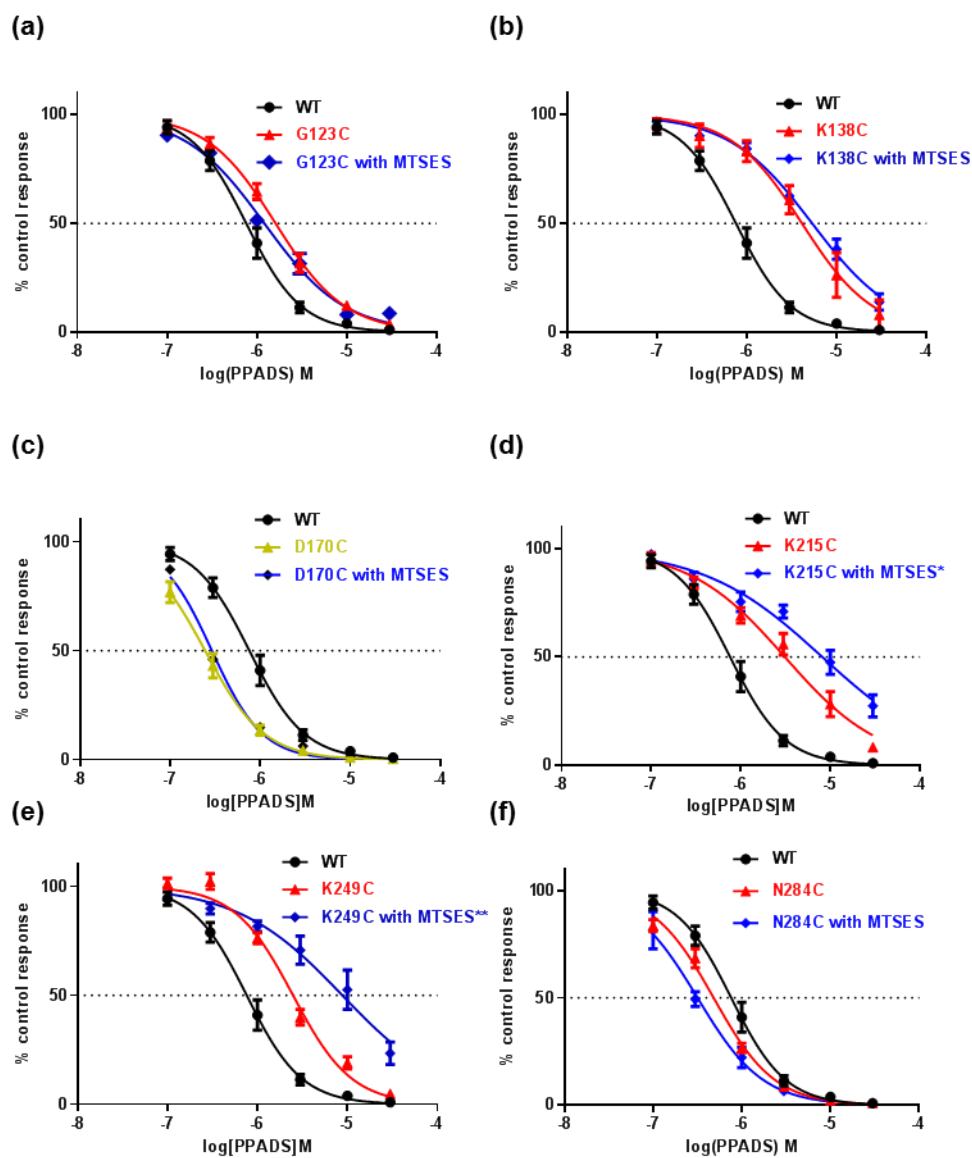


Figure 5.14 Effect of MTSES on PPADS concentration responses at cysteine mutants of the hP2X1R PPADS concentration-response curves of the hP2X1R mutant (a) G123C, (b) K138C, (c) D170C, (d) K215C, (e) K249C and (f) N284C with (blue) and without (red) 100 μ M MTSES. All mutants were incubated in the presence of MTSES for ≥ 1 h. The IC_{50} values are shown by the dashed line. Data are plotted on mean \pm SEM ($n=3$). Significant differences in pIC_{50} of mutants between with and without MTSES are indicated (* $p < 0.05$, ** $p < 0.01$).

Effect of MTSEA and MTS-TPAE on sensitivity

In order to further investigate contributions of these positively charged residues to PPADS binding, positively charged MTSEA was used to modify the cysteines. For the current response of hP2X1Rs to an EC₅₀ value of ATP, positively charged MTSEA (100 µM) potentiated the amplitude of responses at WT P2X1Rs by ~10.1%, similar to that described previously for WT P2X1Rs (Roberts and Evans 2007, Roberts et al. 2009b). Following 5-min washout of MTSEA, WT receptors returned to control values. The change on WT receptors could be a non-specific effect by the modification of cysteine mutants or trafficking of new P2X1Rs from the intracellular space that have not been modified by MTSEA could account for this partial reversal and a similar phenomenon was

seen for cysteine mutants of the P2X4R (Roberts et al. 2008). It was previously shown that 1 h pre-incubation followed by washing with membrane permeant MTSEA was sufficient to modify the pool of P2X4Rs and overcome the apparent reversibility of the effect (Roberts et al. 2008). Therefore, the cysteine mutant hP2X1Rs were incubated with MTSEA for more than 1 h and then their effect on PPADS sensitivity was tested. At mutants K138C and K215C, the positively charged MTSEA did not rescue the decreased PPADS sensitivity. The positive charge of MTSEA at D170C also did not show further effect on PPADS sensitivity (Figure 5.15).

In order to investigate contribution of the size of the side chain of these residues to PPADS binding, a large cysteine-reactive agent MTS-TPAE was used. MTS-TPAE did not have any further significant change on PPADS sensitivity at K138C and K170C compared to the effect caused by the mutants alone (Figure 5.15).

For residues in which MTS compounds have no effect on PPADS sensitivity, it is unclear whether this is because the charge of the residue does not directly contribute to the actions of PPADS at the receptor or whether the residue is inaccessible by the MTS compounds. In the future work, the two possibilities can be determined by testing whether MTSEA-biotin can bind to the individual cysteine mutants of the hP2X1Rs after incubation with MTSES.

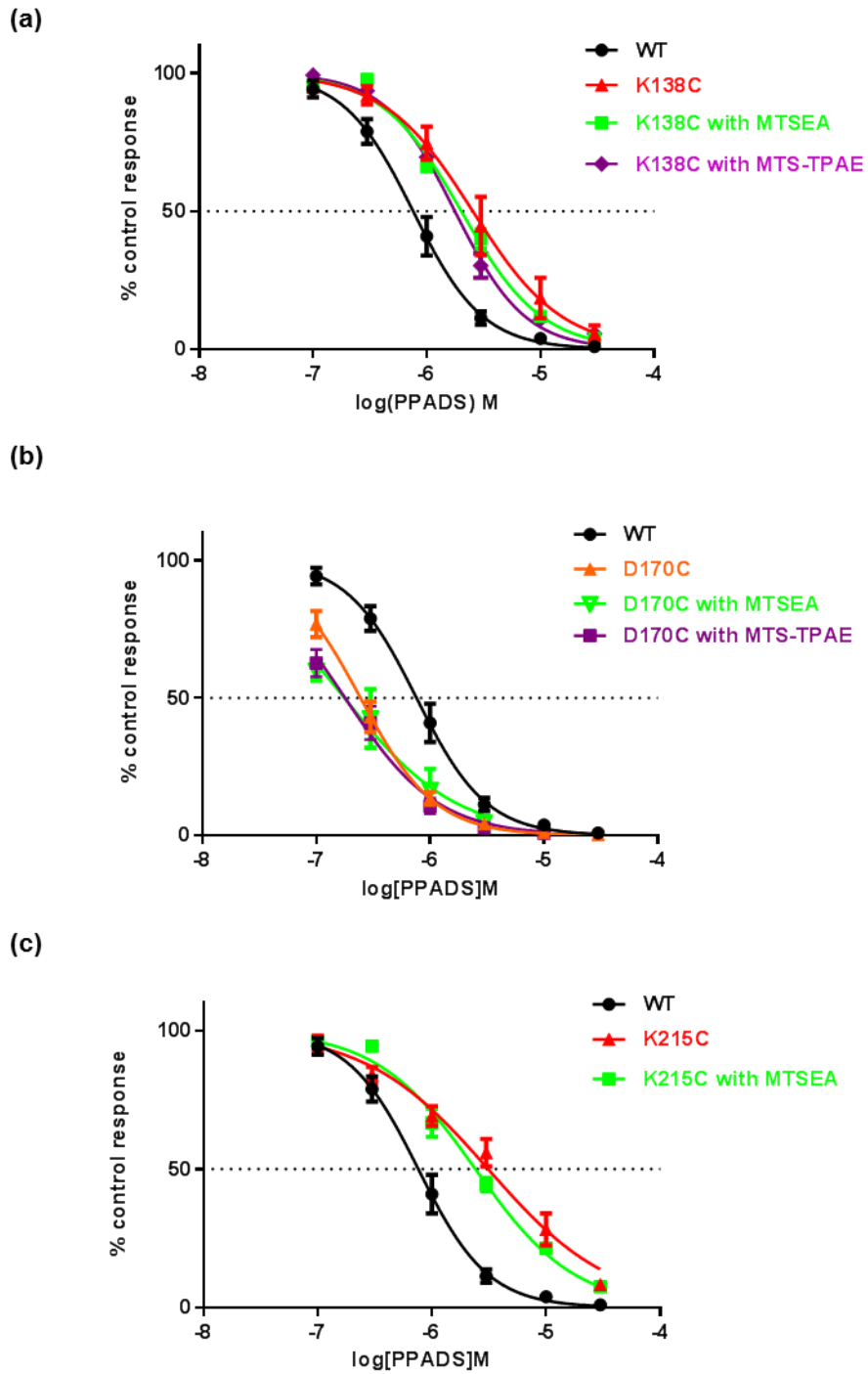


Figure 5.15 Effect of MTSEA and MTS-TPAE on PPADS concentration responses at cysteine mutants of the hP2X1R PPADS concentration-response curves of the hP2X1R mutant (a) K138C (b) D170C and (c) K215C with and without 100 μ M MTSEA (green) and MTS-TPAE (purple). All mutants were incubated in the presence of 100 μ M MTSEA or MTS-TPAE for ≥ 1 h. The IC_{50} values are shown by the dashed line. Data are plotted on mean \pm SEM (n=3).

Mutants	pEC ₅₀	EC ₉₀ (μM)	pIC ₅₀
WT	6.12±0.08	10	6.12±0.07
S64C	5.90±0.06	10	6.12±0.13
S66C	5.75±0.02	10	6.14±0.19
K70C	4.30±0.04 ****	300	5.64±0.06 *
V74C	5.96±0.10	10	6.10±0.01
T75C	5.65±0.06 ***	10	5.82±0.14
L77C	5.94±0.05	10	5.90±0.14
G123C	5.21±0.04 ****	30	5.79±0.07
K138C	6.34±0.05	10	5.36±0.11 ***
R139C	6.22±0.04	10	5.78±0.06
D170C	5.65±0.07 ***	10	6.62±0.08 ***
S175C	-	10	6.02±0.05
A182C	6.26±0.14	10	6.32±0.05
K190C	5.46±0.03 ****	30	5.54±0.13 **
R203C	5.58±0.17***	10	5.61±0.10**
A211C	5.47±0.11****	30	6.28±0.17
K215C	4.83±0.04****	300	5.55±0.12**
Q237C	-	10	6.19±0.04
E248C	6.70±0.14 ****	10	5.88±0.12
K249C	6.25±0.11	10	5.60±0.05 ***
L279C	6.35±0.07	10	5.74±0.11
E282C	5.79±0.06	10	6.60±0.17*
K283C	5.70±0.03**	10	6.01±0.05
N284C	5.64±0.04**	30	6.32±0.06
L285C	5.17±0.10****	30	6.4±0.06
S286C	5.10±0.05****	30	6.44±0.10
P287C	5.31±0.08****	30	6.09±0.17
G288C	5.10±0.07****	30	6.37±0.03

Table 5.1 The sensitivity of WT and single cysteine mutant P2X1Rs.to ATP (pEC₅₀), the EC₉₀ concentration used for determination of antagonist sensitivity and PPADS pIC₅₀ are given. Data are shown as mean ± SEM (n>3) (**p*<0.05, ***p*<0.01, ****p*<0.001, *****p*<0.0001).

Mutants	pEC ₅₀	EC ₉₀ (μM)	pIC ₅₀
WT	6.12±0.08	10	6.12±0.07
K249C+G123C	5.43±0.14	10	4.95±0.10****
K249C+K138C	6.08±0.11	3	5.31±0.08
K249C+K190C	5.62±0.04	10	5.44±0.12
K249C+K215C	5.97±0.05	10	4.98±0.06**
K249C+G123C+K215C	3.61±0.15	1000	5.22±0.12

Table 5.2 The sensitivity of WT and double/triple cysteine mutant P2X1Rs. to ATP (pEC₅₀), the EC₉₀ concentration used for determination of antagonist sensitivity and PPADS pIC₅₀ are given. Data are shown as mean ± SEM (n>3) Significant difference was calculated by t-test between single mutant and combinations of mutants (**p*<0.05, ***p*<0.01, ****p*<0.001, *****p*<0.0001).

Mutants	Peak (μA)	Hillslope	Rise-time (ms)	Decay-time (ms)
WT	-10.06 \pm 0.59	1.11 \pm 0.17	174.35 \pm 14.85	987.94 \pm 92.67
S64C	-13.47 \pm 0.43	1.02 \pm 0.05	63.87\pm1.92**	425.97 \pm 15.79
S66C	-11.56 \pm 0.36	1.12 \pm 0.13	61.99\pm1.57**	805.02 \pm 342.73
K70C	-4.21\pm0.51*	0.94 \pm 0.06	146.78 \pm 13.37	1001.68 \pm 128.20
V74C	-10.46 \pm 0.33	2.18\pm0.40**	85.53\pm3.93**	622.98 \pm 76.33
T75C	-7.60 \pm 1.28	1.65 \pm 0.37	142.68 \pm 32.55	1447.15 \pm 258.69
L77C	-11.23 \pm 0.95	1.51 \pm 0.05	71.16\pm2.87**	467.23 \pm 81.31
G123C	-6.61 \pm 1.89	1.69 \pm 0.37	127.34 \pm 19.19	761.44 \pm 63.39
K138C	-14.47\pm1.08*	1.03 \pm 0.18	152.59 \pm 8.43	934.55 \pm 17.78
R139C	16.96\pm0.52****	1.11 \pm 0.03	135.7 \pm 9.01	2187\pm132.48****
D170C	-10.90 \pm 0.25	1.5 \pm 0.20	119.11 \pm 9.11	1824.65\pm143.31**
A182C	-7.24 \pm 1.06	1.06 \pm 0.06	138.48 \pm 13.83	716.06 \pm 169.87
K190C	-5.39\pm0.25*	1.33 \pm 0.16	102.24 \pm 6.52	1287.82 \pm 160.48
R203C	-9.64 \pm 2.08	1.21 \pm 0.09	80.8\pm4.77*	1131.09 \pm 75.71
K215C	-6.15 \pm 0.64	0.9 \pm 0.03	112.3\pm13.23*	1173.84 \pm 201.64
E248C	-12.76 \pm 1.60	0.91 \pm 0.09	157.73 \pm 19.23	561.49 \pm 15.24
K249C	-11.87 \pm 0.93	1.02 \pm 0.18	72.24\pm4.38*	445.71 \pm 27.87
L279C	-12.59 \pm 0.66	0.90 \pm 0.11	172.68 \pm 15.05	1103.61 \pm 91.28
N284C	-2.25 \pm 0.28	1.21 \pm 0.24	156.65 \pm 13.29	1471.41 \pm 203.67

Table 5.3 Peak currents to a maximal concentration of ATP, time-course of ATP (100 μM) evoked currents and hillslope of the ATP concentration curve for WT and single cysteine mutant hP2X1Rs. Data are shown as mean \pm SEM ($n > 3$) (* $p < 0.05$, ** $p < 0.01$, *** $p < 0.001$, **** $p < 0.0001$).

5.3 Discussion

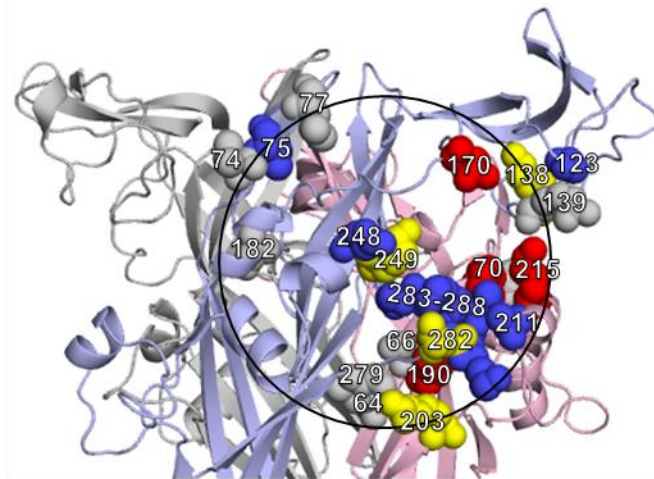
In this chapter, effects of cysteine mutants in the ring centred on K249 on PPADS sensitivity of the hP2X1Rs were investigated. Cysteine substitutions were well tolerated, and functional responses were recorded from all of the cysteine mutant hP2X1Rs. Based on their effect on PPADS potency, 27 cysteine mutants were discriminated into three groups, (i) those that decreased PPADS potency (ii) those that increased PPADS potency and (iii) those showing no change in PPADS potency. The majority of these mutants showed decreased accessibility by PPADS binding (see detail in Chapter 4). Interestingly, mapping the residues showing effect (decrease/increase) on PPADS potency showed they were around the orthosteric pocket (Figure 5.17). This suggests that PPADS is more likely to bind to the orthosteric area. However, some residues in the allosteric area (for example V74, T75 and A182) had no effect on PPADS potency, suggesting that they do not directly contribute to antagonist binding and their changes in accessibility are likely to result from antagonist induced conformational changes.

5.3.1 Effect of residues on PPADS potency within and around the orthosteric pocket

Plotting the individual cysteine mutants (K70C, K138C, K190C, R203C, K125C and K249C) showing decreased (~3-fold) PPADS potency on the hP2X1R homology model highlights a region around the orthosteric site of equivalent dimension to the antagonist. Interestingly, they all removed positive charge from the surface (Figure 5.17). This suggests that positive charges play an important role in PPADS binding, which is consistent with the negatively charged molecule of PPADS.

At K249C, negative charged MTSES treatment produced a further decrease (~10-fold) in PPADS potency, highlighting the importance of charge at this position. This is consistent with previous studies showing reverse of the charge with E249K mutation in rP2X4R recovered its sensitivity to PPADS (Buell et al. 1996). Similarly, MTSES also had a further effect on PPADS at K215C (~10-fold). K215C showed increased accessibility following PPADS binding (Figure

(a)



(b)

PPADS potency

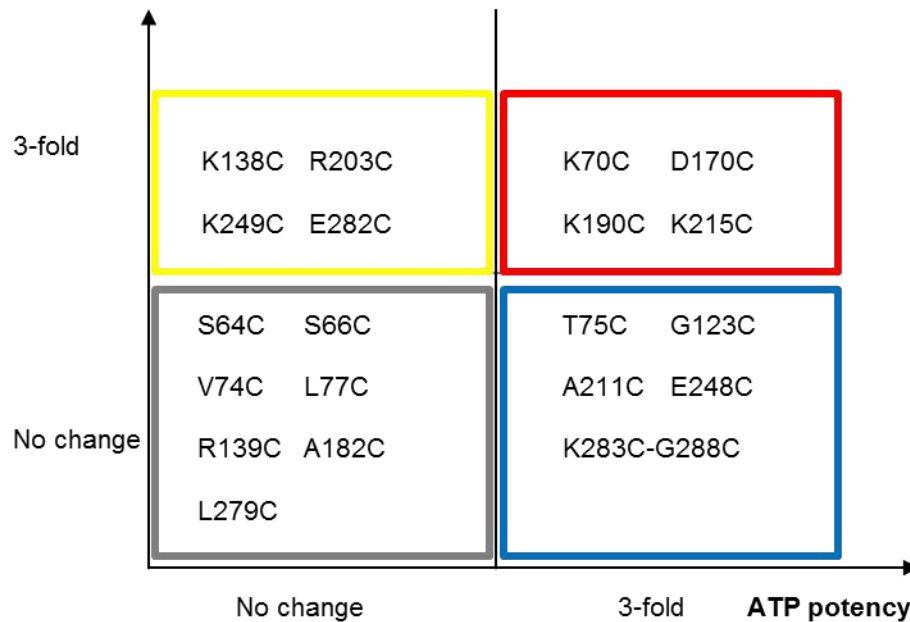


Figure 5.16 Comparison of effects on cysteine mutants on ATP and PPADS potency (a) The closed state homology model of the hP2X1R zoomed in on the extracellular loop showing the location of individual cysteine mutants, yellow spheres indicate no change in ATP potency but 3-fold decrease/increase in PPADS potency; red spheres indicate 3-fold decrease/increased in both PPADS and ATP potency; grey spheres indicate no change in either PPADS or ATP potency; blue spheres indicate 3-fold decrease in ATP potency but no change in PPADS potency. **(b)** Summary of the effects of the individual cysteine mutants on PPADS and ATP potency.

4.6). Therefore, K215 may not directly interact with PPADS but this positive charge contributes to attracting PPADS binding. Combination of these two mutants showed further decrease (~10-fold) on PPADS potency compared to the single mutant, suggesting the importance of these two positive charges. The modest effects of point mutants suggest that multiple residues would be involved in PPADS, consistent with the multiple charges in the PPADS molecule.

At mutant K138C in the cysteine rich head region, PPADS affinity was reduced ~3-fold but it showed increased accessibility by PPADS, suggesting that the positive charge contributed to the conformational rearrangement associated with binding of the antagonist. K138 was previously reported to contribute to the antagonism of suramin and NF449 (El-Ajouz et al. 2012a, Farmer et al. 2015). Interactions between the residue in head region and the antagonists may block the movements required for ATP evoked channel gating (Hattori and Gouaux 2012).

At R203C PPADS potency was decreased by ~3-fold but there was no change in accessibility following PPADS binding (Figure 4.12). This suggests that R203 does not directly line the PPADS binding site but that the positive charge may contribute to the electrostatic pull towards the orthosteric site. In support of the importance of positive charges to PPADS binding, removal of the negative charges in the pocket (D170 and E282C) increased sensitivity to PPADS ~3-fold. Overall, PPADS binding site is predicted to be at orthosteric site, interacting with positive charges at the P2XR.

5.3.2 Residues outside the orthosteric pocket showing no effect on PPADS potency

Five cysteine mutants (V74C, T75C, L77C, A182C and E248C) opposite the ATP binding site showed decreased accessibility by PPADS binding but had no effect on PPADS potency. This suggests that they are not likely to directly contribute to PPADS binding and their decreased accessibility may result from PPADS induced conformational changes. Interestingly, V74C, L77C and A182C also showed no change in ATP potency but decreased accessibility by ATP binding (see detail in Chapter 4). The crystal structure shows they are not in the

ATP binding pocket (Hattori and Gouaux 2012). The decreased accessibility by ATP results from ATP-evoked conformational changes. Therefore, PPADS and ATP may cause similar conformational changes at these positions.

For some cysteine mutants showing no change in accessibility following PPADS binding, there are two possible reasons. One is that they are not involved in PPADS binding and the other is that they may be key residues in the PPADS binding site and mutating at these positions may cause PPADS not binding to the receptor. At S175C and Q237C there was no change in accessibility by PPADS binding and no change in PPADS potency. It indicates that they are not key residues for PPADS binding. It rules out the possibility that they showed no change in accessibility because the mutations abolished binding of the antagonist. In summary, the PPADS binding site is not likely to be located in this area opposite to the ATP binding pocket. This is consistent with the previous hypothesis that PPADS is more likely to bind close to the orthosteric pocket.

5.3.3 Comparison of effects of cysteine mutants on ATP and PPADS potency

Based on effects of the cysteine mutants on PPADS and ATP potency, mutants can be classified into four groups (i) those that had no effect on PPADS and ATP potency; (ii) those that had effect on PPADS potency but no change to ATP potency; (iii) those that had effect on both PPADS and ATP potency; (iv) those that had an effect on ATP potency but no effect on PPADS potency (Figure 5.17). This suggests the PPADS binding site and the ATP binding site may include at least two residues (K70 and K190) in common. Interactions between PPADS and these common residues (conserved residues) may block ATP binding, which may be part of PPADS mode of action. However, these two residues have a great effect on ATP binding (Ennion et al. 2000) but modest effect on PPADS potency (~3-fold). This suggests that these two residues do not dominate in the response to PPADS and multiple residues would work together for PPADS binding.

In addition, some residues (K138, R203, E282 and K249) are unique in the PPADS binding site. Although there is evidence showing PPADS binds to the

orthosteric pocket, it is likely that the PPADS binding site overlaps the ATP binding region and therefore blocks the channel gating.

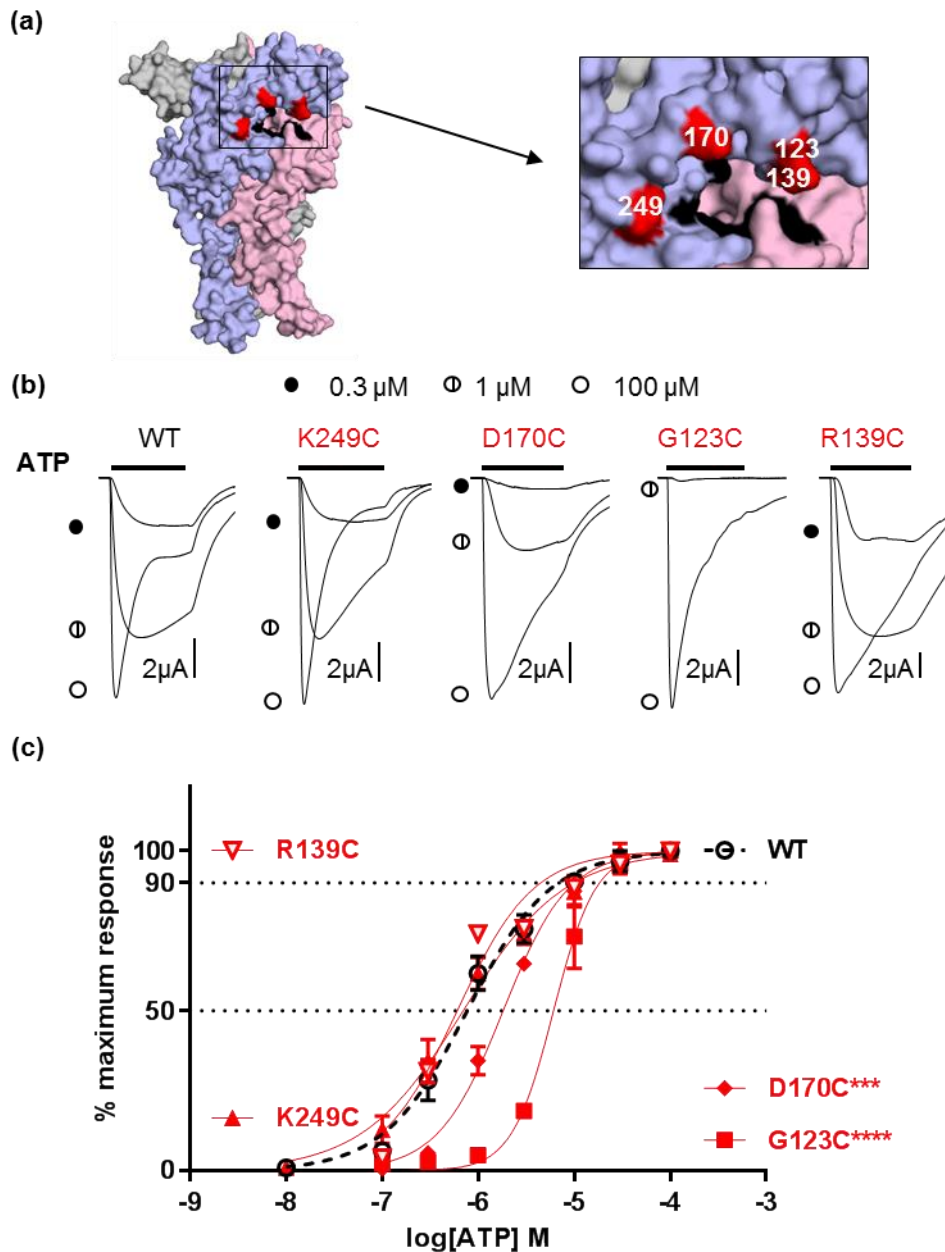


Figure S5.1 Effect of the mutants showing decreased accessibility by PPADS binding around the ATP binding sites on ATP sensitivity of the hP2X1R (a) Homology model of the hP2X1R in the closed state showing the location of individual cysteine mutants showing decreased accessibility by PPADS binding. Residues consisting of the ATP binding site are labelled in black. (b) Representative responses to ATP (0.3, 1, 100 μ M) of the WT P2X1R and the individual mutant showing decreased accessibility following PPADS treatment. Black bar indicates 3 second application of ATP. (c) ATP concentration response curves for the WT hP2X1R and mutants. The EC_{50} and EC_{90} values are shown by the dashed line. Data are plotted on mean \pm SEM ($n=3$). Significant differences in pEC_{50} compared with WT are indicated (** $p < 0.001$, **** $p < 0.0001$).

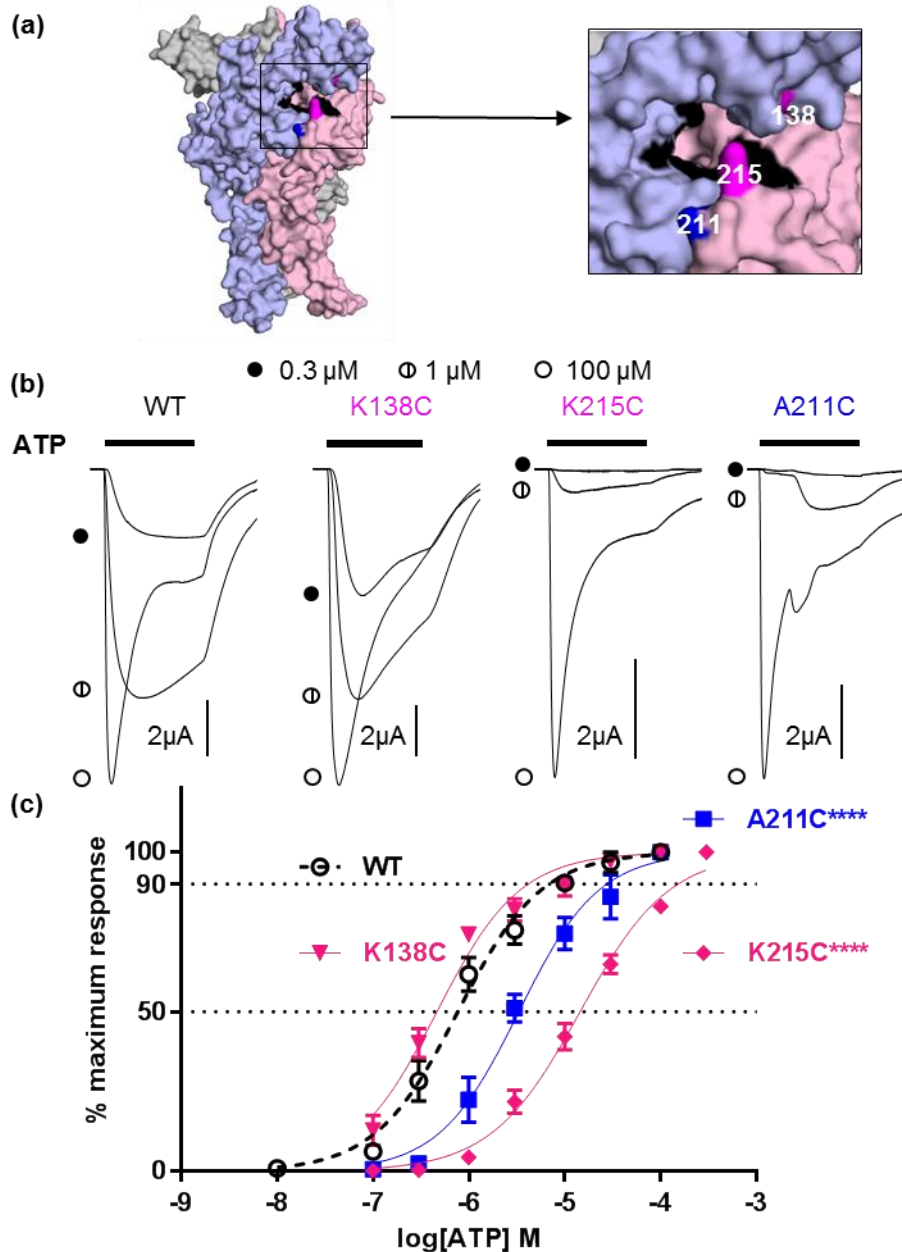


Figure S5.2 Effect of the mutants showing increased accessibility by PPADS binding or inaccessibility around the ATP binding sites on ATP sensitivity of the hP2X1R (a) Homology model of the hP2X1R showing the location of cysteine mutants showing increased accessibility by PPADS binding (pink) and those were inaccessible (blue). Residues consisting of the ATP binding site are labelled in black. (b) Representative concentration responses to ATP (0.3, 1, 100 μ M) of the WT P2X1R and the individual mutant. Black bar indicates 3 second application of ATP. (c) ATP concentration response curves for the WT P2X1R and mutants showing increased accessibility (pink) and inaccessibility (blue). The EC_{50} and EC_{90} values are shown by the dashed line. Data are plotted on mean \pm SEM ($n=3$). Significant differences in pEC_{50} compared with WT are indicated (**** $p<0.0001$).

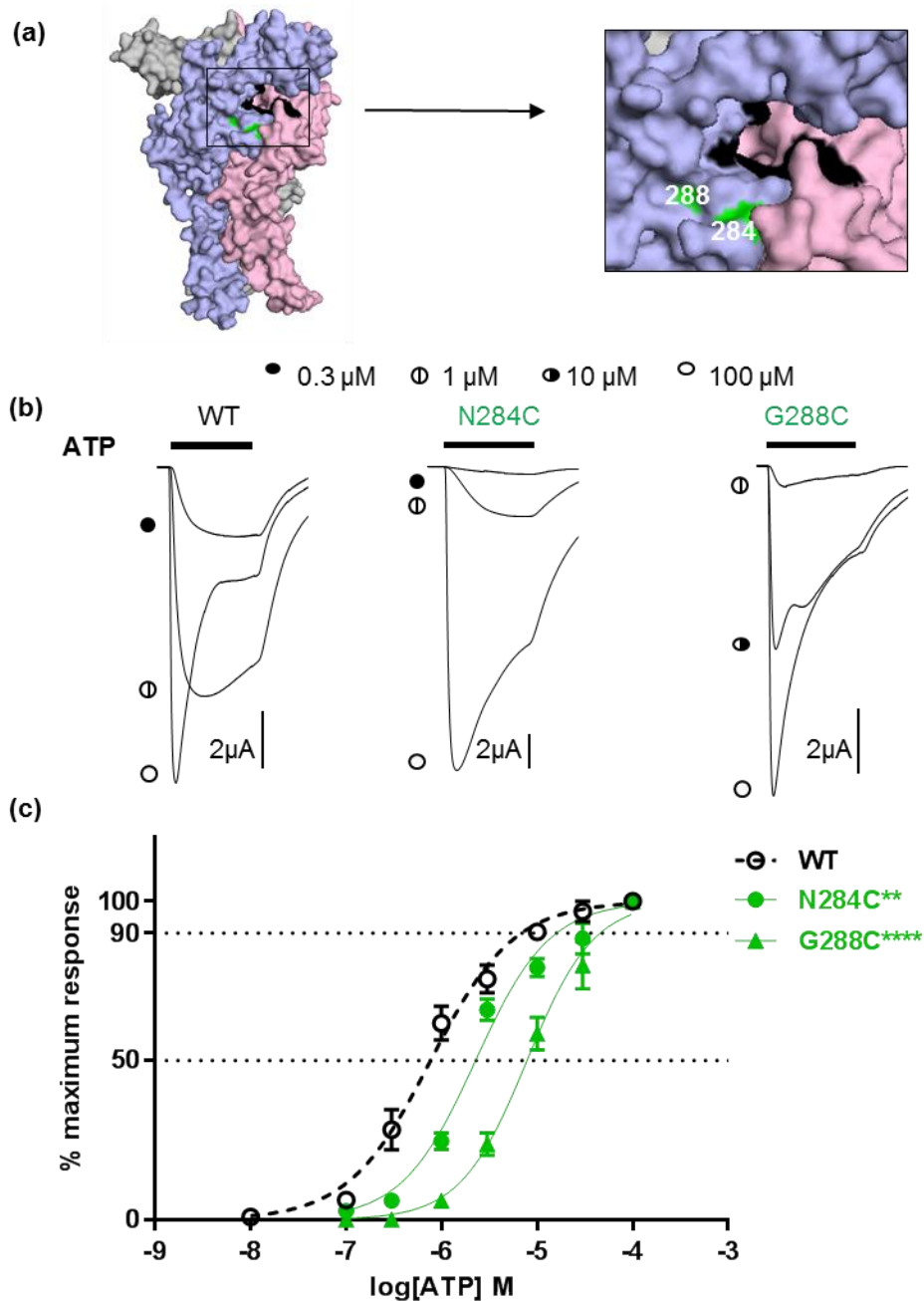


Figure S5.3 Effect of the mutants showing no change in accessibility by PPADS binding around the ATP binding sites on ATP sensitivity of the hP2X1R (a) Homology model of the hP2X1R showing the location of cysteine mutants showing on change in accessibility by PPADS binding. Residues consisting of the ATP binding site are labelled in black. (a) Representative concentration responses to ATP (0.3, 1, 100 μ M) of the WT P2X1R and the individual mutant showing decreased accessibility (red). Black bar indicates 3 second application of ATP. (b) ATP concentration response curves for the WT P2X1R and mutants. The EC_{50} and EC_{90} values are shown by the dashed line. Data are plotted on mean \pm SEM (n=3). Significant differences in pEC_{50} compared with WT are indicated (** $p < 0.01$, **** $p < 0.0001$).

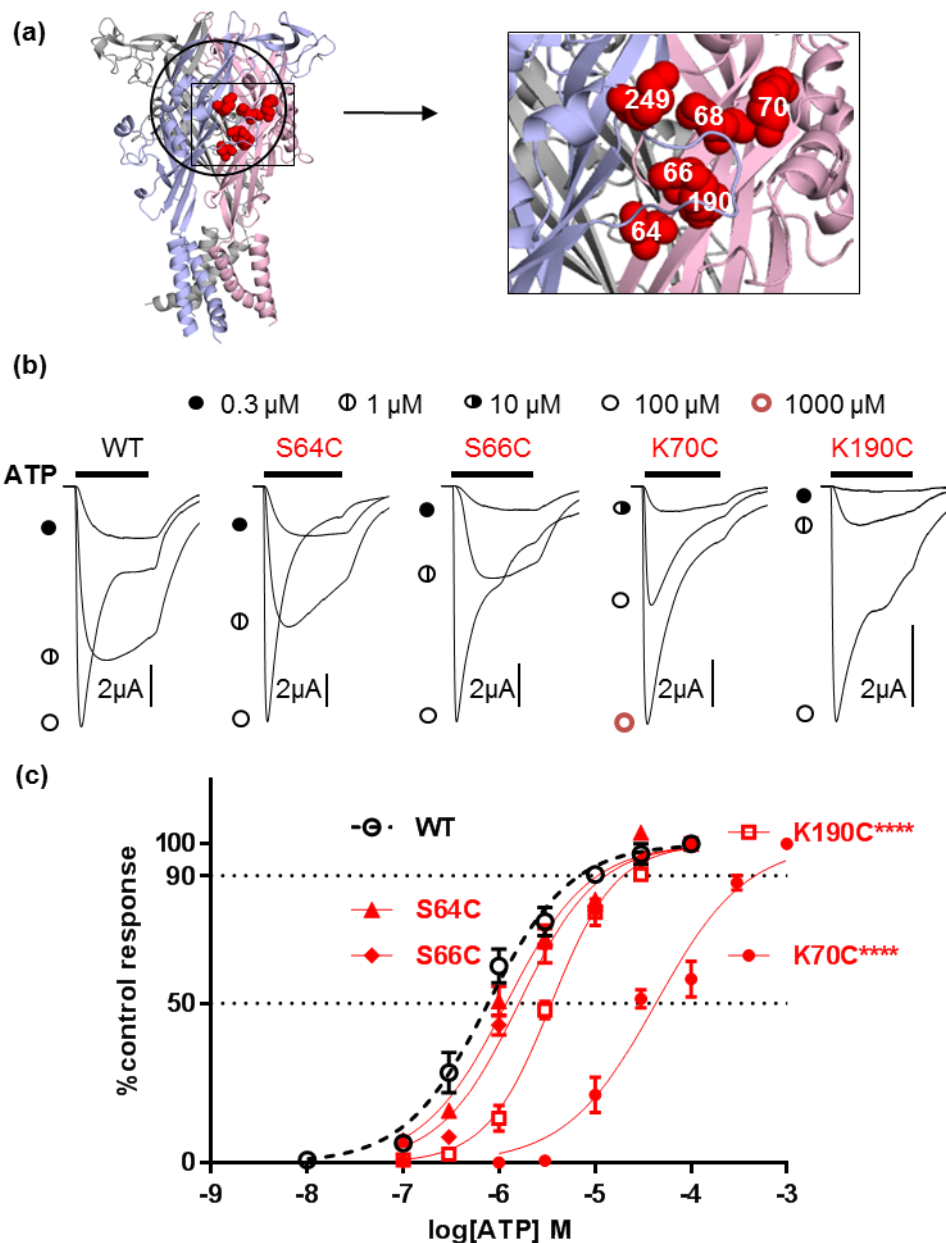


Figure S5.4 Effect of the mutants within the ATP binding sites on ATP sensitivity of the hP2X1R (a) Homology model of the hP2X1R in the closed state showing the location of individual cysteine mutants showing decreased accessibility by PPADS binding. (b) Representative concentration responses to ATP (0.3, 1, 100 μM) of the WT hP2X1R and the individual mutant. Black bar indicates 3 second application of ATP. (c) ATP concentration response curves for the WT P2X1R and mutants showing decreased accessibility. The EC_{50} and EC_{90} values are shown by the dashed line. Data are plotted on mean \pm SEM ($n=3$). Significant differences in pEC_{50} compared with WT are indicated (**** $p<0.0001$).

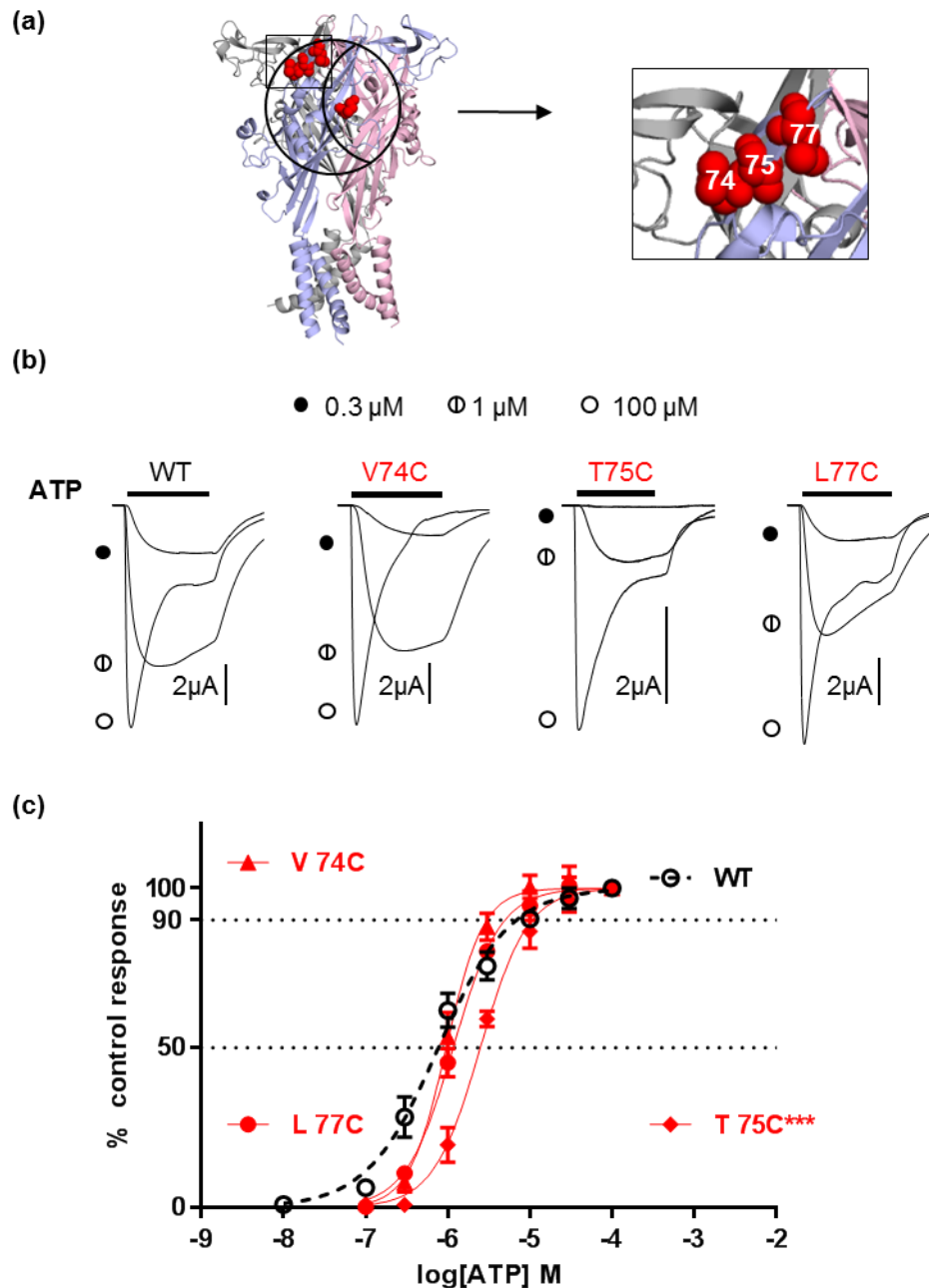


Figure S5.5 Effect of the mutants on the upper body opposite to the ATP binding sites on ATP sensitivity of hP2X1R (a) Homology model of the hP2X1R in the closed state showing the location of individual cysteine mutants showing decreased accessibility by PPADS binding. (b) Representative concentration responses to ATP (0.3, 1, 100 μM) of the WT hP2X1R and the individual mutant. Black bar indicates 3 second application of ATP. (c) ATP concentration response curves for the WT hP2X1R and mutants showing decreased accessibility. The EC_{50} and EC_{90} values are shown by the dashed line. Data are plotted on mean \pm SEM ($n=3$). Significant differences in pEC_{50} compared with WT are indicated ($***p<0.001$).

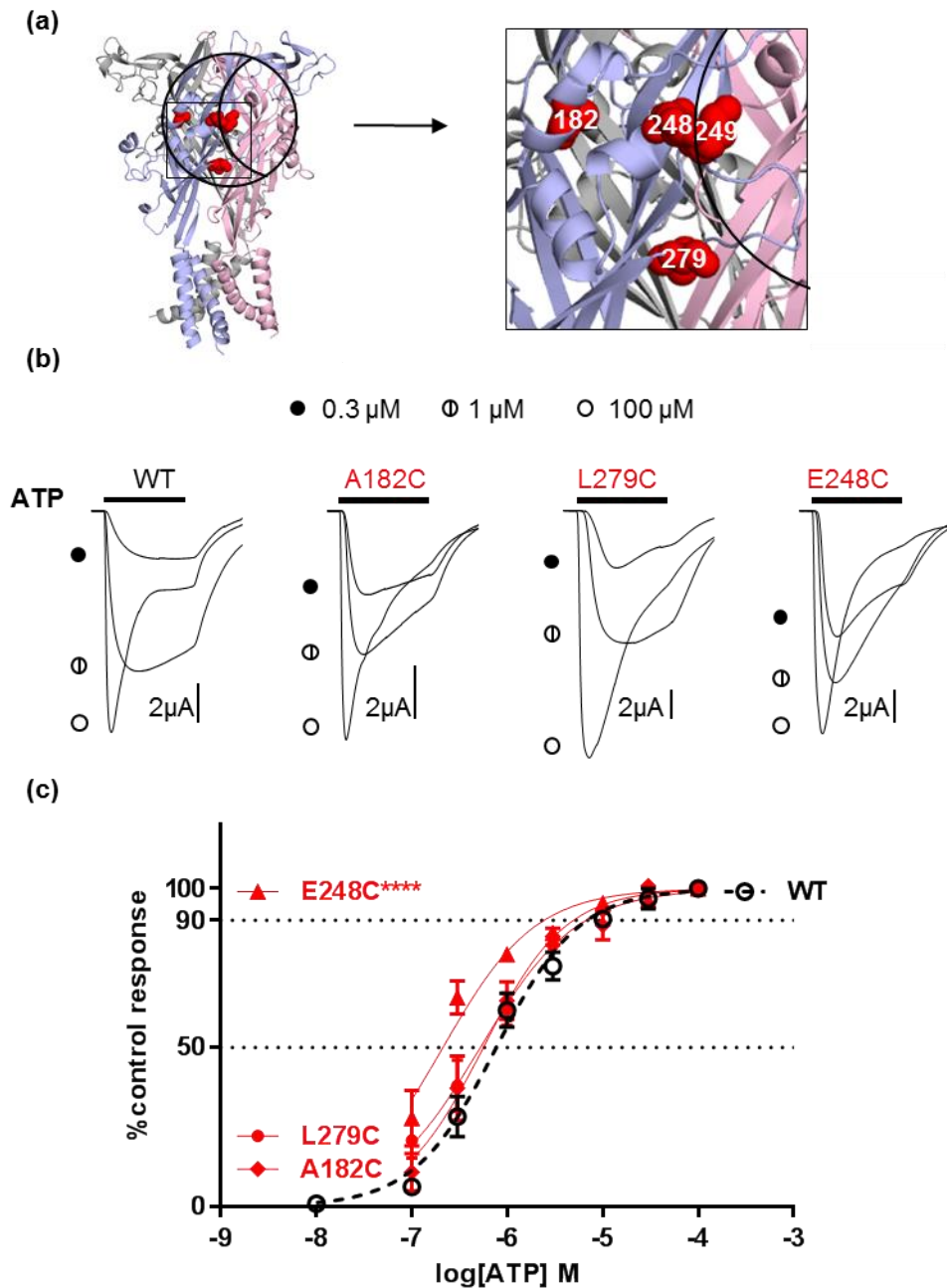


Figure S5.6 Effect of the mutants around dorsal fin opposite to the ATP binding sites on ATP sensitivity of the hP2X1R (a) Homology model of the hP2X1R in the closed state showing the location of individual cysteine mutants showing decreased accessibility by PPADS binding. (b) Representative concentration responses to ATP (0.3, 1, 100 μM) of the WT hP2X1R and the individual mutant. Black bar indicates 3 second application of ATP. (c) ATP concentration response curves for the WT hP2X1R and mutants showing decreased accessibility. The EC_{50} and EC_{90} values are shown by the dashed line. Data are plotted on mean \pm SEM ($n=3$). Significant differences in pEC_{50} compared with WT are indicated (**** $p<0.0001$).

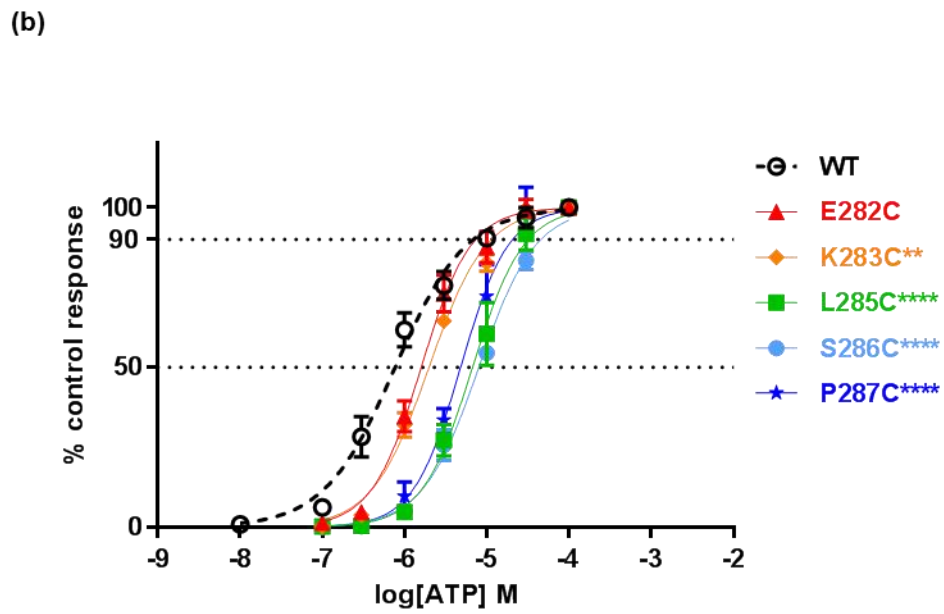
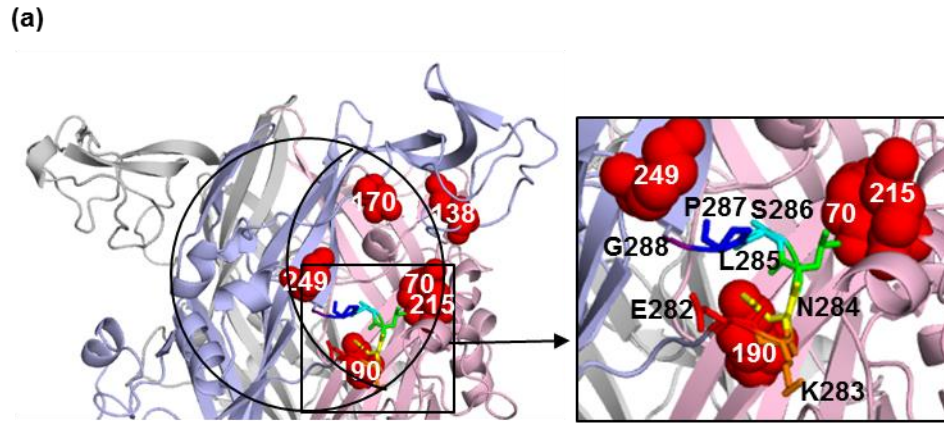
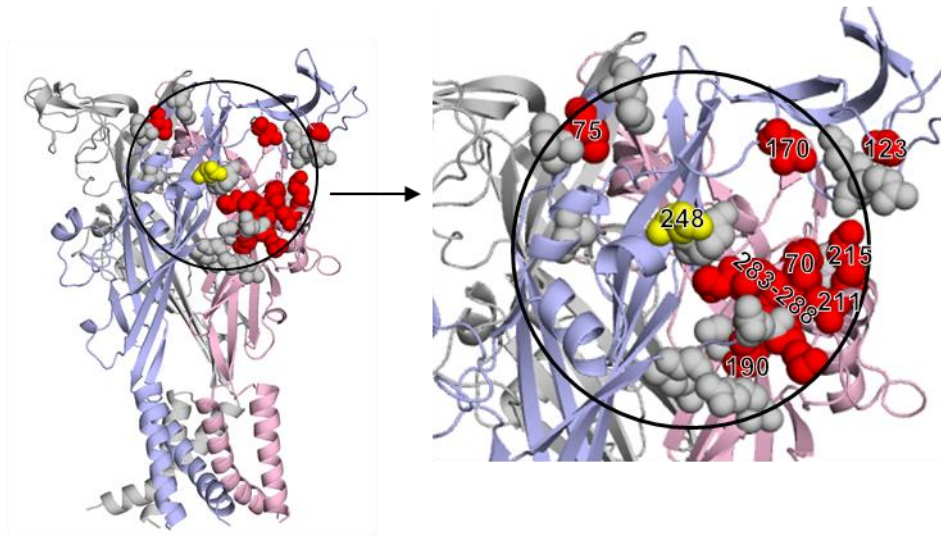


Figure S5.7 Effect of the mutants in the left flipper on ATP sensitivity (a) Homology model of the hP2X1R in the closed state showing the location of individual cysteine mutants in the left flipper as sticks. **(b)** ATP concentration response curves for the WT P2X1R and mutants. The EC₅₀ and EC₉₀ values are shown by the dashed line. Data are plotted on mean \pm SEM ($n=3$). Significant differences in pEC₅₀ compared with WT are indicated (**** $p < 0.0001$).

(a)



(b)

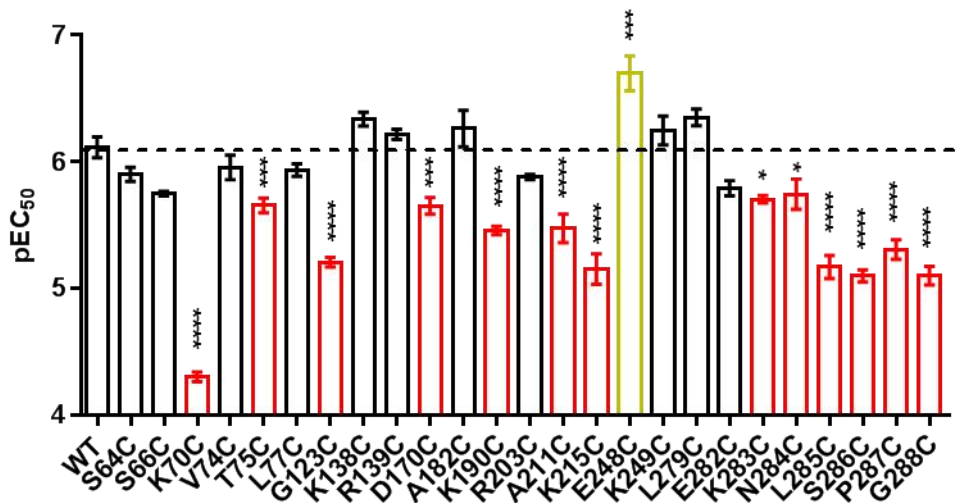


Figure S5.8 Summary of the effect of the mutants showing decreased accessibility on ATP sensitivity (a) Residues showing decreased accessibility in the presence of PPADS were shown as sphere at homology model of P2X1 receptor. Mutants decreasing ATP sensitivity were shown in red and those showing no significant change were in grey. **(b)** Comparison of ATP potency (pEC₅₀ values) between WT and mutant hP2X1Rs. Statistical analysis was performed by one-way ANOVA. Error bars indicate SEM (n=3) (**p*<0.05, ***p*<0.01, ****p*<0.001, *****p*<0.0001).

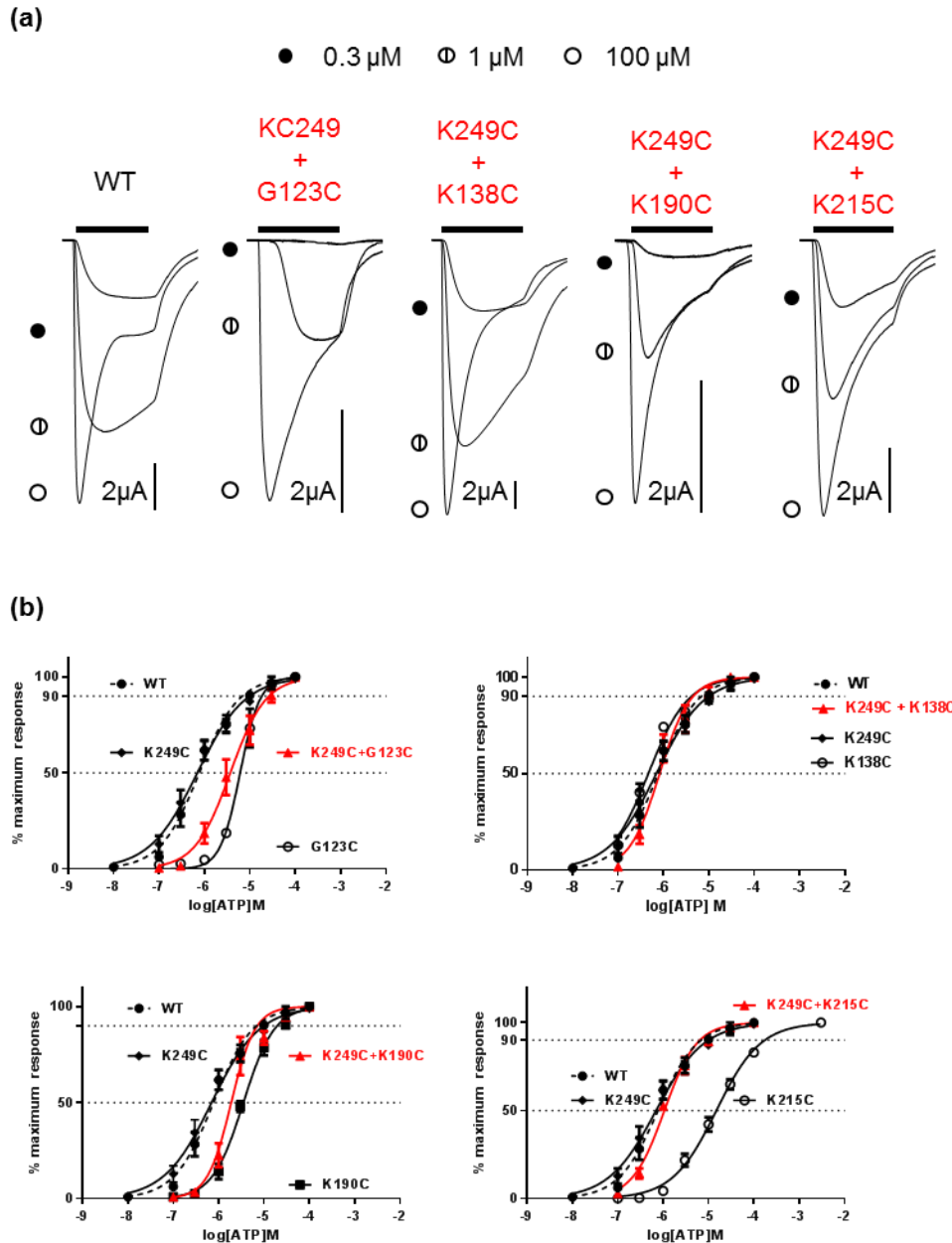


Figure S5.9 Effect of the double mutants on the sensitivity of hP2X1 receptor to ATP (a) Representative concentration responses to ATP (0.3, 1, 100 μ M) of WT hP2X1R and the double mutants. Black bar indicates 3 second application of ATP. (b) ATP concentration response curves for WT, single mutant and the double mutants (red). The EC_{50} and EC_{90} values are shown by the dashed line. Data are plotted on mean \pm SEM (n=3).

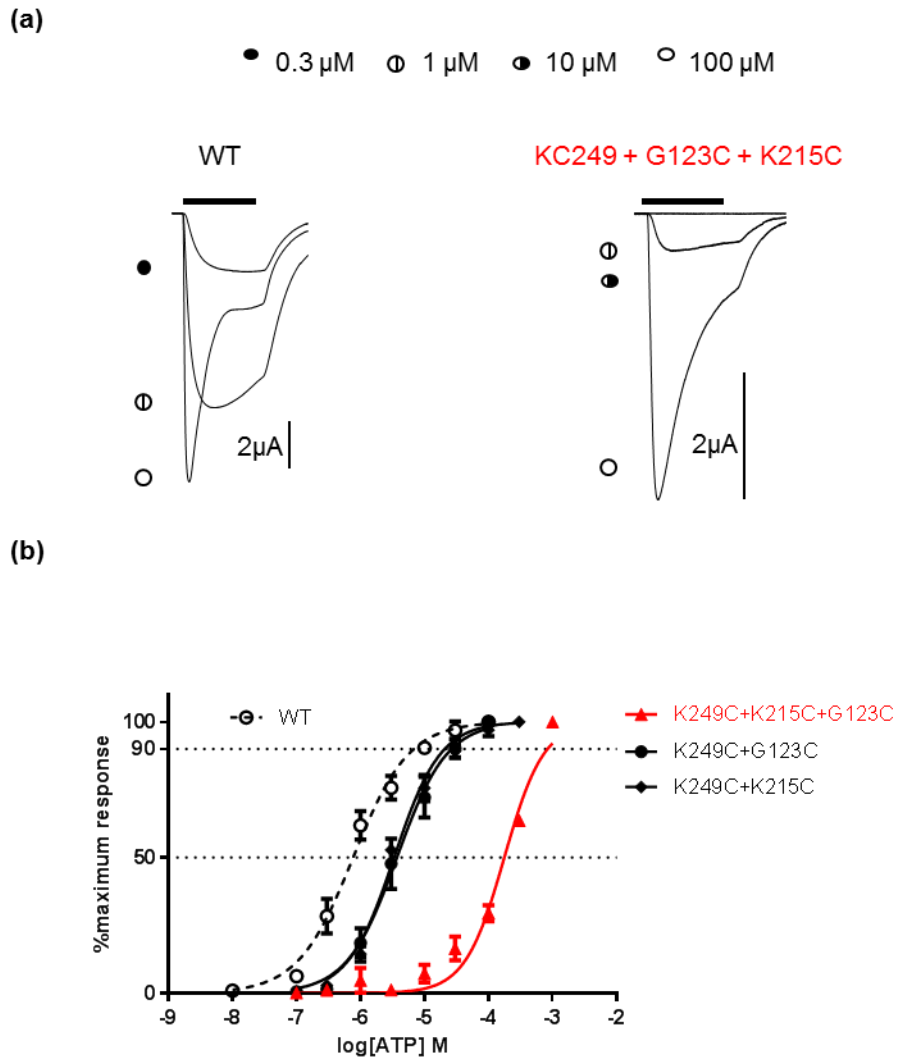


Figure S5.10 Effect of the triple mutants on the sensitivity of hP2X1 receptor to ATP and PPADS (a) Representative concentration responses to ATP of WT hP2X1R and the triple mutant (red). Black bar indicates 3 second application of ATP. **(b)** ATP concentration response curves for WT, double mutants and the triple mutant (red). The EC_{50} and EC_{90} values are shown by the dashed line. Data are plotted on mean \pm SEM ($n=3$).

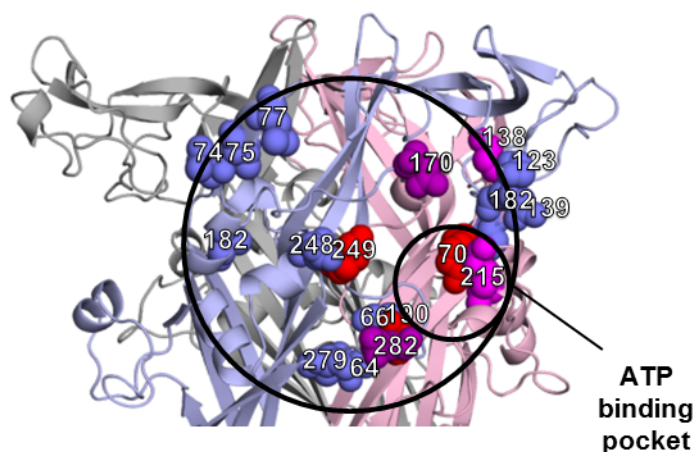
Chapter 6 General discussion

The main focus of this study was to investigate the molecular basis of antagonism of PPADS at the hP2X1R. This was carried out by cysteine mutagenesis coupled with accessibility and PPADS sensitivity tests. Cysteine mutants in the ring which centres on K249 (P2X1 numbering) with the radius of the length of PPADS were tested. They showed various effect on accessibility by PPADS binding and PPADS sensitivity of the receptor. It was predicted that residues directly involved in PPADS binding would show at least two properties: (i) accessibility of cysteine substitutions of the residues would be decreased by PPADS binding and (ii) the cysteine mutants would have effect on PPADS binding. Four residues (K70, D170, K190 and K249) out of thirty residues met these criteria. Mapping them onto the hP2X1R homology model based on the crystal structure of zfP2X4R showed they defined an area at the orthosteric binding pocket equivalent to that of the PPADS molecule. The change in accessibility at several residues was not accompanied by a change in PPADS sensitivity. These map outside the orthosteric area and it is suggested that the change accessibility results from conformational changes. Similarly, decrease in accessibility is seen for ATP as a result of agonist induced conformational changes (Figure 6.1a).

6.1 The contribution of K249 to PPADS binding at P2XRs

The initial work of this study confirmed the role of K249 to PPADS action at the hP2X1R by showing that K249C significantly decreased (~3-fold) PPADS sensitivity of the receptor and its accessibility was decreased by ~90%. These data suggested that K249 is directly involved in PPADS binding to the hP2X1R. This was consistent with previous studies showing the contribution of K249 to PPADS binding to the rP2X4R (Buell et al. 1996). It was previously shown that the PPADS insensitive rP2X4R (IC_{50} of $>500 \mu M$) has a glutamate (E) at the equivalent position of 249 and the E249K mutation recovered its sensitivity to PPADS (IC_{50} of $\sim 10 \mu M$) (Buell et al. 1996). This suggested that the positive charge at this position may play a dominant role in determining sensitivity to the antagonist PPADS. However, this study on the hP2X1R demonstrated that

(a)



(b)

	IC ₅₀ (μM)	70	138	170	190	215	249	Overall Charges
rP2X5	0.2-0.6	K	V	K	K	K	K	5
hP2X1	1	K	K	D	K	K	K	4
hP2X2	1-3	K	D	G	K	K	K	3
hP2X3	1-5	K	R	D	K	K	T	3
hP2X4	30	K	G	D	K	K	E	1
hP2X7	10-45	K	D	V	K	(absent)	Q	1
rP2X4	>300	K	D	D	K	K	E	0

* Numbering for hP2X1R

● Conserved ● positive ● negative ● neutral

Figure 6.1 (a) hP2X1R homology model showing the positions of the introduced single cysteine residue mutations. Red labelling cysteine mutants with a decrease in MTSEA-biotinylation following PPADS treatment and a decrease in PPADS sensitivity, pink corresponds to residues where MTSEA-biotinylation was increased by PPADS and also showed a decrease in PPADS sensitivity, purple is for those with a decrease in MTSEA-biotinylation following PPADS treatment and increase in PPADS sensitivity and blue labelling indicates cysteine mutants with a PPADS induced decrease in MTSEA-biotinylation but no effect on PPADS sensitivity. (b) Alignment of the P2XR subtypes IC₅₀ values to PPADS and amino acid sequences at potential PPADS binding site (numbering for P2X1R). Positively charged residues represent one, negatively charged residues represent minus one and neutral residues represent zero. Calculation of charges is shown in overall charges.

K249C only had a modest effect on PPADS sensitivity. This supported the finding from other studies showing that the contribution of the positive charge at 249 was also dependent on the species and P2XR subtypes. For example, the hP2X4R also has a glutamic acid at 249 but its IC_{50} was $\sim 30 \mu M$ (Garcia-Guzman et al. 1997). The equivalent residue in the P2X3R (IC_{50} of $\sim 1-5 \mu M$) (Kaczmarek-Hajek et al. 2012) is not charged.

6.2 The contribution of positively charged residues to PPADS binding

At mutants K70C, K190C and K249C PPADS apparent affinity was decreased ~ 3 -fold. They also showed significantly decreased accessibility by PPADS binding. Therefore they are likely to be directly involved in PPADS binding. Interestingly, all these mutants remove a positive charge from the surface of the orthosteric pocket. Mutagenesis studies (Ennion et al. 2000, Evans 2010) and crystal structures (Hattori and Gouaux 2012) showed that one characteristic of ATP binding to P2XRs is the interaction between positively charged residues on the receptor and the negatively charged tri-phosphate moiety of ATP. Like ATP, PPADS is a negatively charged compound so one of the driving forces for PPADS binding is the electrostatic interactions pulled by positively charged residues and the binding mode is characterised by specific charge-charge interactions.

In support of the importance of positive charges to PPADS binding, removal of the negative charges in the pocket (D170 and E282C) increased sensitivity of the receptor to PPADS by ~ 3 -fold. The proposed binding mode allows rationalising the effect of the D170C on PPADS potency. D170 is within the coordination sphere of the PPADS-phosphate group, hence removal a negative charge in this position may increase charge interaction between PPADS and the receptor. A negative charge is also found at the equivalent position in hP2X3&4Rs, there is no charge at P2X2, 6&7Rs, and a positive charge at the rP2X5R. This suggests that variations at this position may contribute to subtype dependent differences in PPADS sensitivity. Interestingly, the negative charge at 282 is only found in P2X1R. There is a positive charge at equivalent position in P2X2, 4, 5&7Rs and on charge in P2X3R (Figure 6.1b). This suggests that

variations at this position may also contribute to subtype dependent differences in PPADS sensitivity.

Furthermore, there are positively charged residues in the proximity of the proposed PPADS binding site which do not interact directly with PPADS. For example K215; it showed increased accessibility by PPADS binding but decreased PPADS sensitivity (~3-fold) of the receptor. This positively charged residue located on the dorsal fin is conserved in P2X1-P2X6Rs (Figure 6.1). It may also contribute to the electrostatic pull to the binding pocket. Interestingly there is a deletion for the P2X7R (IC_{50} of ~10-70 μ M) (P. et al. 1998, F. Rassendren et al. 1997, Surprenant et al. 1996), suggesting that it is not essential for PPADS binding.

The modest ~3-fold change in sensitivity for individual mutants predicted to directly interact with PPADS is consistent with a set of positively charged residues required for PPADS binding. The results suggest that the local electrostatic environment has a large role to play in PPADS action. The maximum effect of combination of the cysteine mutants on PPADS sensitivity was less than ~10-fold, suggesting that PPADS binding involves a series of residues and with no particular residue exerting a dominating effect at the hP2X1R.

Among the core residues potentially involved in PPADS binding, K70, K190 and K215 (numbering for the P2X1R) are conserved in P2XR family (Figure 6.1b). This may explain why PPADS can inhibit most P2XR subtypes. The variation of charges at residues (K138, D170 and K249, numbering for the P2X1R) (Figure 6.1b) may account for subtype dependent differences in PPADS sensitivity. The rP2X5R, with positive charges at most of the positions except a neutral residue at 138, showed highest potency to PPADS (IC_{50} ~0.2-0.6 μ M) (X. Bo et al. 2003). The hP2X1R also has five positive charges but a negative charge at 170. PPADS sensitivity of the hP2X1R (IC_{50} ~1 μ M) (Evans et al. 1995) is slightly lower than that of the rP2X5R. For the hP2X2R and P2X3R, they have one less positive charges and therefore showed less sensitive to PPADS (IC_{50} ~1-5 μ M) (Evans et al. 1995, Lewis et al. 1995). Importantly, two negative charges are present in the hP2X4R (Garcia-Guzman et al. 1997) and three negative

charges are present in the rP2X4R (Buell et al. 1996). This is consistent with the relative insensitivity of P2X4Rs to PPADS. The hP2X7R, with one negative charge at 138 and an absence at 215, showing intermediate PPADS sensitivity between P2X1-3Rs and P2X4Rs (Surprenant et al. 1996). In summary, these data suggests more positive charges and less negative charges would give the P2XR higher sensitivity to PPADS

6.3 PPADS binding quenches fluorescence at MTS-TAMRA labelled cysteine mutants in the antagonist binding pocket

Voltage Clamp Fluorometry (VCF) is a powerful method for investigating conformational changes during ligand binding. Introduced free cysteines can be labelled by a sulfhydryl-reactive fluorescent dyes, for example MTS-TAMRA (MTS-5(6)-carboxytetramethylrhodamine). VCF has been used to record simultaneously agonist evoked currents and fluorescence of labelled cysteine residues (Fryatt and Evans 2014, Lörinczi et al. 2012). Changes in the local environment of the introduced cysteine-reactive fluorophore may be detected as changes in the fluorescent emission to give a real-time measure of conformational rearrangements.

Previously, Dr Fryatt in the lab used fluorescent probes to investigate the PPADS binding site at the hP2X1R. Changes in fluorescence of labelled cysteine residues in the absence and presence of PPADS were tested. Control studies showed that PPADS (10 μ M) had no effect on the fluorescence of MTS-TAMRA (1 μ M, the concentration used to label the cysteine mutants), suggesting that there is no interference between these compounds. However, increasing the PPADS concentration (increasing the probability of PPADS and MTS-TAMRA being in close proximity) resulted in a concentration dependent quenching of fluorescence (50% decrease at ~2 mM) (Figure 6.2). Thus, it was hypothesized that if a dye MTS-TAMRA labelled cysteine is close to the PPADS binding site, PPADS binding would decrease MTS-TAMRA fluorescence. For some residues (D320C, V74C and E181C) outside the potential PPADS binding area, they can be labelled with MTS-TAMRA and fluorescence detected. PPADS (10 μ M) application had no effect on fluorescence at these MTS-TAMRA labelled cysteine

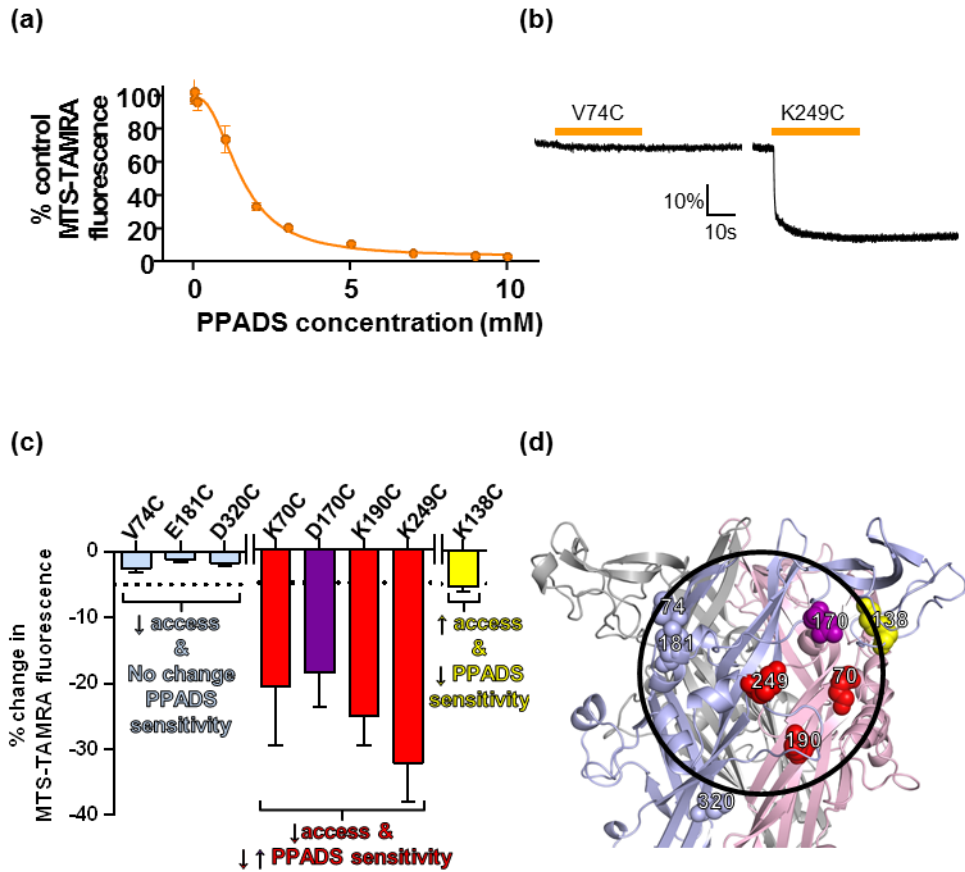


Figure 6.2 PPADS quenches MTS-TAMRA fluorescence and highlights cysteine mutants lining the antagonist binding site. (a.) Graph showing percentage MTS-TAMRA fluorescence remaining after addition of different PPADS concentrations. The baseline fluorescence of 1 μM MTS-TAMRA was measured via Flexstation, then different concentrations of PPADS were added after 20s and any change in fluorescence was monitored (n=3). **(b.)** Example traces of fluorometry recordings from oocytes expressing hP2X1R single cysteine point mutants labelled with MTS-TAMRA. Oocytes were perfused with ND96, then 10 μM PPADS was applied for 30s by perfusion (bar above trace) and any changes in fluorescent output were measured. Changes in fluorescence were quantified as the percentage change in fluorescent output compared to baseline level measured before PPADS application. Scale bars apply to all traces. **(c.)** Graph showing the average change in fluorescence for the mutants tested. A 5% decrease in fluorescence is shown as a dotted line (n≥5). **(d.)** hP2X1R homology model showing the positions of the introduced single cysteine residue mutations. Blue labelling indicates cysteine mutants with a PPADS induced decrease in MTSEA-biotinylation but no effect on PPADS sensitivity, red is for those with a decrease in MTSEA-biotinylation following PPADS treatment and a decrease in PPADS sensitivity and yellow corresponds to residues where MTSEA-biotinylation was increased by PPADS and also showed a decrease in PPADS sensitivity. (Figures taken from Dr Fryatt).

mutants, demonstrating that these residues do not come into close proximity with the antagonist. For the cysteine mutants (K70C, D170C, K190C and K249C), they showed a change in PPADS sensitivity and reduction in MTSEA-biotin access, and MTS-TAMRA fluorescence was reduced significantly by 20-30% following PPADS binding (Figure 6.2). Residue K138C showed increased accessibility by PPADS binding but it decreased PPADS sensitivity. MTS-TAMRA fluorescence was also decreased by PPADS (Figure 6.2). It suggests that the base of the head region moves into closer proximity to the PPADS binding site. These results where MTS-TAMRA fluorescence was reduced, taken together with the biotinylation and antagonist sensitivity data highlight the region defined by K70, D170, K190 and K249 as the site of PPADS binding.

6.4 Molecular docking of PPADS

The molecular docking of PPADS into the hP2X1R was carried out by Dr Ralf Schmid. The data for the K249C mutant demonstrate that this residue forms part of the PPADS binding site, and provides an anchoring point for ligand docking studies to predict potential PPADS binding modes. The docking site was therefore centred at K249. Considering that PPADS induced conformational changes when it binds to the P2XR, closed and open states of the hP2X1R homology models were used for ligand docking. This resulted in a series of docked poses at the orthosteric site where the negative charged sulfonate and phosphate groups of PPADS interact with positively charged side-chains of the receptor. Due to the variety of positively charged residues within and in proximity to the ATP-binding site more than one of these poses seemed plausible, but they were difficult to disentangle based on docking scores alone. Integrating docking results with the measured changes in accessibility of individual cysteine mutants by PPADS binding, the effect of mutation on PPADS potency, and changes of MTS-TAMRA fluorescence by PPADS binding. It determined the binding pose that best supported by experimental data overlaps with the ATP binding site which is best representative pose of the largest, first ranked cluster from PPADS ligand docking to the hP2X1R model in the open state.

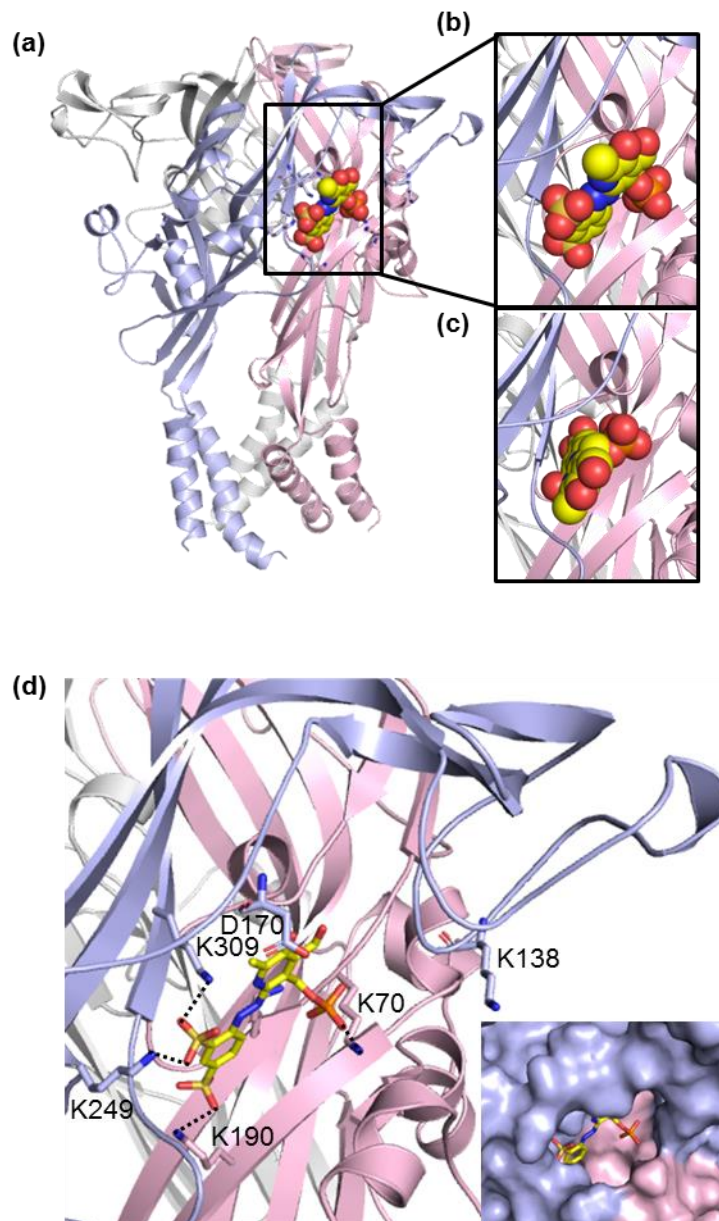


Figure 6.3. PPADS docking poses. (a) Overview of hP2XR1 model with docked PPADS shown as spheres. The three hP2XR1 subunits are shown in cartoon representation in red, blue and white, respectively. (b) and (c) Zoom into representative solutions of the two best ranked docking clusters. (d) Detailed view of (b) indicating key charge interactions between PPADS and hP2XR1 for the docking solution in best agreement with experimental data.

This pose shows PPADS forming salt bridges with K70, K190 and K249. The binding mode also comprises additional charged interactions with residues known to coordinate the triphosphate group of ATP (K68 and K309) (Figure 6.3), indicating that blocking ATP binding may be part of PPADS mode of action. The reduction of accessibility found for S64, S66S and K68 is consistent with PPADS bracing adjacent subunits of hP2X1R via salt bridges between sulfonate groups and the side chains of K190 and K249, and therefore blocking access to the deeper reaches of the pocket where S64, S66 and K68 are located. Combining these data with molecular docking produced a model of the antagonist binding site. PPADS binding overlaps with the orthosteric ATP site and so binding of the antagonist would sterically block access to the agonist.

6.5 PPADS evoked conformational changes

Ligand binding stabilizes a particular receptor structure and can be associated with significant conformation changes from the apo state. At outside the predicted PPADS binding site, some residues (for example, V74C, T75C and A182C) showed decreased accessibility by PPADS binding but no effect on PPADS sensitivity. They were suggested to be involved in PPADS evoked conformational changes around the orthosteric pocket from the closed state. Interestingly, the majority of the mutants also showed decreased accessibility by ATP binding. These results suggest that the PPADS binding caused conformational changes more similar to the ATP-bound than the closed state. Interestingly, PPADS induced conformational changes in the extracellular loop did not cause the channel to open. This suggests that the PPADS-bound structure may show differences in the lower body compared to the open state structure.

A similar move towards the ATP-bound state has been recently reported for the antagonist action of TNP-ATP at the chicken (ck) P2X7R. Although there was no ATP-dependent ckP2X_{crist} associated current in the whole-cell patch clamp recording, the ckP2X_{crist} construct still had TNP-ATP binding activity. Co-crystallization of the ckP2X7R with the competitive antagonist TNP-ATP showed an expanded, incompletely activated conformation that was closer to the ATP

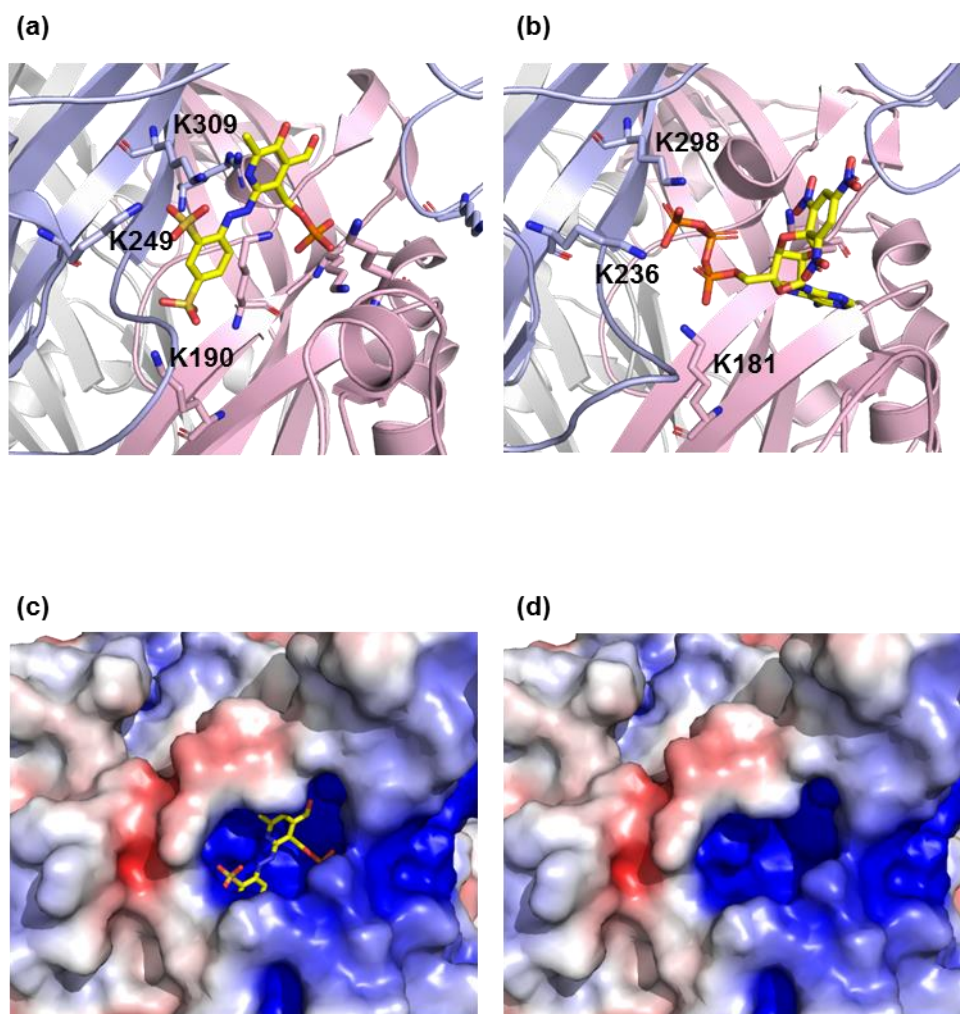


Figure 6.4. (a) Proposed PPADS binding mode for P2X1R. (b) For comparison the X-ray structure of the chP2X7R with TNP-ATP bound is shown. Equivalent lysine residues involved in salt bridges to sulfonate groups of PPADS (a) and phosphate groups of TNP-ATP are labelled. (c) Visualization of electrostatic potential for the P2X1R model used in (a) The electrostatic potential was calculated using the PDB2PQR webserver. (d) as in (c), but PPADS omitted.

bound than the apo state (Kasuya et al. 2017). The PPADS binding mode for the hP2X1R described above shows aspects remarkably similar to the TNP-ATP binding mode in the ckP2X7R. For instance the two sulfonate groups are in equivalent positions and coordination environment to α - and γ - phosphates in TNP-ATP with residues K309, K249 and K190 in the hP2X1R and K298, K1236 and K181 in the ckP2X7 forming salt bridges to the antagonist (Figure 6.4). In comparison to the ckP2X7R the binding mode for TNP-ATP proposed for the hP2X3R shows a different conformation with the receptor essentially in the apo state (Mansoor et al. 2016). This indicates that alternative binding modes for the same antagonist may be possible in different P2XR subtypes. In the context of PPADS binding, this suggests that there may be more than one conformation or PPADS binding mode contributing to potency and differences in subtype specificity.

6.6 The contribution of the cysteine rich head region to PPADS sensitivity

On comparing the effects of PPADS and ATP on accessibility of cysteine mutants, the major differences were at K138C and its adjacent cysteine mutant R139C. The level of biotinylation increased by ~8-fold at K138C and decreased by ~70% at R139C following PPADS treatment respectively whereas there was no change with ATP binding. This study suggests that PPADS induced movement of the cysteine rich head (CRH) region is distinct from that for ATP and raises the possibility that this region contributes to the action of the antagonist. This is supported by previous studies: (i) a region including the CRH region was involved in determining the antagonist PPADS sensitivity differences between rat and human P2X4Rs (Garcia-Guzman et al. 1997); (ii) mutation of the hP2X7R to remove a positively charged arginine residue at the base of the CRH (R126G) reduced PPADS affinity by ~10-fold (Michel et al. 2008b); (iii) a chimera replacing the CRH region (132-184) of the P2X1R with that from the rP2X4R reduced PPADS sensitivity. The introduction of four positive charges (K136, K138, R139 and K140) within this region to rP2X4R greatly increased PPADS efficiency; and (iv) in this study K138C in proximity of the PPADS binding site reduced PPADS sensitivity by ~3-fold. K138 is suggested to not directly interact with PPADS but contribute to the overall positively charged environment which is pulling the

negatively charged PPADS towards the hP2X1R. These results highlight that charge and conformational charge around the CRH region contributes to PPADS binding.

The positive charge at 138 is found at the equivalent position in hP2X1Rs ($IC_{50} \sim 1 \mu\text{M}$) and P2X3Rs ($IC_{50} \sim 3 \mu\text{M}$) which showed high sensitivity to PPADS (Evans et al. 1995, Lewis et al. 1995) whereas there is a negative charge at the rP2X4 ($IC_{50} > 300 \mu\text{M}$) (Buell et al. 1996) and hP2X7R ($IC_{50} \sim 45 \mu\text{M}$) (Surprenant et al. 1996) which showed much less PPADS sensitivity. This suggests that variations at this position may contribute to subtype dependent differences in PPADS sensitivity.

6.7 Using PPADS as a template to develop specific P2XR subtype antagonists

This study provided an experimentally validated model of the binding site of the P2XR antagonist PPADS. This involves interaction of a range of charged residues with the antagonist. Many of these core residues are conserved between P2XR subtypes. The ~3-fold changes in sensitivity for individual cysteine mutants in the current study provide a template for understanding modest differences in sensitivity between P2X1,3,5&6Rs. Mechanistic understanding of the site of PPADS action and the underlying subtype variations in this study provide the potential of medicinal chemistry to develop more subtype selective orthosteric antagonists.

The study has identified core conserved residues in the orthosteric pocket that co-ordinate PPADS binding. In addition, it shows that interactions of PPADS with the CRH region plays a significant role in PPADS sensitivity. Analysis of the different P2XR subtypes shows that there is significant variation in the sequence at the base of the CRH region. The results highlight that this variation could potentially be exploited to develop subtype selective antagonists. It proposes that a family of compounds could be developed that have a core that is compatible with the orthosteric site (but that on its own has low affinity) and subtype selectivity is imparted by specific side group substitutions that have high affinity for variant residues at the base of the CRH found in the different subtypes.

Some PPADS analogues have been generated in previous studies with different sensitivity and selectivity to P2X1Rs (see detail in 1.7.4). The study may explain structural related antagonist sensitivity changes, for example P5P losing 2 negative charges compared to PPADS showed less potency to P2X1Rs (Connolly 1995) may be because it only binds two of the positively charged residues at the receptor and not occupy the ATP binding site. In the future, a range of PPADS derivatives with various sensitivity and selectivity can be modified by adding or deleting the negative charges of the side chains.

Structures of the P2XR bound with PPADS have not been crystallized, suggesting it is difficult to be available. Mutagenesis studies can be a useful tool to further investigate the molecular basis of antagonism PPADS at P2XRs in the future studies. For example, crystal structure of PPADS-bound zfP2X4R can try to be made by recovering its sensitivity to PPADS with these mutations. In the future work, contribution of these conserved residues to PPADS action at other P2XR subtypes would be investigated. For example, mutating lysines (K70, K190 and K249) at the P2X3R to see whether PPADS sensitivity would be decreased. In addition, some PPADS analogues can be used as a tool to investigate PPADS antagonism at the hP2X1R. For example, PPNDS which also contains four negative charges is more potent (~6-fold) than PPADS at P2X1Rs (Lambrecht et al. 2000). Testing PPNDS sensitivity at the hP2X1R with mutants at positive charged residues (K70, K190, K249 and K138) would give indications of their roles in antagonism.

Hopefully, PPADS antagonism at P2XRs can be further confirmed in the future work. However, PPADS and a range of its analogues are still being used as pharmacological research tools. The potential drugs deriving from their molecular structures remain to be identified in the future.

References

- Abbracchio, M. P. and Burnstock, G. (1994) Purinoceptors: are there families of P2X and P2Y purinoceptors? *Pharmacol Ther*, 64(3), pp. 445-75.
- Abbracchio, M. P., Burnstock, G., Boeynaems, J. M., Barnard, E. A., Boyer, J. L., Kennedy, C., Knight, G. E., Fumagalli, M., Gachet, C., Jacobson, K. A. and Weisman, G. A. (2006) International Union of Pharmacology LVIII: update on the P2Y G protein-coupled nucleotide receptors: from molecular mechanisms and pathophysiology to therapy. *Pharmacol Rev*, 58(3), pp. 281-341.
- Abdulqawi, R., Dockry, R., Holt, K., Layton, G., McCarthy, B. G., Ford, A. P. and Smith, J. A. (2015) P2X3 receptor antagonist (AF-219) in refractory chronic cough: a randomised, double-blind, placebo-controlled phase 2 study. *Lancet*, 385(9974), pp. 1198-205.
- Adriouch, S., Bannas, P., Schwarz, N., Fliegert, R., Guse, A. H., Seman, M., Haag, F. and Koch-Nolte, F. (2008) ADP-ribosylation at R125 gates the P2X7 ion channel by presenting a covalent ligand to its nucleotide binding site. *The FASEB Journal*, 22(3), pp. 861-869.
- Akabas, M. H., Stauffer, D. A., Xu, M. and Karlin, A. (1992) Acetylcholine receptor channel structure probed in cysteine-substitution mutants. *Science*, 258(5080), pp. 307-10.
- Akbar, M., Okajima, F., Tomura, H., Shimegi, S. and Kondo, Y. (1994) A single species of A1 adenosine receptor expressed in Chinese hamster ovary cells not only inhibits cAMP accumulation but also stimulates phospholipase C and arachidonate release. *Mol Pharmacol*, 45(5), pp. 1036-1042.
- Alavi, A. M., Dubyak, G. R. and Burnstock, G. (2001) Immunohistochemical Evidence for ATP Receptors in Human Dental Pulp. *Journal of Dental Research*, 80(2), pp. 476-483.
- Allolio, B., Reincke, M., Arlt, W., Deuss, U., Winkelmann, W. and Siekmann, L. (1989) SURAMIN FOR TREATMENT OF ADRENOCORTICAL CARCINOMA. *The Lancet*, 334(8657), pp. 277.
- Allsopp, R. C., Dayl, S., Schmid, R. and Evans, R. J. (2017) Unique residues in the ATP gated human P2X7 receptor define a novel allosteric binding pocket for the selective antagonist AZ10606120. *Scientific Reports*, 7.

Allsopp, R. C., El Ajouz, S., Schmid, R. and Evans, R. J. (2011) Cysteine scanning mutagenesis (residues Glu52-Gly96) of the human P2X1 receptor for ATP: mapping agonist binding and channel gating. *J Biol Chem*, 286(33), pp. 29207-17.

Allsopp, R. C., Farmer, L. K., Fryatt, A. G. and Evans, R. J. (2013) P2X receptor chimeras highlight roles of the amino terminus to partial agonist efficacy, the carboxyl terminus to recovery from desensitization, and independent regulation of channel transitions. *J Biol Chem*, 288(29), pp. 21412-21.

Andre, P., Delaney, S. M., LaRocca, T., Vincent, D., DeGuzman, F., Jurek, M., Koller, B., Phillips, D. R. and Conley, P. B. (2003) P2Y12 regulates platelet adhesion/activation, thrombus growth, and thrombus stability in injured arteries. *J Clin Invest*, 112(3), pp. 398-406.

Aschrafi, A., Sadtler, S., Niculescu, C., Rettinger, J. and Schmalzing, G. (2004) Trimeric Architecture of Homomeric P2X2 and Heteromeric P2X1+2 Receptor Subtypes. *Journal of Molecular Biology*, 342(1), pp. 333-343.

Ase, A. R., Honson, N. S., Zaghdane, H., Pfeifer, T. A. and Seguela, P. (2015) Identification and characterization of a selective allosteric antagonist of human P2X4 receptor channels. *Mol Pharmacol*, 87(4), pp. 606-16.

Balázs, B., Dankó, T., Kovács, G., Köles, L., Hediger, M. A. and Zsembery, Á. (2013) Investigation of the Inhibitory Effects of the Benzodiazepine Derivative, 5-BDBD on P2X₄ Purinergic Receptors by two Complementary Methods. *Cellular Physiology and Biochemistry*, 32(1), pp. 11-24.

Baqi, Y., Hausmann, R., Rosefort, C., Rettinger, J., Schmalzing, G. and Müller, C. E. (2011) Discovery of Potent Competitive Antagonists and Positive Modulators of the P2X2 Receptor. *J Med Chem*, 54(3), pp. 817-830.

Barrera, N. P., Henderson, R. M., Murrell-Lagnado, R. D. and Edwardson, J. M. (2007) The stoichiometry of P2X2/6 receptor heteromers depends on relative subunit expression levels. *Biophys J*, 93(2), pp. 505-12.

Barrera, N. P., Ormond, S. J., Henderson, R. M., Murrell-Lagnado, R. D. and Edwardson, J. M. (2005) Atomic force microscopy imaging demonstrates that P2X2 receptors are trimers but that P2X6 receptor subunits do not oligomerize. *J Biol Chem*, 280(11), pp. 10759-10765.

Berchtold, S., Ogilvie, A. L. J., Bogdan, C., Mühl-Zürbes, P., Ogilvie, A., Schuler, G. and Steinkasserer, A. (1999) Human monocyte derived dendritic cells express functional P2X and P2Y receptors as well as ecto-nucleotidases. *Febs Letters*, 458(3), pp. 424-428.

Bhattacharya, A., Wang, Q., Ao, H., Shoblock, J. R., Lord, B., Aluisio, L., Fraser, I., Nepomuceno, D., Neff, R. A., Welty, N., Lovenberg, T. W., Bonaventure, P., Wickenden, A. D. and Letavic, M. A. (2013) Pharmacological characterization of a novel centrally permeable P2X7 receptor antagonist: JNJ-47965567. *Br J Pharmacol*, 170(3), pp. 624-640.

Bo, X., Jiang, L. H., Wilson, H. L., Kim, M., Burnstock, G., Surprenant, A. and North, R. A. (2003) Pharmacological and biophysical properties of the human P2X5 receptor. *Mol Pharmacol*, 63(6), pp. 1407-16.

Bo, X., Kim, M., Nori, S. L., Schoepfer, R., Burnstock, G. and North, R. A. (2003) Tissue distribution of P2X4 receptors studied with an ectodomain antibody. *Cell and Tissue Research*, 313(2), pp. 159-165.

Bodin, P. and Burnstock, G. (2001) Purinergic signalling: ATP release. *Neurochem Res*, 26(8-9), pp. 959-69.

Bogdanov, Y. D., Wildman, S. S., Clements, M. P., King, B. F. and Burnstock, G. (1998) Molecular cloning and characterization of rat P2Y4 nucleotide receptor. *Br J Pharmacol*, 124(3), pp. 428-430.

Bonora, M., Patergnani, S., Rimessi, A., De Marchi, E., Suski, J. M., Bononi, A., Giorgi, C., Marchi, S., Missiroli, S., Poletti, F., Wieckowski, M. R. and Pinton, P. (2012) ATP synthesis and storage. *Purinergic Signal*, 8(3), pp. 343-57.

Brading, A. F. and Williams, J. H. (1990) Contractile Responses of Smooth-Muscle Strips from Rat and Guinea-Pig Urinary-Bladder to Transmural-Stimulation - Effects of Atropine and Alpha,Beta-Methylene Atp. *Br J Pharmacol*, 99(3), pp. 493-498.

Brake, A. J., Wagenbach, M. J. and Julius, D. (1994) New structural motif for ligand-gated ion channels defined by an ionotropic ATP receptor. *Nature*, 371(6497), pp. 519-23.

Braun, K., Rettinger, J., Ganso, M., Kassack, M., Hildebrandt, C., Ullmann, H., Nickel, P., Schmalzing, G. and Lambrecht, G. (2001) NF449: a subnanomolar potency antagonist at recombinant rat P2X1 receptors. *Naunyn Schmiedebergs Arch Pharmacol*, 364(3), pp. 285-90.

Brotherton-Pleiss, C. E., Dillon, M. P., Ford, A. P. D. W., Gever, J. R., Carter, D. S., Gleason, S. K., Lin, C. J., Moore, A. G., Thompson, A. W., Villa, M. and Zhai, Y. (2010) Discovery and optimization of RO-85, a novel drug-like, potent, and selective P2X3 receptor antagonist. *Bioorganic & Medicinal Chemistry Letters*, 20(3), pp. 1031-1036.

Brown, C., Tanna, B. and Boarder, M. R. (1995) PPADS: an antagonist at endothelial P2Y-purinoceptors but not P2U-purinoceptors. *Br J Pharmacol*, 116(5), pp. 2413-6.

Brown, S. G., Kim, Y. C., Kim, S. A., Jacobson, K. A., Burnstock, G. and King, B. F. (2001) Actions of a Series of PPADS Analogs at P2X1 and P2X3 Receptors. *Drug Dev Res*, 53(4), pp. 281-291.

Brown, S. G., Townsend-Nicholson, A., Jacobson, K. A., Burnstock, G. and King, B. F. (2002) Heteromultimeric P2X_{1/2} Receptors Show a Novel Sensitivity to Extracellular pH. *Journal of Pharmacology and Experimental Therapeutics*, 300(2), pp. 673-680.

Browne, L. E., Jiang, L. H. and North, R. A. (2010) New structure enlivens interest in P2X receptors. *Trends in Pharmacological Sciences*, 31(5), pp. 229-237.

Buchthal, F. and Folkow, B. (1948) Interaction between Acetylcholine and Adenosine Triphosphate in Normal, Curarised and Denervated Muscle. *Acta Physiologica Scandinavica*, 15(2), pp. 150-160.

Buckingham, S. D., Pym, L. and Sattelle, D. B. (2006) Oocytes as an expression system for studying receptor/channel targets of drugs and pesticides. *Methods Mol Biol*, 322, pp. 331-45.

Buell, G., Lewis, C., Collo, G., North, R. and Surprenant, A. (1996) An antagonist-insensitive P2X receptor expressed in epithelia and brain. *The EMBO Journal*, 15(1), pp. 55.

Burnstock, G. (1972) Purinergic nerves. *Pharmacol Rev*, 24(3), pp. 509-81.

Burnstock, G. (1976a) Do some nerve cells release more than one transmitter? *Neuroscience*, 1(4), pp. 239-48.

- Burnstock, G. (1976b) Purinergic receptors. *Journal of Theoretical Biology*, 62(2), pp. 491-503.
- Burnstock, G. (1978) A basis for distinguishing two types of purinergic receptors. *New York, NY: Raven Press*, pp. 107-118.
- Burnstock, G. (2007) Physiology and pathophysiology of purinergic neurotransmission. *Physiol Rev*, 87(2), pp. 659-797.
- Burnstock, G., Campbell, G., Bennett, M. and Holman, M. E. (1963) Inhibition of the Smooth Muscle on the Taenia Coli. *Nature*, 200, pp. 581-2.
- Burnstock, G., Campbell, G., Satchell, D. and Smythe, A. (1970) Evidence That Adenosine Triphosphate or a Related Nucleotide Is Transmitter Substance Released by Ono-Adrenergic Inhibitory Nerves in Gut. *Br J Pharmacol*, 40(4), pp. 668-+.
- Burnstock, G., Dumsday, B. and Smythe, A. (1972) Atropine resistant excitation of the urinary bladder: the possibility of transmission via nerves releasing a purine nucleotide. *Br J Pharmacol*, 44(3), pp. 451-61.
- Burnstock, G. and Kennedy, C. (1985) Is there a basis for distinguishing two types of P2-purinoceptor? *Gen Pharmacol*, 16(5), pp. 433-40.
- Burnstock, G. and Verkhatsky, A. (2010) Vas deferens – A model used to establish sympathetic cotransmission. *Trends in Pharmacological Sciences*, 31(3), pp. 131-139.
- Burton, L. D., Housley, G. D., Salih, S. G., Järlebark, L., Christie, D. L. and Greenwood, D. P2X₂ receptor expression by interstitial cells of Cajal in vas deferens implicated in semen emission. *Autonomic Neuroscience: Basic and Clinical*, 84(3), pp. 147-161.
- Casati, A., Frascoli, M., Traggiai, E., Proietti, M., Schenk, U. and Grassi, F. (2011) Cell-autonomous regulation of hematopoietic stem cell cycling activity by ATP. *Cell Death Differ*, 18(3), pp. 396-404.
- Chambers, J. K., Macdonald, L. E., Sarau, H. M., Ames, R. S., Freeman, K., Foley, J. J., Zhu, Y., McLaughlin, M. M., Murdock, P., McMillan, L., Trill, J., Swift, A., Aiyar, N., Taylor, P., Vawter, L., Naheed, S., Szekeres, P., Hervieu, G., Scott, C., Watson, J. M., Murphy, A. J., Duzic, E., Klein, C., Bergsma, D. J.,

Wilson, S. and Livi, G. P. (2000) A G protein-coupled receptor for UDP-glucose. *J Biol Chem*, 275(15), pp. 10767-71.

Chan, C. M., Unwin, R. J., Bardini, M., Oglesby, I. B., Ford, A. P., Townsend-Nicholson, A. and Burnstock, G. (1998) Localization of P2X1 purinoceptors by autoradiography and immunohistochemistry in rat kidneys. *Am J Physiol*, 274(4 Pt 2), pp. F799-804.

Chang, K., Hanaoka, K., Kumada, M. and Takuwa, Y. (1995) Molecular cloning and functional analysis of a novel P2 nucleotide receptor. *J Biol Chem*, 270(44), pp. 26152-8.

Charlton, S. J., Brown, C. A., Weisman, G. A., Turner, J. T., Erb, L. and Boarder, M. R. (1996a) Cloned and transfected P2Y4 receptors: characterization of a suramin and PPADS-insensitive response to UTP. *Br J Pharmacol*, 119(7), pp. 1301-1303.

Charlton, S. J., Brown, C. A., Weisman, G. A., Turner, J. T., Erb, L. and Boarder, M. R. (1996b) PPADS and suramin as antagonists at cloned P2Y- and P2U-purinoceptors. *Br J Pharmacol*, 118(3), pp. 704-710.

Chen, C. C., Akopian, A. N., Sivilotti, L., Colquhoun, D., Burnstock, G. and Wood, J. N. (1995) A P2X purinoceptor expressed by a subset of sensory neurons. *Nature*, 377(6548), pp. 428-31.

Chen, Y., Zhang, X., Wang, C., Li, G., Gu, Y. and Huang, L.-Y. M. (2008) Activation of P2X7 receptors in glial satellite cells reduces pain through downregulation of P2X3 receptors in nociceptive neurons. *Proceedings of the National Academy of Sciences*, 105(43), pp. 16773-16778.

Chhatrivala, M., Ravi, R. G., Patel, R. I., Boyer, J. L., Jacobson, K. A. and Harden, T. K. (2004) Induction of novel agonist selectivity for the ADP-activated P2Y1 receptor versus the ADP-activated P2Y12 and P2Y13 receptors by conformational constraint of an ADP analog. *J Pharmacol Exp Ther*, 311(3), pp. 1038-43.

Cho, J. H., Jung, K. Y., Jung, Y., Kim, M. H., Ko, H., Park, C. S. and Kim, Y. C. (2013) Design and synthesis of potent and selective P2X(3) receptor antagonists derived from PPADS as potential pain modulators. *Eur J Med Chem*, 70, pp. 811-30.

Cicko, S., Lucattelli, M., Müller, T., Lommatzsch, M., De Cunto, G., Cardini, S., Sundas, W., Grimm, M., Zeiser, R., Dürk, T., Zissel, G., Boeynaems, J.-M.,

Sorichter, S., Ferrari, D., Di Virgilio, F., Virchow, J. C., Lungarella, G. and Idzko, M. (2010) Purinergic Receptor Inhibition Prevents the Development of Smoke-Induced Lung Injury and Emphysema. *The Journal of Immunology*, 185(1), pp. 688-697.

Clark, A. K., Staniland, A. A., Marchand, F., Kaan, T. K. Y., McMahon, S. B. and Malcangio, M. (2010) P2X7-Dependent Release of Interleukin-1 β and Nociception in the Spinal Cord following Lipopolysaccharide. *The Journal of Neuroscience*, 30(2), pp. 573-582.

Clyne, J. D., Wang, L.-F. and Hume, R. I. (2002) Mutational Analysis of the Conserved Cysteines of the Rat P2X₂ Purinoceptor. *The Journal of Neuroscience*, 22(10), pp. 3873-3880.

Cockayne, D. A., Dunn, P. M., Zhong, Y., Rong, W., Hamilton, S. G., Knight, G. E., Ruan, H. Z., Ma, B., Yip, P., Nunn, P., McMahon, S. B., Burnstock, G. and Ford, A. P. (2005) P2X2 knockout mice and P2X2/P2X3 double knockout mice reveal a role for the P2X2 receptor subunit in mediating multiple sensory effects of ATP. *J Physiol*, 567(Pt 2), pp. 621-39.

Cockayne, D. A., Hamilton, S. G., Zhu, Q. M., Dunn, P. M., Zhong, Y., Novakovic, S., Malmberg, A. B., Cain, G., Berson, A., Kassotakis, L., Hedley, L., Lachnit, W. G., Burnstock, G., McMahon, S. B. and Ford, A. P. D. W. (2000) Urinary bladder hyporeflexia and reduced pain-related behaviour in P2X(3)-deficient mice. *Nature*, 407(6807), pp. 1011-1015.

Coddou, C., Yan, Z., Obsil, T., Huidobro-Toro, J. P. and Stojilkovic, S. S. (2011) Activation and regulation of purinergic P2X receptor channels. *Pharmacol Rev*, 63(3), pp. 641-83.

Collo, G., North, R. A., Kawashima, E., Merlo-Pich, E., Neidhart, S., Surprenant, A. and Buell, G. (1996) Cloning OF P2X5 and P2X6 receptors and the distribution and properties of an extended family of ATP-gated ion channels. *J Neurosci*, 16(8), pp. 2495-507.

Communi, D., Gonzalez, N. S., Detheux, M., Brezillon, S., Lannoy, V., Parmentier, M. and Boeynaems, J. M. (2001) Identification of a novel human ADP receptor coupled to G(i). *J Biol Chem*, 276(44), pp. 41479-85.

Communi, D., Govaerts, C., Parmentier, M. and Boeynaems, J. M. (1997) Cloning of a human purinergic P2Y receptor coupled to phospholipase C and adenylyl cyclase. *J Biol Chem*, 272(51), pp. 31969-73.

Communi, D., Piroton, S., Parmentier, M. and Boeynaems, J. M. (1995) Cloning and functional expression of a human uridine nucleotide receptor. *J Biol Chem*, 270(52), pp. 30849-52.

Communi, D., Robaye, B. and Boeynaems, J.-M. (1999) Pharmacological characterization of the human P2Y₁₁ receptor. *Br J Pharmacol*, 128(6), pp. 1199-1206.

Connolly, G. P. (1995) Differentiation by pyridoxal 5-phosphate, PPADS and IsoPPADS between responses mediated by UTP and those evoked by alpha, beta-methylene-ATP on rat sympathetic ganglia. *Br J Pharmacol*, 114(3), pp. 727-31.

Dal Ben, D., Marchenkova, A., Thomas, A., Lambertucci, C., Spinaci, A., Marucci, G., Nistri, A. and Volpini, R. (2017) 2',3'-O-Substituted ATP derivatives as potent antagonists of purinergic P2X₃ receptors and potential analgesic agents. *Purinergic Signal*, 13(1), pp. 61-74.

Danquah, W., Meyer-Schwesinger, C., Rissiek, B., Pinto, C., Serracant-Prat, A., Amadi, M., Iacenda, D., Knop, J.-H., Hammel, A., Bergmann, P., Schwarz, N., Assunção, J., Rotthier, W., Haag, F., Tolosa, E., Bannas, P., Boué-Grabot, E., Magnus, T., Laeremans, T., Stortelers, C. and Koch-Nolte, F. (2016) Nanobodies that block gating of the P2X₇ ion channel ameliorate inflammation. *Science Translational Medicine*, 8(366), pp. 366ra162-366ra162.

Das, A., Ko, H., Burianek, L. E., Barrett, M. O., Harden, T. K. and Jacobson, K. A. (2010) Human P2Y₁₄ receptor agonists: truncation of the hexose moiety of uridine-5'-diphosphoglucose and its replacement with alkyl and aryl groups. *J Med Chem*, 53(1), pp. 471-80.

Davis, I. W. and Baker, D. (2009) RosettaLigand docking with full ligand and receptor flexibility. *J Mol Biol*, 385(2), pp. 381-92.

De Clercq, E. (1979) Suramin: A potent inhibitor of the reverse transcriptase of RNA tumor viruses. *Cancer Letters*, 8(1), pp. 9-22.

Digby, H. R., Roberts, J. A., Sutcliffe, M. J. and Evans, R. J. (2005) Contribution of conserved glycine residues to ATP action at human P2X₁ receptors: Mutagenesis indicates that the glycine at position 250 is important for channel function. *J Neurochem*, 95(6), pp. 1746-1754.

Donnelly-Roberts, D. L., Namovic, M. T., Surber, B., Vaidyanathan, S. X., Perez-Medrano, A., Wang, Y., Carroll, W. A. and Jarvis, M. F. (2009) [3H]A-

804598 ([3H]2-cyano-1-[(1S)-1-phenylethyl]-3-quinolin-5-ylguanidine) is a novel, potent, and selective antagonist radioligand for P2X7 receptors. *Neuropharmacology*, 56(1), pp. 223-229.

Drury, A. N. and Szent-Gyorgyi, A. (1929) The physiological activity of adenine compounds with especial reference to their action upon the mammalian heart. *J Physiol*, 68(3), pp. 213-37.

Dunn, P. M. and Blakeley, A. G. (1988) Suramin: a reversible P2-purinoceptor antagonist in the mouse vas deferens. *Br J Pharmacol*, 93(2), pp. 243-5.

Duplantier, A. J., Dombroski, M. A., Subramanyam, C., Beaulieu, A. M., Chang, S. P., Gabel, C. A., Jordan, C., Kalgutkar, A. S., Kraus, K. G., Labasi, J. M., Mussari, C., Perregaux, D. G., Shepard, R., Taylor, T. J., Trevena, K. A., Whitney-Pickett, C. and Yoon, K. (2011) Optimization of the physicochemical and pharmacokinetic attributes in a 6-azauracil series of P2X7 receptor antagonists leading to the discovery of the clinical candidate CE-224,535. *Bioorg Med Chem Lett*, 21(12), pp. 3708-11.

Eccles, J. C. (1964) *The Physiology of Synapses*, Berlin Heidelberg: Springer

Egan, T. M., Haines, W. R. and Voigt, M. M. (1998) A Domain Contributing to the Ion Channel of ATP-Gated P2X₂ Receptors Identified by the Substituted Cysteine Accessibility Method. *The Journal of Neuroscience*, 18(7), pp. 2350-2359.

Eickhorst, A. N., Berson, A., Cockayne, D., Lester, H. A. and Khakh, B. S. (2002) Control of P2X₂ Channel Permeability by the Cytosolic Domain. *J Gen Physiol*, 120(2), pp. 119-131.

El-Ajouz, S., Ray, D., Allsopp, R. C. and Evans, R. J. (2012a) Molecular basis of selective antagonism of the P2X1 receptor for ATP by NF449 and suramin: Contribution of basic amino acids in the cysteine-rich loop. *Br J Pharmacol*, 165(2), pp. 390-400.

El-Ajouz, S., Ray, D., Allsopp, R. C. and Evans, R. J. (2012b) Molecular basis of selective antagonism of the P2X1 receptor for ATP by NF449 and suramin: contribution of basic amino acids in the cysteine-rich loop. *Br J Pharmacol*, 165(2), pp. 390-400.

El-Tayeb, A., Qi, A., Nicholas, R. A. and Muller, C. E. (2011) Structural modifications of UMP, UDP, and UTP leading to subtype-selective agonists for P2Y2, P2Y4, and P2Y6 receptors. *J Med Chem*, 54(8), pp. 2878-90.

Elliott, R. A., Tonnu, A., Ghaffar, N., Taylor, A. H., Tincello, D. G. and Norman, R. I. (2013) Enhanced purinergic contractile responses and P2X₁ receptor expression in detrusor muscle during cycles of hypoxia-glucopenia and reoxygenation. *Experimental Physiology*, 98(12), pp. 1683-95.

Elneil, S., Skepper, J. N., Kidd, E. J., Williamson, J. G. and Ferguson, D. R. (2001) Distribution of P2X₁ and P2X₃ Receptors in the Rat and Human Urinary Bladder. *Pharmacology*, 63(2), pp. 120-128.

Emmelin, N. and Feldberg, W. (1948) SYSTEMIC EFFECTS OF ADENOSINE TRIPHOSPHATE. *British Journal of Pharmacology and Chemotherapy*, 3(4), pp. 273-284.

Ennion, S., Hagan, S. and Evans, R. J. (2000) The role of positively charged amino acids in ATP recognition by human P2X₁ receptors. *J Biol Chem*, 275(38), pp. 29361-7.

Ennion, S. J. and Evans, R. J. (2002a) Conserved cysteine residues in the extracellular loop of the human P2X₁ receptor form disulfide bonds and are involved in receptor trafficking to the cell surface. *Mol Pharmacol*, 61(2), pp. 303-311.

Ennion, S. J. and Evans, R. J. (2002b) Conserved cysteine residues in the extracellular loop of the human P2X₁ receptor form disulfide bonds and are involved in receptor trafficking to the cell surface. *Mol Pharmacol*, 61(2), pp. 303-11.

Ennion, S. J. and Evans, R. J. (2002c) P2X₁ receptor subunit contribution to gating revealed by a dominant negative PKC mutant. *Biochem Biophys Res Commun*, 291(3), pp. 611-6.

Evans, R. J. (2010) Structural interpretation of P2X receptor mutagenesis studies on drug action. *Br J Pharmacol*, 161(5), pp. 961-971.

Evans, R. J., Lewis, C., Buell, G., Valera, S., North, R. A. and Surprenant, A. (1995) Pharmacological characterization of heterologously expressed ATP-gated cation channels (P2X purinoceptors). *Mol Pharmacol*, 48(2), pp. 178-183.

Fabre, J.-E., Nguyen, M., Latour, A., Keifer, J. A., Audoly, L. P., Coffman, T. M. and Koller, B. H. (1999) Decreased platelet aggregation, increased bleeding time and resistance to thromboembolism in P2Y₁-deficient mice. *Nature Medicine*, 5, pp. 1199.

- Farmer, L. K., Schmid, R. and Evans, R. J. (2015) Use of Chimeras, Point Mutants, and Molecular Modeling to Map the Antagonist-binding Site of 4,4',4'',4'''-(Carbonylbis-(imino-5,1,3-benzenetriylbis(carbonylimino)))tetrakisbenzene-1,3-disulfonic Acid (NF449) at P2X1 Receptors for ATP. *J Biol Chem*, 290(3), pp. 1559-69.
- Finger, T. E., Danilova, V., Barrows, J., Bartel, D. L., Vigers, A. J., Stone, L., Hellekant, G. and Kinnamon, S. C. (2005) ATP Signaling Is Crucial for Communication from Taste Buds to Gustatory Nerves. *Science*, 310(5753), pp. 1495-1499.
- Fisher R, G. R., Blasco HPJ, Kalthof B, Gadea PC, Stelte-Ludwig B, Woltering E, Wutke M (2005) Benzofuro-1,4-diazepin-2-one derivatives.
- Fiske, C. H. and Subbarow, Y. (1929) Phosphorus Compounds of Muscle and Liver. *Science*, 70(1816), pp. 381-2.
- Fortes, P. A., Ellory, J. C. and Lew, V. L. (1973) Suramin: a potent ATPase inhibitor which acts on the inside surface of the sodium pump. *Biochim Biophys Acta*, 318(2), pp. 262-72.
- Franke, H., Grosche, J., Schädlich, H., Krügel, U., Allgaier, C. and Illes, P. (2001) P2X receptor expression on astrocytes in the nucleus accumbens of rats. *Neuroscience*, 108(3), pp. 421-429.
- Fredholm, B. B., AP, I. J., Jacobson, K. A., Linden, J. and Muller, C. E. (2011) International Union of Basic and Clinical Pharmacology. LXXXI. Nomenclature and classification of adenosine receptors--an update. *Pharmacol Rev*, 63(1), pp. 1-34.
- Fredholm, B. B., IJzerman, A. P., Jacobson, K. A., Klotz, K.-N. and Linden, J. (2001) International Union of Pharmacology. XXV. Nomenclature and Classification of Adenosine Receptors. *Pharmacol Rev*, 53(4), pp. 527-552.
- Fryatt, A. G. and Evans, R. J. (2014) Kinetics of conformational changes revealed by voltage-clamp fluorometry give insight to desensitization at ATP-gated human P2X1 receptors. *Mol Pharmacol*, 86(6), pp. 707-715.
- Gachet, C. (2006) Regulation of platelet functions by P2 receptors. *Annu Rev Pharmacol Toxicol*, 46, pp. 277-300.

Gao, Z., Chen, T., Weber, M. J. and Linden, J. (1999) A2B adenosine and P2Y2 receptors stimulate mitogen-activated protein kinase in human embryonic kidney-293 cells. cross-talk between cyclic AMP and protein kinase c pathways. *J Biol Chem*, 274(9), pp. 5972-80.

Garcia-Guzman, M., Soto, F., Gomez-Hernandez, J. M., Lund, P. E. and Stuhmer, W. (1997) Characterization of recombinant human P2X4 receptor reveals pharmacological differences to the rat homologue. *Mol Pharmacol*, 51(1), pp. 109-18.

Garcia-Guzman, M., Soto, F., Laube, B. and Stühmer, W. (1996) Molecular cloning and functional expression of a novel rat heart P2X purinoceptor. *Febs Letters*, 388(2-3), pp. 123-127.

Gever, J. R., Cockayne, D. A., Dillon, M. P., Burnstock, G. and Ford, A. P. D. W. (2006) Pharmacology of P2X channels. *Pflügers Archiv*, 452(5), pp. 513-537.

Giannuzzo, A., Saccomano, M., Napp, J., Ellegaard, M., Alves, F. and Novak, I. (2016) Targeting of the P2X7 receptor in pancreatic cancer and stellate cells. *Int J Cancer*, 139(11), pp. 2540-52.

Ginsburg-Shmuel, T., Haas, M., Grbic, D., Arguin, G., Nadel, Y., Gendron, F. P., Reiser, G. and Fischer, B. (2012) UDP made a highly promising stable, potent, and selective P2Y6-receptor agonist upon introduction of a boranophosphate moiety. *Bioorg Med Chem*, 20(18), pp. 5483-95.

Goldin, A. L. (1992) Maintenance of *Xenopus laevis* and oocyte injection. *Methods Enzymol*, 207, pp. 266-79.

Haines, W. R., Torres, G. E., Voigt, M. M. and Egan, T. M. (1999) Properties of the Novel ATP-Gated Ionotropic Receptor Composed of the P2X₁ and P2X₅ Isoforms. *Mol Pharmacol*, 56(4), pp. 720-727.

Harkat, M., Peverini, L., Cerdan, A. H., Dunning, K., Beudez, J., Martz, A., Calimet, N., Specht, A., Cecchini, M., Chataigneau, T. and Grutter, T. (2017) On the permeation of large organic cations through the pore of ATP-gated P2X receptors. *Proc Natl Acad Sci U S A*, 114(19), pp. E3786-E3795.

Hattori, M. and Gouaux, E. (2012) Molecular mechanism of ATP binding and ion channel activation in P2X receptors. *Nature*, 485(7397), pp. 207-12.

Hauser, R. A., Shulman, L. M., Trugman, J. M., Roberts, J. W., Mori, A., Ballerini, R., Sussman, N. M. and Istradefylline, U. S. S. G. (2008) Study of istradefylline in patients with Parkinson's disease on levodopa with motor fluctuations. *Mov Disord*, 23(15), pp. 2177-85.

Hechler, B., Lenain, N., Marchese, P., Vial, C., Heim, V., Freund, M., Cazenave, J. P., Cattaneo, M., Ruggeri, Z. M., Evans, R. and Gachet, C. (2003) A role of the fast ATP-gated P2X1 cation channel in thrombosis of small arteries in vivo. *J Exp Med*, 198(4), pp. 661-7.

Hechler, B., Magnenat, S., Zighetti, M. L., Kassack, M. U., Ullmann, H., Cazenave, J. P., Evans, R., Cattaneo, M. and Gachet, C. (2005) Inhibition of platelet functions and thrombosis through selective or nonselective inhibition of the platelet P2 receptors with increasing doses of NF449 [4,4',4'',4'''-(carbonylbis(imino-5,1,3-benzenetriylbis-(carbonylimino)))tetrakis-benzene-1,3-disulfonic acid octasodium salt]. *J Pharmacol Exp Ther*, 314(1), pp. 232-43.

Hegde, S. S., Mandel, D. A., Wilford, M. R., Briaud, S., Ford, A. P. D. W. and Eglén, R. M. (1998) Evidence for purinergic neurotransmission in the urinary bladder of pithed rats. *Eur J Pharmacol*, 349(1), pp. 75-82.

Hernandez-Olmos, V., Abdelrahman, A., El-Tayeb, A., Freudendahl, D., Weinhausen, S. and Muller, C. E. (2012) N-substituted phenoxazine and acridone derivatives: structure-activity relationships of potent P2X4 receptor antagonists. *J Med Chem*, 55(22), pp. 9576-88.

Hollopeter, G., Jantzen, H. M., Vincent, D., Li, G., England, L., Ramakrishnan, V., Yang, R. B., Nurden, P., Nurden, A., Julius, D. and Conley, P. B. (2001) Identification of the platelet ADP receptor targeted by antithrombotic drugs. *Nature*, 409(6817), pp. 202-7.

Holton, P. (1959) The liberation of adenosine triphosphate on antidromic stimulation of sensory nerves. *J Physiol*, 145(3), pp. 494-504.

Honore, P., Donnelly-Roberts, D., Namovic, M. T., Hsieh, G., Zhu, C. Z., Mikusa, J. P., Hernandez, G., Zhong, C., Gauvin, D. M., Chandran, P., Harris, R., Medrano, A. P., Carroll, W., Marsh, K., Sullivan, J. P., Faltynek, C. R. and Jarvis, M. F. (2006) A-740003 [*N*-(1-((Cyanoimino)(5-quinolinylamino) methyl)amino)-2,2-dimethylpropyl)-2-(3,4-dimethoxyphenyl)acetamide], a Novel and Selective P2X₇ Receptor Antagonist, Dose-Dependently Reduces Neuropathic Pain in the Rat. *Journal of Pharmacology and Experimental Therapeutics*, 319(3), pp. 1376-1385.

- Hoyle, C. H., Knight, G. E. and Burnstock, G. (1990) Suramin antagonizes responses to P2-purinoceptor agonists and purinergic nerve stimulation in the guinea-pig urinary bladder and taenia coli. *Br J Pharmacol*, 99(3), pp. 617-21.
- HU, B., MEI, Q.-B., YAO, X.-J., SMITH, E., BARRY, W. H. and LIANG, B. T. (2001) A novel contractile phenotype with cardiac transgenic expression of the human P2X4 receptor. *The FASEB Journal*, 15(14), pp. 2739-2741.
- Huang, Y. A., Stone, L. M., Pereira, E., Yang, R., Kinnamon, J. C., Dvoryanchikov, G., Chaudhari, N., Finger, T. E., Kinnamon, S. C. and Roper, S. D. (2011) Knocking Out P2X Receptors Reduces Transmitter Secretion in Taste Buds. *The Journal of Neuroscience*, 31(38), pp. 13654-13661.
- Hulsmann, M., Nickel, P., Kassack, M., Schmalzing, G., Lambrecht, G. and Markwardt, F. (2003) NF449, a novel picomolar potency antagonist at human P2X1 receptors. *Eur J Pharmacol*, 470(1-2), pp. 1-7.
- Ikeda, M. (2007) Characterization of functional P2X₁ receptors in mouse megakaryocytes. *Thrombosis Research*, 119(3), pp. 343-353.
- Inscho, D. A. O. a. E. W. (2010) P2X1 receptor blockade inhibits whole kidney autoregulation of renal blood flow in vivo. *American Journal of Physiology-Renal Physiology*, 298(6), pp. F1360-F1368.
- Inscho, E. W., Cook, A. K., Imig, J. D., Vial, C. and Evans, R. J. (2003) Physiological role for P2X1 receptors in renal microvascular autoregulatory behavior. *Journal of Clinical Investigation*, 112(12), pp. 1895-1905.
- Jacobson, K. A. and Boeynaems, J. M. (2010) P2Y nucleotide receptors: promise of therapeutic applications. *Drug Discov Today*, 15(13-14), pp. 570-8.
- Jacobson, K. A., Kim, Y. C., Wildman, S. S., Mohanram, A., Harden, T. K., Boyer, J. L., King, B. F. and Burnstock, G. (1998) A pyridoxine cyclic phosphate and its 6-azoaryl derivative selectively potentiate and antagonize activation of P2X1 receptors. *J Med Chem*, 41(13), pp. 2201-6.
- Jahangir, A., Alam, M., Carter, D. S., Dillon, M. P., Bois, D. J. D., Ford, A. P. D. W., Gever, J. R., Lin, C., Wagner, P. J., Zhai, Y. and Zira, J. (2009) Identification and SAR of novel diaminopyrimidines. Part 2: The discovery of RO-51, a potent and selective, dual P2X3/P2X2/3 antagonist for the treatment of pain. *Bioorganic & Medicinal Chemistry Letters*, 19(6), pp. 1632-1635.

Jarvis, M. F., Burgard, E. C., McGaraughty, S., Honore, P., Lynch, K., Brennan, T. J., Subieta, A., Van Biesen, T., Cartmell, J., Bianchi, B., Niforatos, W., Kage, K., Yu, H., Mikusa, J., Wismer, C. T., Zhu, C. Z., Chu, K., Lee, C. H., Stewart, A. O., Polakowski, J., Cox, B. F., Kowaluk, E., Williams, M., Sullivan, J. and Faltynek, C. (2002) A-317491, a novel potent and selective non-nucleotide antagonist of P2X3 and P2X2/3 receptors, reduces chronic inflammatory and neuropathic pain in the rat. *Proc Natl Acad Sci U S A*, 99(26), pp. 17179-84.

Jasti, J., Furukawa, H., Gonzales, E. B. and Gouaux, E. (2007) Structure of acid-sensing ion channel 1 at 1.9 Å resolution and low pH. *Nature*, 449, pp. 316.

Jiang, L.-H., Kim, M., Spelta, V., Bo, X., Surprenant, A. and North, R. A. (2003) Subunit Arrangement in P2X Receptors. *The Journal of Neuroscience*, 23(26), pp. 8903-8910.

Jiang, L. H., Rassendren, F., Surprenant, A. and North, R. A. (2000) Identification of amino acid residues contributing to the ATP-binding site of a purinergic P2X receptor. *Journal of Biological Chemistry*, 275(44), pp. 34190-34196.

Jiang, R., Taly, A., Lemoine, D., Martz, A., Cunrath, O. and Grutter, T. (2012) Tightening of the ATP-binding sites induces the opening of P2X receptor channels. *EMBO J*, 31(9), pp. 2134-43.

Jiang, R. T., Taly, A. and Grutter, T. (2013) Moving through the gate in ATP-activated P2X receptors. *Trends in Biochemical Sciences*, 38(1), pp. 20-29.

Johansson, B., Halldner, L., Dunwiddie, T. V., Masino, S. A., Poelchen, W., Gimenez-Llort, L., Escorihuela, R. M., Fernandez-Teruel, A., Wiesenfeld-Hallin, Z., Xu, X. J., Hardemark, A., Betsholtz, C., Herlenius, E. and Fredholm, B. B. (2001) Hyperalgesia, anxiety, and decreased hypoxic neuroprotection in mice lacking the adenosine A1 receptor. *Proc Natl Acad Sci U S A*, 98(16), pp. 9407-12.

Jones, C. A., Chessell, I. P., Simon, J., Barnard, E. A., Miller, K. J., Michel, A. D. and Humphrey, P. P. A. (2000) Functional characterization of the P2X4 receptor orthologues. *Br J Pharmacol*, 129(2), pp. 388-394.

Jones, C. A., Vial, C., Sellers, L. A., Humphrey, P. P. A., Evans, R. J. and Chessell, I. P. (2004) Functional Regulation of P2X6 Receptors by N-Linked Glycosylation: Identification of a Novel $\alpha\beta$ -Methylene ATP-Sensitive Phenotype. *Mol Pharmacol*, 65(4), pp. 979-985.

- Kaczmarek-Hajek, K., Lorinczi, E., Hausmann, R. and Nicke, A. (2012) Molecular and functional properties of P2X receptors--recent progress and persisting challenges. *Purinergic Signal*, 8(3), pp. 375-417.
- Kanjhan, R., Housley, G. D., Burton, L. D., Christie, D. L., Kippenberger, A., Thorne, P. R., Luo, L. and Ryan, A. F. (1999) Distribution of the P2X2 receptor subunit of the ATP-gated ion channels in the rat central nervous system. *J Comp Neurol*, 407(1), pp. 11-32.
- Karasawa, A. and Kawate, T. (2016) Structural basis for subtype-specific inhibition of the P2X7 receptor. *Elife*, 5.
- Karlin, A. (2002) Emerging structure of the nicotinic acetylcholine receptors. *Nat Rev Neurosci*, 3(2), pp. 102-14.
- Kasakov, L. and Burnstock, G. (1982) The use of the slowly degradable analog, α,β -methylene ATP, to produce desensitisation of the P2-purinoceptor: Effect on non-adrenergic, non-cholinergic responses of the guinea-pig urinary bladder. *Eur J Pharmacol*, 86(2), pp. 291-294.
- Kasuya, G., Fujiwara, Y., Takemoto, M., Dohmae, N., Nakada-Nakura, Y., Ishitani, R., Hattori, M. and Nureki, O. (2016) Structural Insights into Divalent Cation Modulations of ATP-Gated P2X Receptor Channels. *Cell Rep*, 14(4), pp. 932-44.
- Kasuya, G., Yamaura, T., Ma, X. B., Nakamura, R., Takemoto, M., Nagumo, H., Tanaka, E., Dohmae, N., Nakane, T., Yu, Y., Ishitani, R., Matsuzaki, O., Hattori, M. and Nureki, O. (2017) Structural insights into the competitive inhibition of the ATP-gated P2X receptor channel. *Nat Commun*, 8(1), pp. 876.
- Kaur, M., Reed, E., Sartor, O., Dahut, W. and Figg, W. D. (2002) Suramin's Development: What Did we Learn? *Investigational New Drugs*, 20(2), pp. 209-219.
- Kawate, T., Michel, J. C., Birdsong, W. T. and Gouaux, E. (2009) Crystal structure of the ATP-gated P2X(4) ion channel in the closed state. *Nature*, 460(7255), pp. 592-8.
- Kawate, T., Robertson, J. L., Li, M., Silberberg, S. D. and Swartz, K. J. (2011) Ion access pathway to the transmembrane pore in P2X receptor channels. *J Gen Physiol*, 137(6), pp. 579-90.

Ke, H. Z., Qi, H., Weidema, A. F., Zhang, Q., Panupinthu, N., Crawford, D. T., Grasser, W. A., Paralkar, V. M., Li, M., Audoly, L. P., Gabel, C. A., Jee, W. S. S., Dixon, S. J., Sims, S. M. and Thompson, D. D. (2003) Deletion of the P2X7 Nucleotide Receptor Reveals Its Regulatory Roles in Bone Formation and Resorption. *Molecular Endocrinology*, 17(7), pp. 1356-1367.

Keystone, E. C., Wang, M. M., Layton, M., Hollis, S., McInnes, I. B. and Team, D. C. S. (2012) Clinical evaluation of the efficacy of the P2X7 purinergic receptor antagonist AZD9056 on the signs and symptoms of rheumatoid arthritis in patients with active disease despite treatment with methotrexate or sulphasalazine. *Ann Rheum Dis*, 71(10), pp. 1630-5.

Kidd, E. J., Grahames, C. B., Simon, J., Michel, A. D., Barnard, E. A. and Humphrey, P. P. (1995) Localization of P2X purinoceptor transcripts in the rat nervous system. *Mol Pharmacol*, 48(4), pp. 569-573.

King, B. F., Townsend-Nicholson, A., Wildman, S. S., Thomas, T., Spyer, K. M. and Burnstock, G. (2000) Coexpression of Rat P2X₂ and P2X₆ Subunits in *Xenopus* Oocytes. *The Journal of Neuroscience*, 20(13), pp. 4871-4877.

Klapperstück, M., Büttner, C., Nickel, P., Schmalzing, G., Lambrecht, G. and Markwardt, F. (2000) Antagonism by the suramin analogue NF279 on human P2X1 and P2X7 receptors. *Eur J Pharmacol*, 387(3), pp. 245-252.

Koshimizu, T., Tomic, M., Koshimizu, M. and Stojilkovic, S. S. (1998) Identification of amino acid residues contributing to desensitization of the P2X2 receptor channel. *J Biol Chem*, 273(21), pp. 12853-7.

Kotnis, S., Bingham, B., Vasilyev, D., Miller, S., Bai, Y., Yeola, S., Chanda, P., Bowlby, M., Kaftan, E., Samad, T. and Whiteside, G. (2010) Genetic and Functional Analysis of Human P2X5 Reveals a Distinct Pattern of Exon 10 Polymorphism with Predominant Expression of the Non-functional Receptor Isoform. *Mol Pharmacol*.

Kwon, H. J. (2012) Extracellular ATP signaling via P2X(4) receptor and cAMP/PKA signaling mediate ATP oscillations essential for prechondrogenic condensation. *J Endocrinol*, 214(3), pp. 337-48.

Labasi, J. M., Petrushova, N., Donovan, C., McCurdy, S., Lira, P., Payette, M. M., Brissette, W., Wicks, J. R., Audoly, L. and Gabel, C. A. (2002) Absence of the P2X7 receptor alters leukocyte function and attenuates an inflammatory response. *J Immunol*, 168(12), pp. 6436-45.

Lalo, U., Pankratov, Y., Wichert, S. P., Rossner, M. J., North, R. A., Kirchhoff, F. and Verkhratsky, A. (2008) P2X₁ and P2X₅ Subunits Form the Functional P2X Receptor in Mouse Cortical Astrocytes. *The Journal of Neuroscience*, 28(21), pp. 5473-5480.

Lambrecht, G., Braun, K., Damer, M., Ganso, M., Hildebrandt, C., Ullmann, H., Kassack, M. U. and Nickel, P. (2002) Structure-activity relationships of suramin and pyridoxal-5'-phosphate derivatives as P2 receptor antagonists. *Curr Pharm Des*, 8(26), pp. 2371-99.

Lambrecht, G., Friebe, T., Grimm, U., Windscheif, U., Bungardt, E., Hildebrandt, C., Baumert, H. G., Spatz-Kumbel, G. and Mutschler, E. (1992) PPADS, a novel functionally selective antagonist of P2 purinoceptor-mediated responses. *Eur J Pharmacol*, 217(2-3), pp. 217-9.

Lambrecht, G., Rettinger, J., Baumert, H. G., Czeche, S., Damer, S., Ganso, M., Hildebrandt, C., Niebel, B., Spatz-Kumbel, G., Schmalzing, G. and Mutschler, E. (2000) The novel pyridoxal-5'-phosphate derivative PPNDS potently antagonizes activation of P2X(1) receptors. *Eur J Pharmacol*, 387(3), pp. R19-21.

Lê, K.-T., Babinski, K. and Séguéla, P. (1998) Central P2X₄ and P2X₆ Channel Subunits Coassemble into a Novel Heteromeric ATP Receptor. *The Journal of Neuroscience*, 18(18), pp. 7152-7159.

Lê, K. T., Boué-Grabot, E., Archambault, V. and Séguéla, P. (1999) Functional and biochemical evidence for heteromeric ATP-gated channels composed of P2X1 and P2X5 subunits. *J Biol Chem*, 274(22), pp. 15415-15419.

Ledent, C., Vaugeois, J.-M., Schiffmann, S. N., Pedrazzini, T., Yacoubi, M. E., Vanderhaeghen, J.-J., Costentin, J., Heath, J. K., Vassart, G. and Parmentier, M. (1997) Aggressiveness, hypoalgesia and high blood pressure in mice lacking the adenosine A2a receptor. *Nature*, 388, pp. 674.

Lewis, C., Neidhart, S., Holy, C., North, R. A., Buell, G. and Surprenant, A. (1995) Coexpression of P2X2 and P2X3 receptor subunits can account for ATP-gated currents in sensory neurons. *Nature*, 377(6548), pp. 432-5.

Lewis, C. J., Surprenant, A. and Evans, R. J. (1998) 2',3'-O-(2,4,6-trinitrophenyl) adenosine 5'-triphosphate (TNP-ATP) - A nanomolar affinity antagonist at rat mesenteric artery P2X receptor ion channels. *Br J Pharmacol*, 124(7), pp. 1463-1466.

Li, C. (2000) Novel mechanism of inhibition by the P2 receptor antagonist PPADS of ATP-activated current in dorsal root ganglion neurons. *J Neurophysiol*, 83(5), pp. 2533-41.

Li, M., Chang, T. H., Silberberg, S. D. and Swartz, K. J. (2008) Gating the pore of P2X receptor channels. *Nat Neurosci*, 11(8), pp. 883-7.

Li, M., Silberberg, S. D. and Swartz, K. J. (2013) Subtype-specific control of P2X receptor channel signaling by ATP and Mg²⁺. *Proc Natl Acad Sci U S A*, 110(36), pp. E3455-63.

Li, Q., Luo, X., Zeng, W. and Muallem, S. (2003) Cell-specific behavior of P2X7 receptors in mouse parotid acinar and duct cells. *J Biol Chem*, 278(48), pp. 47554-61.

Libert, F., Parmentier, M., Lefort, A., Dinsart, C., Van Sande, J., Maenhaut, C., Simons, M. J., Dumont, J. E. and Vassart, G. (1989) Selective amplification and cloning of four new members of the G protein-coupled receptor family. *Science*, 244(4904), pp. 569-72.

Lohmann, K. (1929) Über die Pyrophosphatfraktion im Muskel. *Naturwissenschaften*, 17(31), pp. 624-625.

Lörinczi, É., Bhargava, Y., Marino, S. F., Taly, A., Kaczmarek-Hájek, K., Barrantes-Freer, A., Dutertre, S., Grutter, T., Rettinger, J. and Nicke, A. (2012) Involvement of the cysteine-rich head domain in activation and desensitization of the P2X1 receptor. *Proceedings of the National Academy of Sciences*, 109(28), pp. 11396-11401.

Lustig, K. D., Shiau, A. K., Brake, A. J. and Julius, D. (1993) Expression cloning of an ATP receptor from mouse neuroblastoma cells. *Proc Natl Acad Sci U S A*, 90(11), pp. 5113-7.

Lynch, K. J., Touma, E., Niforatos, W., Kage, K. L., Burgard, E. C., van Biesen, T., Kowaluk, E. A. and Jarvis, M. F. (1999) Molecular and functional characterization of human P2X(2) receptors. *Mol Pharmacol*, 56(6), pp. 1171-81.

Lythgoe, B. and Todd, A. R. (1945) Structure of Adenosine Di- and Tri-Phosphate. *Nature*, 155, pp. 695.

Malmsjö, M., Hou, M., Pendergast, W., Erlinge, D. and Edvinsson, L. (2003) Potent P2Y6 receptor mediated contractions in human cerebral arteries. *BMC Pharmacology*, 3(1), pp. 4.

Mansoor, S. E., Lu, W., Oosterheert, W., Shekhar, M., Tajkhorshid, E. and Gouaux, E. (2016) X-ray structures define human P2X(3) receptor gating cycle and antagonist action. *Nature*, 538(7623), pp. 66-71.

Marteau, F., Le Poul, E., Communi, D., Communi, D., Labouret, C., Savi, P., Boeynaems, J. M. and Gonzalez, N. S. (2003) Pharmacological characterization of the human P2Y13 receptor. *Mol Pharmacol*, 64(1), pp. 104-12.

McLaren, G. J., Lambrecht, G., Mutschler, E., Baumert, H. G., Sneddon, P. and Kennedy, C. (1994) Investigation of the actions of PPADS, a novel P2x-purinoceptor antagonist, in the guinea-pig isolated vas deferens. *Br J Pharmacol*, 111(3), pp. 913-7.

Mei, Q. and Liang, B. T. (2001) P2 purinergic receptor activation enhances cardiac contractility in isolated rat and mouse hearts. *Am J Physiol Heart Circ Physiol*, 281(1), pp. H334-41.

Metzger, M. W., Walser, S. M., Dedic, N., Aprile-Garcia, F., Jakubcakova, V., Adamczyk, M., Webb, K. J., Uhr, M., Refojo, D., Schmidt, M. V., Friess, E., Steiger, A., Kimura, M., Chen, A., Holsboer, F., Arzt, E., Wurst, W. and Deussing, J. M. (2017) Heterozygosity for the Mood Disorder-Associated Variant Gln460Arg Alters P2X7 Receptor Function and Sleep Quality. *J Neurosci*, 37(48), pp. 11688-11700.

Michel, A. D., Chambers, L. J., Clay, W. C., Condreay, J. P., Walter, D. S. and Chessell, I. P. (2007) Direct labelling of the human P2X7 receptor and identification of positive and negative cooperativity of binding. *Br J Pharmacol*, 151(1), pp. 84-95.

Michel, A. D., Chambers, L. J. and Walter, D. S. (2008a) Negative and positive allosteric modulators of the P2X7 receptor. *Br J Pharmacol*, 153(4), pp. 737-750.

Michel, A. D., Clay, W. C., Ng, S. W., Roman, S., Thompson, K., Condreay, J. P., Hall, M., Holbrook, J., Livermore, D. and Senger, S. (2008b) Identification of regions of the P2X(7) receptor that contribute to human and rat species differences in antagonist effects. *Br J Pharmacol*, 155(5), pp. 738-51.

Michel, A. D., Miller, K. J., Lundström, K., Buell, G. N. and Humphrey, P. P. A. (1997) Radiolabeling of the Rat P2X₄ Purinoceptor: Evidence for Allosteric Interactions of Purinoceptor Antagonists and Monovalent Cations with P2X Purinoceptors. *Mol Pharmacol*, 51(3), pp. 524-532.

Mio, K., Kubo, Y., Ogura, T., Yamamoto, T. and Sato, C. (2005) Visualization of the trimeric P2X₂ receptor with a crown-capped extracellular domain. *Biochem Biophys Res Commun*, 337(3), pp. 998-1005.

Mitsuya, H., Popovic, M., Yarchoan, R., Matsushita, S., Gallo, R. C. and Broder, S. (1984) Suramin protection of T cells in vitro against infectivity and cytopathic effect of HTLV-III. *Science*, 226(4671), pp. 172-4.

Mulryan, K., Gitterman, D. P., Lewis, C. J., Vial, C., Leckle, B. J., Cobb, A. L., Brown, J. E., Conley, E. C., Buell, G., Pritchard, C. A. and Evans, R. J. (2000) Reduced vas deferens contraction and male infertility in mice lacking P2X₁ receptors. *Nature*, 403(6765), pp. 86-89.

Nagata, K., Imai, T., Yamashita, T., Tsuda, M., Tozaki-Saitoh, H. and Inoue, K. (2009) Antidepressants inhibit P2X₄ receptor function: a possible involvement in neuropathic pain relief. *Molecular Pain*, 5(1), pp. 20.

Nagaya, N., Tittle, R. K., Saar, N., Dellal, S. S. and Hume, R. I. (2005) An intersubunit zinc binding site in rat P2X₂ receptors. *J Biol Chem*, 280(28), pp. 25982-93.

Nicholas, R. A., Watt, W. C., Lazarowski, E. R., Li, Q. and Harden, K. (1996) Uridine nucleotide selectivity of three phospholipase C-activating P2 receptors: identification of a UDP-selective, a UTP-selective, and an ATP- and UTP-specific receptor. *Mol Pharmacol*, 50(2), pp. 224-229.

Nicke, A., Baumert, H. G., Rettinger, J., Eichele, A., Lambrecht, G., Mutschler, E. and Schmalzing, G. (1998) P2X₁ and P2X₃ receptors form stable trimers: a novel structural motif of ligand-gated ion channels. *EMBO J*, 17(11), pp. 3016-28.

Nicke, A., Kerschensteiner, D. and Soto, F. (2005) Biochemical and functional evidence for heteromeric assembly of P2X₁ and P2X₄ subunits. *J Neurochem*, 92(4), pp. 925-933.

Niitsu, Y., Jakubowski, J. A., Sugidachi, A. and Asai, F. (2005) Pharmacology of CS-747 (prasugrel, LY640315), a novel, potent antiplatelet agent with in vivo P2Y₁₂ receptor antagonist activity. *Semin Thromb Hemost*, 31(2), pp. 184-94.

Nörenberg, W. and Illes, P. (2000) Neuronal P2X receptors: localisation and functional properties. *Naunyn Schmiedebergs Arch Pharmacol*, 362(4), pp. 324-339.

Norenberg, W., Sobottka, H., Hempel, C., Plotz, T., Fischer, W., Schmalzing, G. and Schaefer, M. (2012) Positive allosteric modulation by ivermectin of human but not murine P2X7 receptors. *Br J Pharmacol*, 167(1), pp. 48-66.

North, R. A. (2004) P2X3 receptors and peripheral pain mechanisms. *J Physiol*, 554(2), pp. 301-308.

North, R. A. and Surprenant, A. (2000) Pharmacology of cloned P2X receptors. *Annu Rev Pharmacol Toxicol*, 40, pp. 563-80.

Offermanns, S. and Simon, M. I. (1995) G alpha 15 and G alpha 16 couple a wide variety of receptors to phospholipase C. *J Biol Chem*, 270(25), pp. 15175-80.

Ormond, S. J., Barrera, N. P., Qureshi, O. S., Henderson, R. M., Edwardson, J. M. and Murrell-Lagnado, R. D. (2006) An Uncharged Region within the N Terminus of the P2X₆ Receptor Inhibits Its Assembly and Exit from the Endoplasmic Reticulum. *Mol Pharmacol*, 69(5), pp. 1692-1700.

Ortells, M. O. and Lunt, G. G. (1995) Evolutionary history of the ligand-gated ion-channel superfamily of receptors. *Trends Neurosci*, 18(3), pp. 121-7.

P., C. I., D., M. A. and A., H. P. P. (1998) Effects of antagonists at the human recombinant P2X7 receptor. *Br J Pharmacol*, 124(6), pp. 1314-1320.

Palea, S., Artibani, W., Ostardo, E., Trist, D. G. and Pietra, C. (1993) Evidence for Purinergic Neurotransmission in Human Urinary Bladder Affected by Interstitial Cystitis. *The Journal of Urology*, 150(6), pp. 2007-2012.

Palmer, R. K., Boyer, J. L., Schachter, J. B., Nicholas, R. A. and Harden, T. K. (1998) Agonist Action of Adenosine Triphosphates at the Human P2Y₁ Receptor. *Mol Pharmacol*, 54(6), pp. 1118-1123.

Palmer, T. M., Gettys, T. W. and Stiles, G. L. (1995) Differential interaction with and regulation of multiple G-proteins by the rat A3 adenosine receptor. *J Biol Chem*, 270(28), pp. 16895-902.

- Palygin, O., Lalo, U., Verkhatsky, A. and Pankratov, Y. (2010) Ionotropic NMDA and P2X1/5 receptors mediate synaptically induced Ca²⁺ signalling in cortical astrocytes. *Cell Calcium*, 48(4), pp. 225-231.
- Prado, F. C., Araldi, D., Vieira, A. S., Oliveira-Fusaro, M. C., Tambeli, C. H. and Parada, C. A. (2013) Neuronal P2X3 receptor activation is essential to the hyperalgesia induced by prostaglandins and sympathomimetic amines released during inflammation. *Neuropharmacology*, 67, pp. 252-8.
- R., A. A., Louis-Philippe, B., Dominique, B., Yuriy, P. and Philippe, S. (2010) Modulation of heteromeric P2X1/5 receptors by phosphoinositides in astrocytes depends on the P2X1 subunit. *J Neurochem*, 113(6), pp. 1676-1684.
- Rasar, M. A. and Hammes, S. R. (2006) The physiology of the *Xenopus laevis* ovary. *Methods Mol Biol*, 322, pp. 17-30.
- Rassendren, F., Buell, G., Newbolt, A., North, R. A. and Surprenant, A. (1997) Identification of amino acid residues contributing to the pore of a P2X receptor. *The EMBO Journal*, 16(12), pp. 3446-3454.
- Rassendren, F., Buell, G. N., Virginio, C., Collo, G., North, R. A. and Surprenant, A. (1997) The permeabilizing ATP receptor, P2X7. Cloning and expression of a human cDNA. *J Biol Chem*, 272(9), pp. 5482-6.
- Ray, F. R., Huang, W., Slater, M. and Barden, J. A. (2002) Purinergic receptor distribution in endothelial cells in blood vessels: a basis for selection of coronary artery grafts. *Atherosclerosis*, 162(1), pp. 55-61.
- Ren, J., Bian, X., DeVries, M., Schnegelsberg, B., Cockayne, D. A., Ford, A. P. D. W. and Galligan, J. J. (2003) P2X2 subunits contribute to fast synaptic excitation in myenteric neurons of the mouse small intestine. *J Physiol*, 552(3), pp. 809-821.
- Rettinger, J., Braun, K., Hochmann, H., Kassack, M. U., Ullmann, H., Nickel, P., Schmalzing, G. and Lambrecht, G. (2005) Profiling at recombinant homomeric and heteromeric rat P2X receptors identifies the suramin analogue NF449 as a highly potent P2X1 receptor antagonist. *Neuropharmacology*, 48(3), pp. 461-8.
- Rettinger, J., Schmalzing, G., Damer, S., Muller, G., Nickel, P. and Lambrecht, G. (2000) The suramin analogue NF279 is a novel and potent antagonist selective for the P2X(1) receptor. *Neuropharmacology*, 39(11), pp. 2044-53.

Riksen, N. P., Zhou, Z., Oyen, W. J., Jaspers, R., Ramakers, B. P., Brouwer, R. M., Boerman, O. C., Steinmetz, N., Smits, P. and Rongen, G. A. (2006) Caffeine prevents protection in two human models of ischemic preconditioning. *J Am Coll Cardiol*, 48(4), pp. 700-7.

Robaye, B., Boeynaems, J.-M. and Communi, D. (1997) Slow desensitization of the human P2Y6 receptor. *Eur J Pharmacol*, 329(2), pp. 231-236.

Robaye, B., Ghanem, E., Wilkin, F., Fokan, D., Van Driessche, W., Schurmans, S., Boeynaems, J.-M. and Beauwens, R. (2003) Loss of Nucleotide Regulation of Epithelial Chloride Transport in the Jejunum of P2Y₄-Null Mice. *Mol Pharmacol*, 63(4), pp. 777-783.

Roberts, J. A., Allsopp, R. C., El Ajouz, S., Vial, C., Schmid, R., Young, M. T. and Evans, R. J. (2012) Agonist binding evokes extensive conformational changes in the extracellular domain of the ATP-gated human P2X1 receptor ion channel. *Proceedings of the National Academy of Sciences*, 109(12), pp. 4663-4667.

Roberts, J. A., Allsopp, R. C., El Ajouza, S., Vial, C., Schmid, R., Young, M. T. and Evans, R. J. (2012) Agonist binding evokes extensive conformational changes in the extracellular domain of the ATP-gated human P2X1 receptor ion channel. *Proceedings of the National Academy of Sciences of the United States of America*, 109(12), pp. 4663-4667.

Roberts, J. A., Digby, H. R., Kara, M., El Ajouz, S., Sutcliffe, M. J. and Evans, R. J. (2008) Cysteine substitution mutagenesis and the effects of methanethiosulfonate reagents at P2X2 and P2X4 receptors support a core common mode of ATP action at P2X receptors. *Journal of Biological Chemistry*, 283(29), pp. 20126-20136.

Roberts, J. A. and Evans, R. J. (2004) ATP binding at human P2X1 receptors: Contribution of aromatic and basic amino acids revealed using mutagenesis and partial agonists. *Journal of Biological Chemistry*, 279(10), pp. 9043-9055.

Roberts, J. A. and Evans, R. J. (2006) Contribution of conserved polar glutamine, asparagine and threonine residues and glycosylation to agonist action at human P2X1 receptors for ATP. *J Neurochem*, 96(3), pp. 843-852.

Roberts, J. A. and Evans, R. J. (2007) Cysteine substitution mutants give structural insight and identify ATP binding and activation sites at P2X receptors. *Journal of Neuroscience*, 27(15), pp. 4072-4082.

Roberts, J. A., Valente, M., Allsopp, R. C., Watt, D. and Evans, R. J. (2009a) Contribution of the region Glu181 to Val200 of the extracellular loop of the human P2X1 receptor to agonist binding and gating revealed using cysteine scanning mutagenesis. *J Neurochem*, 109(4), pp. 1042-52.

Roberts, J. A., Valente, M., Allsopp, R. C., Watt, D. and Evans, R. J. (2009b) Contribution of the region Glu181 to Val200 of the extracellular loop of the human P2X1 receptor to agonist binding and gating revealed using cysteine scanning mutagenesis1. *J Neurochem*, 109(4), pp. 1042-1052.

Roberts, J. A., Vial, C., Digby, H. R., Agboh, K. C., Wen, H., Atterbury-Thomas, A. and Evans, R. J. (2006) Molecular properties of P2X receptors. *Pflugers Archiv European Journal of Physiology*, 452(5), pp. 486-500.

Roe, D. R. and Cheatham, T. E., 3rd (2013) PTRAJ and CPPTRAJ: Software for Processing and Analysis of Molecular Dynamics Trajectory Data. *J Chem Theory Comput*, 9(7), pp. 3084-95.

Rong, W., Gourine, A. V., Cockayne, D. A., Xiang, Z., Ford, A. P. D. W., Spyer, K. M. and Burnstock, G. (2003) Pivotal Role of Nucleotide P2X₂ Receptor Subunit of the ATP-Gated Ion Channel Mediating Ventilatory Responses to Hypoxia. *The Journal of Neuroscience*, 23(36), pp. 11315-11321.

Ryten, M., Hoebertz, A. and Burnstock, G. (2001) Sequential expression of three receptor subtypes for extracellular ATP in developing rat skeletal muscle. *Developmental Dynamics*, 221(3), pp. 331-341.

Ryten, M., Koshi, R., Knight, G. E., Turmaine, M., Dunn, P., Cockayne, D. A., Ford, A. P. W. and Burnstock, G. (2007) Abnormalities in neuromuscular junction structure and skeletal muscle function in mice lacking the P2X₂ nucleotide receptor. *Neuroscience*, 148(3), pp. 700-711.

Salvatore, C. A., Tilley, S. L., Latour, A. M., Fletcher, D. S., Koller, B. H. and Jacobson, M. A. (2000) Disruption of the A₃ adenosine receptor gene in mice and its effect on stimulated inflammatory cells. *J Biol Chem*, 275(6), pp. 4429-34.

Savi, P., Pereillo, J. M., Uzabiaga, M. F., Combalbert, J., Picard, C., Maffrand, J. P., Pascal, M. and Herbert, J. M. (2000) Identification and biological activity of the active metabolite of clopidogrel. *Thromb Haemost*, 84(5), pp. 891-6.

Schumann, H. J. (1958) [Noradrenalin and ATP content of sympathetic nerves]. *Naunyn Schmiedebergs Arch Exp Pathol Pharmacol*, 233(3), pp. 296-300.

Serrano, A., Mo, G., Grant, R., Paré, M., O'Donnell, D., Yu, X. H., Tomaszewski, M. J., Perkins, M. N., Séguéla, P. and Cao, C. Q. (2012) Differential Expression and Pharmacology of Native P2X Receptors in Rat and Primate Sensory Neurons. *The Journal of Neuroscience*, 32(34), pp. 11890-11896.

Shcherbatko, A., Foletti, D., Poulsen, K., Strop, P., Zhu, G., Hasa-Moreno, A., Melton Witt, J., Loo, C., Krimm, S., Pios, A., Yu, J., Brown, C., Lee, J. K., Stroud, R., Rajpal, A. and Shelton, D. (2016) Modulation of P2X3 and P2X2/3 Receptors by Monoclonal Antibodies. *J Biol Chem*, 291(23), pp. 12254-70.

Shink, E., Harvey, M., Tremblay, M., Gagne, B., Belleau, P., Raymond, C., Labbe, M., Dube, M. P., Lafreniere, R. G. and Barden, N. (2005) Analysis of microsatellite markers and single nucleotide polymorphisms in candidate genes for susceptibility to bipolar affective disorder in the chromosome 12Q24.31 region. *Am J Med Genet B Neuropsychiatr Genet*, 135B(1), pp. 50-8.

Sibley, G. N. (1984) A comparison of spontaneous and nerve-mediated activity in bladder muscle from man, pig and rabbit. *J Physiol*, 354(1), pp. 431-443.

Silva, C. G., Metin, C., Fazeli, W., Machado, N. J., Darmopil, S., Launay, P. S., Ghestem, A., Nesa, M. P., Bassot, E., Szabo, E., Baqi, Y., Muller, C. E., Tome, A. R., Ivanov, A., Isbrandt, D., Zilberter, Y., Cunha, R. A., Esclapez, M. and Bernard, C. (2013) Adenosine receptor antagonists including caffeine alter fetal brain development in mice. *Sci Transl Med*, 5(197), pp. 197ra104.

Sim, J. A., Broomhead, H. E. and North, R. A. (2008) Ectodomain lysines and suramin block of P2X1 receptors. *J Biol Chem*, 283(44), pp. 29841-6.

Sim, J. A. and North, R. A. (2010) Amitriptyline does not block the action of ATP at human P2X4 receptor. *Br J Pharmacol*, 160(1), pp. 88-92.

Sim, J. A., Park, C. K., Oh, S. B., Evans, R. J. and North, R. A. (2007) P2X 1 and P2X 4 receptor currents in mouse macrophages. *Br J Pharmacol*, 152(8), pp. 1283-1290.

Smolen, J. E. and Weissmann, G. (1978) Mg²⁺-ATPase as a membrane ectoenzyme of human granulocytes. Inhibitors, activators and response to phagocytosis. *Biochimica et Biophysica Acta (BBA) - Biomembranes*, 512(3), pp. 525-538.

Solle, M., Labasi, J., Perregaux, D. G., Stam, E., Petrushova, N., Koller, B. H., Griffiths, R. J. and Gabel, C. A. (2001) Altered cytokine production in mice lacking P2X(7) receptors. *J Biol Chem*, 276(1), pp. 125-32.

Sonin, D., Zhou, S.-Y., Cronin, C., Sonina, T., Wu, J., Jacobson, K. A., Pappano, A. and Liang, B. T. (2008) Role of P2X purinergic receptors in the rescue of ischemic heart failure. *American Journal of Physiology-Heart and Circulatory Physiology*, 295(3), pp. H1191-H1197.

Soto, F., Garcia-Guzman, M., Gomez-Hernandez, J. M., Hollmann, M., Karschin, C. and Stühmer, W. (1996) P2X4: an ATP-activated ionotropic receptor cloned from rat brain. *Proceedings of the National Academy of Sciences*, 93(8), pp. 3684-3688.

Soto, F., Lambrecht, G., Nickel, P., Stühmer, W. and Busch, A. E. (1999) Antagonistic properties of the suramin analogue NF023 at heterologously expressed P2X receptors. *Neuropharmacology*, 38(1), pp. 141-149.

Souslova, V., Cesare, P., Ding, Y. N., Akopian, A. N., Stanfa, L., Suzuki, R., Carpenter, K., Dickenson, A., Boyce, S., Hill, R., Nebenius-Oosthuizen, D., Smith, A. J. H., Kidd, E. J. and Wood, J. N. (2000) Warm-coding deficits and aberrant inflammatory pain in mice lacking P2X(3) receptors. *Nature*, 407(6807), pp. 1015-1017.

Spelta, V., Jiang, L. H., Surprenant, A. and North, R. A. (2002) Kinetics of antagonist actions at rat P2X2/3 heteromeric receptors. *Br J Pharmacol*, 135(6), pp. 1524-30.

Sperlágh, B. and Vizi, S. E. (1996) Neuronal synthesis, storage and release of ATP. *Seminars in Neuroscience*, 8(4), pp. 175-186.

Stehle, J. H., Rivkees, S. A., Lee, J. J., Weaver, D. R., Deeds, J. D. and Reppert, S. M. (1992) Molecular cloning and expression of the cDNA for a novel A2-adenosine receptor subtype. *Molecular Endocrinology*, 6(3), pp. 384-393.

Stelmashenko, O., Lalo, U., Yang, Y., Bragg, L., North, R. A. and Compan, V. (2012) Activation of Trimeric P2X2 Receptors by Fewer than Three ATP Molecules. *Mol Pharmacol*, 82(4), pp. 760-766.

Stokes, L., Jiang, L. H., Alcaraz, L., Bent, J., Bowers, K., Fagura, M., Furber, M., Mortimore, M., Lawson, M., Theaker, J., Laurent, C., Braddock, M. and Surprenant, A. (2006) Characterization of a selective and potent antagonist of human P2X7 receptors, AZ11645373. *Br J Pharmacol*, 149(7), pp. 880-887.

Stokes, L., Scurrah, K., Ellis, J. A., Cromer, B. A., Skarratt, K. K., Gu, B. J., Harrap, S. B. and Wiley, J. S. (2011) A loss-of-function polymorphism in the human P2X4 receptor is associated with increased pulse pressure. *Hypertension*, 58(6), pp. 1086-92.

Sun, B., Li, J., Okahara, K. and Kambayashi, J. (1998) P2X1 purinoceptor in human platelets. Molecular cloning and functional characterization after heterologous expression. *J Biol Chem*, 273(19), pp. 11544-7.

Surprenant, A., Rassendren, F., Kawashima, E., North, R. A. and Buell, G. (1996) The cytolytic P2Z receptor for extracellular ATP identified as a P2X receptor (P2X7). *Science*, 272(5262), pp. 735-8.

Surprenant, A., Schneider, D. A., Wilson, H. L., Galligan, J. J. and North, R. A. (2000) Functional properties of heteromeric P2X1/5 receptors expressed in HEK cells and excitatory junction potentials in guinea-pig submucosal arterioles. *Journal of the Autonomic Nervous System*, 81(1), pp. 249-263.

Tabor, S. (1990) Expression Using the T7 RNA Polymerase/Promoter System. *Current Protocols in Molecular Biology*, 11(1), pp. 16.2.1-16.2.11.

Tempest, H. V., Dixon, A. K., Turner, W. H., Elneil, S., Sellers, L. A. and Ferguson, D. R. (2004) P2X2 and P2X3 receptor expression in human bladder urothelium and changes in interstitial cystitis. *BJU Int*, 93(9), pp. 1344-1348.

Torres, G. E., Egan, T. M. and Voigt, M. M. (1998) N-Linked glycosylation is essential for the functional expression of the recombinant P2X2 receptor. *Biochemistry*, 37(42), pp. 14845-51.

Torres, G. E., Egan, T. M. and Voigt, M. M. (1999) Hetero-oligomeric assembly of P2X receptor subunits. Specificities exist with regard to possible partners. *J Biol Chem*, 274(10), pp. 6653-9.

Torres, G. E., Haines, W. R., Egan, T. M. and Voigt, M. M. (1998) Co-Expression of P2X₁ and P2X₅ Receptor Subunits Reveals a Novel ATP-Gated Ion Channel. *Mol Pharmacol*, 54(6), pp. 989-993.

Treize, D. J., Kennedy, I. and Humphrey, P. P. (1994) The use of antagonists to characterize the receptors mediating depolarization of the rat isolated vagus nerve by alpha, beta-methylene adenosine 5'-triphosphate. *Br J Pharmacol*, 112(1), pp. 282-8.

Tsuda, M., Kuboyama, K., Inoue, T., Nagata, K., Tozaki-Saitoh, H. and Inoue, K. (2009) Behavioral phenotypes of mice lacking purinergic P2X4 receptors in acute and chronic pain assays. *Molecular Pain*, 5(1), pp. 28.

Tsuda, M., Shigemoto-Mogami, Y, Koizumi, S, Mizokoshi, A, Kohsaka, S, Salter, MW & Inoue, K (2003) P2X4 receptors induced in spinal microglia gate tactile allodynia after nerve injury. *Nature*, 424(6950), pp. 778-783.

Ulmann, L., Hirbec, H. and Rassendren, F. (2010) P2X4 receptors mediate PGE2 release by tissue-resident macrophages and initiate inflammatory pain. *The EMBO Journal*, 29(14), pp. 2290-2300.

Valera, S., Hussy, N., Evans, R. J., Adami, N., North, R. A., Surprenant, A. and Buell, G. (1994) A new class of ligand-gated ion channel defined by P2x receptor for extracellular ATP. *Nature*, 371(6497), pp. 516-9.

Valera, S., Talabot, F., Evans, R. J., Gos, A., Antonarakis, S. E., Morris, M. A. and Buell, G. N. (1995) Characterization and chromosomal localization of a human P(2X) receptor from the urinary bladder. *Receptors and Channels*, 3(4), pp. 283-289.

Vanderwinden, J.-M., Timmermans, J.-P. and Schiffmann, S. N. (2003) Glial cells, but not interstitial cells, express P2X7, an ionotropic purinergic receptor, in rat gastrointestinal musculature. *Cell and Tissue Research*, 312(2), pp. 149-154.

Vial, C. and Evans, R. J. (2000) P2X receptor expression in mouse urinary bladder and the requirement of P2X 1 receptors for functional P2X receptor responses in the mouse urinary bladder smooth muscle. *Br J Pharmacol*, 131(7), pp. 1489-1495.

Vial, C., Hechler, B., Leon, C., Cazenave, J. P. and Gachet, C. (1997) Presence of P2X1 purinoceptors in human platelets and megakaryoblastic cell lines. *Thromb Haemost*, 78(6), pp. 1500-4.

von Kugelgen, I. and Harden, T. K. (2011) Molecular pharmacology, physiology, and structure of the P2Y receptors. *Adv Pharmacol*, 61, pp. 373-415.

von Kugelgen, I. and Hoffmann, K. (2016) Pharmacology and structure of P2Y receptors. *Neuropharmacology*, 104(Supplement C), pp. 50-61.

Voogd, T. E., Vansterkenburg, E. L., Wilting, J. and Janssen, L. H. (1993) Recent research on the biological activity of suramin. *Pharmacol Rev*, 45(2), pp. 177-203.

Vulchanova, L., Riedl, M. S., Shuster, S. J., Buell, G., Surprenant, A., North, R. A. and Elde, R. (1997) Immunohistochemical study of the P2X2 and P2X3 receptor subunits in rat and monkey sensory neurons and their central terminals. *Neuropharmacology*, 36(9), pp. 1229-1242.

Waldo, G. L. and Harden, T. K. (2004) Agonist Binding and Gq-Stimulating Activities of the Purified Human P2Y₁ Receptor. *Mol Pharmacol*, 65(2), pp. 426-436.

Wareham, K., Vial, C., Wykes, R. C. E., Bradding, P. and Seward, E. P. (2009) Functional evidence for the expression of P2X1, P2X4 and P2X7 receptors in human lung mast cells. *Br J Pharmacol*, 157(7), pp. 1215-1224.

Webb, T. E., Simon, J., Krishek, B. J., Bateson, A. N., Smart, T. G., King, B. F., Burnstock, G. and Barnard, E. A. (1993) Cloning and Functional Expression of a Brain G-Protein-Coupled Atp Receptor. *Febs Letters*, 324(2), pp. 219-225.

Wei, L., Syed Mortadza, S. A., Yan, J., Zhang, L., Wang, L., Yin, Y., Li, C., Chalon, S., Emond, P., Belzung, C., Li, D., Lu, C., Roger, S. and Jiang, L.-H. (2018) ATP-activated P2X7 receptor in the pathophysiology of mood disorders and as an emerging target for the development of novel antidepressant therapeutics. *Neuroscience & Biobehavioral Reviews*, 87, pp. 192-205.

Weigand, L. A., Ford, A. P. and Udem, B. J. (2012) A role for ATP in bronchoconstriction-induced activation of guinea pig vagal intrapulmonary C-fibres. *J Physiol*, 590(16), pp. 4109-20.

White, C. W., Choong, Y. T., Short, J. L., Exintaris, B., Malone, D. T., Allen, A. M., Evans, R. J. and Ventura, S. (2013) Male contraception via simultaneous knockout of alpha1A-adrenoceptors and P2X1-purinoceptors in mice. *Proc Natl Acad Sci U S A*, 110(51), pp. 20825-30.

Whittaker, V. P., Dowdall, M. J., Dowe, G. H., Facino, R. M. and Scotto, J. (1974) Proteins of cholinergic synaptic vesicles from the electric organ of Torpedo: characterization of a low molecular weight acidic protein. *Brain Res*, 75(1), pp. 115-31.

Wildman, S. S., Brown, S. G., Rahman, M., Noel, C. A., Churchill, L., Burnstock, G., Unwin, R. J. and King, B. F. (2002) Sensitization by extracellular Ca(2+) of

rat P2X(5) receptor and its pharmacological properties compared with rat P2X(1). *Mol Pharmacol*, 62(4), pp. 957-66.

Wildman, S. S., King, B. F. and Burnstock, G. (1999) Modulatory activity of extracellular H⁺ and Zn²⁺ on ATP-responses at rP2X1 and rP2X3 receptors. *Br J Pharmacol*, 128(2), pp. 486-92.

Wills, E. D. and Wormald, A. (1950) Studies on suramin; the action of the drug on some enzymes. *Biochem J*, 47(2), pp. 158-70.

Windscheif, U., Pfaff, O., Ziganshin, A. U., Hoyle, C. H., Baumert, H. G., Mutschler, E., Burnstock, G. and Lambrecht, G. (1995) Inhibitory action of PPADS on relaxant responses to adenine nucleotides or electrical field stimulation in guinea-pig taenia coli and rat duodenum. *Br J Pharmacol*, 115(8), pp. 1509-17.

Wolf, C., Rosefort, C., Fallah, G., Kassack, M. U., Hamacher, A., Bodnar, M., Wang, H., Illes, P., Kless, A., Bahrenberg, G., Schmalzing, G. and Hausmann, R. (2011) Molecular Determinants of Potent P2X2 Antagonism Identified by Functional Analysis, Mutagenesis, and Homology Docking. *Mol Pharmacol*, 79(4), pp. 649-661.

Wu, T., Dai, M., Shi, X. R., Jiang, Z. G. and Nuttall, A. L. (2011) Functional expression of P2X4 receptor in capillary endothelial cells of the cochlear spiral ligament and its role in regulating the capillary diameter. *Am J Physiol Heart Circ Physiol*, 301(1), pp. H69-78.

Xiang, Z., Bo, X. and Burnstock, G. (1998) Localization of ATP-gated P2X receptor immunoreactivity in rat sensory and sympathetic ganglia. *Neurosci Lett*, 256(2), pp. 105-8.

Xiong, K., Peoples, R. W., Montgomery, J. P., Chiang, Y., Stewart, R. R., Weight, F. F. and Li, C. (1999) Differential modulation by copper and zinc of P2X2 and P2X4 receptor function. *J Neurophysiol*, 81(5), pp. 2088-94.

Yamada, K., Kobayashi, M. and Kanda, T. (2014) Involvement of adenosine A2A receptors in depression and anxiety. *Int Rev Neurobiol*, 119, pp. 373-93.

Yamamoto, K., Korenaga, R., Kamiya, A. and Ando, J. (2000a) Fluid Shear Stress Activates Ca²⁺ Influx Into Human Endothelial Cells via P2X4 Purinoceptors. *Circulation Research*, 87(5), pp. 385-391.

Yamamoto, K., Korenaga, R., Kamiya, A., Qi, Z., Sokabe, M. and Ando, J. (2000b) P2X4 receptors mediate ATP-induced calcium influx in human vascular endothelial cells. *American Journal of Physiology-Heart and Circulatory Physiology*, 279(1), pp. H285-H292.

Yamamoto, K., Sokabe, T., Matsumoto, T., Yoshimura, K., Shibata, M., Ohura, N., Fukuda, T., Sato, T., Sekine, K., Kato, S., Isshiki, M., Fujita, T., Kobayashi, M., Kawamura, K., Masuda, H., Kamiya, A. and Ando, J. (2005) Impaired flow-dependent control of vascular tone and remodeling in P2X4-deficient mice. *Nature Medicine*, 12, pp. 133.

Yan, D., Zhu, Y., Walsh, T., Xie, D., Yuan, H., Sirmaci, A., Fujikawa, T., Wong, A. C., Loh, T. L., Du, L., Grati, M., Vljakovic, S. M., Blanton, S., Ryan, A. F., Chen, Z. Y., Thorne, P. R., Kachar, B., Tekin, M., Zhao, H. B., Housley, G. D., King, M. C. and Liu, X. Z. (2013) Mutation of the ATP-gated P2X(2) receptor leads to progressive hearing loss and increased susceptibility to noise. *Proc Natl Acad Sci U S A*, 110(6), pp. 2228-33.

Yan, Z., Liang, Z., Tomić, M., Obsil, T. and Stojilkovic, S. S. (2005) Molecular Determinants of the Agonist Binding Domain of a P2X Receptor Channel. *Mol Pharmacol*, 67(4), pp. 1078-1088.

Young, M. T. (2010) P2X receptors: dawn of the post-structure era. *Trends in Biochemical Sciences*, 35(2), pp. 83-90.

Young, M. T., Fisher, J. A., Fountain, S. J., Ford, R. C., North, R. A. and Khakh, B. S. (2008) Molecular shape, architecture, and size of P2X4 receptors determined using fluorescence resonance energy transfer and electron microscopy. *J Biol Chem*, 283(38), pp. 26241-51.

Yu, Y., Ugawa, S., Ueda, T., Ishida, Y., Inoue, K., Kyaw Nyunt, A., Umemura, A., Mase, M., Yamada, K. and Shimada, S. (2008) Cellular localization of P2X7 receptor mRNA in the rat brain. *Brain Research*, 1194, pp. 45-55.

Zhang, K., Zhang, J., Gao, Z. G., Zhang, D., Zhu, L., Han, G. W., Moss, S. M., Paoletta, S., Kiselev, E., Lu, W., Fenalti, G., Zhang, W., Muller, C. E., Yang, H., Jiang, H., Cherezov, V., Katritch, V., Jacobson, K. A., Stevens, R. C., Wu, B. and Zhao, Q. (2014) Structure of the human P2Y12 receptor in complex with an antithrombotic drug. *Nature*, 509(7498), pp. 115-8.

Zhang, X.-J., Zheng, G.-G., Ma, X.-T., Yang, Y.-H., Li, G., Rao, Q., Nie, K. and Wu, K.-F. Expression of P2X7 in human hematopoietic cell lines and leukemia patients. *Leukemia Research*, 28(12), pp. 1313-1322.

Zhao, W.-S., Wang, J., Ma, X.-J., Yang, Y., Liu, Y., Huang, L.-D., Fan, Y.-Z., Cheng, X.-Y., Chen, H.-Z., Wang, R. and Yu, Y. (2014) Relative motions between left flipper and dorsal fin domains favour P2X4 receptor activation. *Nature Communications*, 5, pp. 4189.

Zheng, L., Zhang, X., Yang, F., Zhu, J., Zhou, P., Yu, F., Hou, L., Xiao, L., He, Q. and Wang, B. (2014) Regulation of the P2X7R by microRNA-216b in human breast cancer. *Biochem Biophys Res Commun*, 452(1), pp. 197-204.

Zhou, Q. Y., Li, C., Olah, M. E., Johnson, R. A., Stiles, G. L. and Civelli, O. (1992) Molecular cloning and characterization of an adenosine receptor: the A3 adenosine receptor. *Proc Natl Acad Sci U S A*, 89(16), pp. 7432-6.

Ziganshin, A. U., Hoyle, C. H., Bo, X., Lambrecht, G., Mutschler, E., Baumert, H. G. and Burnstock, G. (1993) PPADS selectively antagonizes P2X-purinoceptor-mediated responses in the rabbit urinary bladder. *Br J Pharmacol*, 110(4), pp. 1491-5.

Ziganshin, A. U., Hoyle, C. H., Lambrecht, G., Mutschler, E., Bumert, H. G. and Burnstock, G. (1994) Selective antagonism by PPADS at P2X-purinoceptors in rabbit isolated blood vessels. *Br J Pharmacol*, 111(3), pp. 923-9.

Zimmermann, H. (1994) Signalling via ATP in the nervous system. *Trends in Neurosciences*, 17(10), pp. 420-426.

Zimmermann, H. (2001) Ectonucleotidases: Some recent developments and a note on nomenclature. *Drug Development Research*, 52(1-2), pp. 44-56.